Thermoplastic Composites for Polymer Electrolyte Membrane Fuel Cell Bipolar Plates

by

Taylor J. Mali

A thesis
presented to the University of Waterloo
in fulfillment of the
thesis requirement for the degree of
Master of Applied Science
in
Chemical Engineering

Waterloo, Ontario, Canada, 2006

I hereby declare that I am the sole author of this thesis. This is a true copy of the thesis, including any required final revisions, as accepted by my examiners.

I understand that my thesis may be made electronically available to the public.

Abstract

Polymer electrolyte membrane fuel cells (PEMFCs) exhibit encouraging potential as an enabling technology for the Hydrogen Economy. Currently an important barrier to commercialization is the cost associated with existing PEMFC materials; this project's goal was to investigate alternative materials for PEMFC bipolar plates. Conductive thermoplastic materials offer the promise of low density, low cost processing, and inexpensive resins, and were the focus of material development for PEMFC bipolar plate applications.

In order to develop a thermoplastic bipolar plate this study utilized the combination of a low cost injection moldable commodity polymer resin, and low cost carbon materials as conductive fillers. The materials selected and tested included; a polypropylene copolymer; acetylene carbon black; Vulcan carbon black; and short carbon fiber. The components were combined in a twin screw extruder and injection molded into samples for testing. The result was a spectrum of composite samples with a range of filler loadings from 0 to 60 wt% and varying filler type ratios. Synergy between the different carbon types was achieved which led to better physical properties, specifically conductivity.

The novel blends produced were tested for electrical conductivity, mechanical properties, rheology, microscopy, and actual plates were made and tested in a single cell PEMFC. These trials enabled discussion around the feasibility of the materials with respect to processability, cost, and performance (both in the fuel cell and in potential applications).

The most significant results were measured using a composite blend with 54 wt% filler loading and a 1:1:1 filler ratio. Mechanical results achieved 68% and 100% of the industry targets for tensile and flexural strength, respectively. Tensile strength attained 27.7 MPa and flexural strength measured 82.8 MPa. Electrical conductivity results for the same samples varied between the two methods of measurement used. Using a fuel cell industry recommended procedure 2.2 S/cm was achieved and using a four point ASTM measurement technique 12.0 S/cm was reported. These values represent 3% to 12% of the industry target.

Actual 16 cm^2 fuel cell plates were produced, fuel cell hardware constructed and assembled, and the power output was found to be 51% relative to graphite plates.

Thermoplastic bipolar plates for PEMFCs made of composite materials is promising, but optimum filler loading that balances all properties is still required in order to achieve conductivity targets. Nevertheless this study has demonstrated that conductive thermoplastic bipolar plates can be produced via injection molding.

Acknowledgements

I would like to acknowledge the support of my supervisor, collaborators, colleagues, and co-operative undergraduate students, which influenced this research. This research would not have been possible without the use of equipment from the University of Waterloo polymer research groups under Dr. Costas Tzoganakis and Dr. Leonardo Simon. Special thanks are extended to Dr. Michael Fowler, Sumit Kundu, and Matthew Stevens for their contributions.

Dedication

I would like to dedicate my thesis to my Parents and my Fiancé for all of their support and understanding throughout my education.

Table of Contents

List of Tables

List of Figures

Glossary

1:1:1	equal ratio of ACB, VCB, and CF
ACB	acetylene carbon black
ADL	Arthur D. Little
AFC	alkaline fuel cell
ANOVA	analysis of variance
CB	carbon black
CF	carbon fiber
CO	carbon monoxide
CO_2	carbon dioxide
CO_3^{2-}	carbonate ion
DTI	Direct Technologies Inc.
e^-	electron
EMF	electromotive force
EPDM	ethylene-propylene-norbornene
EVA	ethylene vinyl acetate
F	fluorine atom
GDL	gas diffusion layer
GF	graphite fiber
H	hydrogen atom
H^+	hydrogen ion
H_2	hydrogen gas
HDPE	high density polyethylene
H_2O	water
ICP	inherently conductive polymer
K	consistency factor (shear viscosity relationship)
m_i	mass of species i
MCFC	molten carbonate fuel cell
MEA	membrane electrode assembly
NO_x	nitrogen oxides
O	oxygen atom
O_2	oxygen gas
O^{2-}	oxygen ion
OCV	open circuit voltage
OH^-	hydroxide ion

P	percolation fraction
P_c	percolation threshold
P_{max}	percolation maximum
PA	polyaniline
PAFC	phosphoric acid fuel cell
PANI	polyaniline
PEM	polymer electrolyte membrane
PEMFC	polymer electrolyte membrane fuel cell
PET	polyethylene terephthalate
PFSA	perfluorinated sulfonic acid
PP	polypropylene
PPS	polyphenylene sulfide
PDVF	polyvinyldifluoride
PVE	polyvinyl ester
S	sulfur atom
SEM	scanning electron microscope
SO_x	sulfur oxides
SOFC	solid oxide fuel cell
TGA	thermal gravimetric analysis
USD	United States dollar
VCB	Vulcan carbon black
X_i	mass fraction of species i
Y_i	volume fraction of species i
ρ	density
η	shear viscosity
γ	shear rate

1 Introduction

This project's intention is to contribute to a solution for the current energy challenges that society faces. One proposed solution, which this research intends to development, is the Hydrogen Economy through polymer electrolyte membrane fuel cells (PEMFCs). One aspect of PEMFCs that need to be improved before an energy shift of such significance is financially viable is the development of PEMFC components that can stand up to the rigorous demands placed on the energy industry and potential applications such as automobiles. Traditional materials have proven to be cost prohibitive and other options have shown limitations such as reduced component durability or functionality. One important component of PEMFCs is the bipolar plates or flow plates, which have traditionally been made from graphite. Conductive composites as an alternative material have shown promise toward achieving this goal due to strong compatibility in a fuel cell environment and low cost / high volume manufacturing options. The research efforts of this project will investigate the feasibility of a specific conductive composite family to be used as bipolar plates in a PEMFC.

1.1 Energy Evolution

The evolution of the energy sector continues to be driven by society's need and desire to have a convenient energy supply for daily living, transportation, and commercial advancement. This trend is becoming more difficult to maintain and as suggested by many organizations around the globe, changes are required in the near future to regain control of the world's energy challenges. These problems include foreign energy dependence, declining energy supply, negative environmental impacts, and an increase in health problems.[1]

The primary contributor to these negative effects is fossil fuels, which is non-sustainable, non-renewable, and creates pollution when burned. The pollution is the result of emissions such as CO, CO_2, NOx, and SOx to name a few.[2]

Due to these concerns there has already been a significant shift in the design relationship from previous decades. In the past we have seen energy technology design be primarily driven by technology capabilities and customer desired performance. As a result the one directional relationship between design, emissions, and energy has only considered technology performance and not the impact it has on energy or environmental resources.

In recent years the mindset of organizations and society as a whole has shifted this relationship and we now see a much more different cycle where design, emissions, and energy are all interacting factors. Figure 1-1 shows the three factors in this more balanced approach.

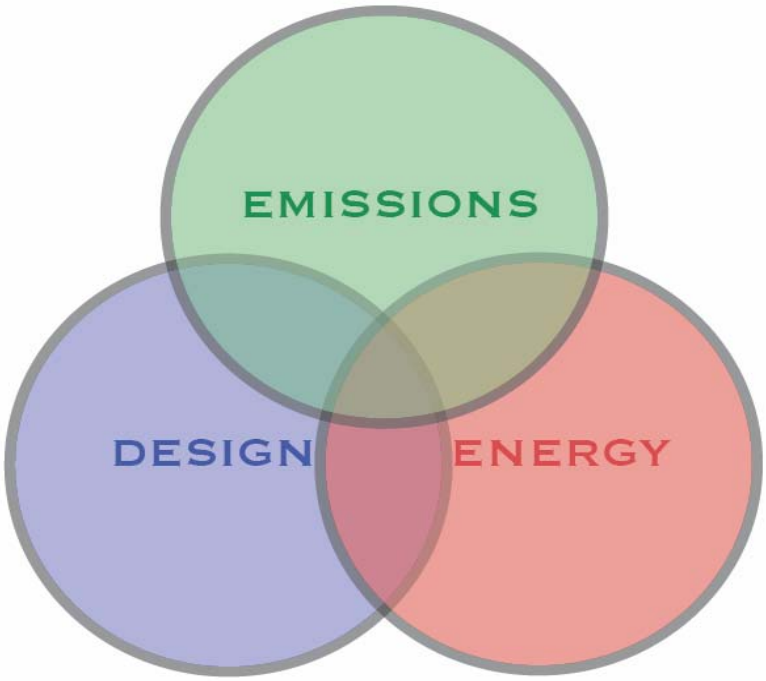

Figure 1-1 – Current Energy Design Relationship

It is necessary to maintain this balanced approach when addressing the problems which are being faced by the energy sector. New solutions to our future energy shortage, among other problems need to be found and a new design approach has evolved to incorporate a balance between energy, emissions, and design. Although many areas of the energy industry show promise for the coming years, for this discussion it is necessary to focus on one technology in this very large energy market.

1.2 Hydrogen Economy

One area of focus within the energy and transportation industries has been towards the hydrogen economy. When produced from renewable resources hydrogen is sustainable, renewable and has the potential to produce zero emissions, addressing many of the current concerns faced by the energy sector. There have been many interpretations of the hydrogen economy; the ideal 'utopist' interpretation limits hydrogen generation to ideal power sources such as wind and solar. However, the implementation of such an economy is not possible due to the limitations associated with capital cost and the inability to produce large amounts of energy using these methods.

The more realistic interpretation of a future energy economy that incorporates hydrogen is illustrated in Figure 1-2. In addition to all efforts which should focus on reducing energy consumption the introduction of the hydrogen economy incorporates many alternatives for the production, distribution, and conversion of hydrogen along with the use of direct electrical energy use.

This approach enables an increase in energy supply, ensures the continuation of energy independence, and reduces emissions, which works toward a decrease in pollution and health related concerns.

Figure 1-2 indicates a very complicated arrangement of energy vectors. The era where there exists one primary source of energy, as seen in the past and still in the present with fossil fuels, is coming to an end. Energy conversion technologies in future fuels such as hydrogen, bio-diesel, ethanol, and other renewables will be vastly diverse. One suggested conversion technology for either local energy distribution or transportation is fuel cell technology.

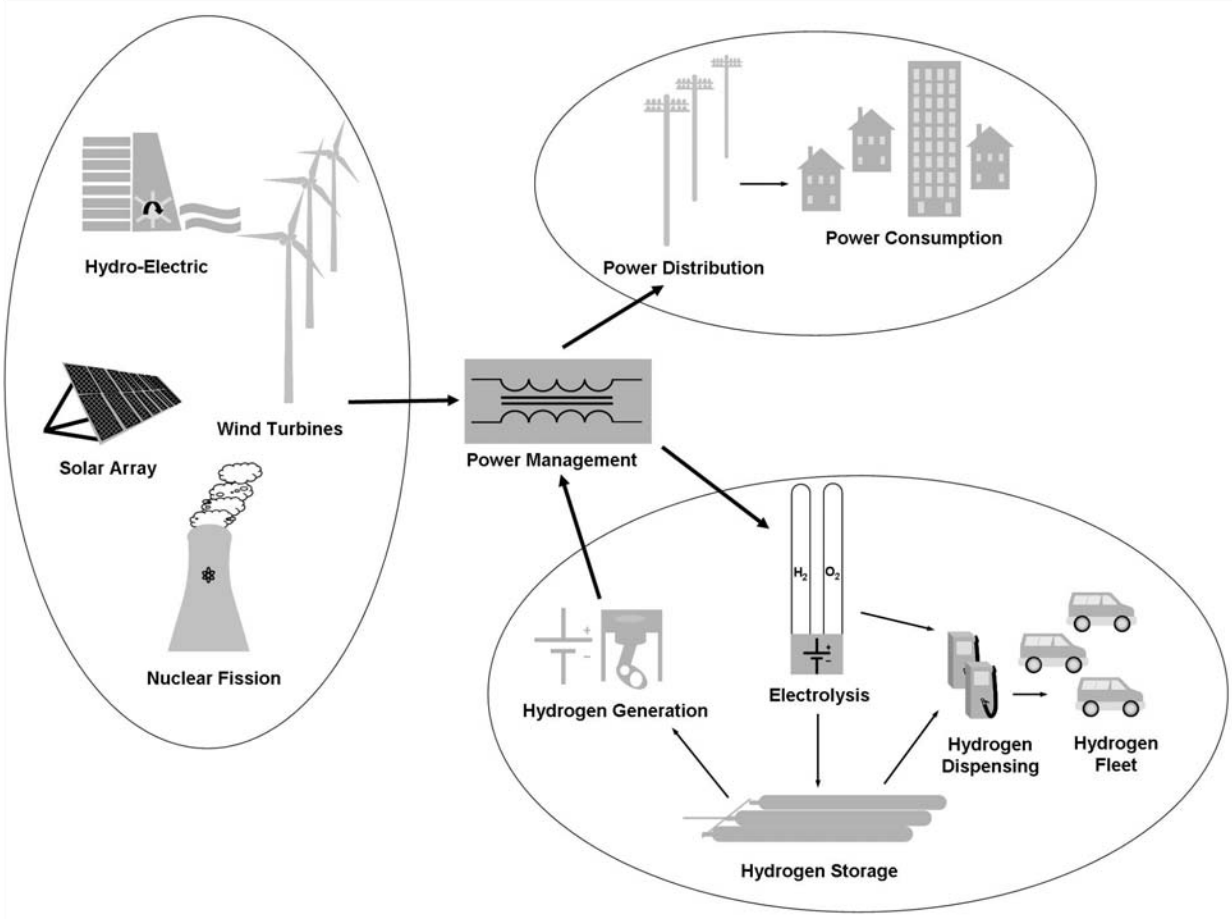

Figure 1-2 –Integrated Hydrogen Economy

1.3 Fuel Cells

Fuel cells are an electrochemical device similar to a battery that can convert chemical energy into electrical energy. The primary difference between a fuel cell and a battery is its ability to continually supply the reactants which partake in the half cell reactions. Therefore fuel cells are a continuous electrochemical device that can maintain the production of electricity provided both oxidant and fuel are supplied.

Figure 1-3 illustrates the transport of materials in a generalized fuel cell flow diagram. The fuel enters on one side, the oxidant on the other side and two half cell reactions transfer ions from one side to the other through an electrolyte. During this flow of mass, electrons travel externally from the fuel side (anode) to the oxidant side (cathode) to complete the reaction and create power through the load placed in the circuit.

Therefore the primary components of any fuel cell include:

- Fuel delivery system to anode;
- Electrolyte (ion conductor);
- Oxidant delivery system to the cathode;
- Depleted fuel, oxidant, and product gas removal systems, and
- External circuit with load.

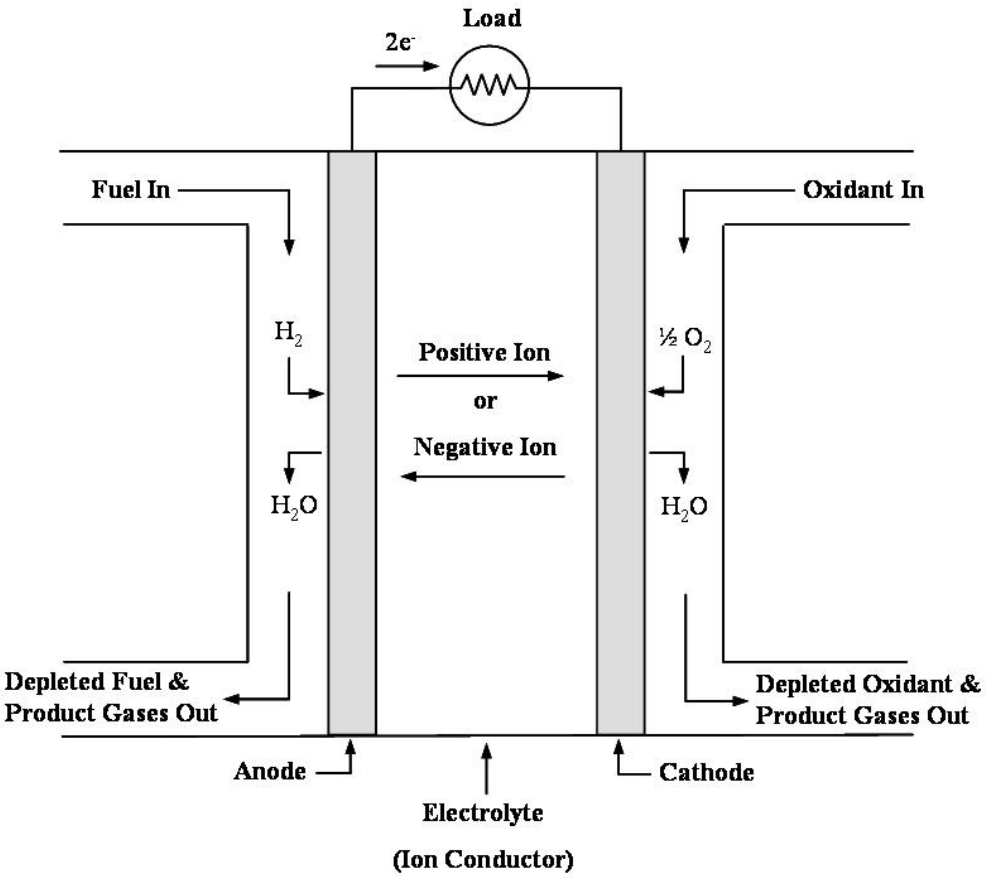

Figure 1-3 – Material Flow in a Fuel Cell [3]

These components are common to all types of fuel cells; however, there are many types of fuel cells each with there own independent set of half cell reactions. The various types of fuel cells include:

1 Proton Exchange Membrane Fuel Cell (PEMFC)
2 Alkaline Fuel Cell (AFC)
3 Phosphoric Acid Fuel Cell (PAFC)
4 Molten Carbonate Fuel Cell (MCFC)
5 Solid Oxide Fuel Cell (SOFC)

Some of the major differences in characteristics between each type of fuel cell are described in Table 1-1. The most influential characteristics with respect to potential applications include fuel cell operating temperature, half cell reactions, and size.

The low to mid temperature range fuel cells (<200^{o}C) are well suited for mobile applications such as transportation or portable electronics. They tend to be smaller and have high power densities; however, require a high purity fuel to be supplied. The higher temperature fuel cells (>600^{o}C) are better suited for stationary applications such as distributed power. These fuel cells tend to be much larger and have the ability to process fuels which have a variety of impurities. Table 1-2 shows a detailed summary of the half cell reactions for a range of fuel cell chemistries. Note that "Polymer Electrolyte Membrane" fuel cells are a specific type of "Proton Exchange Membrane" fuel cells. PEMFC in the following sections continues to refer to the former.

Table 1-1 – Types of Fuel Cells and Some Associated Properties [3]

	PEMFC	AFC	PAFC	MCFC	SOFC
Electrolyte	Ion Exchange Membrane	Potassium Hydroxide	Liquid Phosphoric Acid	Liquid Molten Carbonate	Ceramic
Operating Temperature	80^{o}C	65-220^{o}C	205^{o}C	650^{o}C	600-1000^{o}C
Charge Carrier	H^{+}	OH^{-}	H^{+}	CO_3^{2-}	O^{2-}
Prime Cell Components	Carbon-based	Carbon-based	Graphite-based	Stainless-based	Ceramic
Catalyst	Platinum	Platinum	Platinum	Nickel	Perovskites

Table 1-2 – Various Fuel Cell Chemistries [3]

Fuel Cell	Anode Reaction	Cathode Reaction
Proton Exchange Membrane and Phosphoric Acid	$H_2 \rightarrow 2H^+ + 2\ e^-$	$½\ O_2 + 2H^+ + 2e^- \rightarrow H_2O$
Alkaline	$H_2 + 2\ OH^- \rightarrow 2H_2O + 2\ e^-$	$½\ O_2 + H_2O + 2e^- \rightarrow 2OH^-$
Molten Carbonate	$H_2 + CO_3^{2-} \rightarrow H_2O + CO_2 + 2\ e^-$ $CO + CO_3^{2-} \rightarrow 2CO_2 + 2\ e^-$	$½\ O_2 + CO_2 + 2e^- \rightarrow CO_3^{2-}$
Solid Oxide	$H_2 + O^{2-} \rightarrow H_2O + CO_2 + 2\ e^-$ $CO + O^{2-} \rightarrow CO_2 + 2\ e^-$ $CH_4 + 4O^{2-} \rightarrow 2H_2O + CO_2 + 8\ e^-$	$½\ O_2 + 2e^- \rightarrow O^{2-}$

CO – carbon monoxide	e^- – electron	H_2O – water
CO_2 – carbon dioxide	H^+ – hydrogen ion	O_2 – oxygen
CO_3^{2-} – carbonate ion	H_2 – hydrogen	OH^- – hydroxyl ion

The quality and functionality of fuel cells and their components can be reported in many ways such as conductivity, mechanical strength, permeability, reliability, durability, and power output. Ultimately the key metric of the entire system is the continuous power output which can be converted to useful energy. Power is often presented in graphical form as a relationship between voltage and current density. This relationship when plotted is referred to as a polarization curve.

The various aspects of a polarization curve are illustrated in Figure 1-4. The plotted curve relates the cell voltage to a changing current density. The maximum cell voltage, which occurs when the current density is zero, is referred to as the open circuit voltage (OCV). In electrochemical systems the voltage decreases as the current density increases and can be divided into three general areas: activation polarization; ohmic polarization; and concentration polarization. It is important to note that the ohmic polarization leads to ohmic losses, which are largely due to the conductivity of the fuel cell components, specifically the conductivity of the bipolar plate materials.

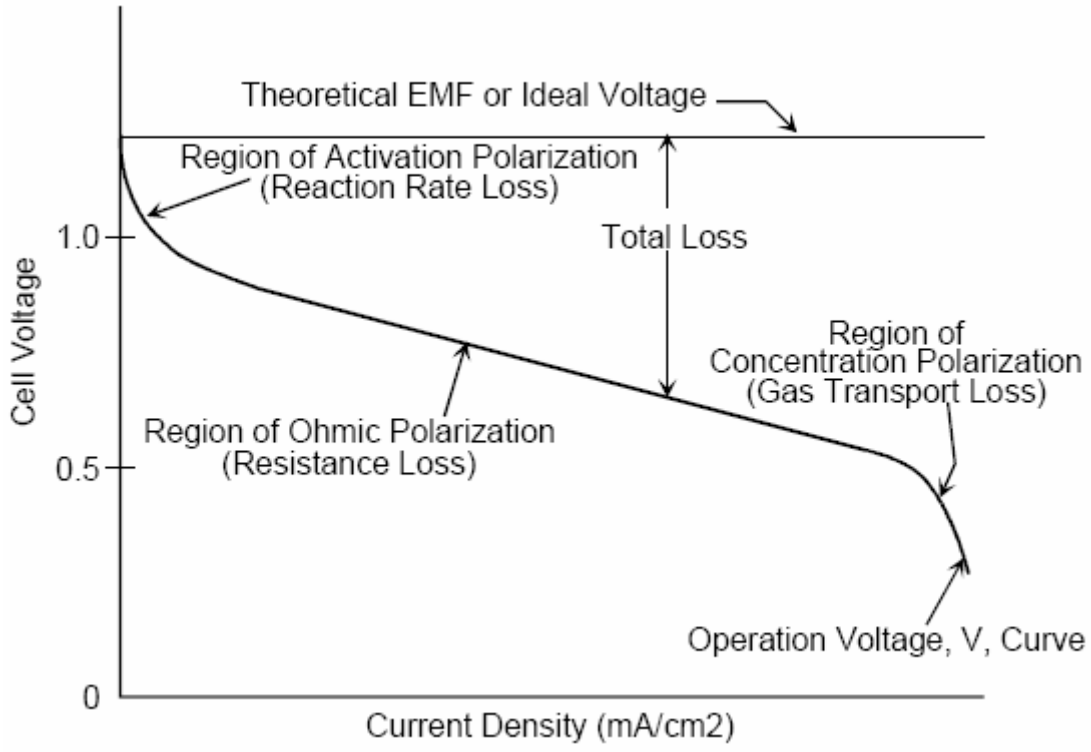

Figure 1-4 – Fuel Cell Polarization Curve [3]

The research presented will focus on only one type of fuel cell, hydrogen polymer electrolyte membrane fuel cells. Any reference to fuel cells here after will refer directly to PEMFCs.

1.4 Polymer Electrolyte Membrane Fuel Cells

PEMFCs are unique in that their electrolyte consists of a layer of solid polymer which, when hydrated, allows protons to be transmitted from one face to the other. This is the most promising technology for transportation applications. The inputs to the system are humidified hydrogen and oxygen (or air) and the outputs are electrons, water and heat. The operating temperature is much lower than other fuel cells because of the limitations of both the thermal properties and hydration requirement imposed by the membrane (above 100°C the water will not be a liquid at atmospheric pressure).

The basic operation of a PEMFC involves a hydrogen-rich fuel stream that flows across the porous anode electrode where the following half-cell reaction occurs:

$$H_2 \rightarrow 2H^+ + 2e^- \qquad \textbf{Equation 1-1}$$

The released electrons flow through an external circuit traveling to the cathode. Parallel to the electron flow, the proton, solvated in water, diffuses through the membrane to the cathode. An oxidant, usually air, oxygen or helium/oxygen, flows across the cathode and combines with the protons and electrons. The following is the half-cell reaction that occurs at the cathode.

$$\tfrac{1}{2} O_2 + 2H^+ + 2e^- \rightarrow H_2O \qquad \textbf{Equation 1-2}$$

Combining both half cell reactions gives the net reaction:

$$H_2 + \tfrac{1}{2} O_2 \rightarrow H_2O \qquad \textbf{Equation 1-3}$$

Illustrating all the specific components which facilitate the reaction in a PEMFC are Figure 1-5 and Figure 1-6.

The heart of the PEMFC and the location of all the half cell reactions is referred to as the membrane electrode assembly (MEA). The MEA consists of a polymer electrolyte membrane, and two catalyst layers. Within a fuel cell stack MEAs are compressed between two gas diffusion layers (GDL), two bipolar plates and are held together by the balance of hardware.

Therefore the key components of a PEMFC are:

1. Polymer electrolyte membrane;
2. Catalyst layers;
3. Gas diffusion layers;
4. Bipolar plates; and,
5. Balance of hardware (current collectors, gaskets, and endplates).

Previously mentioned, the fuel (hydrogen) and oxidant (air) flow into the fuel cell at opposite sides traveling through holes or manifolding in the endplates, current collectors, and gaskets into the bipolar plates. The gases then travel throughout the flow path within the plates distributing the gases across the entire cross-section of the active area.

Further dispersion occurs as reactants travel through the gas diffusion layer towards the catalyst layers on either side of the membrane where the reactions can proceed.

The following sections will further discuss the operation of each component of the fuel cell once the hydrogen has arrived at the anode catalyst layer and the oxygen (or air) has traveled to the cathode catalyst layer.

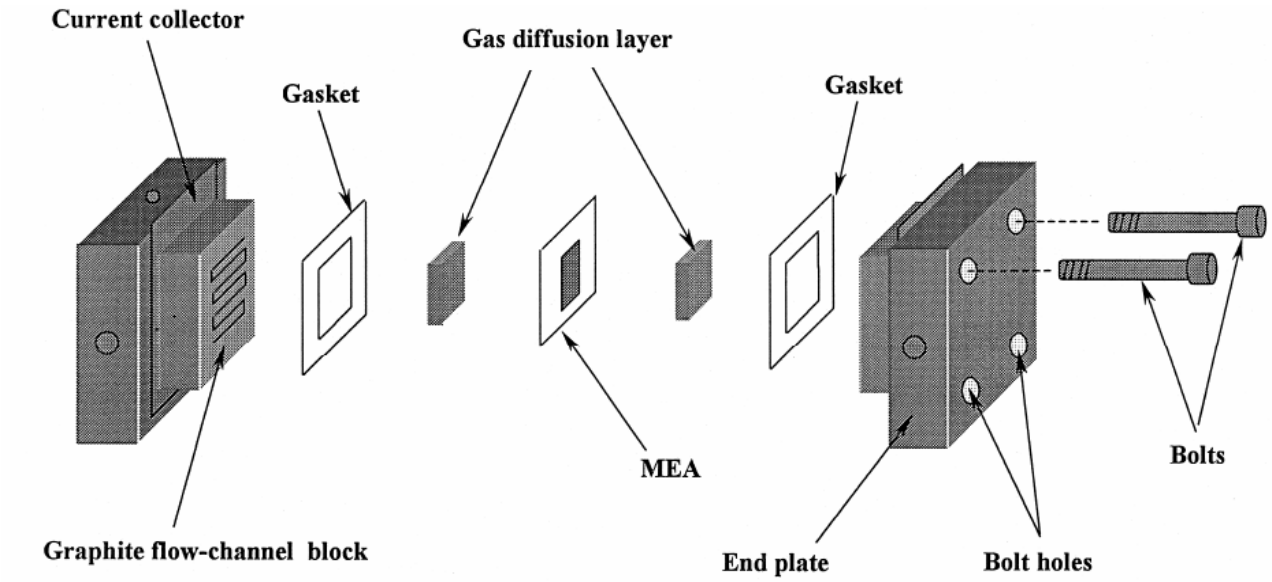

Figure 1-5 – Basic Schematic of a PEMFC [4]

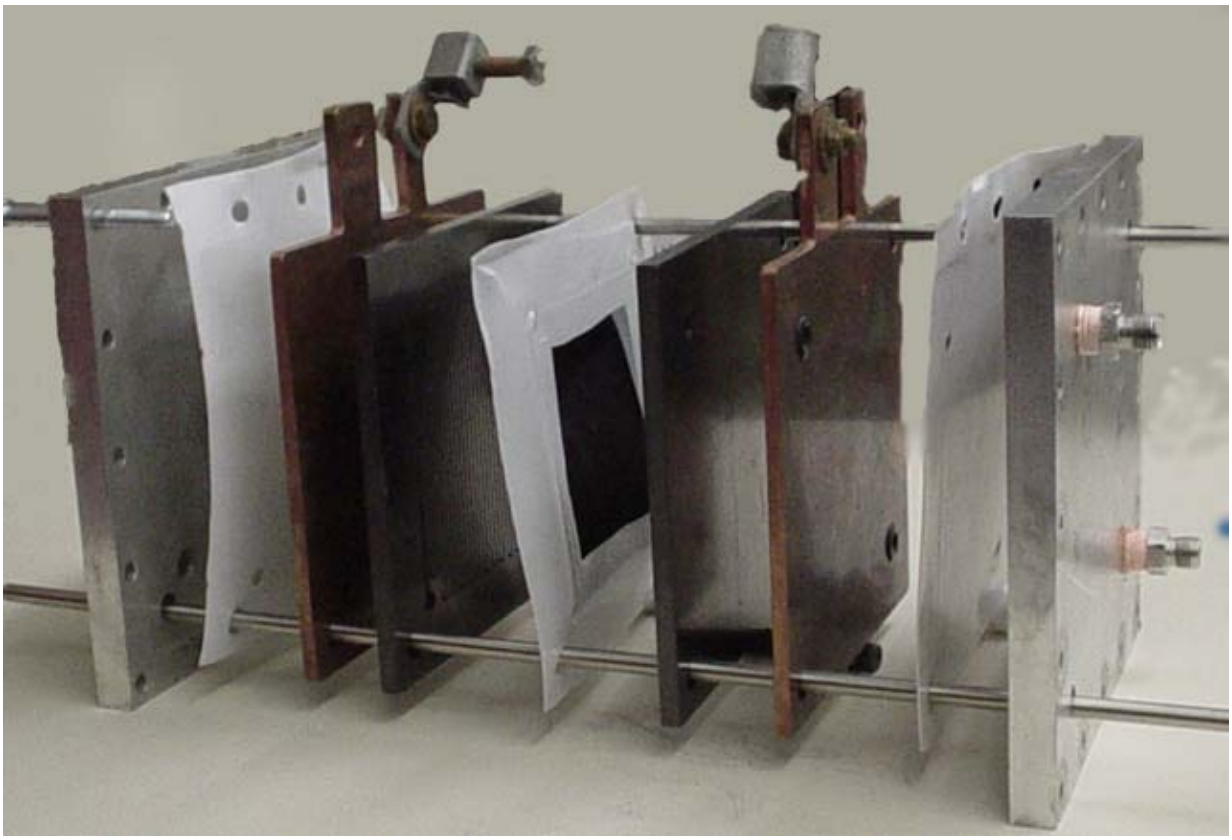

Figure 1-6 – Photograph of a PEMFC Constructed at University of Waterloo (retired cell)

1.4.1 Polymer Electrolyte Membrane

The polymer electrolyte membrane (PEM) enables the transportation of protons from the anode to the cathode catalyst layers, completing each half cell reaction. The PEM is the most specialized component in the fuel cell as it is not permeable by either fuel or oxidant gases, nor is it electrically conductive.

The membrane used in PEMFCs is almost exclusively sulphonated polytetrafluroethylene (PFSA) to date. This PFSA derivative is marketed under the trade name Nafion^{TM}, a patented product of DuPont which consists of a polytetrafluroethylene backbone with sulphonic functional groups through out the structure. The chemical formula is shown as Equation 1-4.

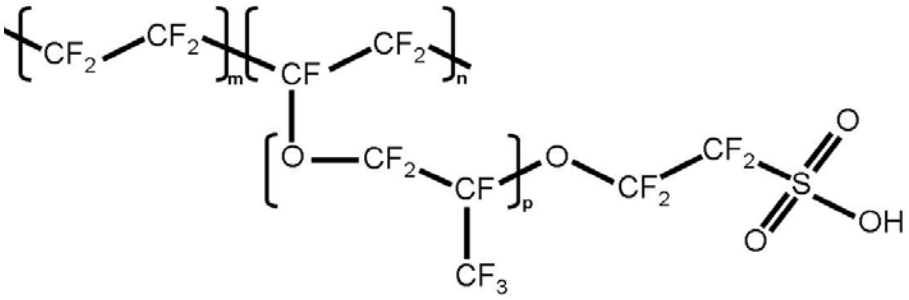

$$[CF_2CF(CF_2CF_2)_n]_m - [OCF_2CFCF_3]_p - OCF_2CF_2SO_3H \qquad \textbf{Equation 1-4}$$

Figure 1-7 is a scanning electron micrograph of a complete MEA with the gas diffusion layer. The center grey layer, surrounded by the two white catalyst layers is the PEM (the woven cloth on the outside is a carbon cloth gas diffusion layer).

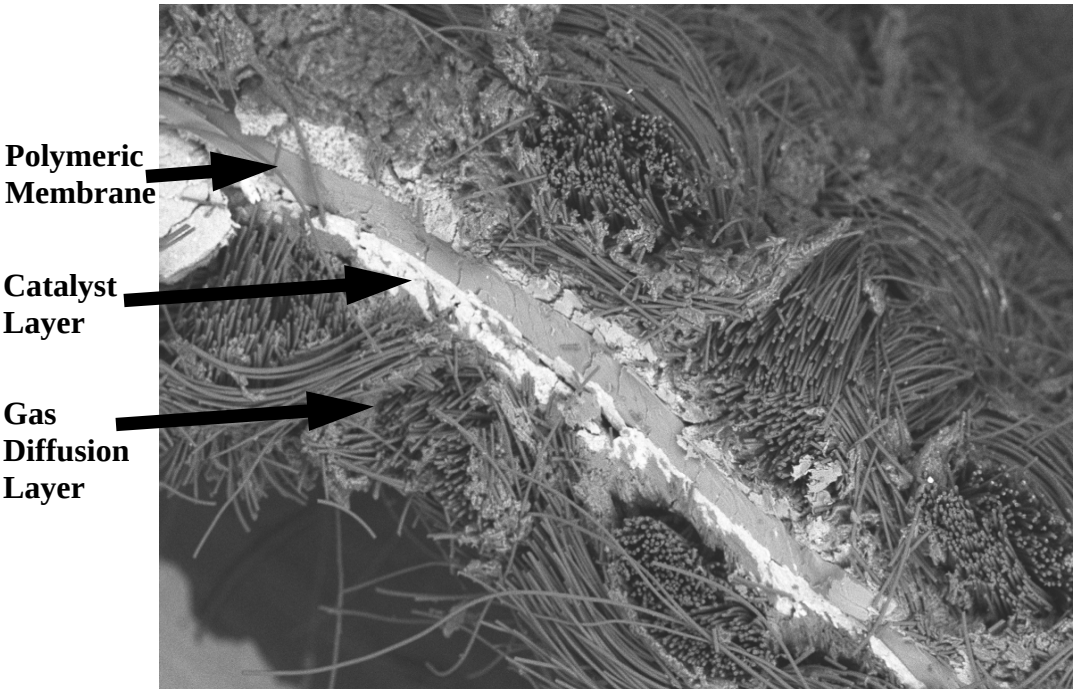

Figure 1-7 – PEMFC MEA Image Using a Scanning Electron Microscope

1.4.2 Catalyst Layers

The catalyst layers facilitate the two half cell reactions described in Equation 1-1 and Equation 1-2 and are the points of interaction between the membrane and the gas diffusion

layer. It is at this 'triple point', the membrane, the catalyst, and the gas diffusion layer that each half cell reaction takes place.

Table 1-1 indicated the use of a platinum based catalyst for the PEMFC. The catalyst has a carbon support and is held together by an ionomer. A representation of the catalyst layer structure is shown in Figure 1-8.

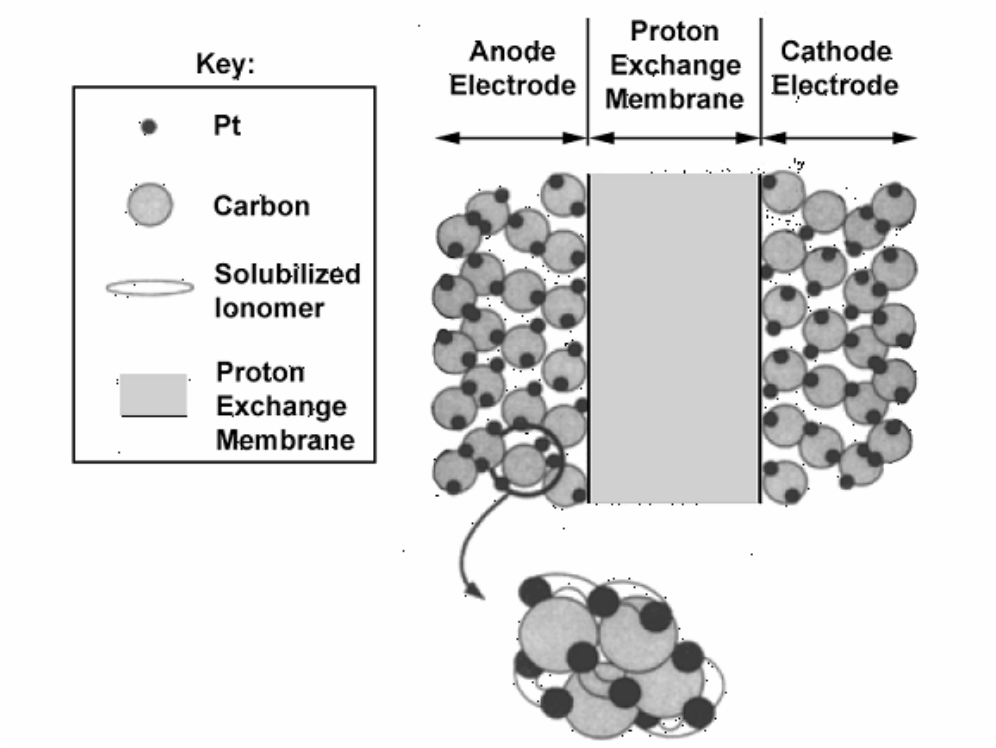

Figure 1-8 – PEMFC Catalyst Layer Structure [5]

1.4.3 Gas Diffusion Layers

The last component of the MEA and an important part of the triple point is the gas diffusion layer (GDL). The GDL further distributes the gases as they flow from the bipolar plates over the entire active area of the catalyst layer. In addition to distributing the gases the anode GDL also conducts the electrons away from the anode, back to the anode bipolar plate and current collector. At the same time the cathode GDL conducts the electrons to the cathode

catalyst layer from the cathode bipolar plate and current collector ensuring the complete flow of electrons as shown in Figure 1-3.

The gas diffusion layer is typically made from carbon paper or carbon fabric which promotes the flow of reactants, products, and electrons. Some GDL materials may also have an ionomer to ensure a more robust product. An example of the GDL layers was shown in Figure 1-7.

1.4.4 Bipolar Plates

The MEA is the heart of the fuel cell; however, the components surrounding the MEA must be compatible with the MEA and ensure the reactants, products, electrons, and heat flow in and out of the fuel cell. The bipolar plates direct the fuel and oxidant gases towards each GDL / catalyst layer and facilitate the flow of electrons from the anode to the cathode. Since the bipolar plates are the focus of this research it is important to define the relevant properties.

There are a number of properties that must be considered for bipolar plates. These characteristics ensure fuel cell functionality and in order of importance are:

1. Electrical conductivity;
2. Mechanical strength and durability;
3. Chemically inert;
4. Thermal conductivity; and
5. Low permeability.

Other characteristics that are equally important for the ability to use fuel cells in an application in order of importance are:

1. Low cost;
2. Ability to mass manufacture; and
3. Low density.

Though all of these characteristics need to be considered, as opposed to most previous work, this research will focus on economically viable materials for fuel cell commercialization. As a result the second group of characteristics will take precedence. Much of the research to date (as will be outlined later) has focused on improving conductivity and chemical inertness.

1.4.5 Balance of Hardware

The balance of the hardware includes the current collectors, gaskets, and endplates. The current collectors complete the electrical circuit moving electrons from inside the fuel cell to the adjoining external electrical circuit. Gaskets are required between the various components to ensure the fuel cell is completely sealed when compressed together. The endplates are the most external plates on either side of the fuel cell enabling the ability to seal in the gases by clamping the cell together, providing mechanical strength and rigidity for fuel cell operation.

1.5 Objective

The objective of this research work is to build on the energy-emissions-design relationship through the hydrogen economy by making fuel cells more viable due to improved bipolar plates. Specifically with respect to PEMFCs the objective is to

Design, prototype, and test commercially viable bipolar plate materials.

This will be achieved by combining commodity thermoplastics and carbon-based fillers.

1.6 Motivation

Fuel cells have the potential to significantly impact the energy and transportation industries. In order to facilitate this commercial implementation all the respective components must be optimized, including bipolar plates. The bipolar plate contribution to fuel cell cost has been expressed in a number of developed models; two such models include work from Direct Technologies Inc. (DTI) and Arthur D. Little (ADL). Figure 1-9 illustrates these models with the bipolar plate contribution ranging from 15-29% of the total fuel cell cost. Figure 1-10

indicates that more than 80% of fuel cell weight is attributed to the bipolar plates. Both weight and cost could be significantly improved with the use of alternative materials such as composites. It is hoped that this work will help bring about lighter, less expensive fuel cells making them more commercially viable.

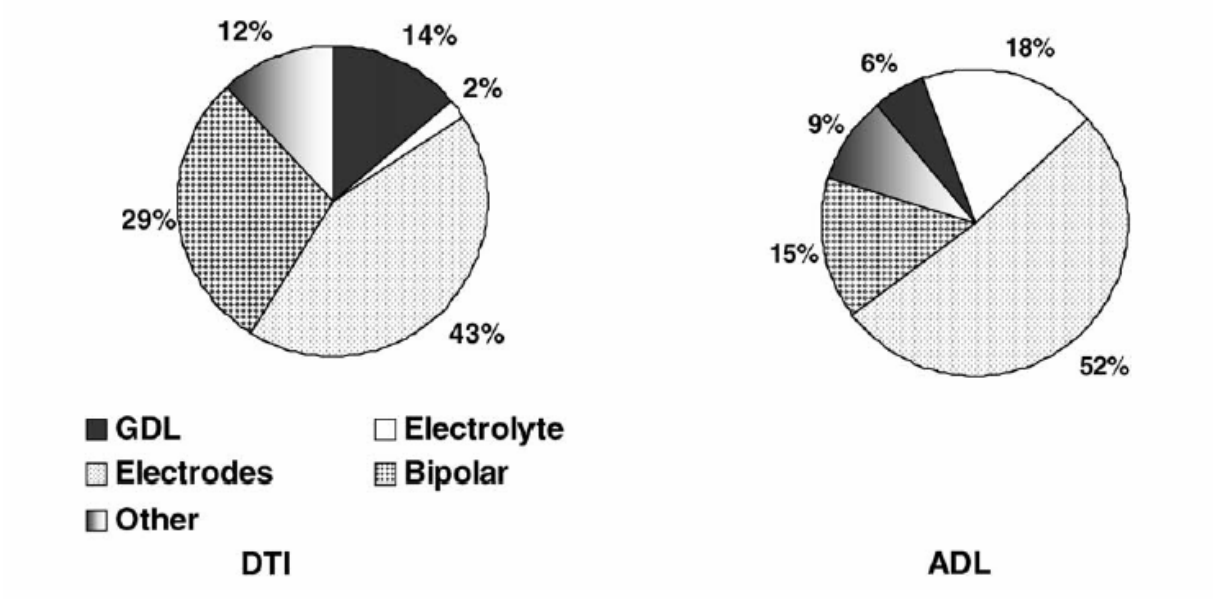

Figure 1-9 – Analysis of Fuel Cell Cost by Component [6]

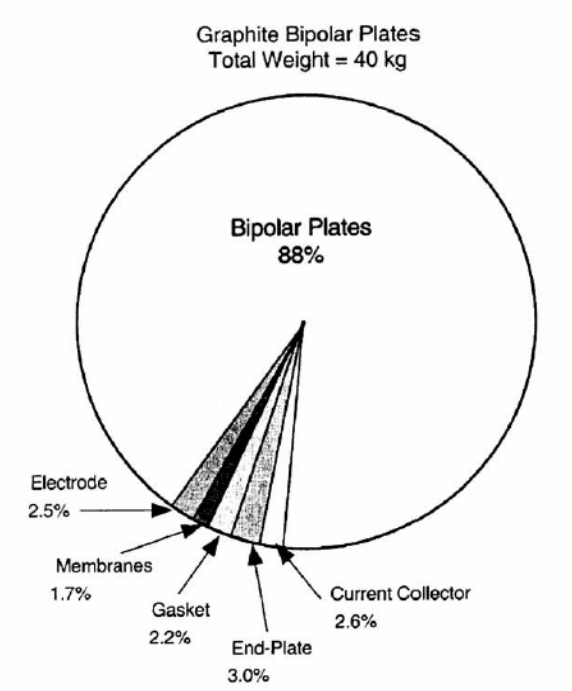

Figure 1-10 – Analysis of Fuel Cell Weight by Component [7]

2 Theory and Literature Review

As eluded to before, the focus of this research is on material selection and manufacturing of bipolar plates for Polymer Electrolyte Membrane Fuel Cells. In the initial stages of the project two functional properties were used to measure the results: electrical conductivity; and mechanical performance. In order to analyze the conductivity and mechanical properties thoroughly the relevant concepts must be understood, the discussion of these concepts will follow.

In addition to these two functional characteristics the three important characteristics necessary for commercial viability include the ease of mass manufacturing, a low material density and low cost. For composite systems these properties will be verified using rheology analysis, density measurements, and financial estimations.

Specific to composites, conductivity is described using percolation theory. The development of percolation concepts will be presented along with a review of literature with respect to bipolar plate material properties. This review includes electrical conductivity, mechanical properties, rheology (composites only), density, and cost estimations.

2.1 Electrical Conductivity and Percolation Theory

Electrical conductivity is a chemical property indicating a material's ability to allow the flow of electrons through itself. The path of travel may consider flow across the surface (surface or in-plane conductivity S/m), through a cross section (transverse or through-plane conductivity S/m^2), or both (volumetric conductivity S/m). The measurement of volumetric conductivity is used for material testing associated with this project. For the remainder of the report the terms 'volumetric conductivity' and 'conductivity' are used synonymously.

Typical values for material conductivity are 10^{-15} to 10^{-12} for polymers, 10^4 for carbon black, 10^6 for carbon fiber, and 10^7 to 10^8 for metals such as aluminum and copper (all values in S/m). [8T] The inverse of volumetric conductivity (S/m) is volumetric resistivity (Ω-m). Either method of reporting measurements is acceptable and easily comparable, however it is

important to use standardized measuring techniques when measuring and comparing material properties. Specific procedures will be discussed in Chapter 3.

Important theory for understanding conductivity within composite materials, especially where the polymer matrix and the filler(s) have very different characteristics, is the concept of percolation. A simple definition of percolation is to 'pass through'. The notion of percolation theory is to quantitatively analyze the ease of movement of a species through a medium or matrix. In this case the species are electrons and the matrix is a composite thermoplastic.

The development of percolation theory is illustrated in Figure 2-1. The sites occupied by filler are denoted © and the empty sites represent a polymer occupied site. The first step (a) shows the composite before the percolation threshold is reached. There is no available path (along the filler sites) that could transport the flow of electrons.

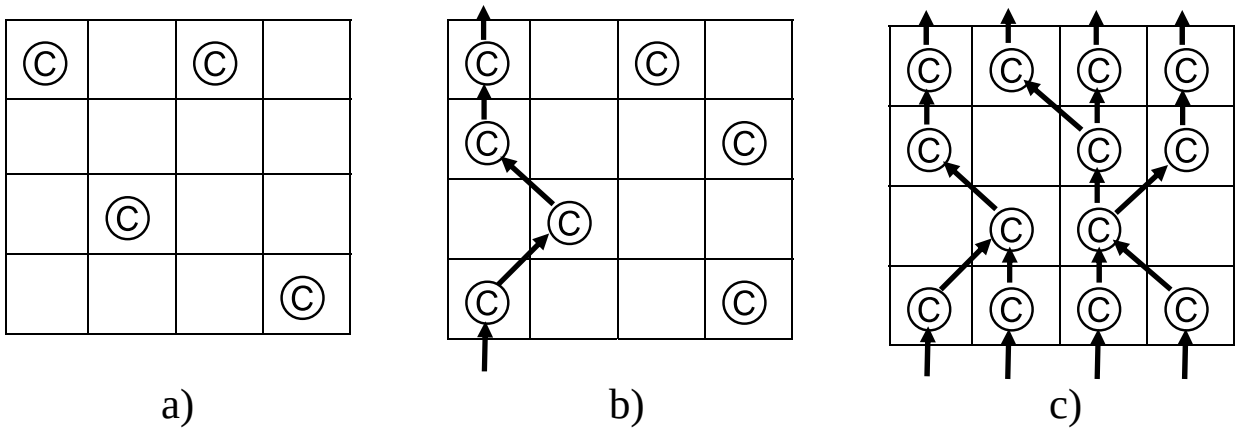

Figure 2-1 -Percolation Theory Development

At this stage the conductivity will closely resemble that of the virgin polymer matrix. In the second step (b) the composite just reaches the percolation threshold. This is the point at which the first available path through the filler is made for the transport of electrons. A path is indicated by successive arrows from the bottom to the top of the matrix. The third and final step (c) shows the maximum percolation value. Any further addition of filler will not significantly increase the ease of electron flow since any electron entering the system already

has the shortest available path to reach the other side. At this point the conductivity will resemble that of the filler.

Figure 2-2 shows a pictorial of percolation theory with respect to conductivity. Relative conductivity refers to the conductivity of the composite in comparison to the conductivity of the pure filler. Percolation, as described above, is a measure of the number of composite sites which are filler occupied with respect to the total number of available sites. At a value of P equal to zero no path exists for electron transport, when P is equal to unity there are an infinite amount of paths for the electrons to flow; all of the cells are occupied by filler. The point at which the addition of more filler does not increase the ease of electron movement is labeled P_{max}. The addition of more filler will not enhance the conductivity to any significant degree. [9]

At a relative conductivity of 1, the composite would have the same conductivity as the pure filler. Theoretically the composite can only approach this value asymptotically, since when relative conductivity reaches 1 the percolation would reach a value of 1 and the sample would have reached 100% filler (no polymer matrix).

The graphical shape expressed in Figure 2-2 could take many variations depending on the specific system. An experimental relationship reported in literature is shown in Figure 2-3, which displays volume fraction on the x-axis instead of percolation. It should be noted that volume fraction is directly proportional to percolation and the section from P_c to P_{max} is the area of importance for future research opportunities.

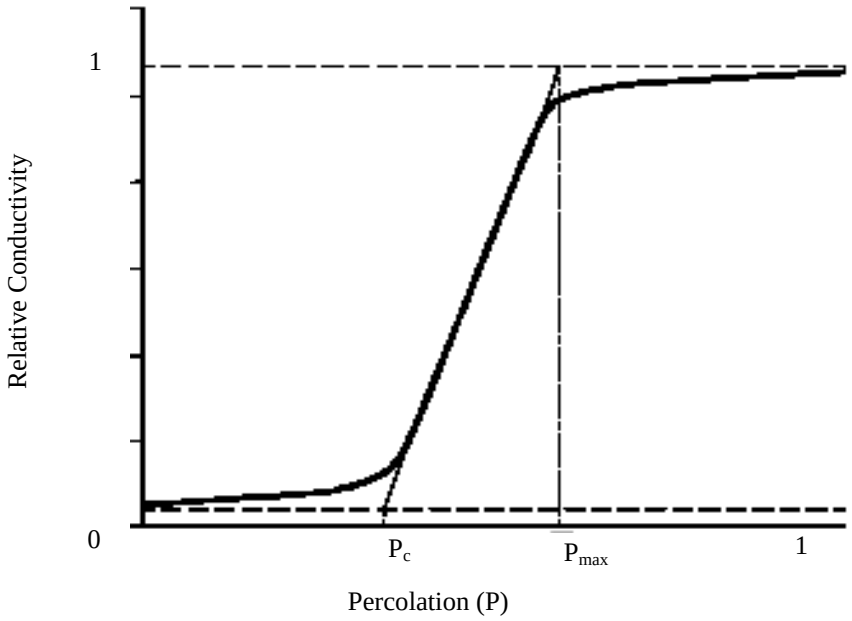

Figure 2-2 - Percolation S-Curve

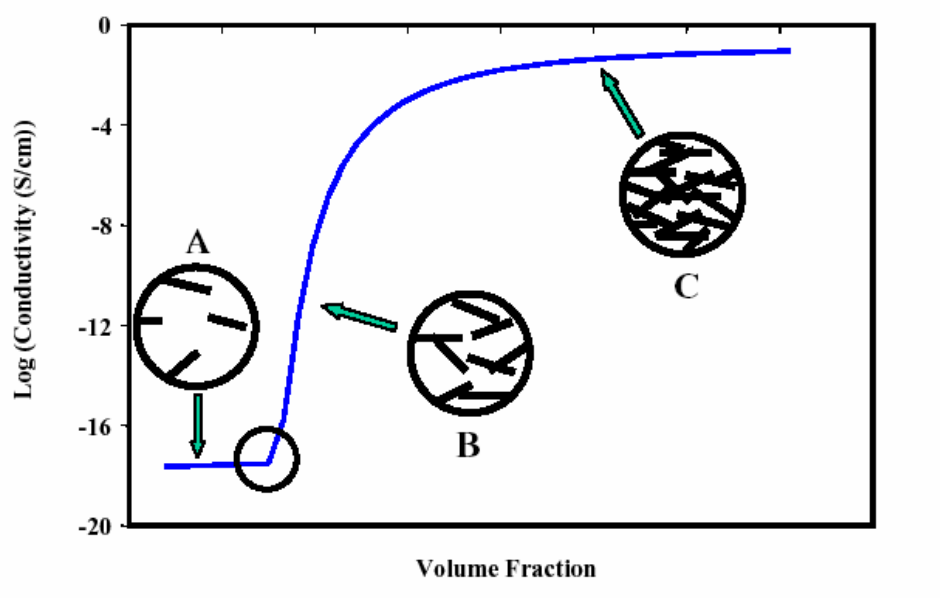

Figure 2-3 – Literature Results for Percolation S-Curve [10]

2.2 Literature Review

There has been a significant degree of work with respect to both conductive composites and PEMFC bipolar plate material development; however, an effective low cost solution has not been achieved. Since it is important to understand the characteristics for bipolar plate material selection a macroscopic review of the general design criteria for bipolar plates was presented by Cooper, shown in Table 2-1. Focusing on material properties only (not flow path etc.) the specific properties of importance can be summarized in four categories. These categories include chemical/physical properties, mechanical properties, manufacturing properties, and environmental impact. The current research focused on the first three categories.

Table 2-1 – Macroscopic Review of Bipolar Plate Design Criteria [11]

Category	Requirements
Stack performance related design criteria	Electrical resistance is minimized/conductivity is maximized
	Thermal resistance is minimized/conductivity is maximized
	Allows distribution of the fuel, oxidant, residual gases, and water without leaks
	Withstand mechanical loads during operation
	Resistant to corrosion/passivation in contact with an acidic electrolyte, oxygen, heat, and humidity
	Minimizes differences in the coefficient of thermal expansion between metal plates and any coatings
System performance related design criteria	Mass/kW is minimized (plates should be light weight)
	Volume/kW is minimized (plates should be slim)
	Stacks must operate in freeze and cold conditions
	The design life is maximized
Manufacturing related design criteria	The stack is inexpensive to manufacture (materials, fabrication including machine tools, assembly, etc.)
	Plate designs should call for manufacturing processes with high yields relative to mass production
	Length/width should be system defined (flexible cross section)
	The plate surface finish requirements are minimized to increase manufacturing options
	Plate tolerances should be maximized to increase manufacturing options
Environmental impact related design criteria	Plate materials are recyclable at vehicle service, following a vehicle accident, or when the vehicle is retired
	Plates are made of recycled materials

Table 2-2 illustrates these properties along with suggested targets, primarily from two literature compilations. Targets for conductivity and mechanical properties are important in addition to mass manufacture capabilities, low density and low cost.

Table 2-2 – Applicable Bipolar Plate Material Properties and Suggested Targets

PROPERTY	TARGET	UNITS	REFERENCE
Chemical/Physical Properties			
Electrical Conductivity	<100	Ohm-cm	[12]
	>100	S/cm	[13]
Thermal Conductivity	>10	W/m-K	[12]
	>10	W/m-K	[13]
Chemical Stability (Corrosion)	<16	$\mu A/cm^2$	[13]
Density	<5	g/cm^3	[13]
Gas Permeability (H_2)	$>2x10^{-16}$	$cm^3/(cm^2\text{-}s)$	[13]
Water Absorption	>0.3	%	[12]
Mechanical Properties			
Flexural Strength	>500	Kg_f/cm^2	[12]
	>59	MPa	[13]
Tensile Strength	>41	MPa	[13]
Impact Strength	>40.5	J/m	[13]
Crush Strength	>4200	kPa	[13]
Manufacturing Properties			
Rapid Processability (Ease of Manufacturing)	High Volume		
Low Cost	<10	$/plate	[14]
	<0.0045	$/cm^2$	[15]
Rheology (Composites)	Not Available	Not Available	

The bipolar plate material options can be categorized into three groups which include non-porous graphite, coated metals, and composite plates. Mehta et al. has described materials which have been used or proposed to manufacture bipolar plates.[15] These materials have all shown promise, however, the early performance success of using graphite plates has set it

as the standard for comparing new material development. A detailed list of materials is shown in Figure 2-4.

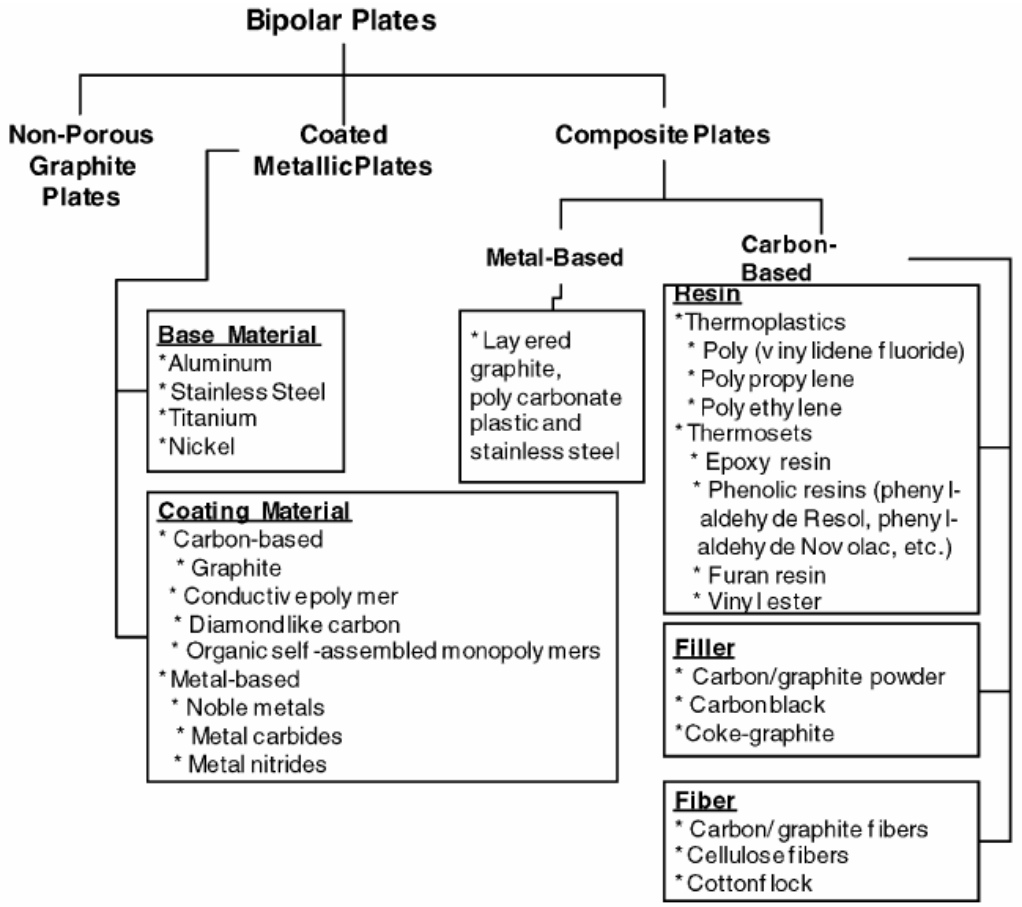

Figure 2-4 – Summary of Bipolar Plate Materials [15]

The manufacturing of the bipolar plate materials described in Figure 2-4 was also presented by Mehta et al. within the same three categories. All the processes are illustrated in Figure 2-5, with the standard being the graphite material manufacturing process. This approach is very expensive and time consuming as the flow path must be machined for each plate. The cost contributed from this process is one of the largest motivations to develop new materials and manufacturing techniques.

2.2.1 Non-Porous Graphite

Bipolar plates have traditionally been made from non-porous graphite and machined to exhibit an appropriate flow path for both anode (hydrogen) and cathode (oxidant) gases.

Graphite was a natural selection due to its high electrical conductivity and chemical inertness. The disadvantage of this material for bipolar plates is the high cost of machining the flow path and the brittleness exhibited. These properties make mass manufacturing difficult due to the mechanical properties and the cost associated with this technique.

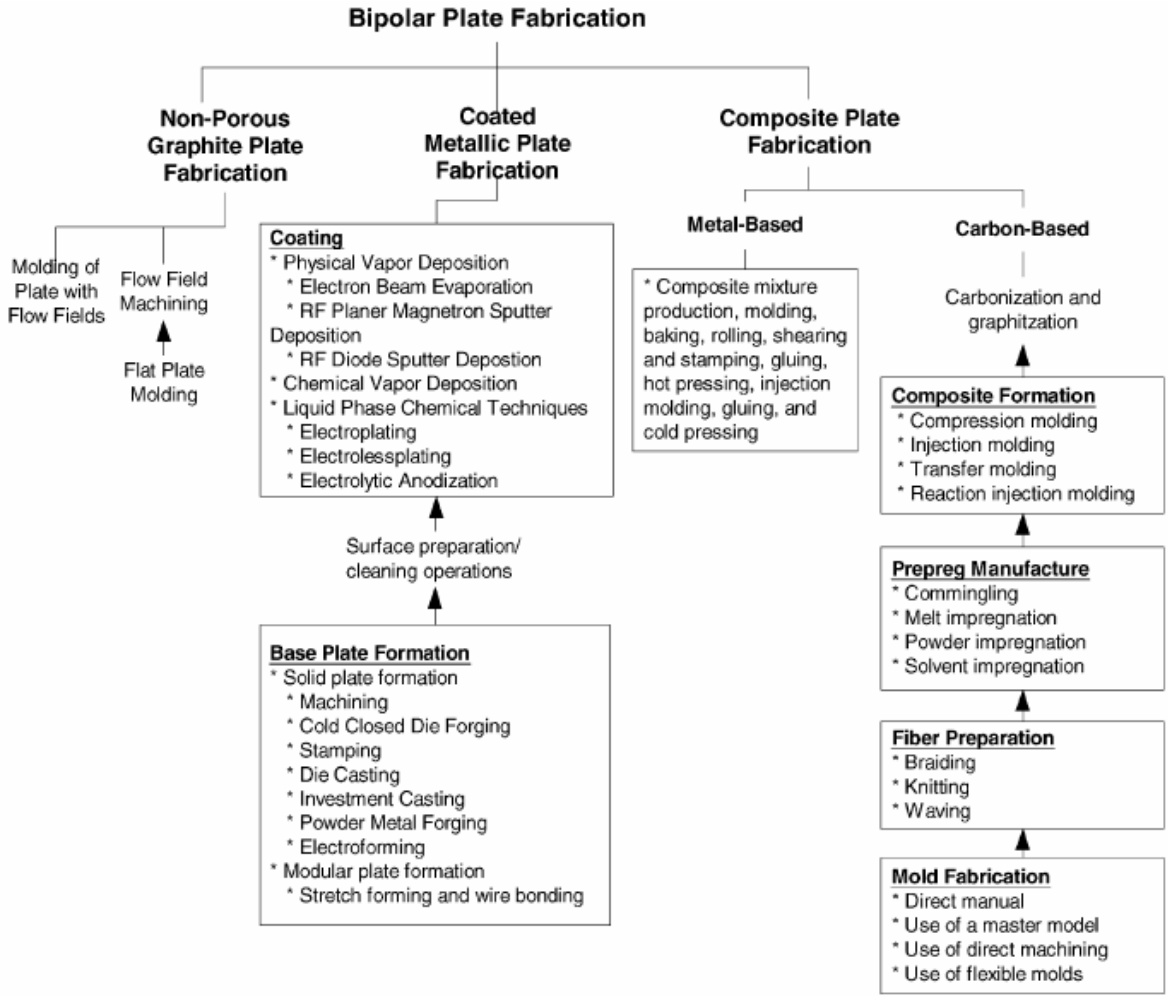

Figure 2-5 – Bipolar Plate Material Manufacturing Techniques [15]

2.2.2 Coated Metals

Metals would naturally be a candidate for bipolar plates due to the very high electrical conductivity they possess. However, leaching of metal ions in a fuel cell environment would lead to membrane contamination and eventually failure, therefore the use of special coatings are used in conjunction with metals to reduce this phenomenon. Table 2-3 summarizes the

materials that have been previously investigated along with some advantages and disadvantages of using coated metals for bipolar plates. [15,16,17,18,19,20, 21,22,23,24,25]

Stainless steel has been the most sought after metal due to its low cost and beneficial properties such as conductivity, strength, and chemical inertness (as compared to other metals). Hentall et al. investigated stainless steel with a gold coating and compared fuel cell results with and without the gold coating to graphite. The performance results of this work are illustrated in Figure 2-6. Using a coating such as gold delivers results which compare very closely to graphite plates, the conventional industry standard. The associated problem with gold coated stainless steel plates or any coated metal for that mater is that metals, even "inert" metals can eventually lead to membrane contamination and fuel cell loss of performance over time. In addition to this, the coatings and metals themselves can be cost prohibitive especially depending on the mode of manufacturing. In order to overcome some of these concerns various materials and coatings have been investigated with different processing approaches.

Table 2-3 – Summary of Metals and Coatings for PEMFCs

Metals	Coatings	Advantages	Disadvantages
Stainless steel	Gold	High Conductivity	High Coating Cost
Stainless Steel Foam	Titanium	Low Material Cost	Membrane Contamination
Titanium	Polymer	Low Volume	High Mass
Aluminum	Graphite	High Strength	
Gold	Silicon Carbide		
Nickel	Nitride Alloys		
Nickel Foam	Carbide Alloys		
Iron Alloys			

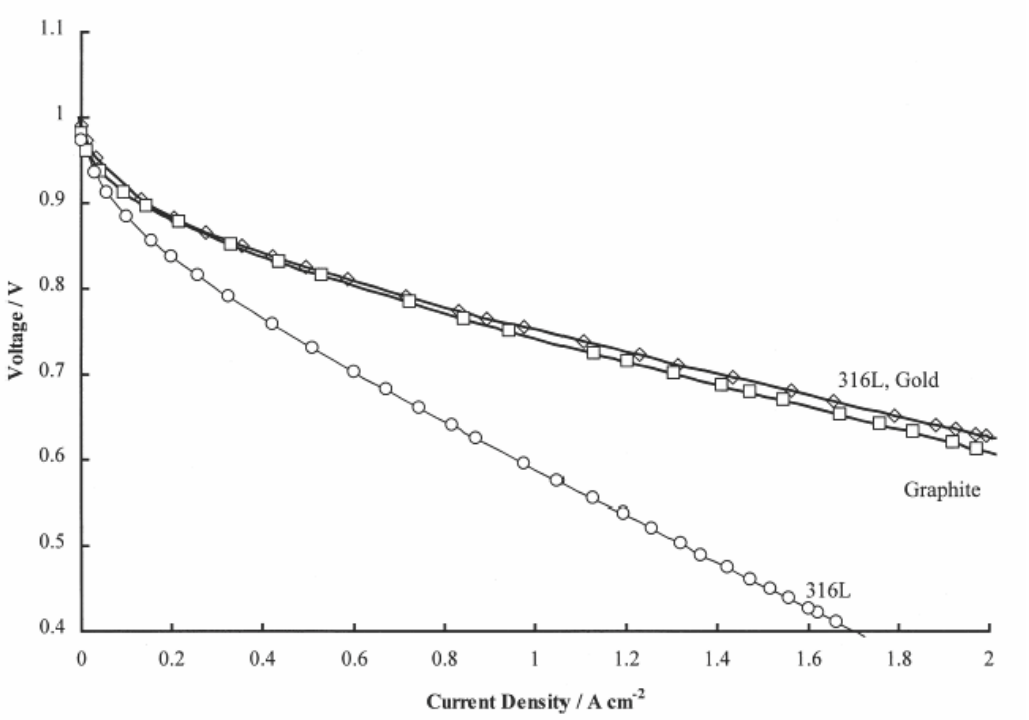

Figure 2-6 – Polarization Curves Comparing Graphite and Stainless Steel 316L with and without a Gold Coating [16]

Table 2-4 - Summary of Polymers and Fillers for PEMFCs

Polymer	Fillers	Advantages	Disadvantages
HDPE	Carbon Black	Chemically Inert	Low Electrical Conductivity
PP	Synthetic Graphite	Very Low Cost	Low Thermal Conductivity
PA	Natural Graphite	Low Density	
PANI	Carbon Fiber		
PET	Carbon Nano-tubes		
PVDF	Copper		
EVA	Particles/Fibers/Flakes		
EPDM	Nickel		
Ethylene-Octene	Particles/Fibers/Flakes		
Vinyl Ester	Stainless Steel		
Polyepoxy	Particles/Fibers/Flakes		
Polyester			
Phenolic Resin			
PPS			

Table 2-5 – Polymer Composite Electrical and Mechanical Properties with a Focus on Bipolar Plates for PEMFCs [8,13,26,27,28,29,30,31,32,33,34]

Polymer [reference]	Filler (%wt)	Conductivity (S/cm)		Mechanical Strength (MPa)	
		Through-plane	In-plane	Tensile	Flexural
EPDM/PP [28]	CB (50)		1	24	
Nylon 6,6 [8]	CB(5), SG(30),CF(20)	3.1			
PET [30]	CNT (12-vol%)		0.25		
PET [30]	CNT (6-vol%)		0.0023	25	
PET [13,32]	SG (65), GF (7)	18-25	230	36.5	53
PET/PVDF [30]	CNT (6-vol%)		0.059	34	
Phenolic Resin [32]	SG (77.5)		53		
Phenolic Resin [32]	CF (N/A)		200-300		
Phenol-Formaldehyde [27]	CB (15)		35.7		150
PP [29]	SG (85)		71		48.6
PP [31]	CB(16.5),SG(38.5)	2.78			45
PP [31]	CB (16.5),SG (33),CF (5.5)	2.5			52
PP [34]	CB (5),SG (15),CF (30)		30.3		
PPS [13]	SG (70), CF (6)	19	271	57.5	95.8
PPS [31]	CB (8.5),SG (43.8),CF (4)	10			84.0
PVDF [13]	SG (74)		119		36.2
PVDF [13]	SG (64), CF (16)		109		42.7
PVDF [29]	SG (75)		43		62.6
PVDF [26]	CB (40)	2.3			
PVE [13]	SG (68)		60	23.4	29.6
PVE [13]	SG (68)		85	24.1	28.2
PVE [13]	SG (69)		30	26.2	37.9
PVE [13]		50	100	30.3	40
PVE [13]	SG (68)	20	55	26.2	40
PVE [34]	SG (85)		250		
Unknown [13]	Unknown	25-33		25.1	53.1
Unknown [13]	Unknown	20	100		40
Unknown [13]	Unknown		67		29.4
Unknown [13]	Unknown		105	25.1	20.7
Unknown [13]	Unknown		217.4		

2.2.3 Composites

Composites can cover a very broad combination of materials as indicated in Table 2-4; however, the focus for composite literature review will be towards polymer matrices loaded with carbon based fillers. Other composites such as polymer-metal filler systems have

received limited attention thus far, as they require more specialized processing and also have the potential of ion dissolution into the fuel cell membrane, thus degrading performance. The composite approach can be divided into two types of polymers: thermoset; and thermoplastic. An in depth summary of literature results for both thermosets and thermoplastics are summarized for bipolar plates (Table 2-5) and other relevant work (Table 2-6).

Table 2-6 - Polymer Composite Electrical and Mechanical Properties with a Focus on other Applications [35,36,37,38,39,40,41]

Polymer (reference)	Filler [%wt]	Conductivity (S/cm)		Mechanical Strength (MPa)	
		Through-plane	In-plane	Tensile	Flexural
Ethylene-Octene [38]	CB [~10.5 vol%]		$\sim10^{-5.5}$	~18	
EVA [38]	CB [~14.5-vol%]		~0.001	~17	
EVA/PP [36]	CB [10.5-vol%]		0.1	28	
HDPE [39]	CF [20]		~10.7		
HDPE [39]	SG [75]		~10.9		
HDPE [39]	CF [34], SG [26]		~28.5		
PA [37]	NG [15-vol%]		~6		
PANI [37]	NG [42-vol%]		~50		
Polyepoxy [35]	CF [3.1]		0.8		
Polyester [35]	CF [2.5]		1.3		
PP [40]	CB [39]		~2.5	32.5	
PP [38]	CB[~11-vol%]		$\sim10^{-5}$	~17.5	
PP [37]	NG [40-vol%]		~3		
PP [39]	CB [6]		~0.001	38	
PP [39]	CF [15]		~0.001	41	

Thermoset composites

Thermoset polymers become more rigid upon heating which can hinder processing, but when formed tend to have a higher mechanical strength then thermoplastics. Thermosets that have been used for bipolar plates include phenolic resin and carbon fibers reported by Besmann et al.[14], research which includes polyester and polyepoxy with carbon fibers completed by Feller et al.,[35] and studies with phenol-formaldehyde resin and carbon black from Ryu et al.[27] Thermosets have shown a great deal of promise with results reaching as high as 200-300 S/cm (in-plane)[32] and 50 S/cm (through-plane).[13] The disadvantages with thermosets are the costs often associated with the specialized materials and manufacturing techniques. Techniques such as slurry molding, chemical vapour infiltration, and other pre or post processing manufacturing methods.[15]

Thermoplastic composites

Thermoplastic composites have been investigated in much more detail than thermosets, in large part due to their abundance and ease of manufacturing. Heiser demonstrated an improved electrical conductivity of 3.1 S/cm with the addition of carbon fillers in nylon.[8] Research from Huang et al. has shown results for both PET and PPS combined with carbon fillers.[13] The PET measured 18-25 S/cm through-plane and 230 S/cm in-plane, while the PPS measured 19 S/cm and 271 S/cm for through-plane and in-plane, respectively. Del Rio et al. used polyvinylidene fluoride (PVDF) and carbon black to achieve a conductivity of 2.36 S/cm, while graphite filled composites produced by Nedstack have reached conductivities as high as 217.4 S/cm (in-plane).[13,26]

Results that have specifically used polypropylene (PP) with carbon fillers are shown in Table 2-7. Polypropylene was compression molded by Blunk et al. with graphite, carbon black and carbon fibers attaining 30.3 S/cm (in-plane).[34] Mighri et al. showed that higher structured carbon black yields the same resistivity results in a PP matrix as lower structured carbon blacks but at a lower loading (24 wt% as compared to 35 wt%). The conductivity ranged from 2.5 – 2.8 S/cm.[31] Figure 2-7 illustrates a comparison of Mighri's work with both PP and PPS polymers.

Table 2-7 – Subset of Table 2-4 for PP-Carbon Composites and Material Details

Polypropylene		Filler		Conductivity (S/cm)		Mechanical Strength (MPa)	
Supplier [reference]	MFI	Type (Supplier)	Particle Size / Loading (wt%)	Through-plane	In-plane	Tensile	Flexural
Sun Allomer Ltd [29]	0.4 g/10 min (230 C, 21.2 N load)	Graphite powder (Showa Denko K.K.)	20 µm / 85		71		48.6
Basel [31]	50 dg/min	Carbon Black (Degussa/Huls) Synthetic Graphite (Asbury)	70 nm / 16.5 15 µm / 38.5	2.78			45
Basel [31]	50 dg/min	Carbon Black (Degussa/Huls) Synthetic Graphite (Asbury) Carbon Fibers (Asbury)	70 nm / 16.5 15 µm / 33 15 µm / 5.5	2.5			52
Russia-A36 [37]		Natural Graphite (Russia – EUZ-M)	40-60 µm / 40-vol%		~3		
Tatren TF-411 [40]	10 g/10 min	Carbon Black (Cabot)	?/ 39		~2.5		
Profax 6323 [38]		Carbon Black (Cabot)	12 nm / ~11-vol%		~0.2	~17.5	
Carmel Olefins [39]		Carbon Fiber (Tenax)	6 mm / 15		~0.001	41	
Carmel Olefins [39]		Carbon Black (Akzo)	? /11		~0.001	38	

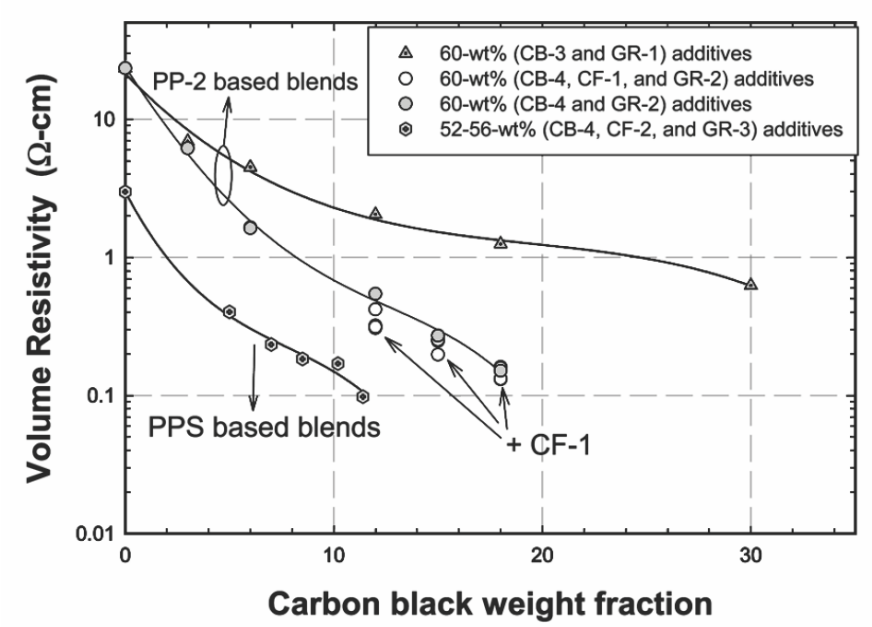

Figure 2-7 –Volume Resistivity versus Carbon black Weight Fraction in Multi-filler Composites [31]

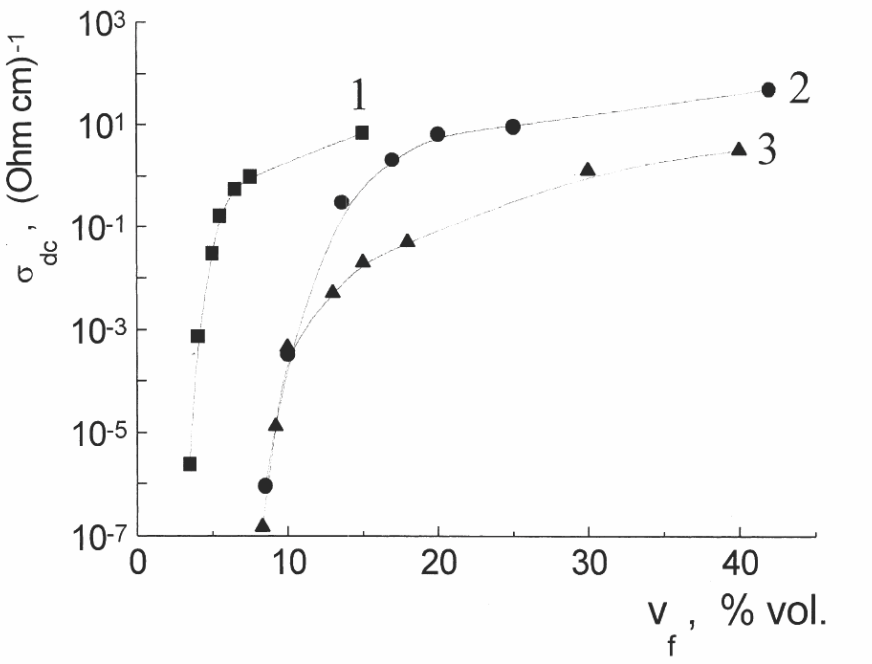

Figure 2-8 – Conductivity of Graphite Composites using PA (1), PANI (2), PP (3) Polymer Matrices for Various Filler Loadings by Volume[37]

Tchmutin et al. also investigated PP composites along with PA and PANI matrices using natural graphite. Conductivity for the PP composite was approximately 3 S/cm at a filler

loading of 40 vol%.[37] Figure 2-8 illustrates the conductivity versus filler loading, showing the percolation curves for each of the polymer matrices.

Inherently conductive polymers (ICPs) have also been investigated and they often are placed in their own class. ICPs include such polymer families as polythiophenes, polyanilines, polypyrroles, polyphenylene, polyfluorenes, polynaphthalene, and polyacetylenes. These polymers are often combined with other polymers in addition to conductive fillers to improve processability.[42] Results for PANI and PA as shown in Figure 2-8 are approximately 50 S/cm and 6 S/cm (in-plane), respectively.

Mechanical properties are also important to the durability of PEMFCs, specifically tensile and flexural strength. Table 2-5 to Table 2-7 display tensile and flexural strength (MPa) where information was available in the literature.

Specific examples of tensile results are shown in Figure 2-9 and Figure 2-10 for virgin polypropylene (PP), PP with fiber (carbon and glass) and PP with carbon black. From the literature the expected range for tensile strength is 15-40 MPa and for flexural strength is 30-55 MPa.

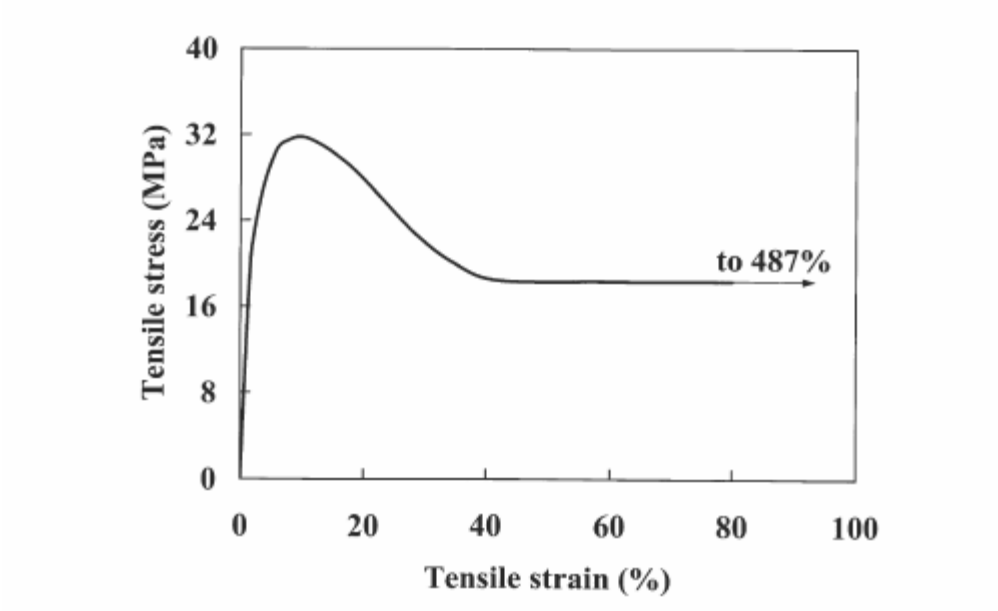

a)

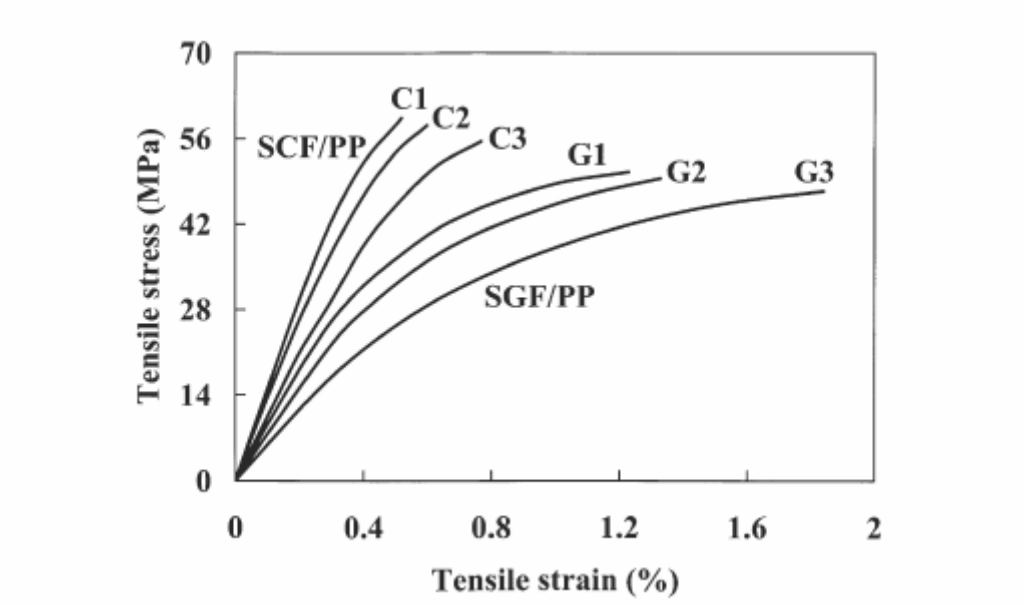

b)

Figure 2-9 – Examples from Literature of Typical Tensile Stress-Strain Curves for PP a) and PP-CF or PP-GF b) Systems [43]

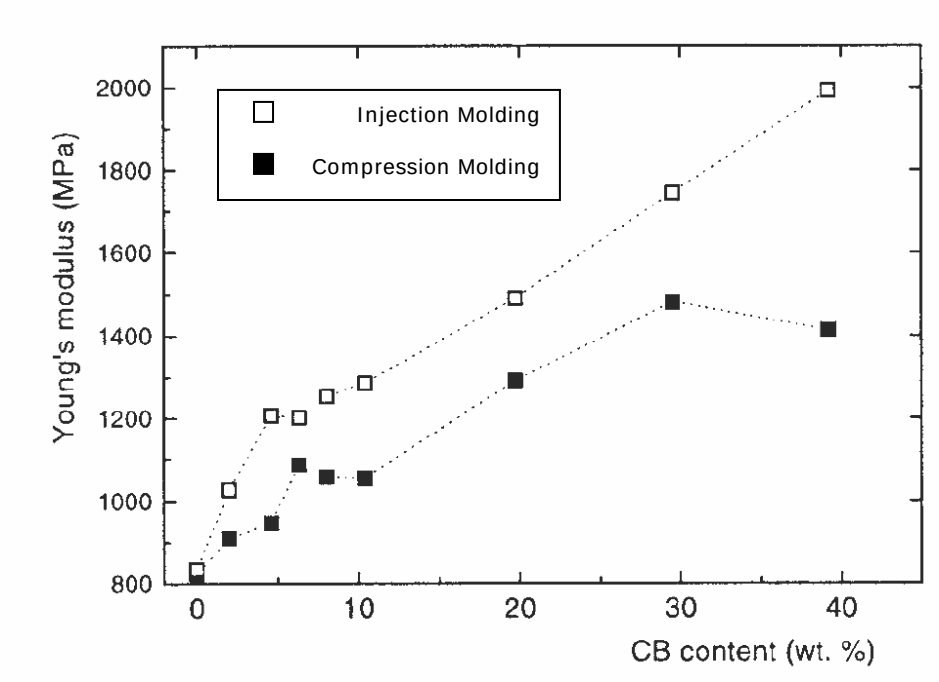

a)

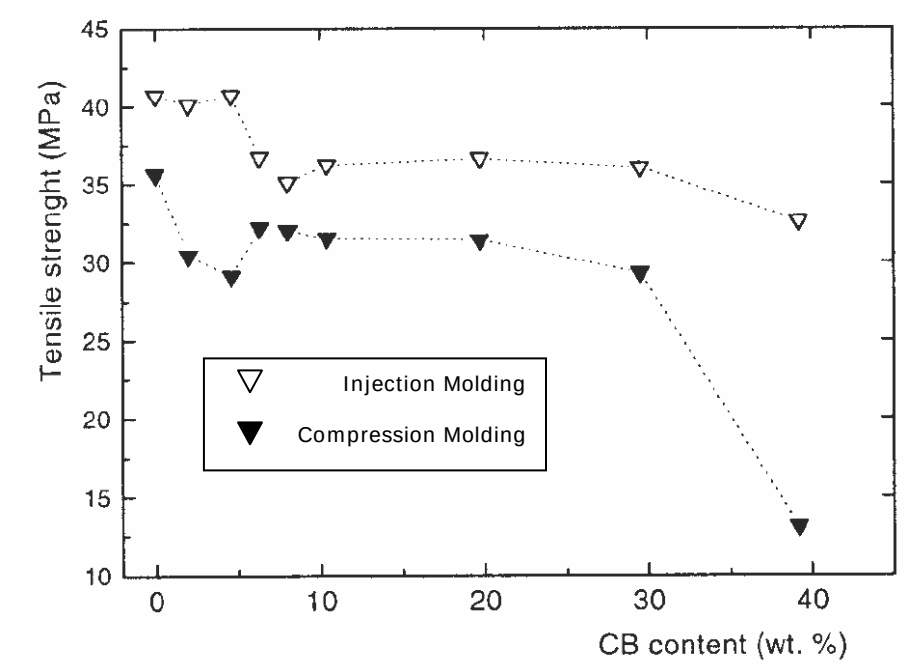

b)

Figure 2-10 - Examples from Literature of Typical Tensile Modulus a) and Strength b) PP -CB Systems [40]

2.2.4 Bipolar Plate Cost

Another focus of this research project is minimizing material and manufacturing cost for bipolar plate development. Since there are more than 300 bipolar flow plates within a fuel cell stack for applications such as transportation it is important to minimize weight, volume and cost.[44] There have been various analyses conducted to estimate or suggest appropriate cost targets for bipolar plates such as \$10/plate USD [14] and \$0.0045/cm^2 USD [15].

Heinzel et al. provided some insight into comparing the cost of injection molded bipolar plates as production volumes increased. Figure 2-11 illustrates the findings and suggests that at high volumes cost targets may be very realistic provided improvements are made with future development.

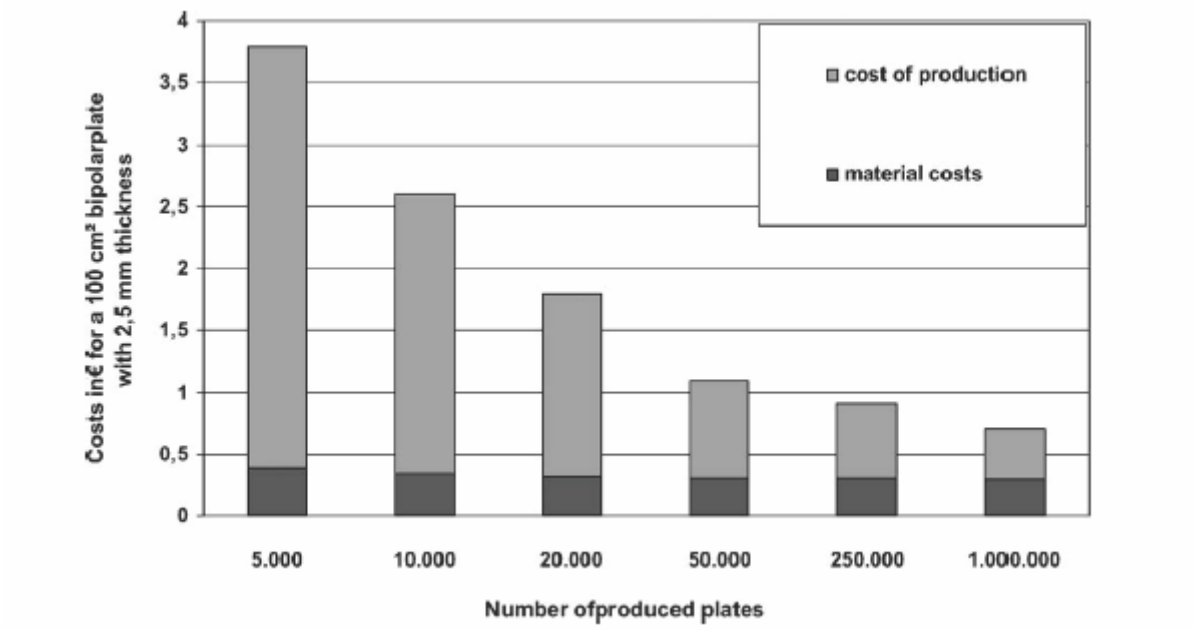

Figure 2-11 – Dependence on Production Related Costs of Injection Molded Bipolar Plates on Production Volume [45]

Middelman et al. financially evaluated NedStack's Conduplate composite material for bipolar plates. The results are summarized in Table 2-8.[33] The findings suggest that if used with a 7 kW/m^2 MEA the bipolar plate cost will be approximately 4 Euros/kW.

Table 2-8 – Summary of Cost Associated with NedStack Bipolar Plate Material [33]

Assumptions		Cost Results (2002 Euros)	
Material Yield	100%	Material	0.65
Cycles per mold	500 000	Molds	0.05
Equipment up-time	80%	Equipment	0.40
Depreciation per year	20%	Energy	0.08
Size	250 x 250 x 2 (mm)	Labor	0.22
Weight	0.1 kg		
Capacity per year	1 000 000 plates	Total	1.40

Bar-On et al. completed a very rigorous analysis looking at two very different cost models for fuel cells. From Chapter 1, Figure 1-9 depicts the two models. Bar-On obtained the models from Lomax et al. for Direct Technologies Inc. (DTI), published in 1998, and Arthur D. Little (ADL) cost model that was prepared for the US Department of Energy Transportation Fuel Cell program in 2000.[6] Figure 2-12 further describes the exact cost value associated with each fuel cell component. These two models serve as the extreme cases to be considered, the DTI model is much more inexpensive as compared to the ADL model. Figure 2-13 and Figure 2-14 are specific for the bipolar plates and provide more insight into the anticipated cost of injection molded bipolar plates at commercial volumes in the future.

It is intended that the values associated with all the models and estimations be used to estimate the cost of the bipolar plates produced through this research project by comparing material cost and assuming similar manufacturing techniques such as extrusion and injection molding.

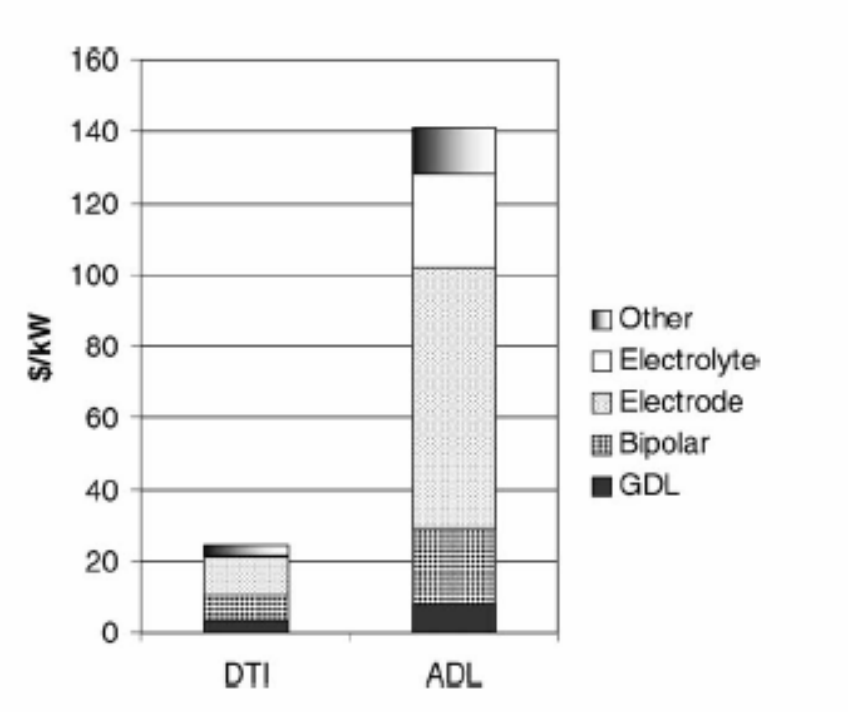

Figure 2-12 – Two Fuel Cell Cost Models and Associated Value in $/kW USD [6]

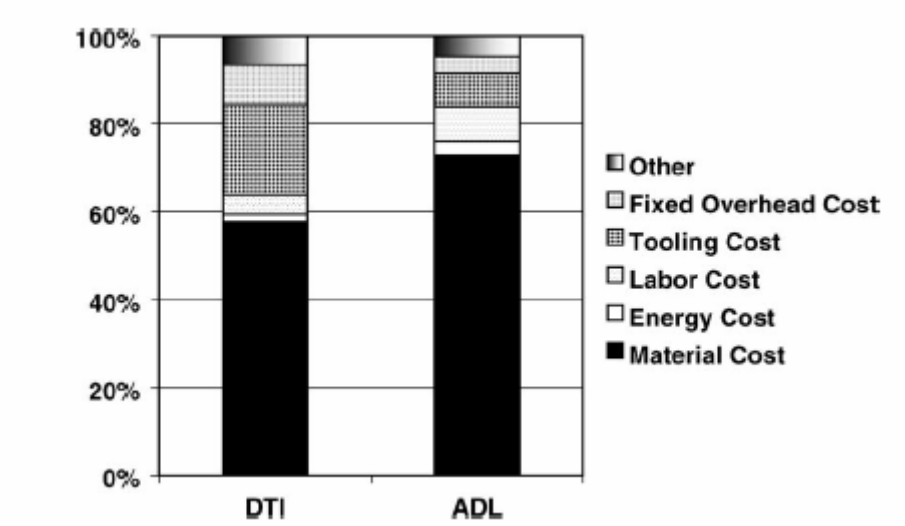

Figure 2-13 – Cost Elements of Bipolar Plates for Each Design Model [6]

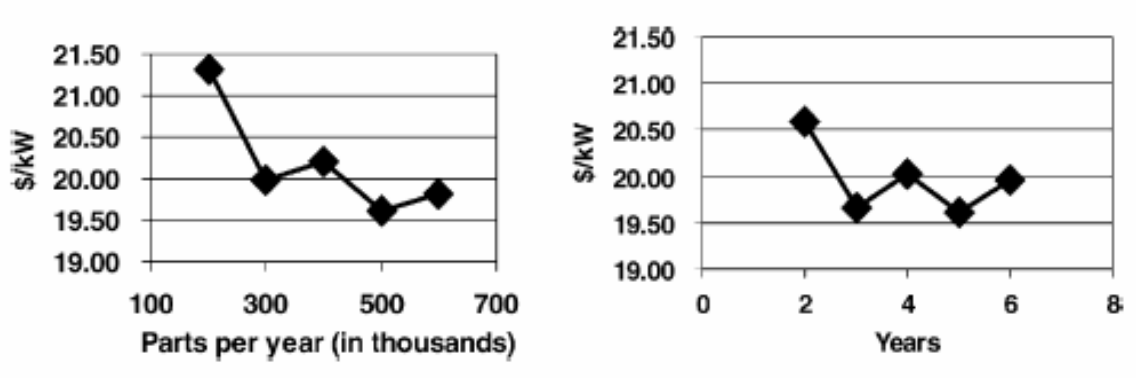

Figure 2-14 – Manufacturing Cost of Injection Molded Bipolar Plates for Varied Production Volumes on the ADL Model [6]

3 Experimental

Based on background literature and the objective of this research, the target for material development was to maximize conductivity while maintaining adequate mechanical strength. Thermoplastic composites were chosen due to the ease of manufacturing, low density, and low cost, as suggested previously. The material selection, manufacturing process, and testing which was performed to verify and validate these goals will be summarized in this chapter.

3.1 Material Selection

The materials used for composite development includes three types of carbon based fillers in polypropylene. The resin matrix chosen for this project was an Equistar polypropylene copolymer. Petrothene PP36KK01 has a melt flow index of 7 and is manufactured for medium impact strength.

Table 3-1 – Petrothene PP36KK01 Polypropylene [46,47]

Property	Nominal Value	Units	ASTM Test Method
Melt Flow Rate	7.0	g/10 min	D 1238
Tensile Strength @ Yield	22.0	MPa	D 638
Elongation @ Yield	6	%	D 638
Flexural Modulus	1100	MPa	D 790
Izod Impact, Notched @ 23°C	500	J/m	D 256
Izod Impact, Notched @ -18°C	75	J/m	D 256
Unnotched Impact @ -18°C	1655	J/m	D 4812
Gardner Impact @ -18°C	36	J	D 5420
Rockwell Hardness	78	R	D 785
Heat Deflection @ 66 psi	73	°C	D 648
Heat Deflection @ 264 psi	56	°C	D 648
Specific Gravity	0.89-0.91		

Table 3-1 has additional information about the virgin resin. The research objectives narrowed the preliminary resin selection to commodity polymers. A melt flow index of 7 incorporates a balance between processability and mechanical rigidity, which are important for the ability to achieve a high filler loading and operate effectively in a fuel cell environment.

Three carbon fillers were used in conjunction with Petrothene to form electrically conductive composites. The fillers included Chevron Phillips Acetylene Carbon Black, Cabot's Vulcan Carbon Black, and Fortafil's Short Carbon Fiber.

Cheveron Phillip's AB100% Shawinigan acetylene carbon black has a mean particle size of 42 nanometers and a specific gravity of 1.75. Further acetylene carbon black properties are shown in Table 3-2.

Table 3-2 – CPChem Shawinigan Acetylene Carbon Black [48]

Specifications	Limits	Typical
Moisture wt%	0.2 Max.	0.05
Ash wt%	0.05 Max.	0.005
Grit (325 Mesh Sieve) wt%	0.02 Max.	0.006
Absorption Stiffness, ml/5gm	19.0 Min.	19.5
Bulk Density lbs/ft^3	12.5-14.5	12.9
Actual Density gm/cc		1.75
Mean Particle Size, nm		42
Surface Area		
BET Method, m/gm		75
Iodine Absorption Number		90
Carbon content %		>99.9

The second type of filler used was Cabot Corporation's XC72R Vulcan carbon black. It has a particle size of 84 ± 40 nm and a specific gravity of approximately 1.8.[49] Additional Vulcan carbon black properties are shown in Table 3-3.

Table 3-3 – Cabot Vulcan XC72R Carbon Black [49, 50]

Specifications	Limits	Typical
Moisture wt%	3.0 max	0.6
Ash wt%	0.20 max	0.03
pH	3.5-9.5	7.1
Bulk Density lbs/ft^3	3.00-9.00	5.20
Actual Density gm/cc	1.7-1.9	
Mean Particle Size, nm	30 nm nom.**	84 +/- 40 nm**
Carbon content %		>99.8

The third and last type of filler used was carbon fiber. Fortafil's 243 short carbon fiber has a specific gravity of 1.8, an aspect ratio of 500 and electrical conductivity of approximately 60 000 S/m. It was anticipated that the fiber will provide an ideal path for electron transport through the material. Table 3-4 shows the properties of Fortafil 243.

Table 3-4 – Fortafil 243 Chopped Carbon Fiber [51]

Specifications	SI
Tensile Strength	>3450 MPa
Tensile Modulus	>207 GPa
Ultimate Elongation	1.7%
Density	1.8 g/cm^3
Cross-Sectional Area/Filament	3.3 x 10^{-5} mm^2
Filament Shape	Round
Filament Diameter	6 microns
Electrical Resistivity	1.67 mOhm-cm
Physical Form	Flakes
Fiber Length	3 mm
Moisture Content	<0.3%

3.2 Experimental Design

The experimental approach consisted of two trials. The first trial used a twenty run mixture response design that was developed using Stat-Ease's Design Expert 6.0 and is shown in Table 3-5. Materials used for this trial include Equistar PP36KK01, CPChem AB100%, Cabot XC72R, and Fortafil 243 fiber. The ratio between the three fillers varied from 0 to 1, with the overall filler loading ranging from 0 to 35 wt %.

Based on Trial 1 results, a second trial was executed. The objective of the Trial 2 experimental work was to explore the conductivity relationship between varying filler loading using a fixed filler ratio of 1:1:1. The identification of a percolation trend (or S-curve) associated with this filler combination was the experimental objective. For Trial 2 the overall filler loading targets ranged from 0 to 60 wt%, with the experimental targets for each run shown in Table 3-6.

Table 3-5 – Runs for Trial 1 Experimental Design

	Targeted Percent Fill (by Weight)			
Run	**Acetylene Black**	**Vulcan Black**	**Carbon Fiber**	**Polypropylene**
1	0	0	0	100
2	0	0	18	83
3	18	18	0	65
4	35	0	0	65
5	0	0	35	65
6	0	18	0	83
7	22	4	4	69
8	5	5	22	69
9	18	0	18	65
10	9	9	9	74
11	0	18	18	65
12	0	0	18	83
13	4	22	4	69
14	4	4	22	69
15	18	0	0	83
16	0	35	0	65
17	4	4	4	87
18	18	0	0	83
19	4	4	4	87
20	0	0	0	100

Table 3-6 – Runs for Trial 2 Experimental Design

Targeted Percent Fill (by Weight)		
Run	**Filler**	**Polypropylene**
1	0	100
2	60	40
3	50	50
4	40	60
5	30	70
6	20	80
7	10	90

3.3 Processing

The samples were fabricated by using the fillers and resin as received from the suppliers. The sample fabrication process is illustrated in Figure 3-1. Prior to the extrusion process the fillers were hand mixed in the appropriate ratios, as such the results assume that the relative filler distribution stayed consistent throughout the process. For Trial 1 all 20 runs went through the entire process. However, for Trial 2 a master batch of the 1:1:1 ratio of filler was prepared using the 'Mixing Process' and was cut using more virgin resin during the 'Molding Process'.

The extruder used, shown in Figure 3-2, was a co-current Leistritz twin screw 30.34 extruder. Following extrusion the material was pelletized using a Berlyn pelletizer, illustrated in Figure 3-3. Finally, as seen in Figure 3-4, the material was injection molded at Polymer Technologies Inc. on an 85 ton Engel injection molder.

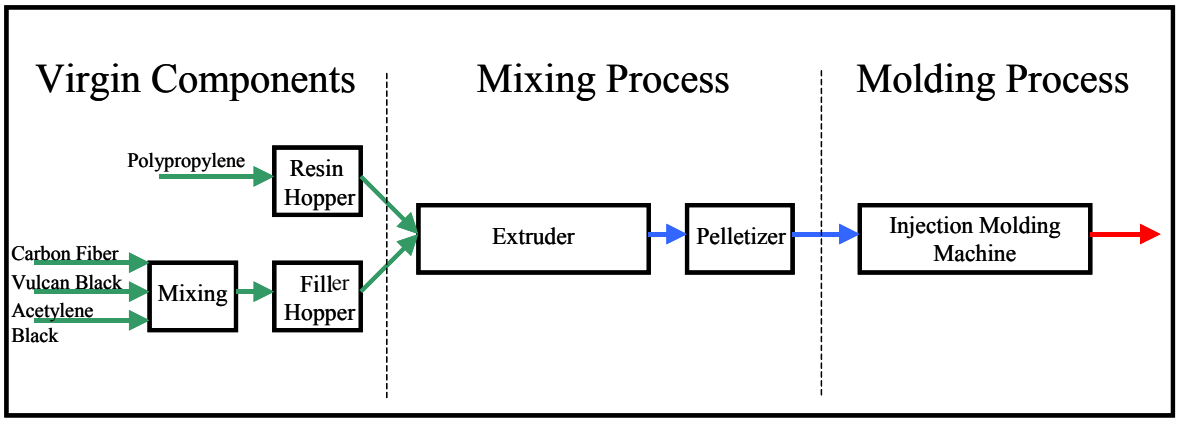

Figure 3-1 – Sample Preparation Process

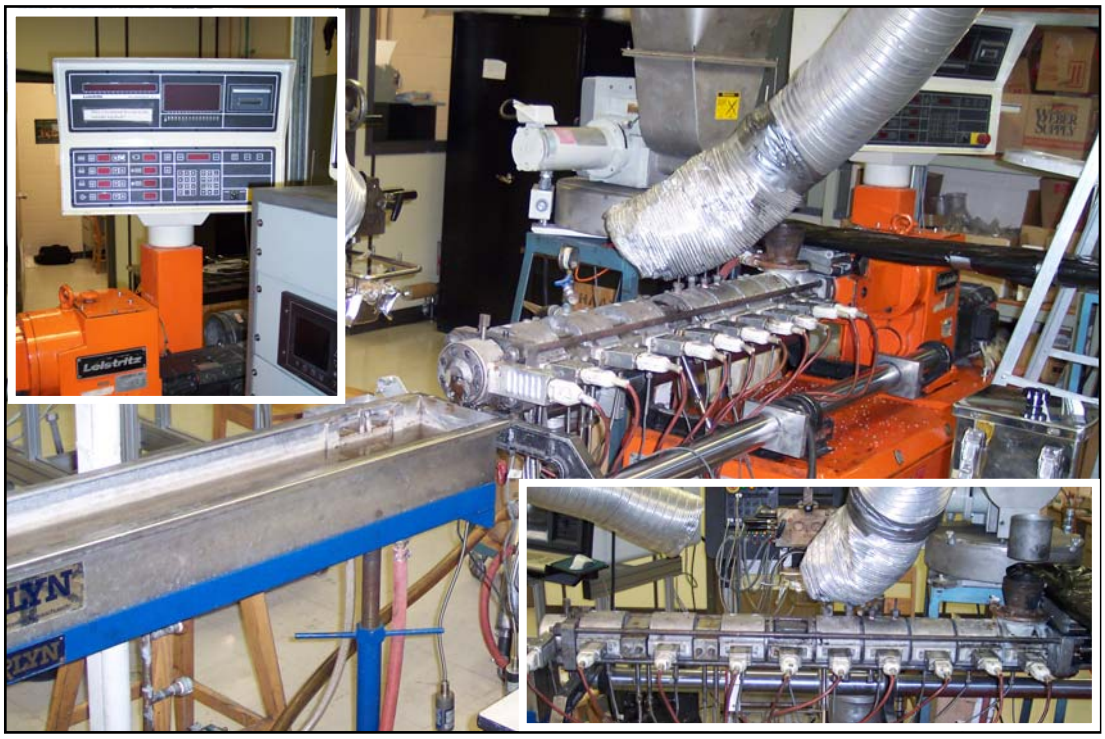

Figure 3-2 – University of Waterloo Leistritz Twin Screw Extruder

Figure 3-3 – University of Waterloo Berlyn Pelletizer

Figure 3-4 – Polymer Technology Inc. Engel 85 Ton Injection Molder

The twin screw configuration used is shown in Figure 3-5. The configuration consisted of two feeding locations, one for the virgin resin and one for the fillers. The option for multiple feed locations ensured that the fibers were exposed to a minimum amount of degradation due to shear forces that could cause fiber fractures and a reduction in the aspect ratio. This arrangement also reduced problems associated with screw torque and filler feeding. The last important aspect of the screw arrangement was the location and size of the kneading blocks. It was a balance of ensuring adequate mixing without excessive fiber degradation.

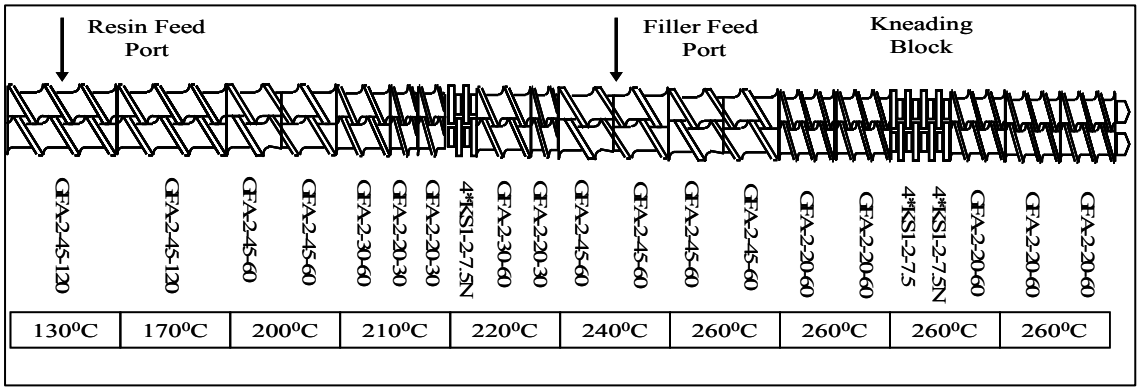

Figure 3-5 – Twin Screw Configuration

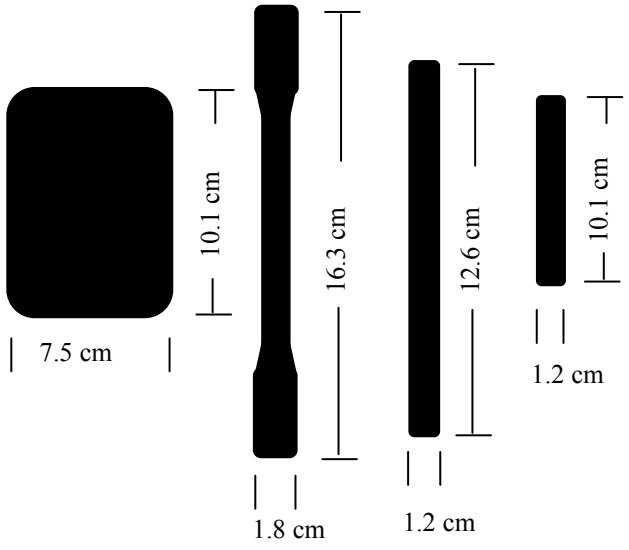

Figure 3-6 – Trial 1 Sample Dimensions

The shape and dimensions of the produced samples are shown in Figure 3-6 and Figure 3-7 for Trials 1 and 2, respectively. The Trial 1 samples were created based on existing test molds available at the manufacturer. The Trial 2 shape was produced from a newly developed and manufactured mold, dictated from the final application requirements in a commercial fuel cell. Appropriately sized samples were cut from the original samples for various mechanical and fuel cell testing.

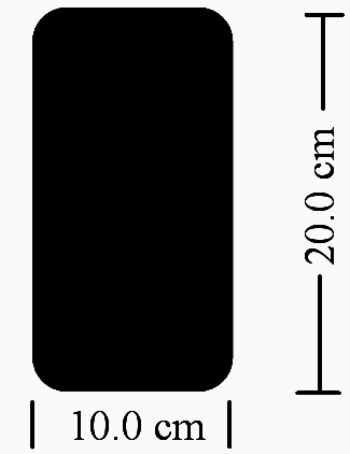

Figure 3-7 – Trial 2 Sample Dimensions

3.4 Ex-Situ Testing

Following the execution of each experiment it was necessary to analyze the results. The properties of interest were related to the filler loading and filler ratio in each case, forming a relationship between that property and the composite mixture. The order of testing is shown below in Figure 3-8. The only underlying assumption that had to be made for multi-filler composites was that the filler ratio remained consistent throughout the process. The overall filler loading, however, was verified using thermal gravimetric analysis.

3.4.1 Thermal Gravimetric Analysis

The uncontrollable inconsistencies with the material feed rate and operation of the twin screw extruder could be verified by using thermal gravimetric analysis (TGA) to obtain the

actual filler loading. TGA measures the mass of a sample over time as the temperature increases at a constant rate. The TGA chamber was continuously swept with a purge gas to remove vapors or formed gases during the instrument's operation.

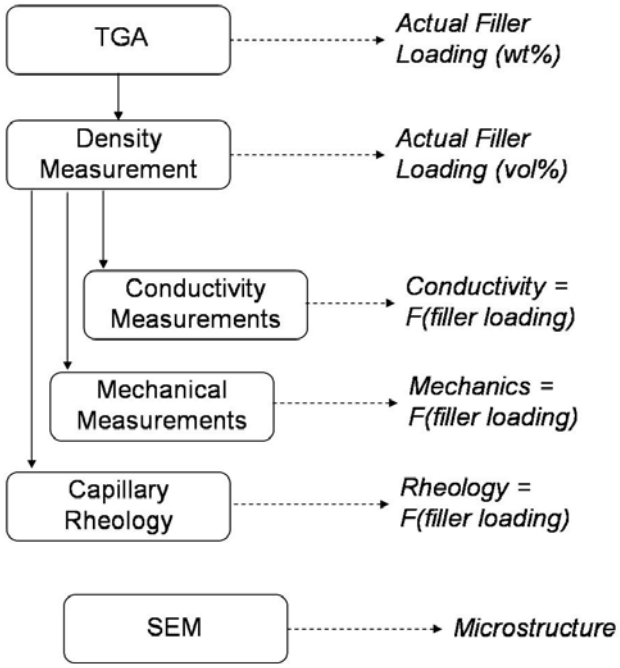

Figure 3-8 – Testing Process Flow Diagram

Thermal gravimetric analysis was performed on a 'TA SDT 2960 Simultaneous DTA-TGA'. Each individual component of the system was characterized in the TGA chamber, resulting in an associated decomposition temperature range. In sequential composite runs each component can be isolated to their characterized temperature range to determine the associated weight fraction of the sample. An example of data from a TGA run is shown in Figure 3-9. There is no mass loss until approximately 400^{o}C. Between 400^{o}C and 500^{o}C almost 50% of the sample's mass is lost and the remaining 50% is lost between 600^{o}C and 900^{o}C. The TGA measurements confirmed the sample's actual filler loading ($X_{fillers}$). This example will be re-iterated and discussed in detail in the results section and further details regarding test procedures can be referenced in Appendix A.

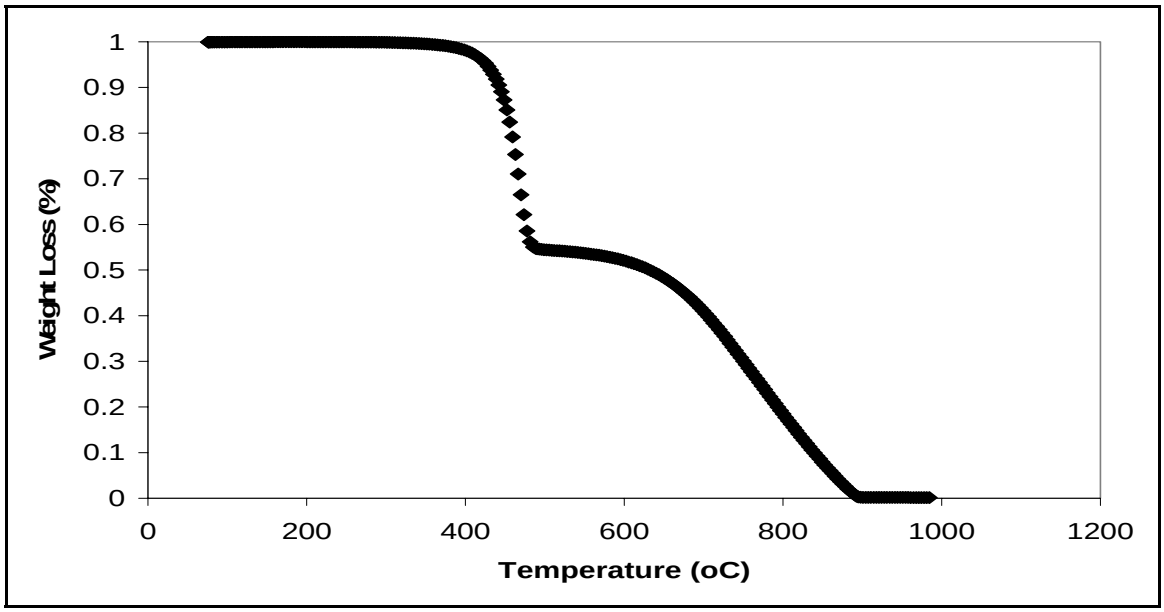

Figure 3-9 – TGA Sample Data

3.4.2 Density

The next step was to convert the actual filler loading from a weight fraction ($X_{fillers}$) to a volume fraction ($Y_{fillers}$). This is possible by determining the density of each sample and using the resin sample (100% Polypropylene) as a reference point.

The density of each sample was determined using an analytical balance and water displacement technique. The mass of each sample was measured on an analytical balance (m_{sample}) and compared to the increased weight difference when submerged in a beaker of water (m_{water}). Further details regarding test procedures can be referenced in Appendix A. The density was then calculated using Equation 3-1.

$$\rho_{sample} = \frac{m_{sample}}{m_{water} / \rho_{water}} \qquad \textbf{Equation 3-1}$$

The density of water was taken from Perry's Chemical Engineers' Handbook corrected for temperature.[52]

Based on the measured densities a statistical linear regression was performed. A statistical density was determined for each component of the system, which enable the calculation of the filler loading as a volume fraction $(Y_{component})_z$ in Equation 3-2 and the void fraction associated with each component $(Y_{void})_z$ in Equation 3-3. The total void fraction is equal to the sum of all the void fraction contributions.

$$\left(Y_{component}\right)_z = \frac{\left(Volume\_Component\right)_z}{Volume\_Sample} = \frac{\frac{\left(X_{component}\right)_z}{\left(\rho^{stat}_{component}\right)_z}}{\sum_{i=1}^{4}\frac{\left(X_{component}\right)_i}{\left(\rho^{stat}_{component}\right)_i}} \qquad \textbf{Equation 3-2}$$

$$\left(Y_{void}\right)_z = \left(Y_{component}\right)_z - \frac{\left(Volume\_Component\right)^{calc}_z}{Volume\_Sample} = \left(Y_{component}\right)_z - \frac{\frac{\left(X_{component}\right)_z}{\left(\rho^{specific}_{component}\right)_z}}{\sum_{i=1}^{4}\frac{\left(X_{component}\right)_i}{\left(\rho^{stat}_{component}\right)_i}}$$

Equation 3-3

X- mass fraction	calc – calculated value based on specific property
Y- volume fraction	component – fillers and resin
ρ - density	stat – value based on regression
	specific – value based on measured value

3.4.3 Conductivity Testing

Two conductivity measurement techniques were examined. The first technique (Method 1) used ASTM D-991 "Volume Resistivity of Electrically Conductive and Antistatic Products".[53] Figure 3-10 and Figure 3-12 illustrate the test apparatus. Labels D and E are current and voltage electrodes respectively, and label C represents the test specimen. The electrical circuit shown in Figure 3-11 represents the electron flow and was the basis for calculating the material volume conductivity using Equation 3-4.

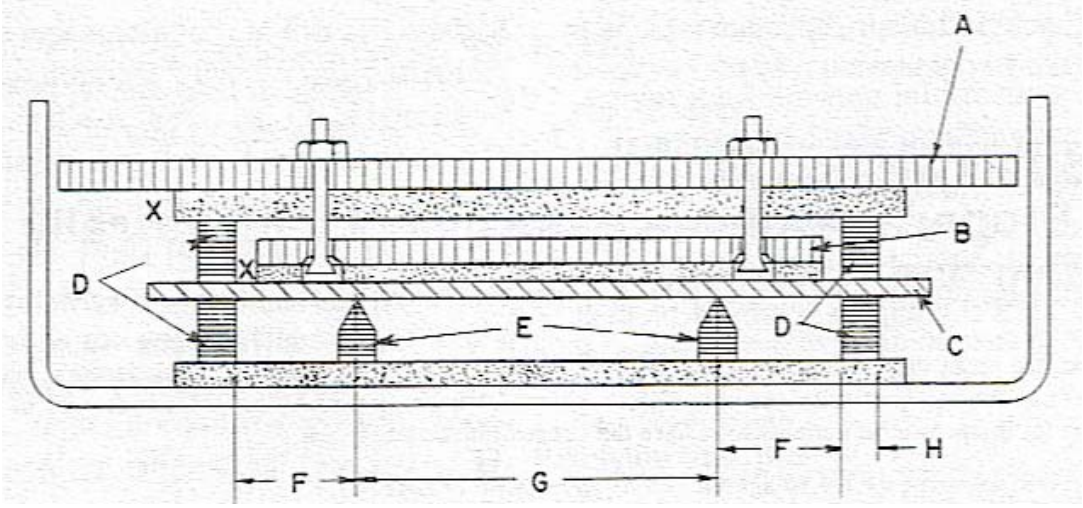

A – Mass for applying contact force between current electrodes and specimen
B – Mass for applying contact force between potential electrodes and specimen
C – Specimen
D – Current Electrodes
E – Potential Electrodes
F – Distance between current and potential electrodes
G – Distance between potential electrodes depending on specimen size
H – Width of current electrodes, 5 to 8 mm
X - Insulation

Figure 3-10 – ASTM D-991 Conductivity Apparatus [53]

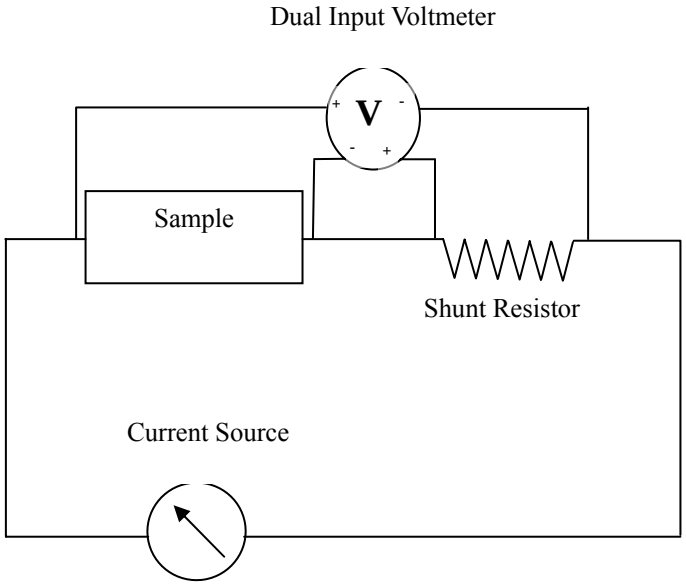

Figure 3-11 – Conductivity Measurement Circuit

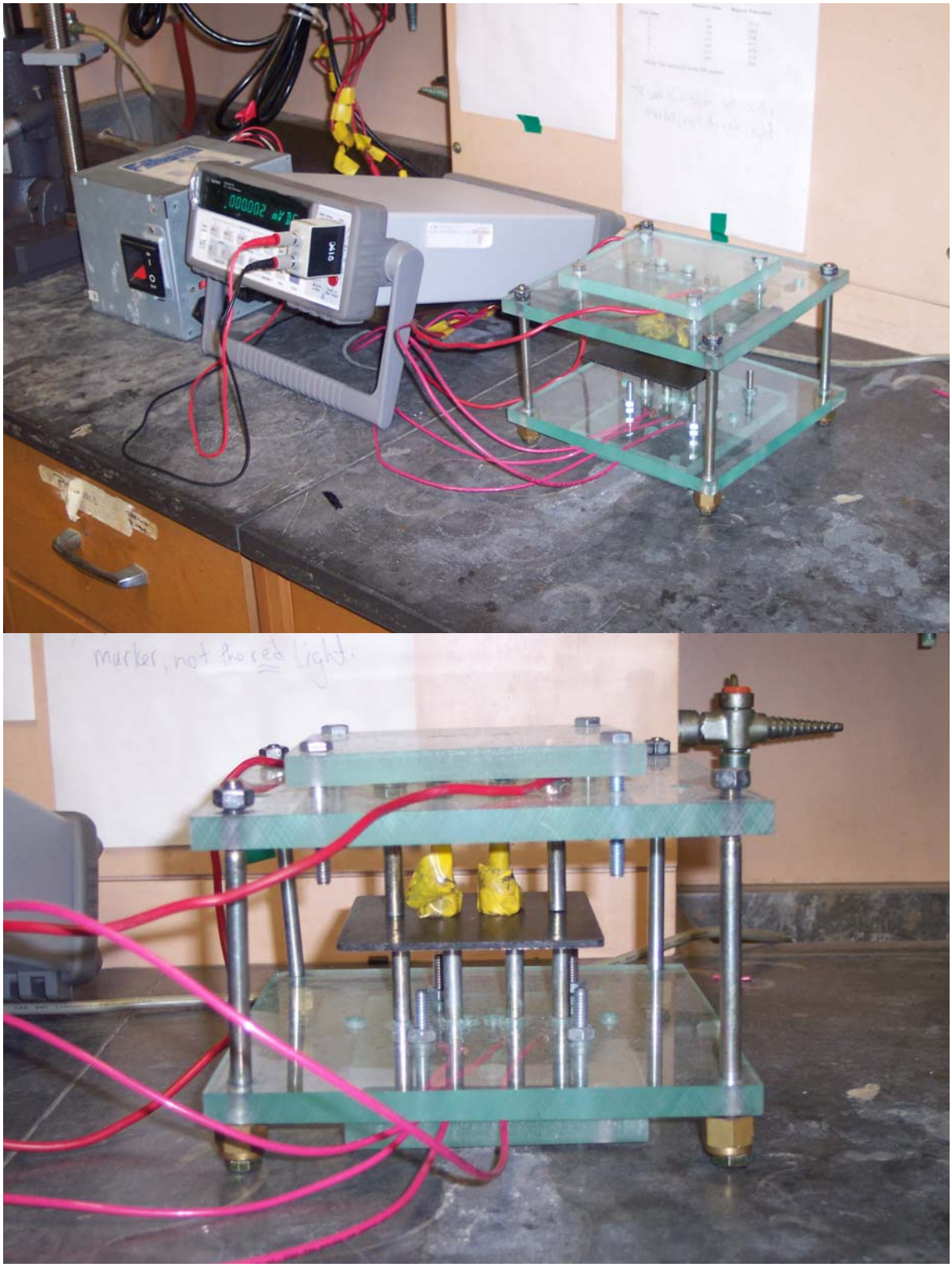

Figure 3-12 – Actual ASTM D-991 Conductivity Measurement Apparatus

$$S = \frac{I \cdot D}{0.001 \cdot v \cdot t \cdot W}$$ **Equation 3-4**

S – conductivity (S/m) v – voltage (V)
I - current (A) t – thickness of sample (mm)
D – distance between electrodes (mm) W – width of sample (mm)

The second conductivity technique (Method 2) was developed from the US Fuel Cell Council's recommended guidelines.[54] Figure 3-13 and Figure 3-14 shows the test apparatus. Two gold-nickel-copper electrode plates were used in a hydraulic press with two pieces of GDL placed on either side of the sample between the electrodes. A clamping pressure of 1000 psi was used and both voltage and current were independently monitored on both electrodes. The conductivity circuit, represented by Figure 3-11, was used to calculate the volume conductivity using Equation 3-5.

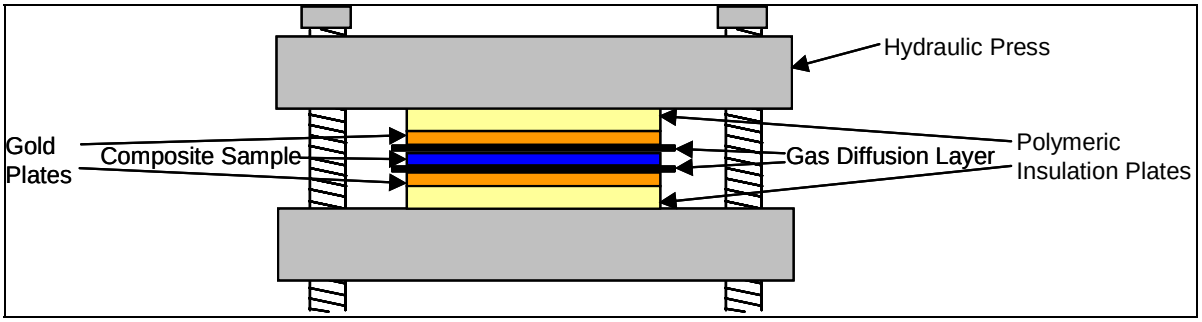

Figure 3-13 – US Fuel Cell Council Conductivity Measurement Apparatus

$$S = \frac{1000 \cdot I \cdot t}{v \cdot L \cdot W}$$ **Equation 3-5**

S – conductivity (S/m) v – voltage (V)
I - current (A) L – length of sample (mm)
t – thickness of sample (mm) W – width of sample (mm)

Calculation details and experimental procedures for both Method 1 and Method 2 can be found in Appendix B.

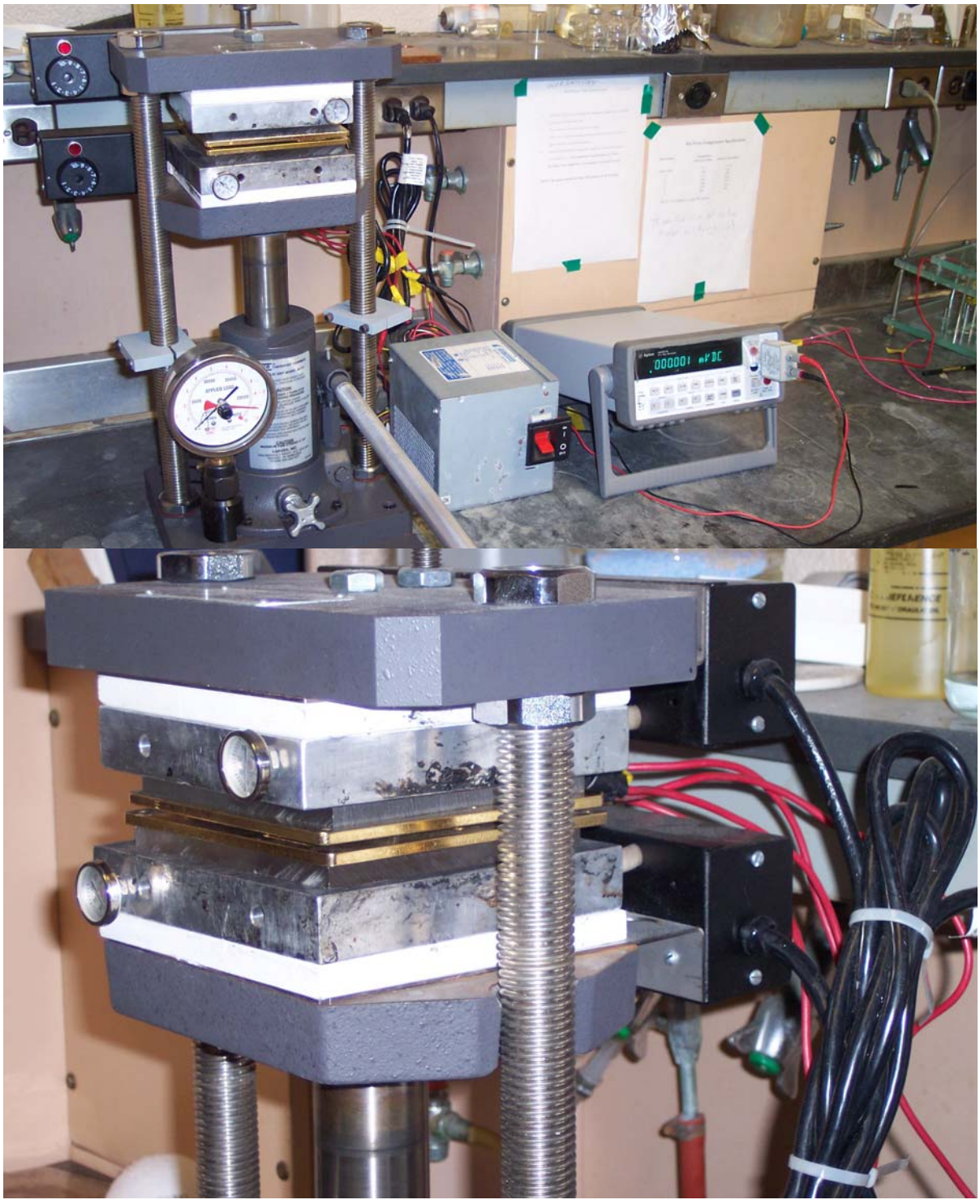

Figure 3-14 – Actual US Fuel Cell Council Conductivity Measurement Apparatus

3.4.4 Mechanical Testing

Mechanical modulus and yield strength were determined for tensile and flexural properties using a Rheometric Scientific Mini-Mat test apparatus. The test procedures that were used for tensile, and flexural analysis in order include: ASTM D-3039/D-3039M-00 "Standard Test Method for Tensile Properties of Polymer Matrix Composite Materials"[55]; ASTM D-5934 "Standard Test Method for Determination of Modulus of Elasticity for Rigid and Semi-Rigid Plastic Specimens by Controlled Rate of Loading Using Three-Point Bending"[56] Small deviations in variables such as testing speed were used for specific materials and sample size. Further details regarding test procedures can be referenced in Appendix C.

3.4.5 Rheology

The previous properties (conductive and mechanical) play a large role in the composite's ability to perform well in a fuel cell environment. However, the ability to process the material was largely dependent on the rheology of the material. The relationship between processability and filler loading was investigated using capillary rheometry.

The apparatus used for rheological testing was the Dynisco Galaxy V Capillary Rheometer and ASTM D3835-02 "Standard Test Method for Determination of Properties of Polymeric Materials by Means of a Capillary Rheometer" was followed.[57] Further details regarding test procedures can be referenced in Appendix D.

The power law associated with this test is defined by Equation 3-6. This equation relates shear viscosity (η) to shear rate (γ). The preceding consistency index (K) will be the factor of interest.

$$\eta = K\gamma^{n-1} \qquad \textbf{Equation 3-6}$$

3.4.6 Microstructure

The analysis of a material's microstructure is important in order to better understand the relationship between the filler loading and various other properties. In order to achieve this, the samples were viewed using a scanning electron microscope (SEM).

The SEM was a LEO1530 field emission SEM with a Gemini column. Images were produced at 5 kV ranging from 100 X to 10 000 X magnification. The samples were prepared by cold fracturing using liquid nitrogen and sputter coated with gold.

3.5 In-Situ Testing

In-situ or in cell testing is the ultimate measure of performance. In order to minimize the amount of material needed for in-situ testing a small fuel cell design was implemented (commercial fuel cells are very large, requiring large amounts of material). This approach required the design and construction of new fuel cell hardware in addition to a bipolar plate mold which could create plates that could be used in a fuel cell operating environment.

3.5.1 Test Fuel Cell Design

A fuel cell with an active area of 365.1 mm by 381.0 mm was designed and built and is shown in Figure 3-15. The detailed 2-D drawing of the accompanying bipolar plate is illustrated in Figure 3-16. The fuel cell was made with aluminum endplates, copper current collectors, and graphite bipolar plates (for a reference point). The components used for testing included an ion power MEA and a SGL 10BA GDL. These materials were held constant for all the in-situ testing, ensuring a direct comparison between the graphite flow plates and the composite molded plates. The fuel cell was clamped to a torque of three N-m.

3.5.2 Bipolar Plate Mold

In order to incorporate the new composite materials a mold was also necessary to fit the new fuel cell design. The design was completed in a way to incorporate capabilities to emboss the flow path into previously injection molded rectangular samples as well as compression molding samples from composite pellets or flakes.

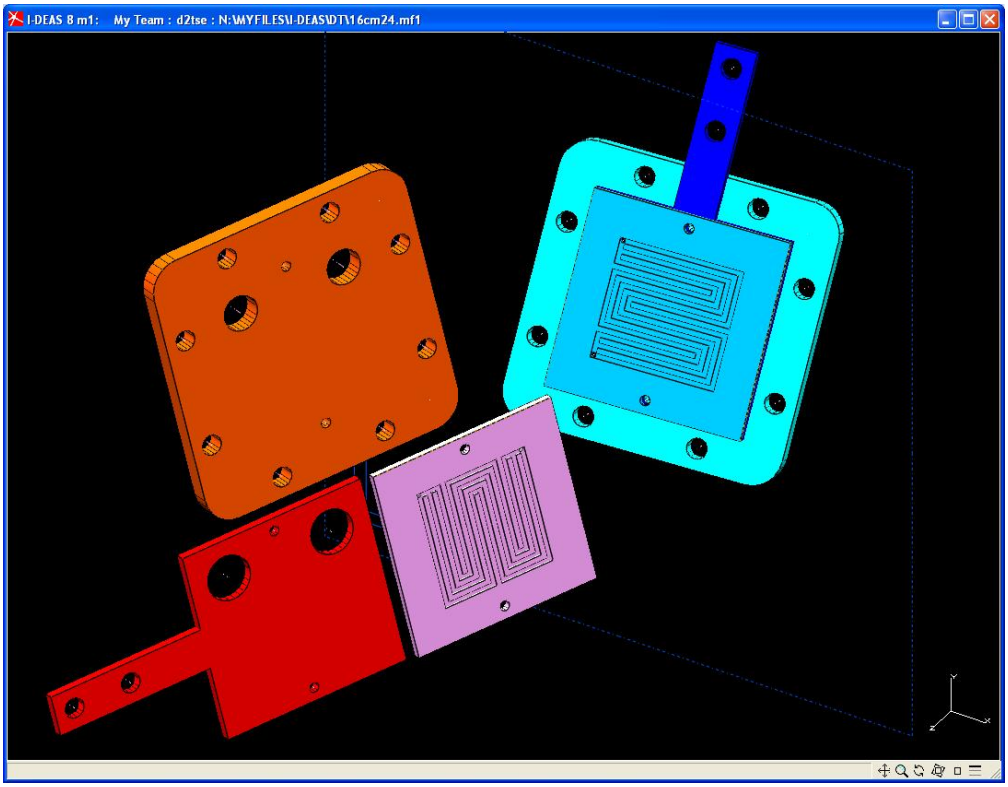

Figure 3-15 – IDEAS 3-D Drawing of Small Fuel Cell Hardware

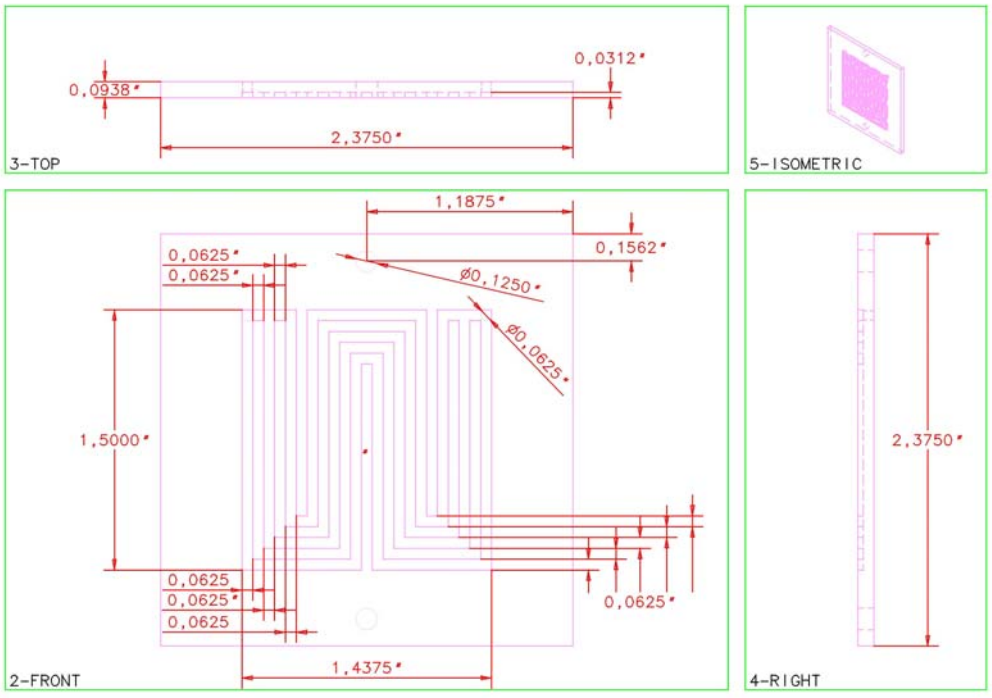

Figure 3-16 – IDEAS 2-D Drawing of Small Fuel Cell Bipolar Plates

The current work only investigated embossing previously injection molded samples; however, future work should investigate compression molding as a potential manufacturing technique.

The mold, shown in Figure 3-17 was designed by Polymer Technologies Inc. and manufactured at the University of Waterloo. The design incorporates numerous chokes to ensure the ability to purge the entrapped air out of the mold as well as ejector pins which are operated by a sling hammer from the underside of the mold.

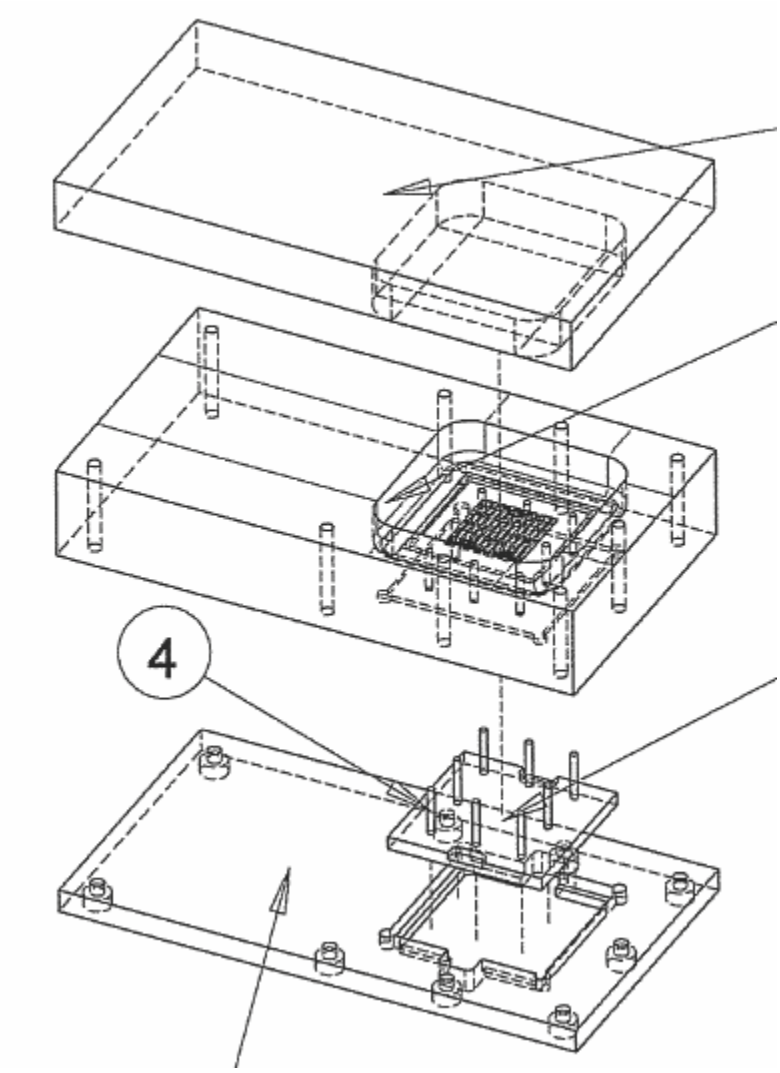

Figure 3-17 –Drawing of Mold Designed by Polymer Technologies

Figure 3-18 - Actual Mold Designed by Polymer Technologies

3.5.3 Fuel Cell Testing

Following the completion of the fuel cell hardware and the bipolar plate mold, composite plate testing was possible. After the fuel cell was assembled it was important to ensure the fuel cell was sealed properly and had no internal crossover. The operating conditions and procedure for the test station can be found in Appendix E.

3.5.3.1 Leak Test

Leak testing was required to ensure the fuel cell was tightened sufficiently to seal in both fuel and oxidant gases. The test consists of pressuring both the anode and cathode to an equal pressure of air or nitrogen and submerging the fuel cell in water. If there was a sealing problem the gas would bubble out of the cell, otherwise the fuel cell was sealed.

3.5.3.2 Cross Over Test

The cross over test was conducted in order to ensure the fuel and oxidant gases can not mix. This would be possible if there was a hole in the membrane or the membrane was not sealed between the gaskets. The test consists of slightly pressuring one side of the fuel cell with air and measuring the flow of gas out the other side. If there was no flow, then there was no cross over problems and the cell was ready to be tested.

3.5.3.3 Test Station

The fuel cell test station and a representative schematic are shown in Figure 3-19 and Figure 3-20. The fuel cell testing was completed in its entirety using this test station arrangement. A detailed description of the system follows.

The reactant gases first flowed through Omega flow meters and pressure transducers before entering the hydrators. It was important to keep the gas streams hydrated, ensuring the MEA did not dry out from water transport to the flowing gas. Perma Pure hydrators were used in this system, which consisted of a small Nafion^{TM} tube inserted into a larger tube. In this design the water was transferred through the inner tube wall, this occurs as the gas streams were allowed to flow in the inner tube while heated deionised water ran through the annulus.

The Nafion™ readily absorbed water while also maintaining a gas barrier, thus as the gas flowed it picked up water from the Nafion™ surface.

Once hydrated, the gas streams flowed into the fuel cell. The cell itself was kept in an oven in order to maintain the cell temperature at 80°C. The anode and cathode current collectors were connected to an external load via load cables, and the cell voltage was measured at the current collectors with voltage taps. The external load was a Dynaload load box which was interfaced with the DAC / PC, and allowed for control and measurement of the current.

The gases, which are saturated, exit the fuel cell and enter knockout drums. These drums condensed much of the water out of the gas streams, preventing the water from entering the mass flow controllers (MFCs) which were found downstream of the knockout drums. The mass flow controllers measured the outlet flow rates of the gases as well as provided the operator with the ability to control backpressure and flow through the system. Once the gases left the MFCs they were vented through a fume hood.

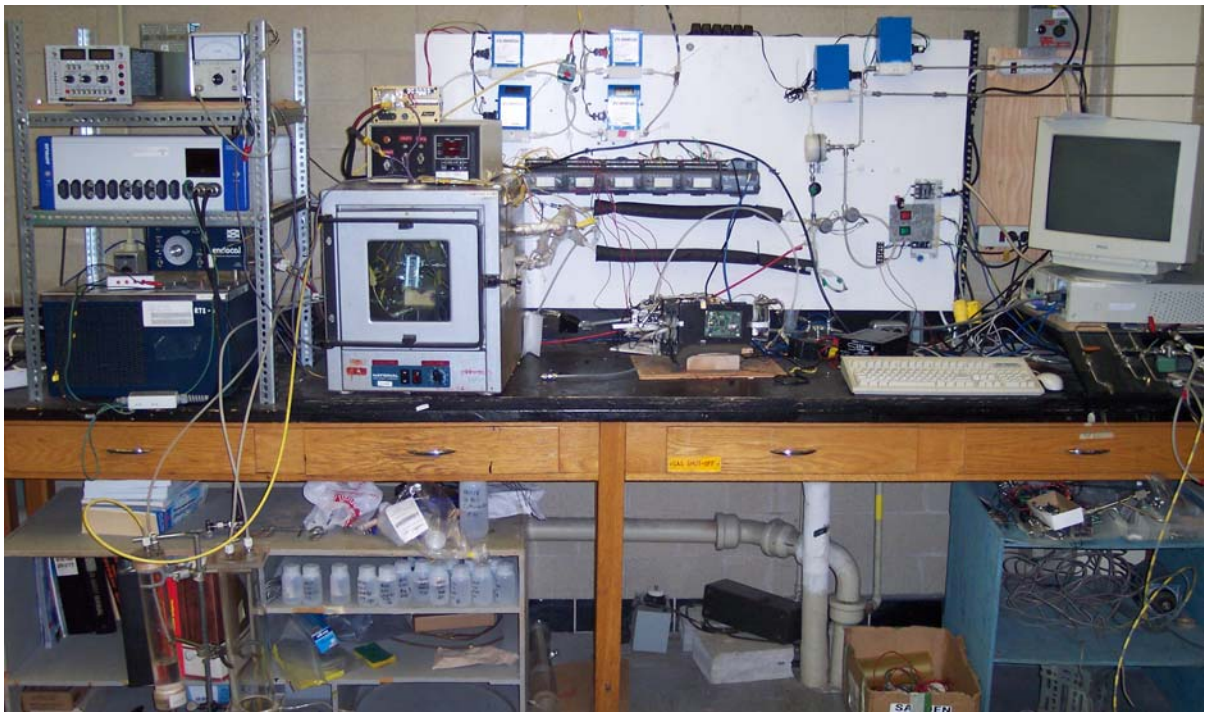

Figure 3-19 – Fuel Cell Test Station

The data acquisition system (DAC) allowed temperature, gas flow rates, pressure, voltage, and current to be monitored and values calculated such as power and efficiency through the PC running LabView.

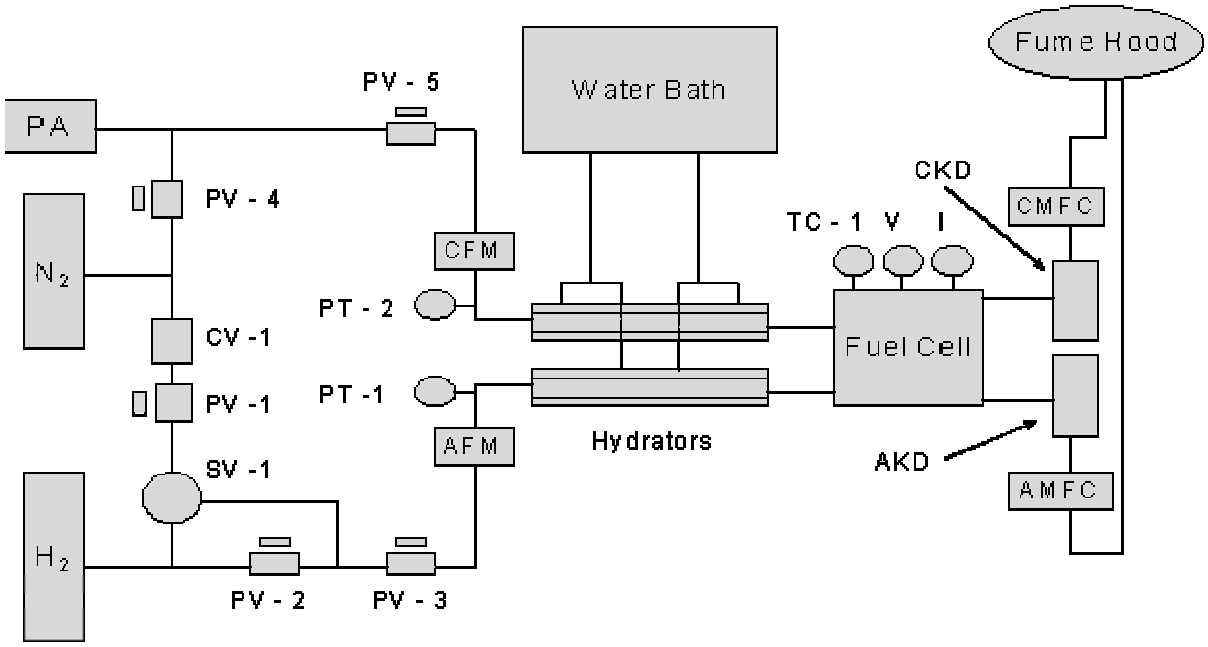

PA – Plant Air Supply
N_2 – Nitrogen Supply
H_2 – Hydrogen Supply
PV – Pressure Regulating Valve
CV – Control Valve
PT – Pressure Transmitter
SV – Solenoid Valve
CFM – Cathode Flow Meter
AFM – Anode Flow Meter
TC – Thermal Couple
V – Voltage Measurement
I – Current Measurement
AKD – Anode Knockout Drum
CKD – Cathode Knockout Drum
CMFC – Cathode Mass Flow Controller
AMFC – Anode Mass Flow Controller

Figure 3-20 – Fuel Cell Test Station Schematic

4 Results and Discussion

The overall objective of this project was to develop bipolar plate materials for PEMFCs. To conclude the benefits and disadvantages for the selected materials a characterization process was required, which has been previously established. The remainder of the thesis will present the results and discuss their meaning.

The results are presented in two sections described as Trial 1 and Trial 2. Trial 1 consisted of the original set of blends based on a designed experiment which was conducted to understand the relationship between the four components in the system (VCB, ACB, CF, & PP). Based on promising conductivity results associated with Trial 1, Trial 2 was executed to obtain information regarding the percolation threshold and 'S-curve' of an equal ratio of all three filler. A brief overview of each trial and their objectives is presented in Table 4-1.

Table 4-1 – Summary of Experimental Trials

	Trial 1	Trial 2
Objective	Understand interaction of 4 component system	Obtain percolation 'S' curve
Filler Mixing Ratio	Varied (1,2, & 3 filler combinations)	Equal mixture of each filler component (1:1:1)
Filler Loading	0-35 wt% (target)	0-60 wt% (target)
Number of Runs	20	7

4.1 Trial 1 – Design of Experiment

4.1.1 Thermal Gravimetric Analysis

Thermal gravimetric analysis (TGA) was used to determine the actual filler loading for each sample of each trial run. The individual components were first analyzed to differentiate between various component characteristics. The trends in Figure 4-1 a) showed the polypropylene resin having a distinct transition, but the individual fillers overlap. Even

magnified as shown in b) the temperature range for each carbon filler is difficult to distinguish. The distinction between fillers is not easily accountable; however the overall filler loading can be calculated assuming the filler ratios are consistent to the initial mixing ratios. Details regarding the TGA method are provided in Appendix A.

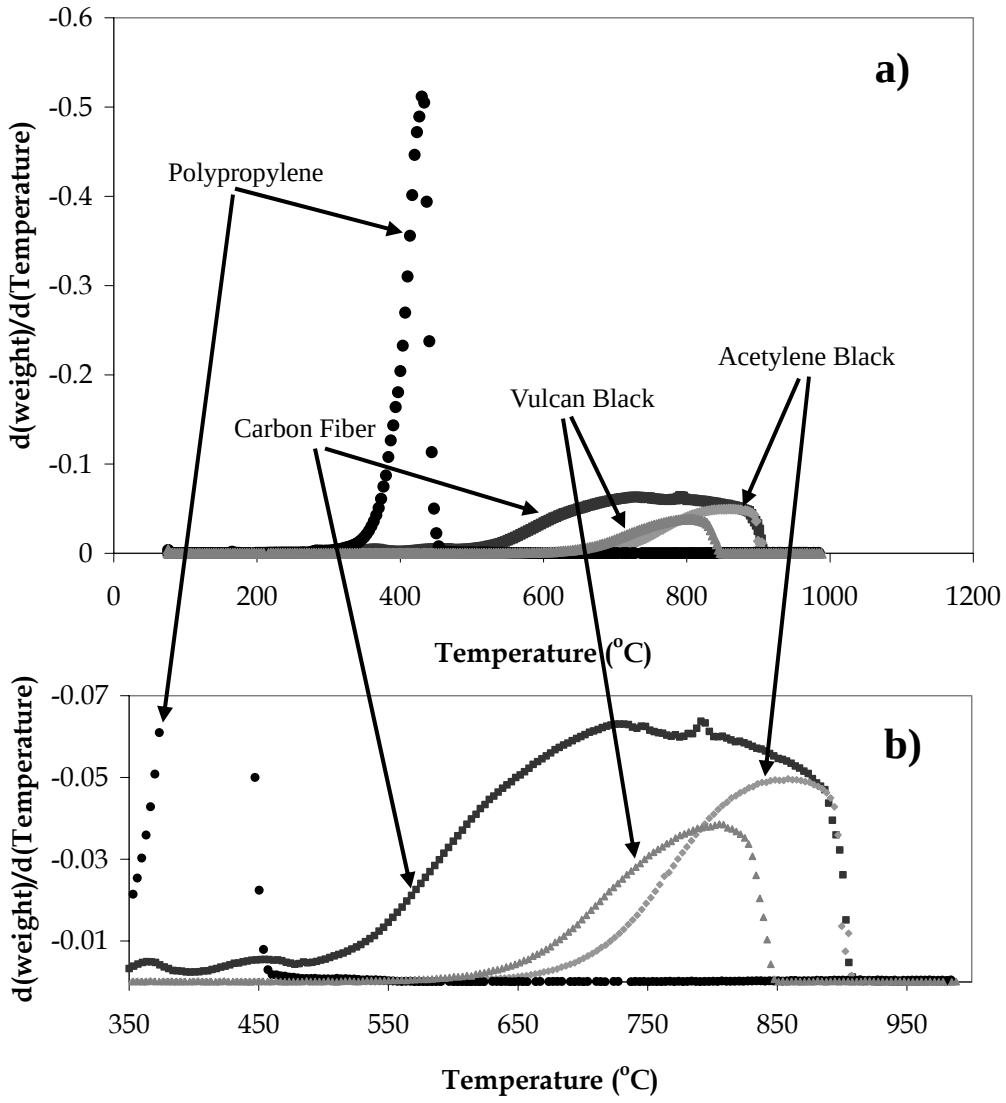

Figure 4-1 – Composite Component TGA a) Entire Range Temperature Range b) Magnification of Carbon Filler Peaks

The polypropylene was removed primarily between 350˚C and 500˚C, while the carbon fillers were oxidized between 550˚C and 900˚C. From this knowledge a confirmation of the sample compositions is possible post processing. Using the originally mixed filler ratios the

actual loading was calculated for each of the individual fillers as a weight percentage. The results for Trial 1 are shown in Table 4-2.

Table 4-2 – Actual Filler Loading (by Mass) – Trial 1

Run	Acetylene Black	Vulcan Black	Carbon Fiber	Polypropylene
1	0	0	0	100
2	0	0	16.97	83.03
3	13.94	13.94	0	72.12
4	34.86	0	0	65.14
5	0	0	29.77	70.23
6	0	16.48	0	83.52
7	21.78	4.36	4.36	69.5
8	3.58	3.58	17.87	74.97
9	16.55	0	16.55	66.9
10	11.64	11.64	11.64	65.08
11	0	14.98	14.98	70.04
12	0	0	18.3	81.7
13	3.99	19.92	3.99	72.1
14	3.81	3.81	19.05	73.33
15	19.86	0	0	80.14
16	0	32.39	0	67.61
17	3.73	3.73	3.73	88.81
18	15.67	0	0	84.33
19	7.51	7.51	7.51	77.47
20	0	0	0	100

4.1.2 Density Measurement

Following the determination of actual filler loadings (wt%), the volumetric filler loading was calculated by inputting the density. The density was measured using a water displacement technique. This procedure is described in Appendix A. The results for Trial 1 are presented in Figure 4-2. The standard deviation is shown with error bars and was based on 5 samples for each of the trial runs. The lowest density obtained in runs 1 and 20 were pure PP, while the highest density was obtained in run 4, which was 35 wt% acetylene black. Runs 5, 7, 9, and 10 also represented significant density increases from the virgin polymer. These runs all had significant contributions from either acetylene black or carbon fiber or both.

Upon analyzing the results of the density measurements a relationship can be established using linear regression. All of the statistical analyses shown in Chapter 4 were facilitated using the software 'Design Expert'. The density relationship is shown below in the form of Equation 4-1.

$$\text{Density} = 1.435(\text{ACB}) + 1.447(\text{VCB}) + 1.440(\text{CF}) + 0.894(\text{PP}) \qquad \textbf{Equation 4-1}$$

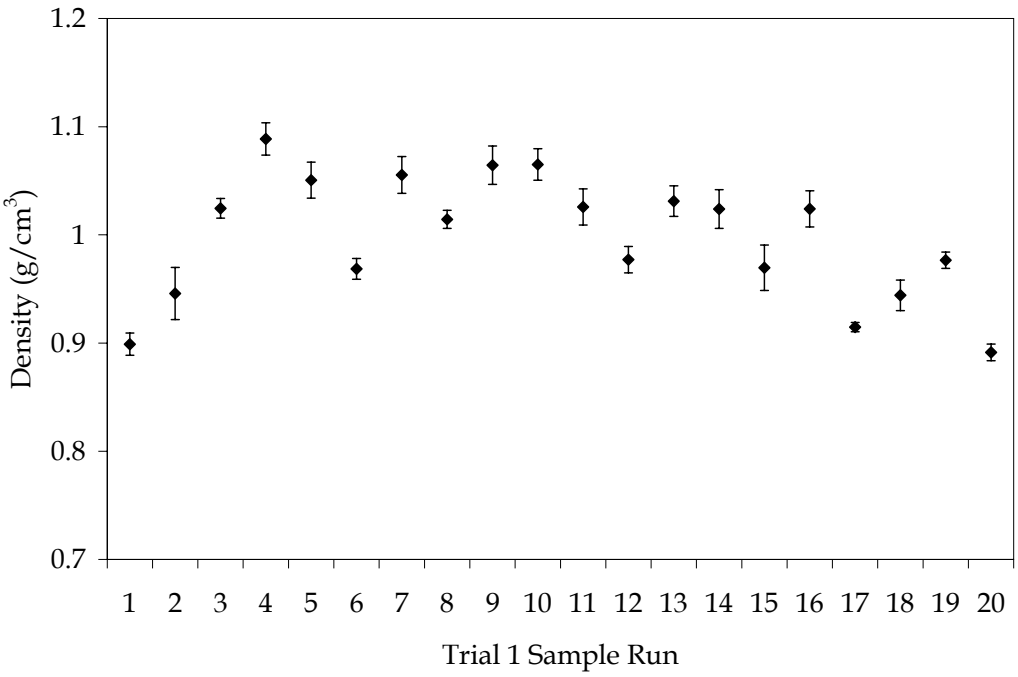

Figure 4-2 – Density of Trial 1 Experimental Runs

Table 4-3 presents the analysis of variance for the regression. The linear model has a very high correlation, which was expected since all the components are immiscible with respect to each other and therefore the density is an additive property in this system.

Table 4-3 – Regression Analysis of Variance for Trial 1 Density

Source of Variance	Sum of Squares	Degrees of Freedom	Mean Square	F Value
Model	0.061	3	0.020	870.06
Residuals	3.752×10^{-4}	16	2.345×10^{-5}	
Total	0.062	19		

R-Squared	0.9939	Pred R-Squared	0.9901
Adj R-Squared	0.9928	Probability >F	<0.0001

One of the benefits of using software in a regression analysis is the ability to easily generate plots such as Figure 4-3, which illustrates one cross-section of the four dimensional design space. In Figure 4-3 the polymer dimension is held constant at 65 wt% while the three other components vary to make up the remaining 35 wt%. These three dimensions are shown using the three points of the triangle. Each corner of the triangle represents a filler loading of 35 wt% for that particular component and correspondingly the opposite side represents 0 wt% of the same component (for each of the three dimensions). Therefore no matter which point you select within the triangle the sum of the three fillers will add up to 35 wt%. For a different value of PP (design space range was from 65 to 100 wt%) there was a slightly different cross-section (or triangle).

The coefficients within Equation 4-1 imply the specific gravity associated with each of the fillers and the polymer matrix. Explicitly the specific gravity was 1.435, 1.447, 1.440, and 0.894 for ACB, VCB, CF, and PP, respectively. Table 4-4 compares the reported densities, the expected density, and the measured density.

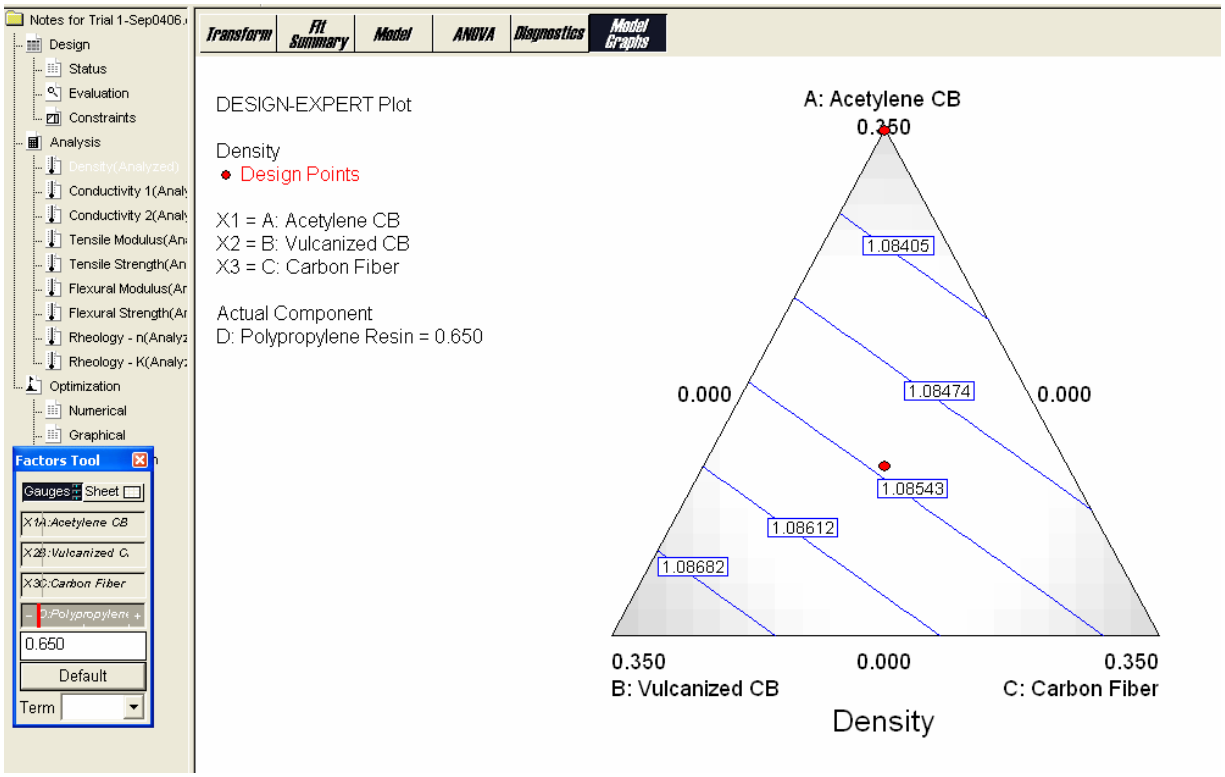

Figure 4-3 – Design Space Plot of Density with the Resin Held Constant at 65%

Table 4-4 – Densities Associated with Each Composite Component [46,48,50,51]

	Bulk Density (g/cm^3)	Actual Density (g/cm^3)	Expected Density (g/cm^3)	Measured Density (g/cm^3)	Deviation
ACB	0.20-0.23	1.75	>1.0	1.435	None
VCB	0.048-0.14	1.7-1.9	>1.0	1.447	None
CF	1.8	1.8	1.8	1.440	Low
PP	0.89-0.91	0.89-0.91	0.89-0.91	0.894	None

The actual density was not expected for ACB and VCB as it was not anticipated that all the voids (bulk versus actual density) would be penetrated by the polymer, some particle agglomerates remained; however, penetration should have occurred in a significant portion of the inter-particle voids. The measured results correlated specific gravity values for ACB and VCB much closer to the reported actual density opposed to the bulk density. The carbon fibers were well dispersed in the polymer matrix and therefore did not have inter-fiber voids.

As a result the density of the fibers should correspond better to the value obtained during the regression. It is believed that voids formed between the fibers and the polymer matrix throughout the composite correlate to the low carbon fiber density coefficient observed. These voids may be due to poor wetting between the polymer and the carbon fibers.

Table 4-5 – Actual Filler Loading (vol%) – Trial 1

Run	Acetylene Black	Vulcan Black	Carbon Fiber	Polypropylene	Voids
1	0.0	0.0	0.0	100.0	0.0
2	0.0	0.0	9.0	88.7	2.3
3	8.0	7.7	0.0	80.7	3.6
4	20.5	0.0	0.0	75.0	4.5
5	0.0	0.0	16.7	79.2	4.2
6	0.0	8.7	0.0	89.1	2.1
7	12.6	2.4	2.4	78.6	4.0
8	2.0	2.0	9.8	82.8	3.4
9	9.7	0.0	9.4	76.5	4.5
10	6.9	6.7	6.7	75.0	4.8
11	0.0	8.4	8.4	79.1	4.1
12	0.0	0.0	9.8	87.8	2.4
13	2.3	11.1	2.2	80.7	3.8
14	2.2	2.1	10.5	81.6	3.6
15	11.0	0.0	0.0	86.6	2.4
16	0.0	18.4	0.0	77.2	4.5
17	2.0	1.9	1.9	92.8	1.4
18	8.5	0.0	0.0	89.6	1.9
19	4.2	4.1	4.1	84.7	2.9
20	0.0	0.0	0.0	100.0	0.0

The inter-particle and interfacial voids attributed to carbon particles and carbon fibers had an impact on mechanical and conductivity properties since the adhesion of the particles and interface of the fibers affected the mechanics and the transmission of electrons. Table 4-5 shows the calculated volume fractions for all the components including the void fractions based on Equation 3-3.

4.1.3 Conductivity

As presented in Chapter 3, two conductivity measurement techniques were used in this project. Figure 4-4 shows that in Method 1 the current is flowing in the same direction as the injection molding direction, and in the Method 2 measures the current is flowing perpendicular to the molding direction. It will be shown further in this chapter the impact of the measurement direction with respect to the molding direction and the direction of fiber alignment.

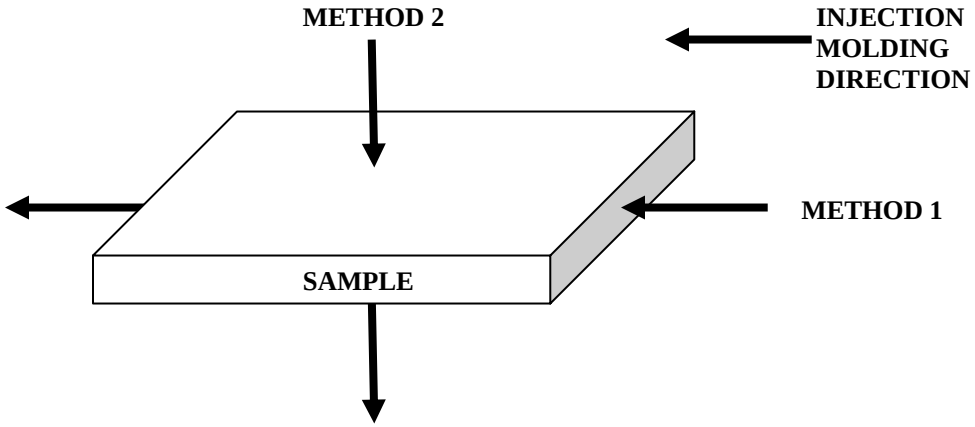

Figure 4-4 – Conductivity Measurement Orientation for Method 1 and Method 2

The complete set of results for all 20 runs is shown in Table 4-6, which includes the five sample averages and standard deviation. Not only are the magnitudes of the results different for each method, the trends are also contradicting. In Method 1 the 1:1:1 ratio (run 10) exhibits the best conductivity of 155 S/m on a wt% basis, suggesting synergistic effects between the three fillers.

Table 4-6 – Summary of All Conductivity Measurements for Trial 1

RUN	Method 1 – In-plane (ASTM)		Method 2 – Through-plane (US FCC)	
	Average (S/m)	Standard Deviation (S/m)	Average (S/m)	Standard Deviation (S/m)
1	0 (No Reading)	N/A	1.00×10^{-4}	6.34×10^{-5}
2	0.22	7.92×10^{-2}	0.130	4.70×10^{-2}
3	20.27	0.244	18.8	0.396
4	22.16	0.381	18.7	0.412
5	3.04	0.891	1.53	0.280
6	1.39	9.54×10^{-2}	0.101	1.35×10^{-2}
7	34.33	0.736	5.01	0.246
8	18.98	2.18	0.940	5.59×10^{-2}
9	15.89	1.71	0.599	2.94×10^{-2}
10	155.44	4.30	18.0	0.350
11	25.21	5.04	0.849	2.89×10^{-2}
12	0.42	8.26×10^{-2}	0.225	2.81×10^{-2}
13	46.40	3.09	6.87	0.742
14	26.67	6.12	1.26	3.60×10^{-2}
15	0.51	2.36×10^{-2}	4.56×10^{-2}	3.13×10^{-3}
16	66.22	0.280	48.3	1.28
17	0 (No Reading)	N/A	1.74×10^{-3}	8.45×10^{-4}
18	0 (No Reading)	N/A	1.69×10^{-4}	2.85×10^{-4}
19	0 (No Reading)	N/A	2.58×10^{-2}	3.64×10^{-3}
20	0 (No Reading)	N/A	1.41×10^{-4}	1.32×10^{-4}

Individually the Vulcan black showed the highest conductivity results (runs 6,16) while the carbon fiber exhibits very low potential on its own (runs 2,5,12) and acetylene black had values between the other two fillers (runs 4,15,18). Method 2 showed much lower conductivities in general and did not exhibit any synergy with the highest conductivity of 48 S/m occurring in run 16 with only the Vulcan carbon black as the filler. The 1:1:1 filler ratio

in run 10 had a similar result to the acetylene black in run 4, while the carbon fiber showed poor conductivity results for both methods of testing.

Using selected runs from Trial 1 the varying trends of the two methods, shown in Figure 4-5 and Figure 4-6, indicated the importance of understanding the mechanism of testing. In Method 1 (based on ASTM D-991) the combination of the three fillers exhibited higher values than Method 2 (based on US Fuel Cell council recommended guidelines). Some degree of synergy was also observed in Method 1, while this was not seen in Method 2.

The difference in measurement technique has not been addressed thus far and becomes very significant in the case of composites where many properties were anisotropic due to fiber alignment and filler-polymer interaction. The trends shown in Method 1 were the primary reasons that the 1:1:1 ratio of fillers was further investigated in Trial 2.

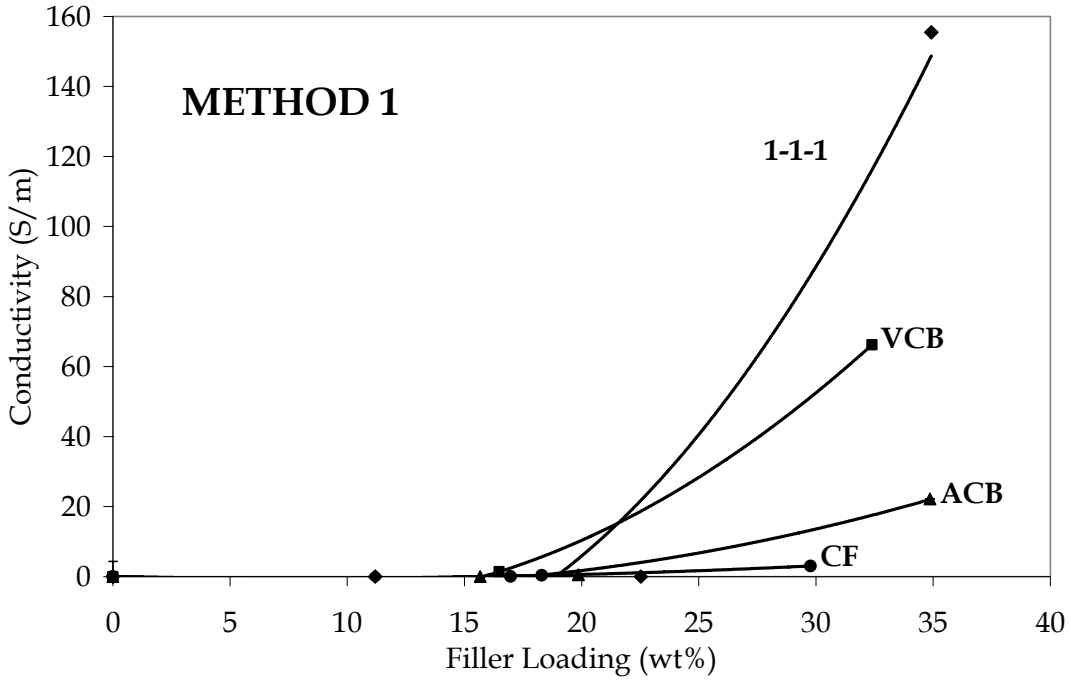

Figure 4-5 – Conductivity Trends in Trial 1 using Method 1 Measurement Technique

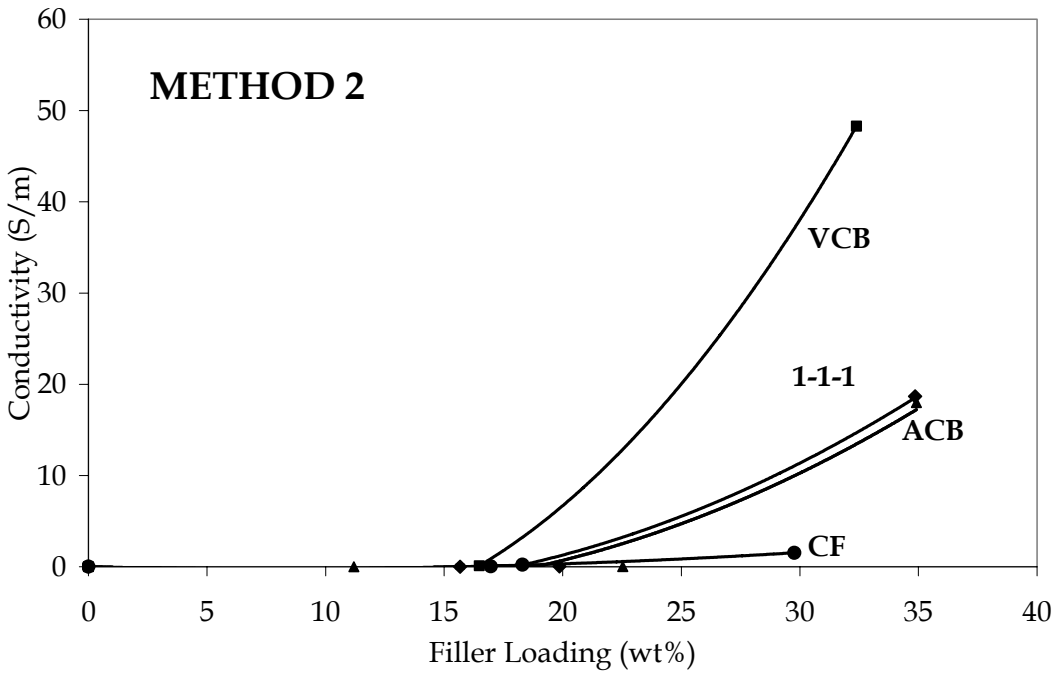

Figure 4-6 – Conductivity Trends in Trial 1 using Method 2 Measurement Technique

Further statistical analysis of the conductivity data reveals Equation 4-2 and Equation 4-3 for measurement techniques 1 and 2, respectively. Both equations are followed by an ANOVA table and the associated R^2 values.

Conductivity 1 (S/m) = 14.42(ACB) + 81.95(VCB) + 7.05(CF) – 1.72(PP) + 444.52(ACB)(VCB) – 136.29(VCB)(PP) + 1892.70(ACB)(VCB)(CF) – 2495.05(ACB)(VCB)(PP)

Equation 4-2

Table 4-7 - Regression Analysis of Variance for Trial 1 Conductivity using Method 1

Source of Variance	Sum of Squares	Degrees of Freedom	Mean Square	F Value
Model	24567.31	7	3506.76	64.88
Residuals	648.58	12	54.05	
Total	25195.89	19		

R-Squared	0.9743	Pred R-Squared	0.7670
Adj R-Squared	0.9592	Probability >F	<0.0001

Conductivity 2 (S/m) = 31.22(ACB) + 796.31(VCB) + 6.47(CF) – 1.29(PP) – 754.45(VCB)(CF) – 962.56(VCB)(PP)

Equation 4-3

Statistically both conductivity relationships were significantly correlated; however, equation form and coefficient interpretation was also relevant.

Table 4-8 - Regression Analysis of Variance for Trial 1 Conductivity using Method 2

Source of Variance	Sum of Squares	Degrees of Freedom	Mean Square	F Value
Model	2411.74	5	482.35	23.46
Residuals	287.91	14	20.56	
Total	2699.64	19		

R-Squared	0.8934	Pred R-Squared	0.6876
Adj R-Squared	0.8553	Probability >F	<0.0001

Table 4-9 – Summary of the Conductivity Equations for Trial 1

Method 1 Conductivity Equation		Method 2 Conductivity Equation	
ACB	14.42	ACB	31.22
VCB	81.95	VCB	796.31
CF	7.05	CF	6.47
PP	- 1.72	PP	- 1.29
ACB x VCB	444.52	VCB x CF	- 754.45
VCB x PP	- 136.29	VCB x PP	- 962.56
ACB x VCB x CF	1892.76		
ACB x VCB x PP	- 4928.96		

In the Method 1 relationship the linear terms showed the observed graphic trends. Vulcan carbon black had the largest individual impact followed by acetylene carbon black, carbon fiber, and finally the polypropylene had a negative impact on conductivity in this design space. The quadratic terms show a constructive interaction between ACB and VCB, while there was a deconstruction interaction between VCB and the PP matrix. Finally the two cubic terms illustrated a synergy between all three fillers while the final term between ACB, VCB and PP works against the previous constructive interaction of ACB and VCB. In the case of Equation 4-2 the only unexpected term was the negative interaction of the two carbon black fillers and the PP resin.

In the Method 2 relationship, the linear terms were also expected as the VCB linear coefficient is much larger than any of the other terms. This was viewed in the conductivity results associated with the composite samples with only VCB. As in the case of the Method 1 the PP linear coefficient was negative, indicating a lower effect of the conductivity property as the PP content increased. The two quadratic terms in this case were both negative and are associated with the VCB-CF and VCB-PP interactions. It was interesting that not only does the interaction of VCB and CF not help the conductivity, but it actually hindered it, and again the VCB-PP interaction was significantly deconstructive as seen in the Method 1 equation.

When comparing the two methods of conductivity measurement it was concluded that when the particle fillers were the only fillers used, the two measurement techniques gave results that were very similar; however, as soon as the carbon fiber was introduced the sample becomes anisotropic with respect to conductivity, resulting in a very large deviation.

Beyond the lack of synergy observed in the Method 2 measurement technique the magnitude of difference in most of the measurements, in large part, may have be due to the contributions from the carbon fibers. However, the Method 2 measurement took place perpendicular to Method 1 and the carbon fiber direction.

Another point of interest was the polymer skin around the composite that could create a significant amount of contact or surface resistance. This phenomenon may have impacted both measurement techniques and reduced the conductivity results.

4.1.4 Tensile Properties

The tensile measurements were conducted using a Rheometric Scientific Mini-Mat test platform, parallel to the injection molding direction. An example of the data output is shown in Figure 4-7, and is representative of the samples tested. One experimental issue that could not be completely overcome was the initial slipping of the clamps on the sample. The result of this occurrence is highlighted in the following figure with a circle and leads to a shift in the curve to the right. This shift consistently occurred and where this was the case the modulus and strength calculations were compensated by shifting the strain percentage back an appropriate amount.

Due to the small amount of initial slipping and the required size of the samples (very small) it resulted in a large amount of variance with respect to mechanical properties. The range of variance for the tensile modulus was 7.48%-25.19% and the range of the tensile strength variance was 1.52%-22.69%. Even with such a large variance it was still useful to perform a statistical analysis to understand the relationships and interactions of all the components involved.

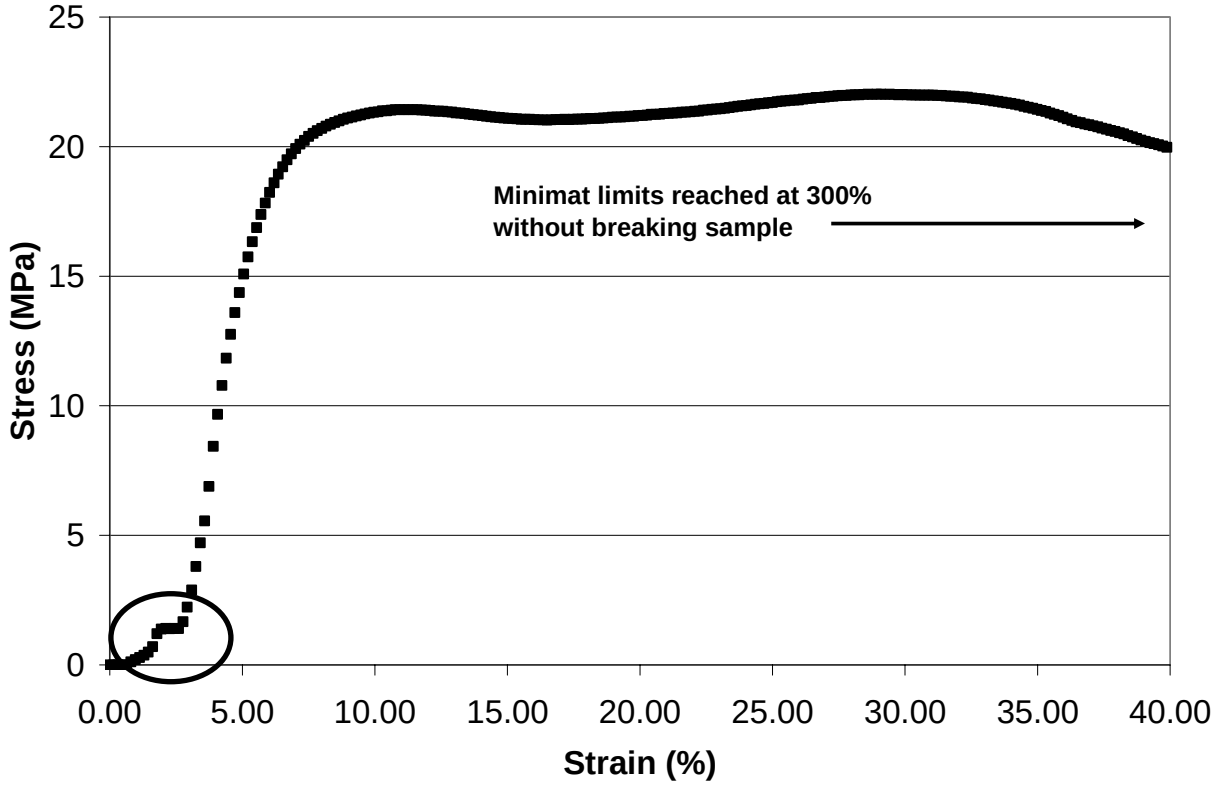

Figure 4-7 – Tensile Results for Run 20 – 100% Polypropylene

Table 4-10 summarizes the tensile results for Trial 1. The highest tensile modulus was observed with an equal amount of each filler at 35 wt% (run 10) and the lowest value was obtained with 35 wt% of acetylene black only (run 4). The tensile strength had a maximum of approximately 25 MPa and also occurred with a combination of all the filler, carbon fiber making up the majority (run 14). The weakest tensile strength was observed with 16 wt% of Vulcan black (run 6).

These values were statistically interpreted and the resulting equations and ANOVA tables are shown in Equation 4-4 and Table 4-11 for tensile modulus and Equation 4-5 and for tensile yield strength. The correlation for the tensile modulus was very high, but the analysis involving the tensile yield strength lacked correlation with and R^2 value of only 0.6950. This low value was attributed back to the problems of measurement discussed previously.

Table 4-10 – Summary of Tensile Results for Trial 1

RUN	Tensile Modulus		Tensile Strength (0.2% offset)	
	Average (MPa)	Standard Dev. (%)	Average (MPa)	Standard Dev. (%)
1	510.00	16.39	20.78	6.78
2	1287.33	16.34	23.15	3.14
3	463.50	18.46	12.37	19.09
4	384.00	15.10	13.46	22.69
5	1659.50	17.94	24.07	3.14
6	421.00	25.19	8.75	20.53
7	1254.00	17.15	19.86	15.97
8	1577.33	10.14	19.59	6.21
9	1435.00	14.39	23.48	13.97
10	1696.67	7.48	18.60	21.92
11	1548.00	18.69	20.96	14.82
12	1312.00	16.77	17.22	6.33
13	728.50	10.58	14.44	12.73
14	1419.67	15.76	24.70	21.54
15	852.00	7.76	19.91	18.40
16	617.5	10.65	11.07	20.95
17	698.33	24.35	15.47	21.65
18	900.50	9.19	19.54	11.91
19	1388.67	16.98	21.15	18.33
20	573.33	8.92	16.30	1.52

Tensile Modulus (MPa) = 451.13(ACB) + 488.52(VCB) + 1881.45(CF) + 521.75(PP)
2037.98(ACB)(CF) + 1641.21(VCB)(CF) + 3008.62(ACB)(PP)

Equation 4-4

Table 4-11 – ANOVA Table for Trial 1 Tensile Modulus Analysis

Source of Variance	Sum of Squares	Degrees of Freedom	Mean Square	F Value
Model	$3.682 \times (10)^6$	6	$6.136 \times (10)^5$	21.31
Residuals	$3.733 \times (10)^5$	13	$2.879 \times (10)^4$	
Total	$4.056 \times (10)^6$	19		

R-Squared	0.9077	Pred R-Squared	0.6222
Adj R-Squared	0.8651	Probability >F	<0.0001

Table 4-12 - ANOVA Table for Trial 1 Tensile Yield Strength Analysis

Source of Variance	Sum of Squares	Degrees of Freedom	Mean Square	F Value
Model	250.39	3	83.46	11.40
Residuals	109.87	15	7.32	
Total	360.26	18		

R-Squared	0.6950	Pred R-Squared	0.5290
Adj R-Squared	0.6340	Probability >F	0.0004

Tensile Strength (MPa) =29.15(ACB) – 5.23(VCB) + 44.33 (CF) + 16.86(PP)

Equation 4-5

Table 4-13 compares the coefficients of the tensile modulus and yield strength. In both cases the carbon fiber had the largest role in mechanical performance. The CF also interacted with both ACB and VCB for the modulus equation. The tensile yield strength exhibits an unusual negative value for the linear coefficient for VCB; there is no interpretation of this result.

Table 4-13 – Summary of Tensile Equations for Trial 1

Tensile Modulus Equation (MPa)		Tensile Yield Strength Equation (MPa)	
ACB	451.13	ACB	29.15
VCB	488.52	VCB	-5.23
CF	1881.45	CF	44.33
PP	521.75	PP	16.86
ACB x CF	2037.98		
VCB x CF	1641.21		
ACB x PP	3008.62		

4.1.5 Flexural Properties

The results for the flexural properties are summarized in Table 4-14 along with the standard deviation of each run. The variance for flexural modulus ranged from 3.21% to 12.30% and the variance for the flexural strength ranged from 2.18% to 10.67%. It also needs to be noted that the flexural strength values that show ‘greater-than’ (>) values are due to the Minimat apparatus having reached its maximum force. The corresponding values were not used in the statistical analysis that follows.

Table 4-14 – Summary of Flexural Results for Trial 1

RUN	Flexural Modulus		Flexural Strength (0.2% offset)	
	Average (MPa)	Standard Dev. (%)	Average (MPa)	Standard Dev. (%)
1	898	10.91	32.1	4.36
2	1738	10.70	42.3	2.84
3	942	6.37	34.2	9.65
4	1019	7.16	32.8	10.67
5	2086	4.84	>45.3	N/A
6	834	7.91	30.8	2.60
7	1214	4.70	35.1	6.84
8	1812	8.72	>43.2	N/A
9	1807	7.58	>44.8	N/A
10	1540	7.27	>44.5	N/A
11	1681	6.31	>44.3	N/A
12	1787	9.85	41.2	2.18
13	1209	4.14	36.8	7.34
14	1819	6.32	>44.7	N/A
15	871	3.21	30.3	5.61
16	912	6.69	30.5	8.85
17	1031	8.34	28.7	6.62
18	812	7.51	30.7	2.28
19	1356	7.82	38.8	5.41
20	878	12.30	30.2	4.97

The flexural modulus maximum value was 2086 MPa and occurred with 30 wt% carbon fiber (run 5). The lowest values were obtained with acetylene black (runs 15, 18). Carbon fiber also had the greatest impact on flexural strength obtaining values exceeding 45 MPa (runs 5,9,10,11,14). The lowest values were again obtained when the carbon particles had an impact.

The statistical interpretation and the resulting equations and ANOVA tables are shown in Equation 4-6 and Table 4-15 for flexural modulus, and Equation 4-7 and Table 4-16 for flexural yield strength.

$$\text{Flexural Modulus (MPa)} = 1210.76(ACB) + 1086.82(VCB) - 962.32\,(CF) + 835.93(PP) + 9014.04(ACB)(CF) + 7950.65(VCB)(CF) + 8550.58(CF)(PP)$$

Equation 4-6

Table 4-15 - ANOVA Table for Trial 1 Flexural Modulus Analysis

Source of Variance	Sum of Squares	Degrees of Freedom	Mean Square	F Value
Model	$3.434 \times (10)^6$	6	$3.724 \times (10)^5$	257.87
Residuals	$2.885 \times (10)^4$	13	2219.56	
Total	$3.463 \times (10)^6$	19		

R-Squared	0.9917	Pred R-Squared	0.9818
Adj R-Squared	0.9878	Probability >F	<0.0001

$$\text{Flexural Strength (MPa)} = 38.74(ACB) + 38.28(VCB) + 99.10\,(CF) + 29.81(PP)$$

Equation 4-7

Table4-16 - ANOVA Table for Trial 1 Flexural Yield Strength Analysis

Source of Variance	Sum of Squares	Degrees of Freedom	Mean Square	F Value
Model	200.19	3	66.73	14.15
Residuals	47.16	10	4.72	
Total	247.35	13		

R-Squared	0.8093	Pred R-Squared	0.6358
Adj R-Squared	0.7521	Probability >F	0.0006

Table 4-17 summarizes both flexural property equations for Trial 1. The yield strength equation coefficients, relative to each other, were expected, as was the trend for the tensile yield strength equation. Carbon fiber had the largest impact by almost three fold over any of the other components, and the carbon black particles both had small positive impact on the strength. The trends were very similar for flexural modulus with the exception of the carbon fiber which had a negative value. This seems very unusual, however this is balanced by the quadratic coefficients which are significantly large and all include CF.

Table 4-17 – Summary of Flexural Equations for Trial 1

Flexural Modulus Equation (MPa)		Flexural Yield Strength Equation (MPa)	
ACB	1210.76	ACB	38.74
VCB	1086.82	VCB	38.28
CF	– 962.32	CF	99.10
PP	835.93	PP	29.81
ACB x CF	9014.04		
VCB x CF	7950.65		
CF x PP	8550.58		

4.1.6 Rheology

Processability is important for the ability to apply composites to fuel cell applications do to the larger number of bipolar plates in a fuel cell stack and the need for low cost processing. A study using capillary rheometry was conducted to gain insight in the ability of the material to flow. The results are displayed in Figure 4-8 to Figure 4-11.[58] The relationship displayed in all the figures shows the non-Newtonian flow of the composite on a log-log scale and is represented by Equation 3-6 presented previously ($\eta = K\gamma^{n-1}$). In this case the y-intercept is equal to the consistency factor (K) and the slope is equal to exponential term (n-1).

Figure 4-8 gives a band of values that encompass the range of the results, and the sequential three graphs look at the results associated with the individual fillers. It is clear that the increase in the consistency factor from 0 to 16-20% was much less than the increase from 16-20% to 30-35% in all three cases. The other interesting observation was that the highest filler loading for the two carbon blacks had a higher shift on the graph than that of the carbon fiber. This result was not expected as it was anticipated that the carbon fiber would create more of a viscosity increase than the carbon particles. However, when multiple fillers are combined, the results were more expected and are discussed with the aid of a statistical interpretation.

Upon statistical analysis the exponential term did not change from run to run and had an average value of 0.267 with a standard deviation of 0.039 (14.7%). This was not the case with the consistency factor (K). The consistency factor's statistical analysis yielded an R^2 value of 0.8090 and a quadratic model. Details of the results are displayed in Equation 4-8, Table 4-18, and Table 4-19. The quadratic model developed shows the linear terms in order of impact as CF>ACB>VCB>PP. This relationship was expected as the fiber component had the highest impact followed by the carbon particles and the polymer matrix had the least impact on increasing the viscosity. The quadratic terms represent the interaction of the various fillers, all of which had negative terms indicating that the interactions help lower the viscosity slightly. The only two quadratic terms that did not have statistical significance were the ACB x VCB and VCB x PP terms.

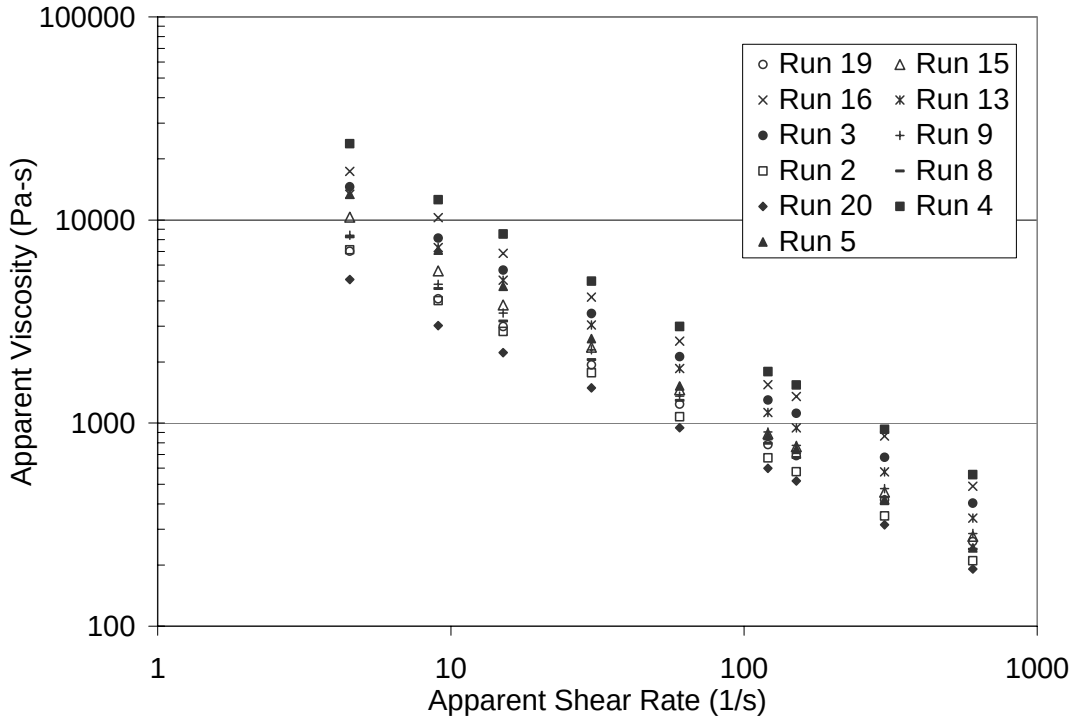

Figure 4-8 – Summary of Rheology Results for Trial 1

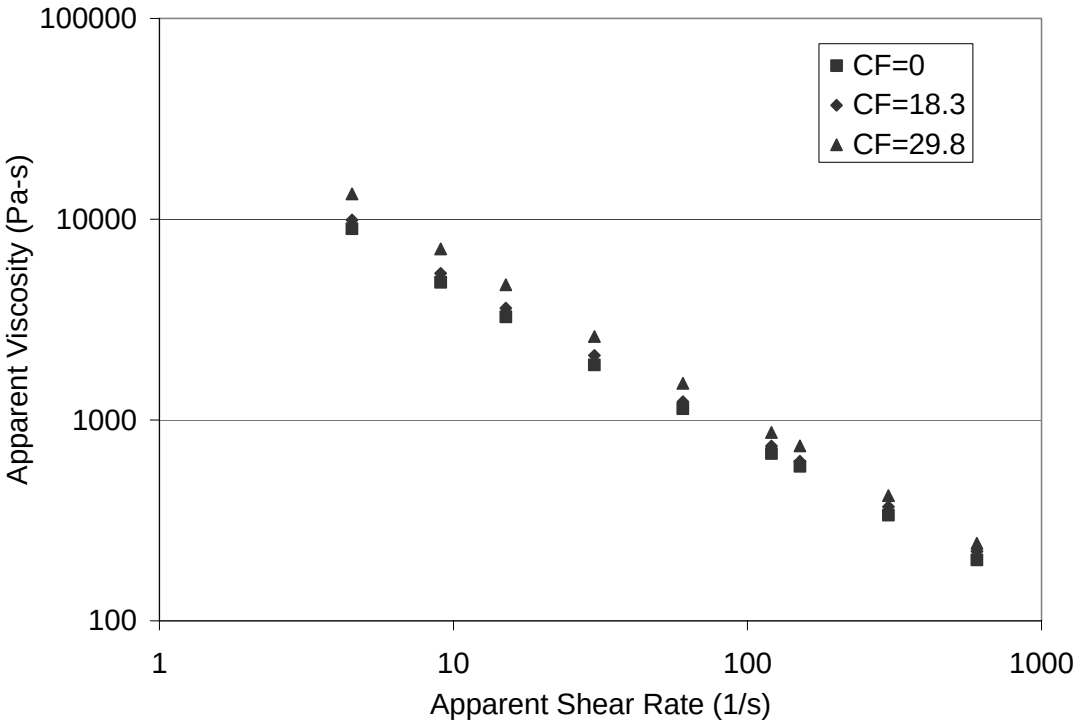

Figure 4-9 – CF-PP Rheology Results for Trial 1

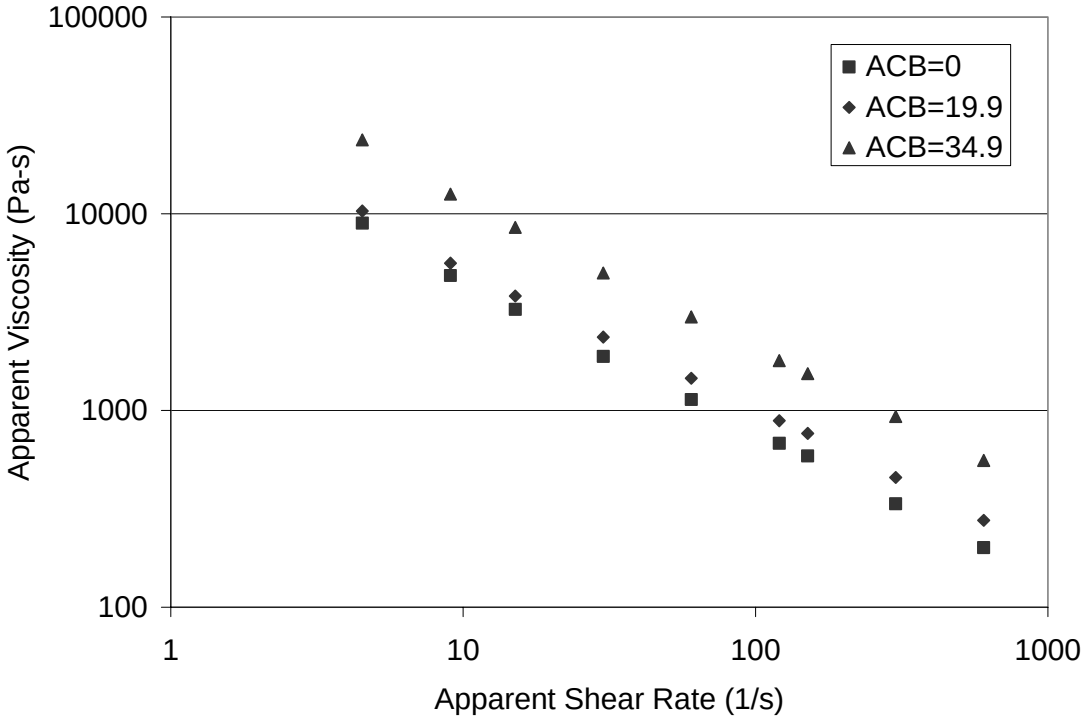

Figure 4-10 – ACB-PP Rheology Results for Trial 1

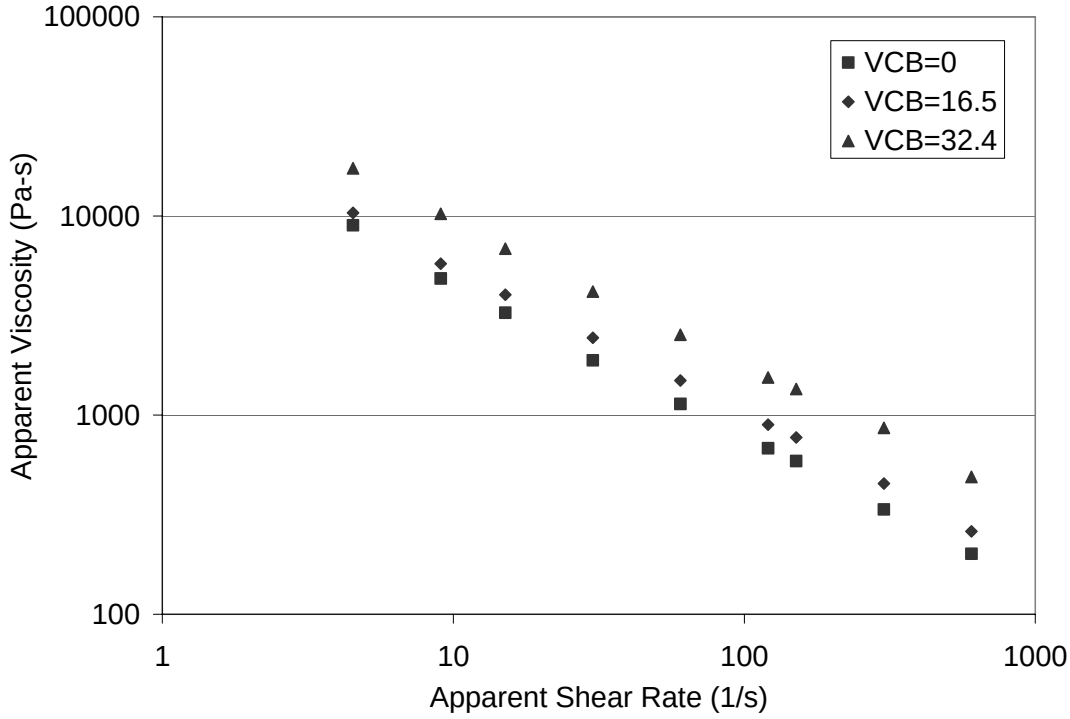

Figure 4-11 – VCB-PP Rheology Results for Trial 1

$$\text{Consistency Factor (K)} = 3.645 \times (10)^5 (ACB) + 9.675 \times (10)^4 (VCB) + 4.654 \times (10)^5 (CF) + 1.895 \times (10)^4 (PP) - 1.052 \times (10)^6 (ACB)(CF) - 3.246 \times (10)^5 (ACB)(PP) - 5.312 \times (10)^5 (VCB)(CF) - 5.140 \times (10)^5 (CF)(PP)$$

Equation 4-8

Table 4-18 – ANOVA Table for Consistency Factor (K) Associated with Trial 1 Rheology

Source of Variance	Sum of Squares	Degrees of Freedom	Mean Square	F Value
Model	$2.445 \times (10)^9$	7	$3.493 \times (10)^8$	7.26
Residuals	$5.773 \times (10)^8$	12	$4.811 \times (10)^7$	
Total	$3.022 \times (10)^9$	19		

R-Squared	0.8090	Pred R-Squared	0.1889
Adj R-Squared	0.6975	Probability >F	0.0016

Table 4-19 – Summary of Rheology Consistency Factor for Trial 1

Consistency Factor (K) $\times (10)^{-4}$
ACB: 36.45
VCB: 9.675
CF: 46.54
PP: 1.895
ACB x CF: – 105.2
ACB x PP: – 32.46
VCB x CF: – 53.12
CF x PP: – 51.40

4.1.7 Scanning Electron Microscopy

In order to understand the microstructure associated with the produced composites, scanning electron microscopy was performed for all the samples. A selected few micrographs are presented. Figure 4-12, Figure 4-13, and Figure 4-14 are SEM images of individual fillers in the PP polymer matrix of ACB, VCB, and CF, respectively.

Figure 4-12 shows 35 wt% Acetylene carbon black in polypropylene. The particle size varied from approximately 20-100 nm, with an average size around 40 or 50 nm, comparable to the mean particle size previously stated. There existed some agglomeration, but the groups of particles were distributed through out the resin.

The Vulcan carbon black microstructure was similar to the Acetylene carbon black with an average particle size between 60 and 80 nm. The Vulcan black in Figure 4-13 was at 32 wt% and exhibits even more agglomeration than the acetylene carbon black resulting in less distribution throughout the polypropylene. Often it is desired to distribute fillers as well as possible, but in this case the less distributed particle exhibited significantly better conductivity. Perhaps some agglomeration and "clumping" enabled better electron flow.

The Fortafil carbon fiber size had two orders of magnitude difference compared to the size of the carbon black particles. With a diameter of 6-7 microns, Figure 4-14 shows the aligned fibers at a 30 wt%. The injection molding direction in this case is shown as 'into the page'. It is easily seen that none of the fibers seem to be in contact and were separated by microns as opposed to the carbon black aggregates which were only separated by nanometers. The ability for electrons to travel through the polymer was very poor and could explain why the carbon fibers (independently from the other fillers) did not enhance the conductivity to the same extent as the carbon black particles. Figure 4-15 is another SEM image of the same CF in the PP matrix at a higher magnification and is an effective image of the voids that exist around some of the fiber, showing the poor wetting that exists between the fibers and the polymer matrix. As suggested previously this phenomenon could have a major impact on both electrical and mechanical properties. Future work to minimize this problem could serve to affect the properties dramatically.

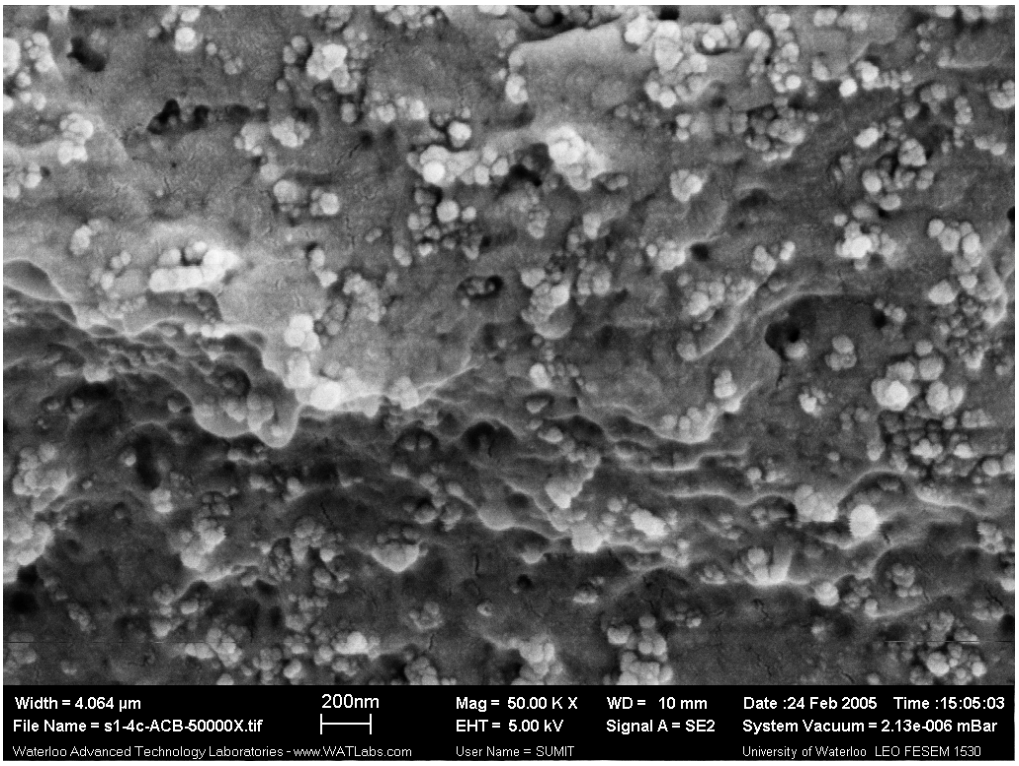

Figure 4-12 – 35 wt% Acetylene Carbon Black in Petrothene Resin - SEM Micrograph at 50000X

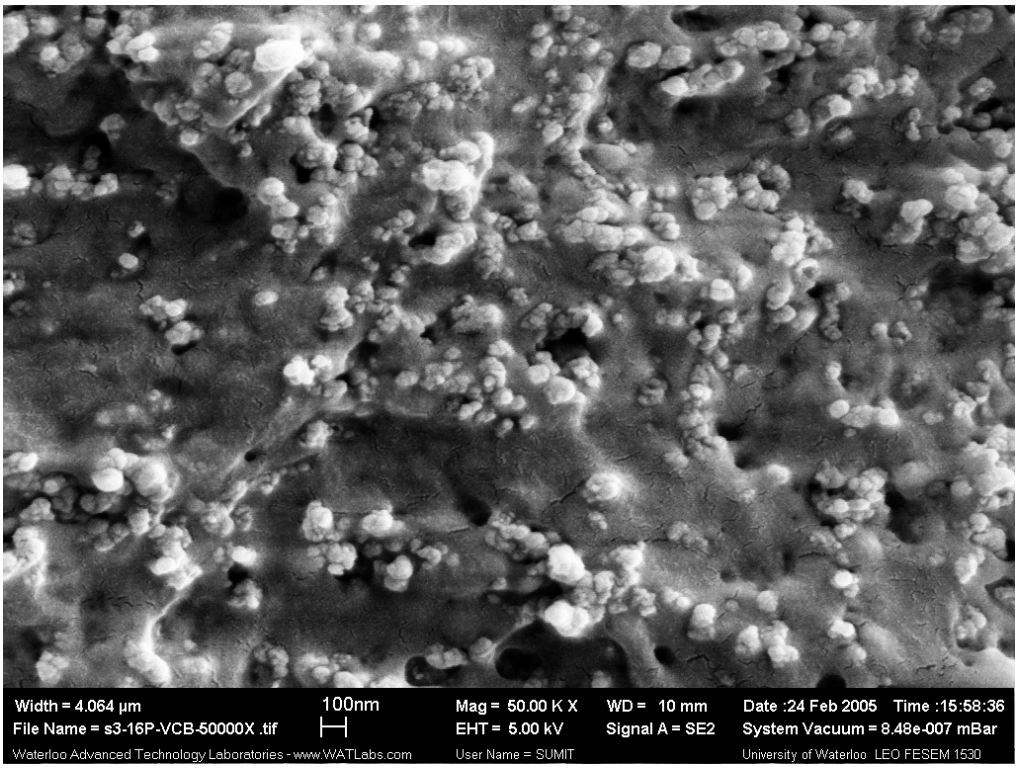

Figure 4-13 – 35 wt% Vulcan Carbon Black in Petrothene Resin - SEM Micrograph at 50000X

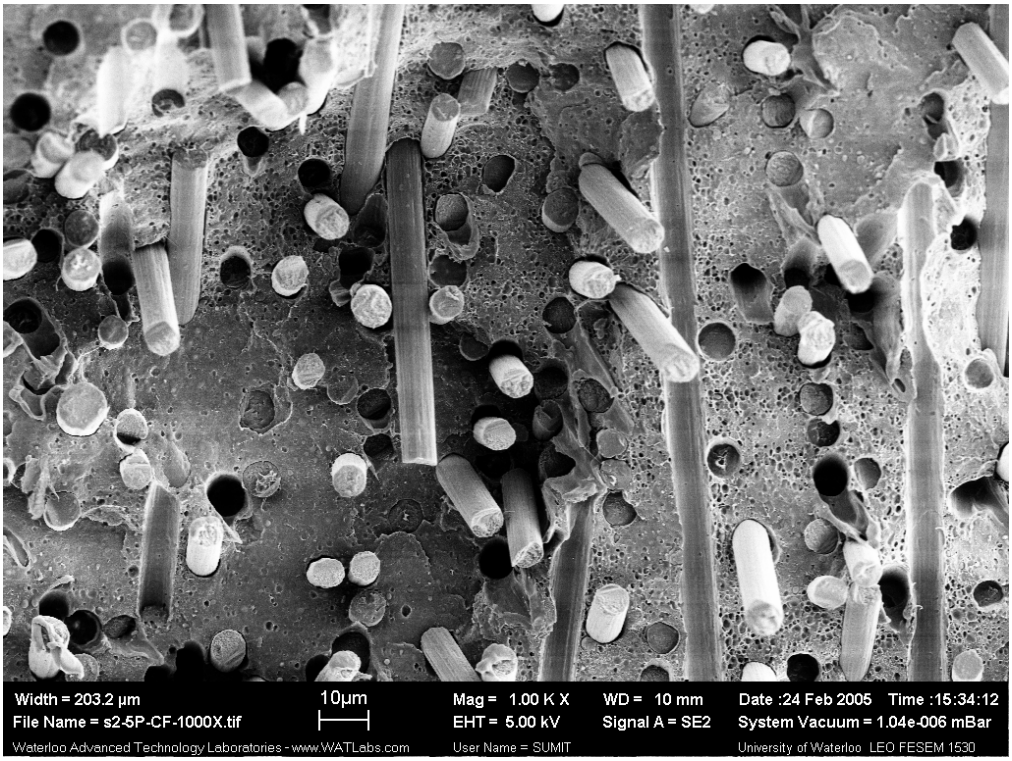

Figure 4-14 – 35 wt % Carbon Fiber in Petrothene Resin - SEM Micrograph at 1000X

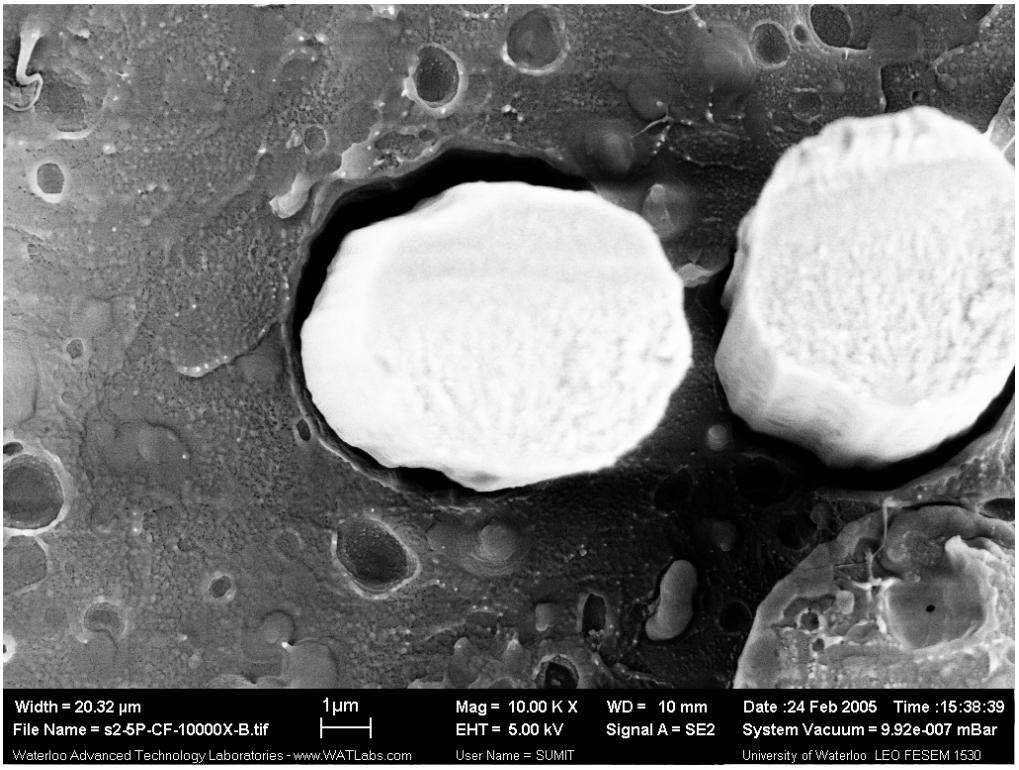

Figure 4-15 – 35 wt % Carbon Fiber in Petrothene Resin - SEM Micrograph at 10000X

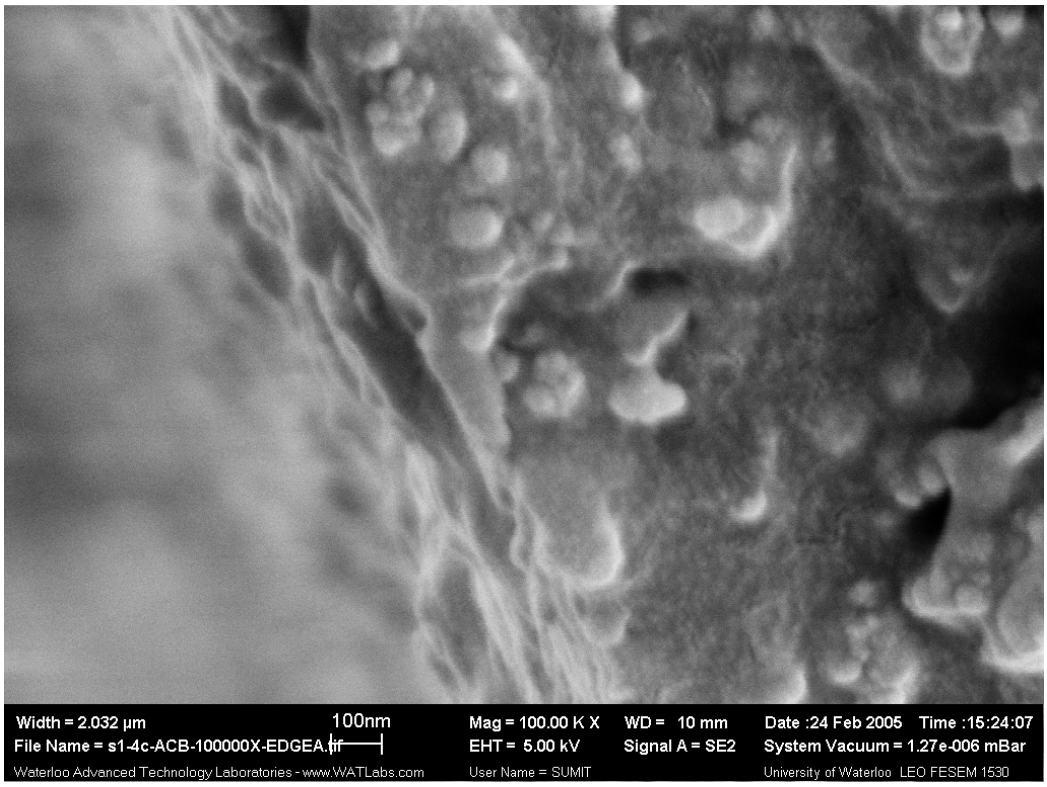

Figure 4-16 – ACB Particles at Edge of Sample - SEM Micrograph at 100k X

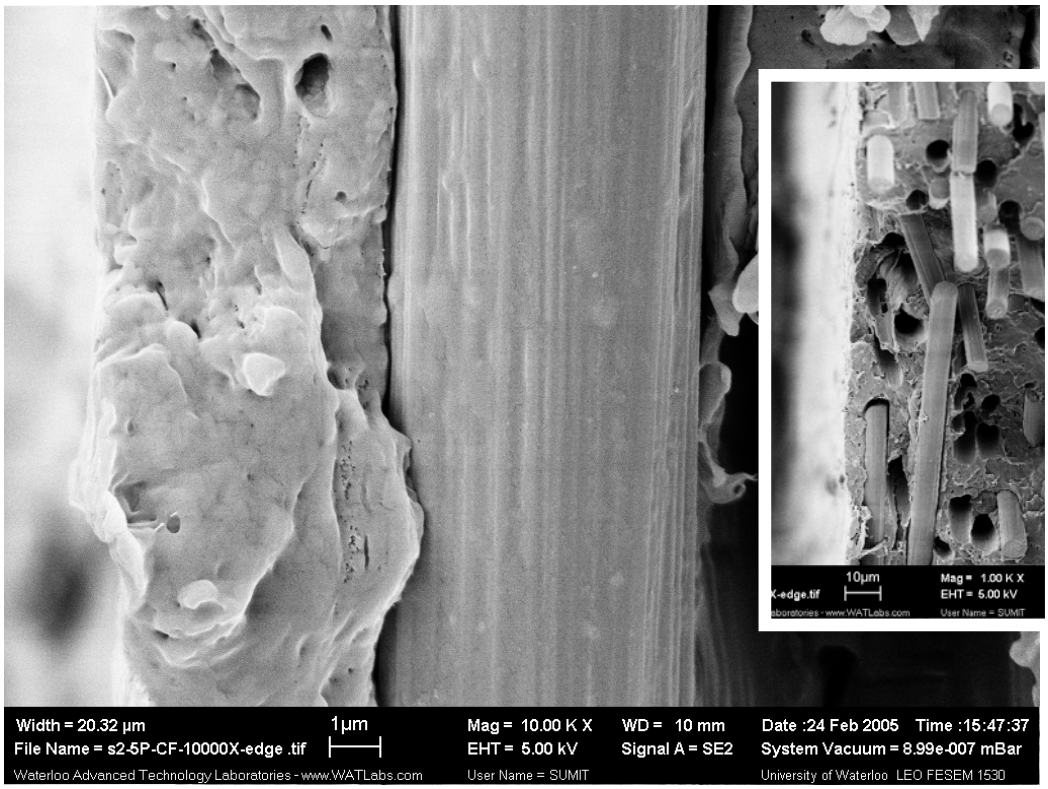

Figure 4-17 – Carbon Fiber at Edge of Sample - SEM Micrograph at 10k X & 1000X

As a result of the polymer processing method (injection molding) there inherently was a polymeric skin at the surface. The micrographs in Figure 4-16 and Figure 4-17 showed this phenomenon for both the small carbon particles and the carbon fibers, respectively. The particles penetrate very close to the edge, within nanometers, where as the fibers are two or three orders of magnitude further away. This could be another reason for the poor performance of the fibers, especially when only the filler were used. This result is also shown in Figure 4-18 especially with respect to Method 1, which takes advantage of the fiber alignment. The CF on its own had very low conductivity, but when combined with either of the other two fillers the conductivity increased significantly. This is very promising, however the wetting issue discussed early still limited the impact of the CF as the VCB on its own still produces better results.

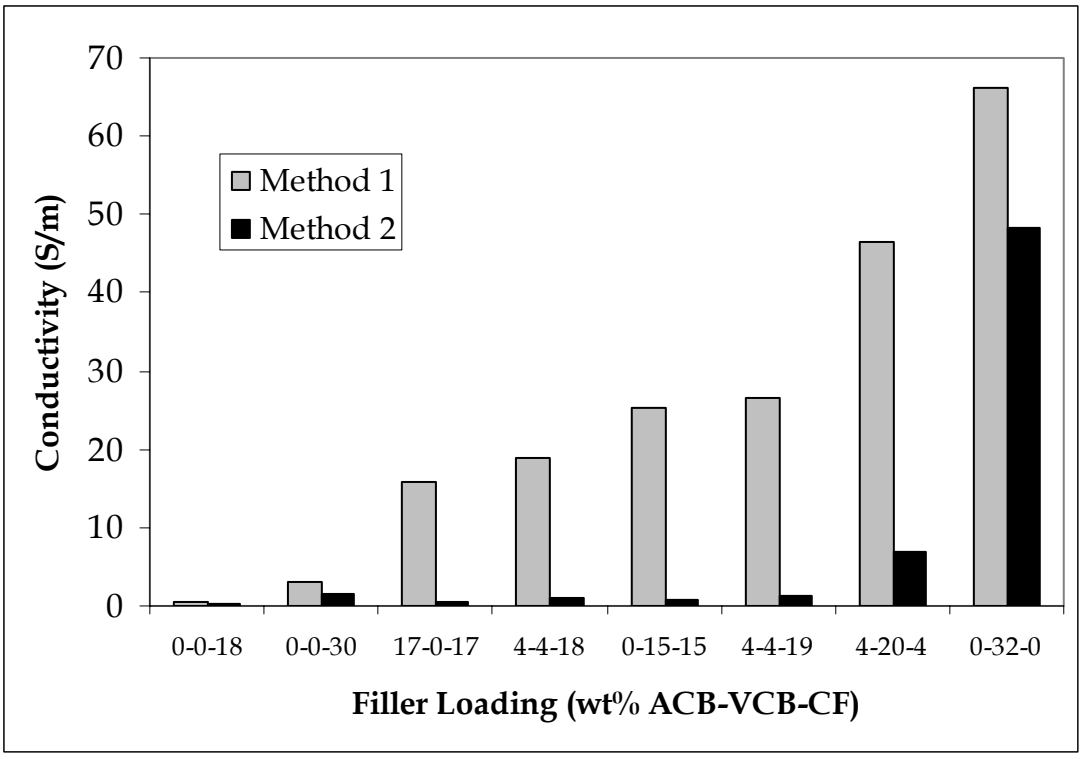

Figure 4-18 – Effect of Carbon Fiber Content on Conductivity

4.1.8 Literature Comparison

In comparison to the literature targets shown in Table 4-20, a great deal of improvement is needed before the targets are achieved. The mechanical properties are achievable with higher filler loading; however, the very low fraction of the conductivity target is of great concern.

From the results of Trial 1 the possible changes that can be explored include:

- increase in filler loading
- processing to limit fiber shearing and orientation
- processing additives to improve filler interaction and fiber wetting

Table 4-20 – Comparison of Literature Targets to Trial 1 Results [13]

	Literature Target	Trial 1 Results	Fraction of Target
Conductivity (S/cm)	>100	0 – 2 (Method 1) 0 – 0.5 (Method 2)	2% 0.5%
Tensile Strength (MPa)	41	9 – 25	61%
Flexural Strength (MPa)	49 – 59	30 – >45	76% – 92%

The first suggested change, increasing filler loading, was the focus of Trial 2 conducted during this work. Since the number of possible trials was limited by resources and time the second trial will looked at only one filler ratio and tried to obtain the composite's percolation 'S-curve'. The filler ratio used was 1:1:1 as it showed the most promise for conductivity synergy using the Method 1 conductivity measurement technique.

4.2 Trial 2 – Percolation 'S – curve'

As discussed previously the transition from Trial 1 to Trial 2 shifted the focus from a general experimental design space to a percolation curve as a function of filler loading for an equal filler ratio of the three fillers (1:1:1).

4.2.1 Thermal Gravimetric Analysis

Thermal gravimetric analysis (TGA) was used to determine the actual filler loading for each sample within each Trial 2 run. In order to better understand the variance of this developed method an analysis of variance was conducted using the master batch. The analysis consisted of two parts. The first part examined the sample population deviation from five different samples in the same run. The mean was 53.87% and the standard deviation was 0.35%. The second part examined the sample population deviation from five different locations in the same sample. The mean was 53.75% and the standard deviation was 0.34%. The 95% confidence interval using a 2 sided t-test is +/- 0.43% for each analysis. The TGA results in Figure 4-19 populates the Trial 2 TGA runs, note there are some small deviations with values of the finishing sample weight on both sides of the axis. With such small deviations the TGA method showed a large degree of accuracy within the sample populations. The determination of the actual (after processing) filler loading by using TGA was conducted in order to confirm the actual loading levels. It was important to have this confirmation due to the variations of feed rate and hopper mixing inherent in the process. The Trial 2 results followed closely with the targeted filler loading. The complete list of results is shown in Table 4-21.

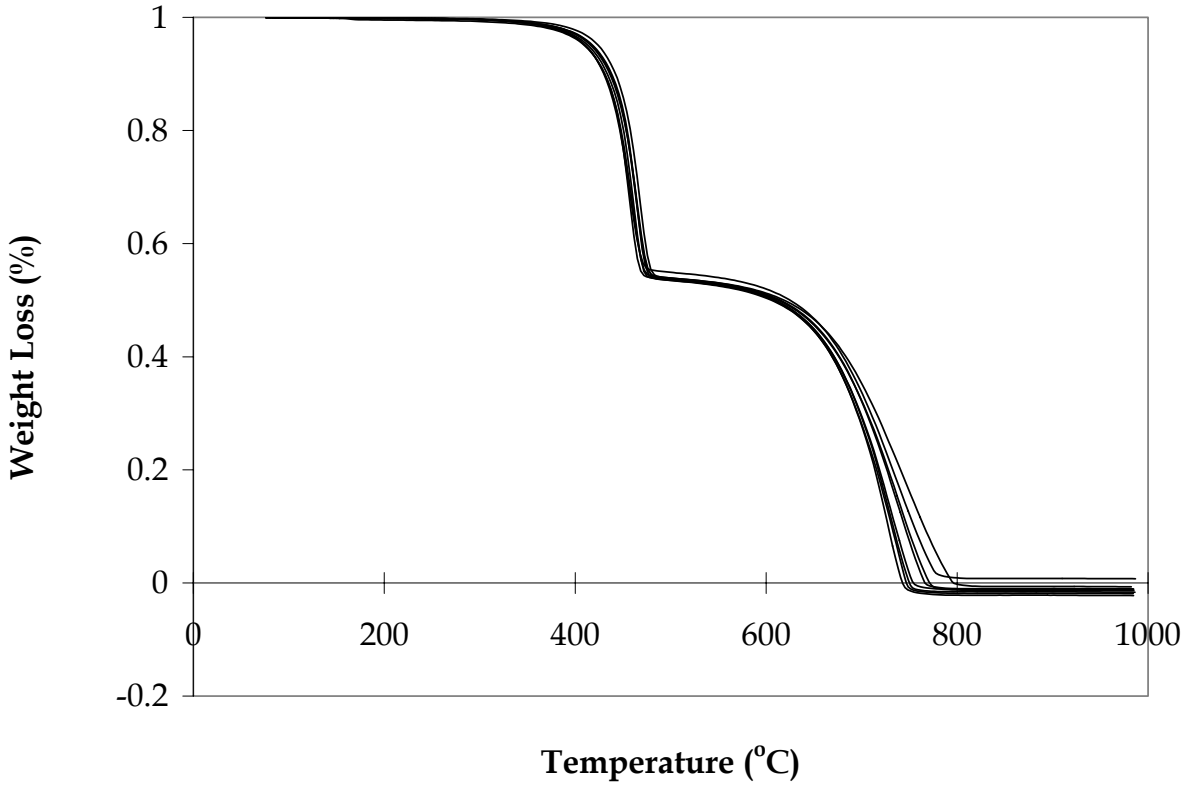

Figure 4-19 – TGA Graphs for Variance Study

Table 4-21 – Actual Filler Loading (wt%) – Trial 2

Run	Filler	Polypropylene
1	0	100
2	53.81	45.74
3	48.97	51.03
4	39.23	60.77
5	28.97	71.03
6	17.98	82.02
7	6.40	93.60

4.2.2 Density Measurement

The values for the density measurements and the corresponding standard deviations (error bars) are presented graphically in Figure 4-20. As expected the density of the samples increased as the filler loading increased with the maximum density of 1.20 g/cm^3 occurring in run 2, which had a filler loading of 54 wt%.

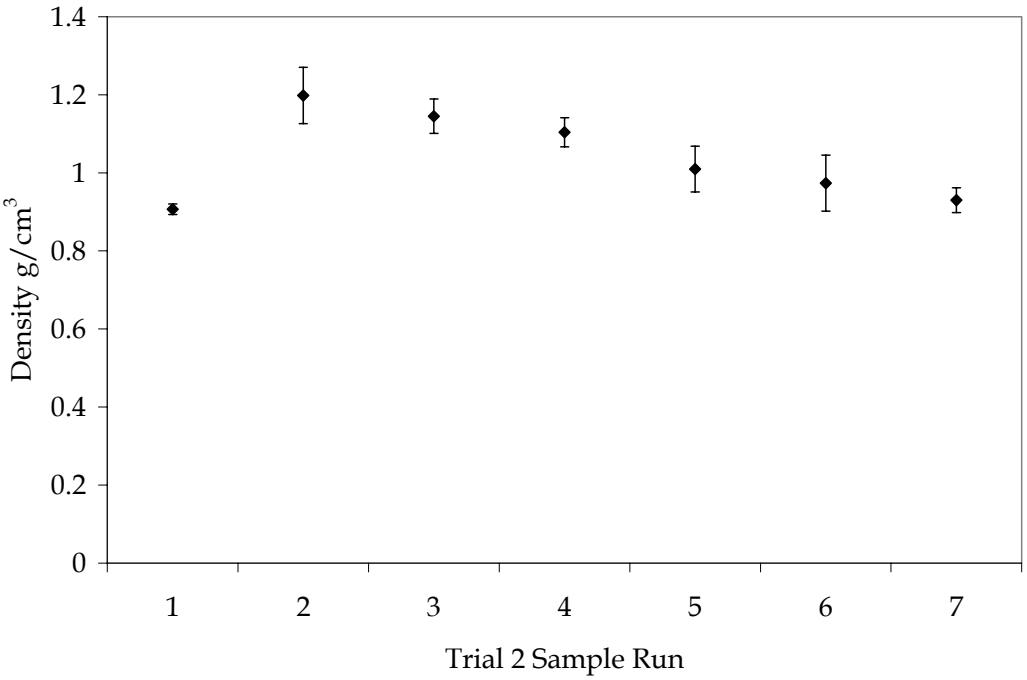

Figure 4-20 – Density of Trial 2 Experimental Runs

Table 4-22 – Actual Filler Loading (vol%) – Trial 2

Run	Filler	Polypropylene	Voids
1	0	100	0
2	33.62	57.83	8.54
3	29.92	62.48	7.60
4	22.94	71.23	5.83
5	16.21	79.67	4.12
6	9.62	87.94	2.44
7	3.27	95.90	0.83

Following the determination of the actual filler loadings the volumetric filler loading can be determined similar to the Trial 1 calculations. The maximum filler loading which occurred in run 2 only reached 34% on a volumetric basis as compared to 54% on a weight basis. The results with standard deviations are shown in Table 4-22.

4.2.3 Conductivity

The second Trial focused only on a 1:1:1 ratio of fillers with the goal of studying the percolation effects, including the percolation threshold. The Trial 2 results are presented in Table 4-23 and the trends associated for both methods are shown for both weight and volume fractions in Figure 4-21 and Figure 4-22. A portion of the percolation 'S-curve' was obtained along with the percolation threshold which varied depending on the measurement technique as well as the loading basis, volume or weight. The highest value attained occurred at the maximum filler loading of 54 wt% and had a value of 1200 S/m and 220 S/m for Method 1 and Method 2, respectively. The trends between the figures are similar when comparing the same method techniques. The difference is simply a shift to the left for the volume fraction as compared to the weight fraction.

Table 4-23 – Method 1 and 2 Conductivity Results for Trial 2

Filler Loading (wt%)	Method 1 Conductivity (S/m)		Method 2 Conductivity (S/m)	
	Average	Stnd Dev	Average	Stnd Dev
53.81	1203.77	55.14	267.80	9.88
48.97	879.52	42.10	158.76	10.91
39.23	328.97	32.48	19.23	4.00
28.97	47.01	31.47	0.46	0.29
17.98	0	N/A	0.09	0.02
6.40	0	N/A	0.05	0.07
0	0	N/A	0.02	0.03

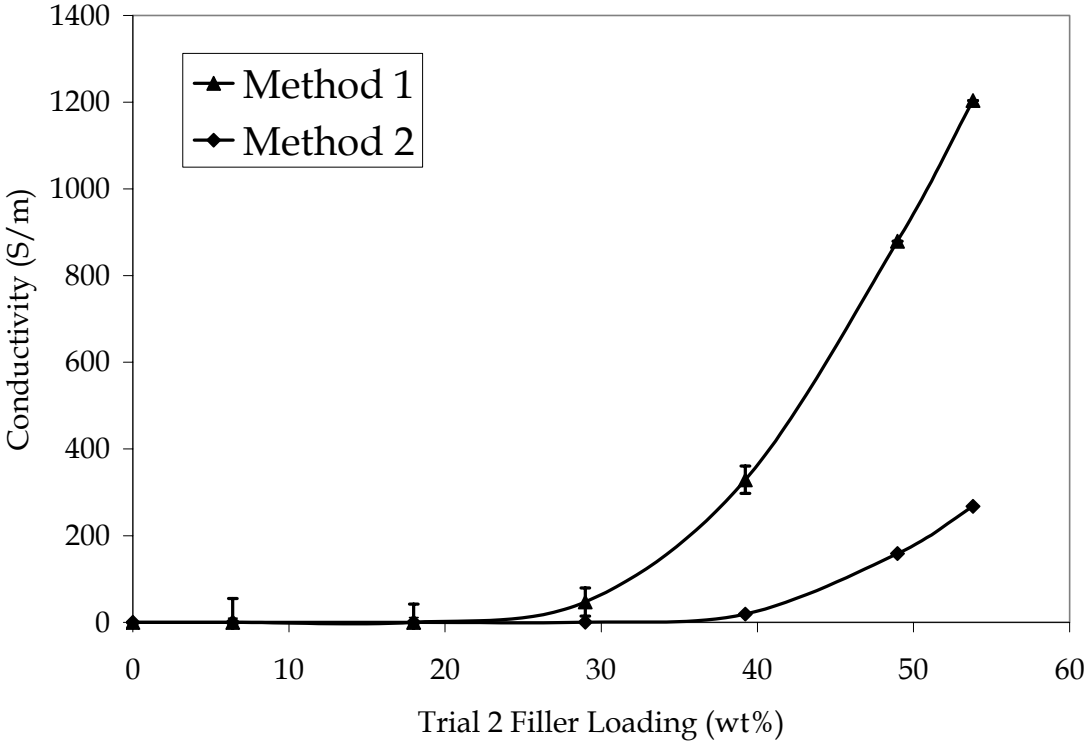

Figure 4-21 – Conductivity Results for Trial 2 in Weight Fraction Loading

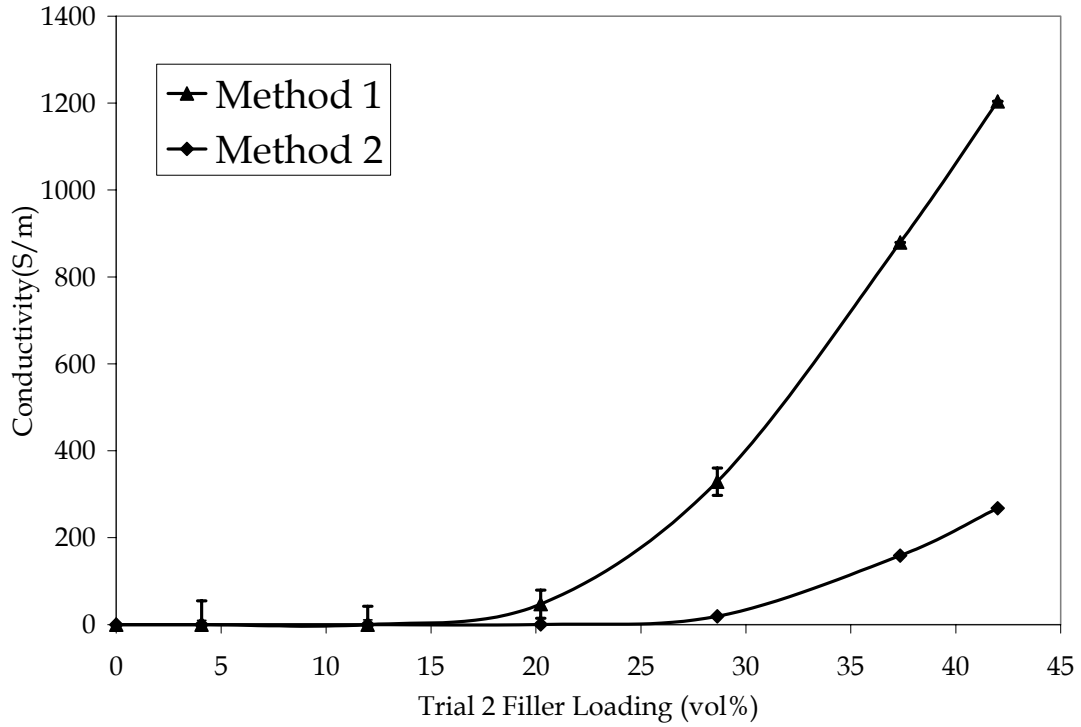

Figure 4-22 – Conductivity Results for Trial 2 in Volume Fraction Loading

For higher filler loadings the conductivity would increase until it reaches a point at which the conductivity would plateau, similar to the initial conductivity values, completing the 'S' shape. In this study these higher loadings could not be obtained because the blends could not be processed.

The difference between Method 1 and Method 2 is clearly shown in each graph. Method 2 had a percolation curve much flatter than Method 1 in both cases. The flat curve suggested that the maximum point of the percolation curve was significantly less for the Method 2 technique.

The percolation threshold seemed to be approximately 30 wt% (or 20 vol%) for Method 1, while the point for Method 2 was much higher at approximately 40 wt% (or 30 vol%) for Method 2. This difference would play a significant role in the effectiveness of the material. If the percolation threshold was lower, the linear portion of the conductivity increase would become significant at lower filler loadings. The slope of the conductivity versus filler loading line, if similar in both methods, would peak sooner for the lower percolation threshold and the processability of the material would be more viable at the higher conductivity regime.

4.2.4 Tensile Properties

The Trial 2 mechanical properties were measured in both the axial (parallel to injection flow) and transversal (perpendicular to the injection flow) modes for this trial. The tensile yield strength results and trends are presented in Figure 4-23. There was adequate correlation in each case as shown through the R^2 value associated with each equation. The standard deviation for each run is also shown with the error bars in each figure. The maximum values for the yield strength was 27.7 MPa and 18.1 MPa, for the axial and transverse directions, respectively. As the filler loading increases the directional difference between axial and transverse tensile properties also increases. This relationship is anticipated since the carbon fiber loading increases proportionally to the total filler loading, which would have a positive effect in the direction of orientation, the axial direction.

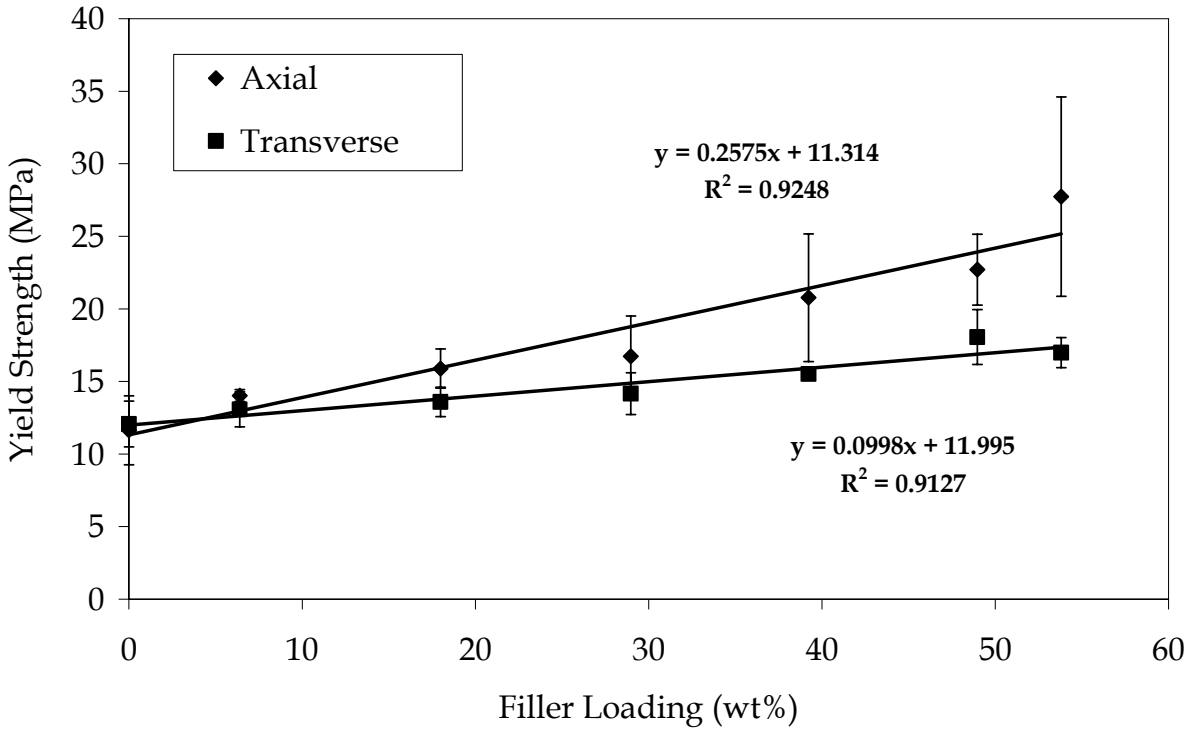

Figure 4-23 – Tensile Strength in the Axial and Transverse Directions for Trial 2

Correlations and analysis for Young's modulus have also been performed; the results and associated trends are shown in Figure 4-24. The modulus reached a maximum of 2969 MPa in the axial direction and 2369 MPa in the transverse direction. Similar to the tensile strength the axial direction increased over the transverse direction as the filler loading increased, however, this trend changes after 40 wt% filler loading. The axial direction began to decrease at higher filler loading, suggesting that the improvements added by the carbon fiber alignment were cancelled by the interaction of the carbon black with the polypropylene, reducing the slope of the stress-strain relationship.

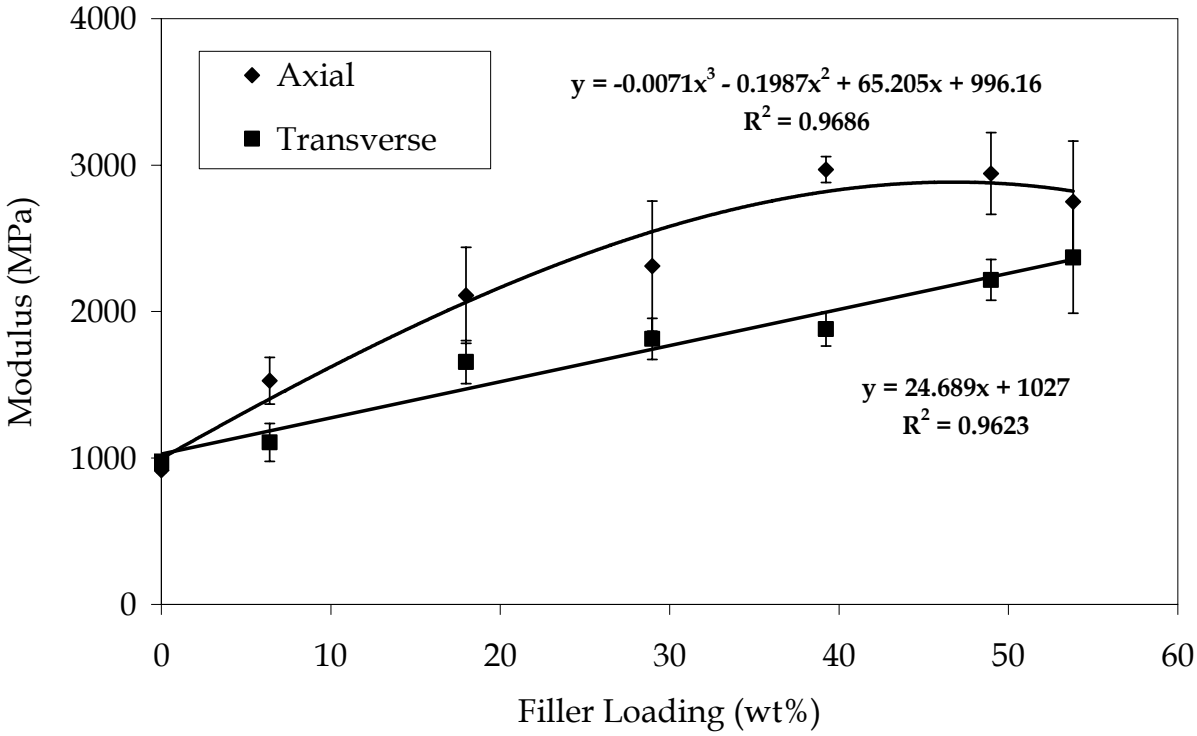

Figure 4-24 - Tensile Modulus in the Axial and Transverse Directions for Trial 2

4.2.5 Flexural Properties

The flexural strength and modulus were tested in a similar fashion to the tensile properties. The flexural strength results for the axial and transverse directions along with the statistical correlations are shown in Figure 4-25. The results yield maximum values of 82.8 MPa for the axial measurement and 43.4 MPa for the transverse measurement. In this case there is no difference in the values up to a filler loading of 30 wt% after which the axial direction increases significantly faster than the transverse direction. This change was associated with the interaction between the carbon fiber and the polypropylene. The transverse direction was very flat, indicating that the filler had little to no affect on the yield strength.

The flexural modulus exhibited very similar trends to that of the flexural strength and the results are shown in Figure 4-26. There was no difference in the direction of measurement up to 30 wt% filler loading, after which the axial direction increased rapidly, but the transverse direction continued the same linear increase. The maximum value for the flexural modulus was 8343 MPa and 3930 MPa for the axial and transverse directions, respectively.

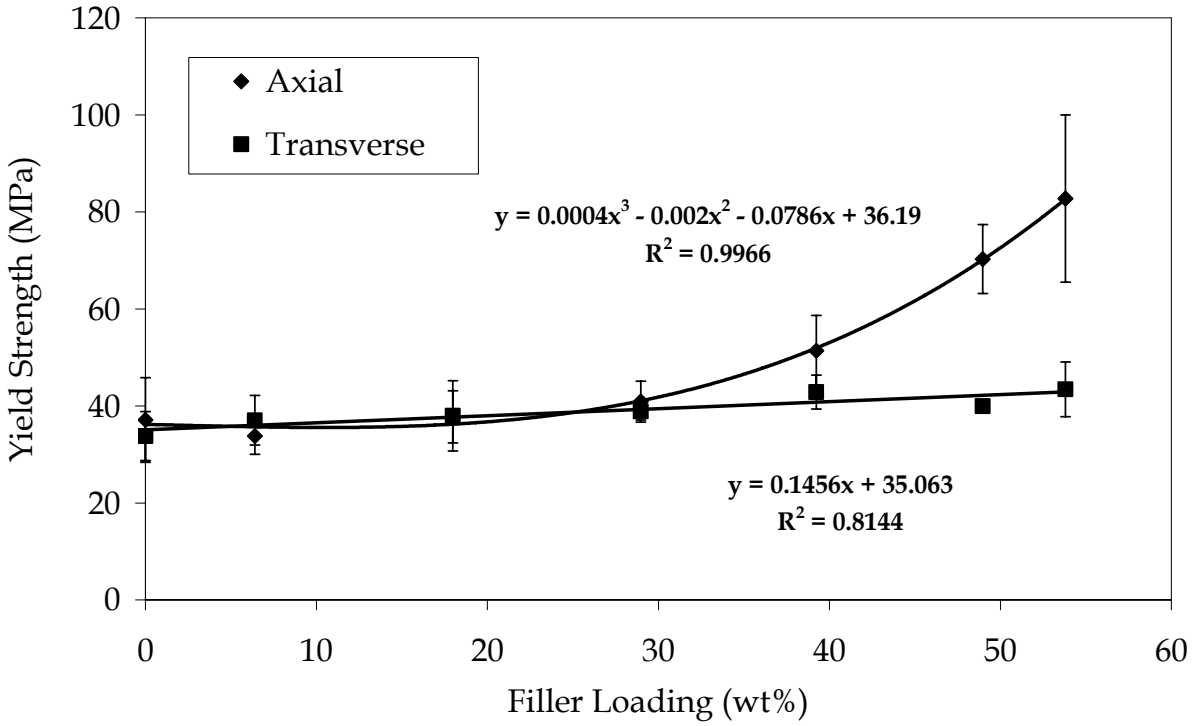

Figure 4-25 – Flexural Strength in the Axial and Transverse Directions for Trial 2

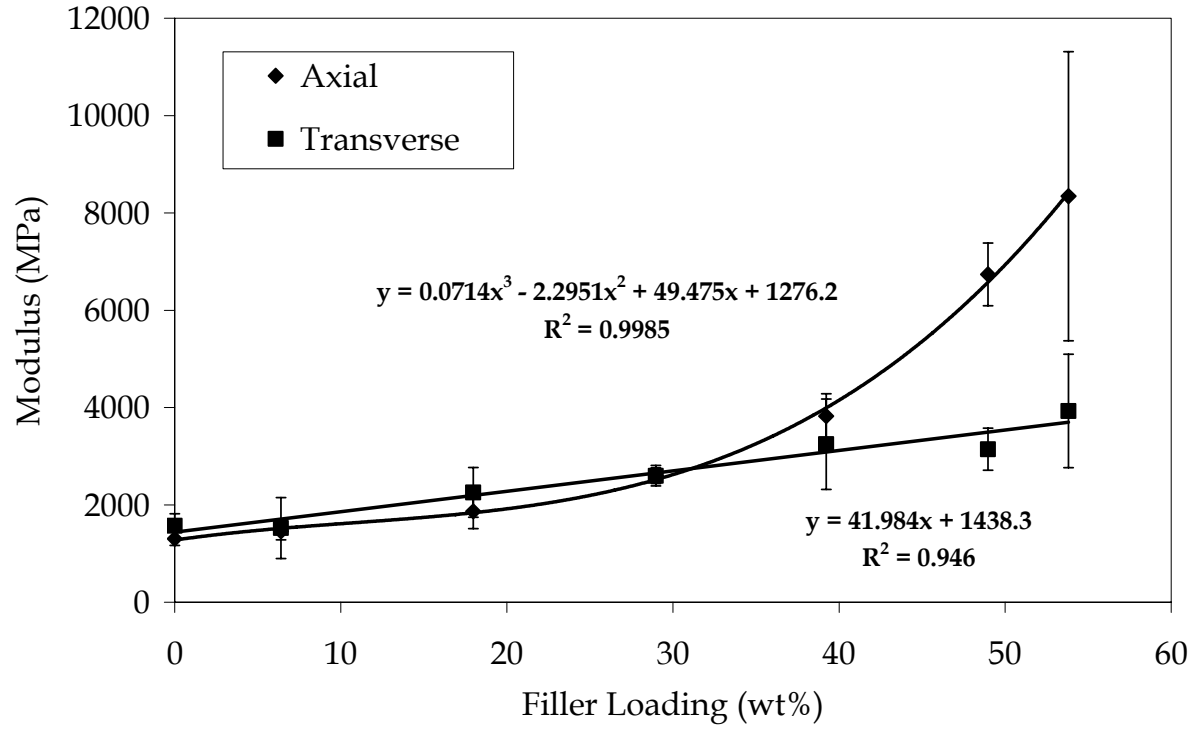

Figure 4-26 - Flexural Modulus in the Axial and Transverse Directions for Trial 2

4.2.6 Rheology

The rheology analysis was performed using capillary methods in the non-Newtonian range. Figure 4-27 presents the rheology results for the samples that maintained the 1:1:1 filler ratio. The lowest range had a filler loading of approximately 12 wt%, while the maximum filler loading was approximately 61 wt%. It should be noted that 61 wt% was not mentioned in any previous analysis due to the fact that a very small amount of this composite was produced due to extruder limitations. As a result fabrication of samples based on 61 wt% was not possible for conductivity or mechanical testing; however, rheology testing was possible.

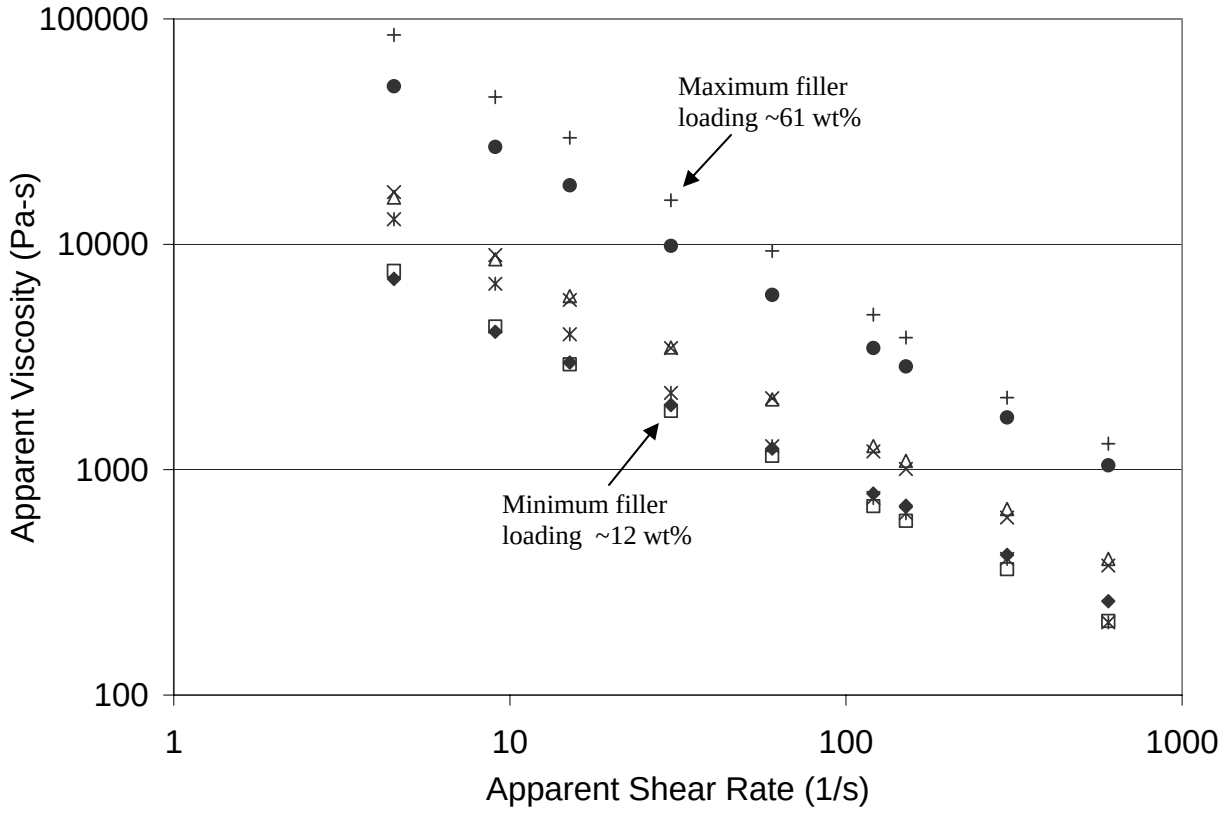

Figure 4-27 – Capilliary Rheology Range for 1:1:1 Composite Samples for Trial 2

Similar to Trial 1, in the Trial 2 analysis, it was found that the power law index for the various runs did not differ, but the consistency index varied with filler loading as shown in Figure 4-28.

The increase of the consistency index was linear with respect to low filler loading and was independent of the filler type. The 1:1:1 combination of all three fillers was consistent with the individual fillers, rising linearly up to 40 wt% and then increased rapidly from 40 to 60 wt%. The sudden increase indicated a threshold point around 40 wt% by which the ability for the composite to flow deteriorates quickly. Note that fill levels in the upper range were desired for the required high conductivity. In this sense, the processability decreased as conductivity increased, so these properties must be balanced.

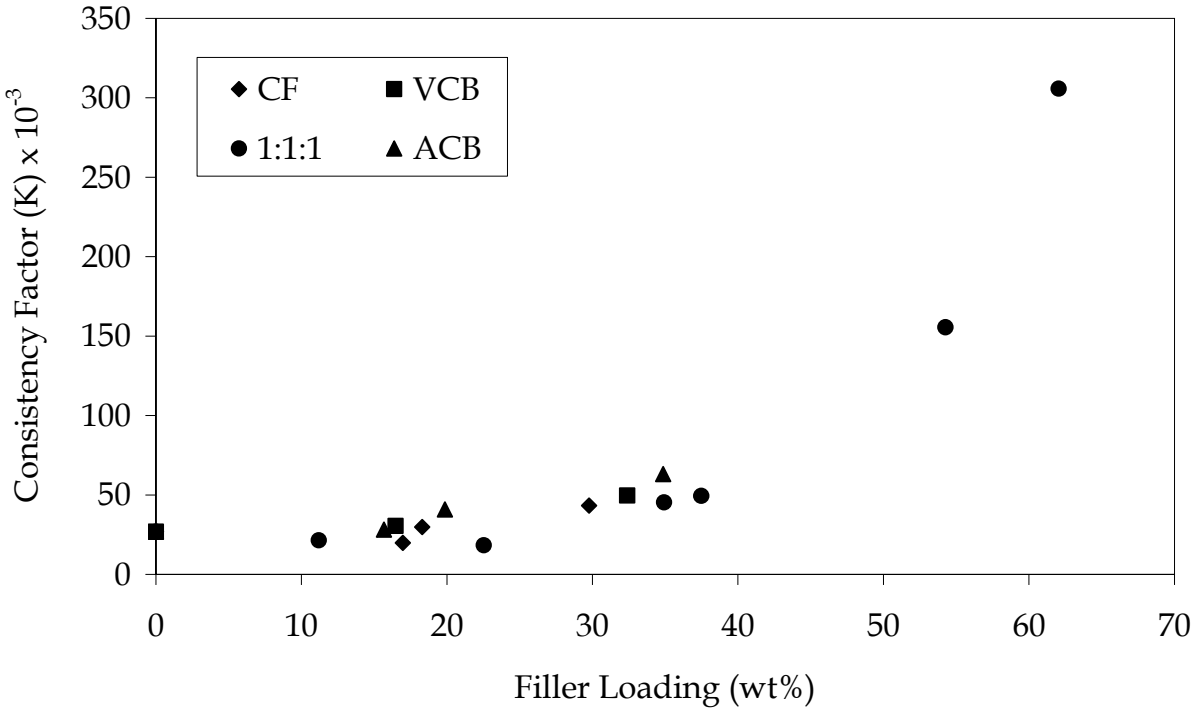

Figure 4-28 - Consistency Index for Each Filler and the 1:1:1 Filler Combination

4.2.7 Scanning Electron Microscopy

In order to investigate the trends that have been observed, it is important to investigate the microstructure of the samples. As suggested in the discussion of Trial 1 there were a number of phenomena that contributed to the electrical and mechanical property results. The microstructure discussion will include a comparison between low and high filler loading in general, carbon fiber alignment in the composites, and edge/surface composition.

The low and high filler loading differed by the population of the filler observed within the matrix. Figure 4-29 and Figure 4-30 compare the microstructure differences between filler loadings of 18 wt% and 50 wt%, respectively. The density of the carbon fiber and the carbon black particles were widely distributed in Figure 4-29, where the concentration of fibers and density of carbon particles in Figure 4-30 were increased creating a 'grainy' appearance.

In many of the presented micrographs, Figure 4-29 through Figure 4-31, it is easy to see the fiber alignment into and out of the page (which was along the injection mold direction); there were however still some disordered fibers. The injection molding direction (also into the page) was inherently responsible for the fiber alignment observed. This alignment would enhance the conductive and mechanical properties in the direction of the alignment. However, it will not help the properties perpendicular to the alignment. The addition of carbon fibers to the composite also hindered the rheology and ultimately the processability of the material.

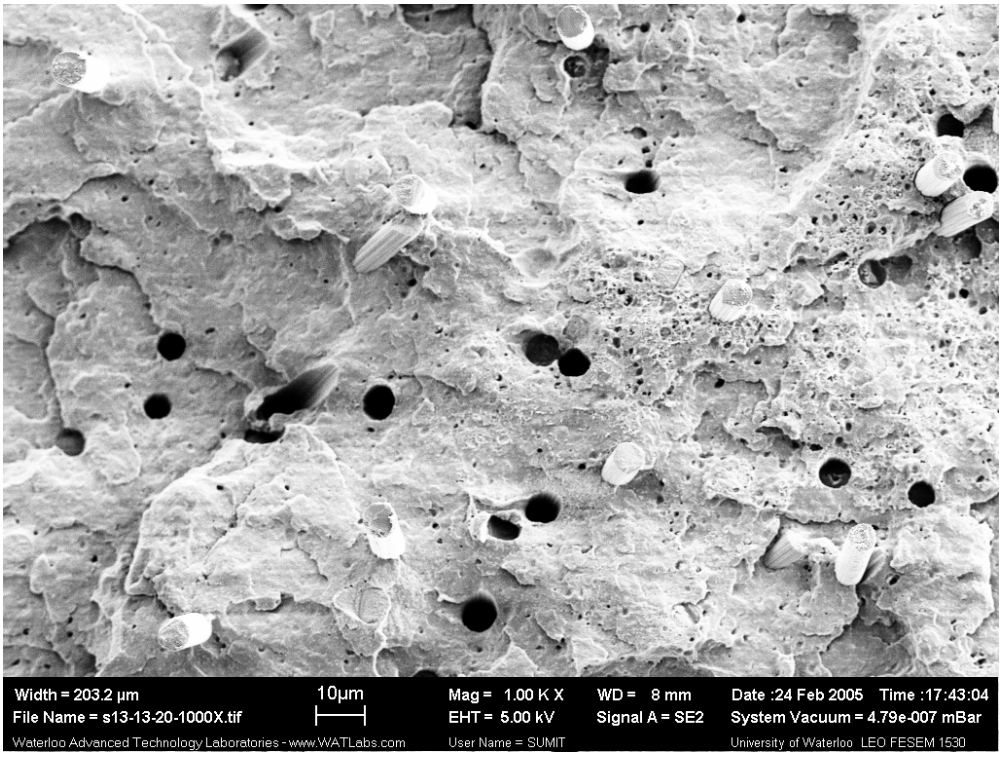

Figure 4-29 – SEM Micrograph of 18 wt% 1:1:1 Composite Sample (1000 X mag.)

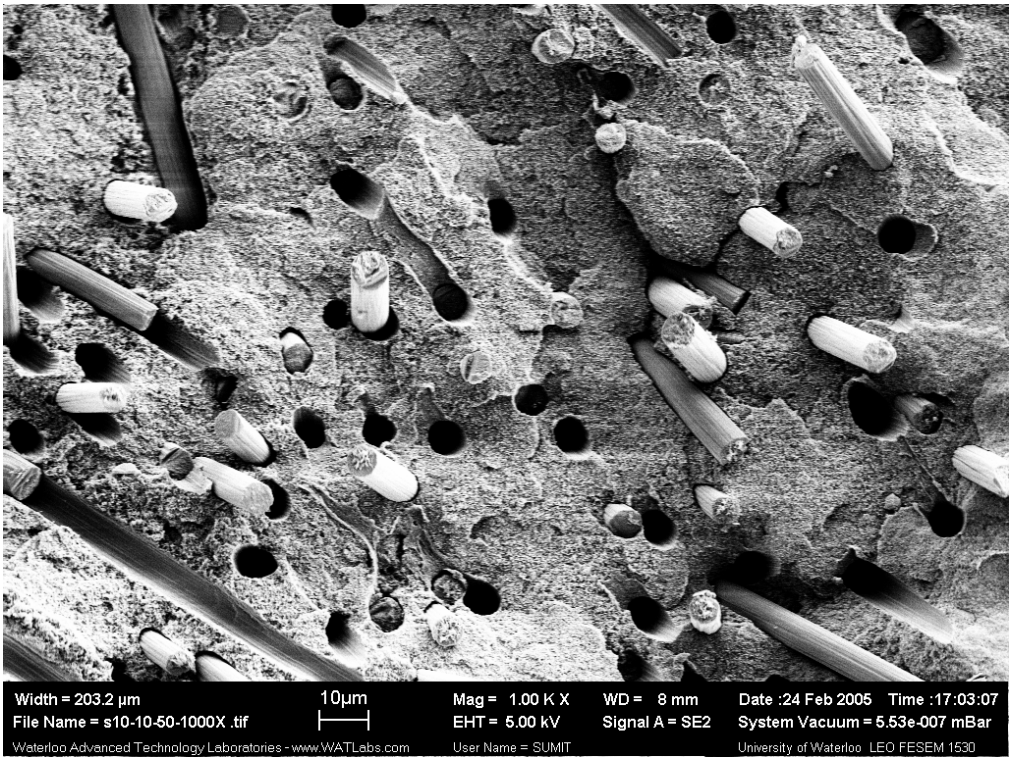

Figure 4-30 - SEM Micrograph of 49 wt% 1:1:1 Composite Sample (1000 X mag.)

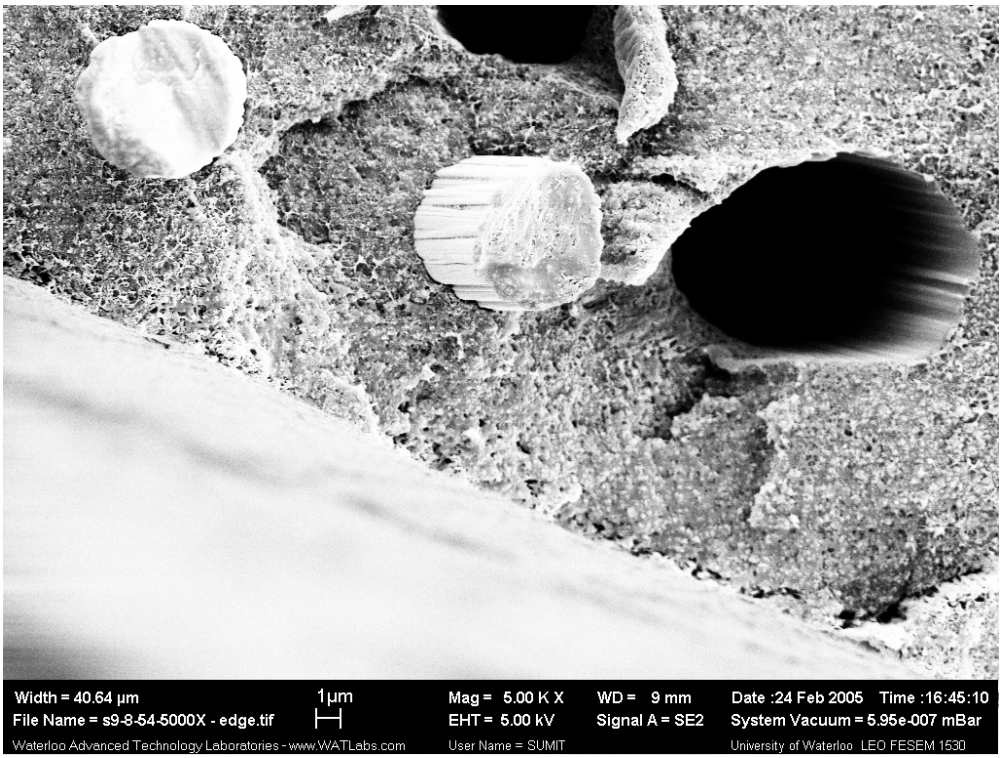

Figure 4-31 – SEM Micrograph of a 54 wt% Composite at the Sample's Edge (5k X mag.)

The final point of interest for the microstructure of Trial 2 samples was the composition and structure at the edge of the sample. In Figure 4-31 the micrograph shows the fibers much further from the edge than the grains of the carbon in the polymer matrix. This contributes to the lack of carbon fiber contribution (especially on its own) to the conductivity.

Zooming in closer the micrograph shown in Figure 4-32 accentuates the degree which the smaller particles can penetrate the edge of the sample. The figure also illustrates the lower filler density observed at the edge of the sample. This more concentrated polymer layer not only lacks filler density it also, in this case, promoted significant voids to form. The lack of filler concentration and the presence of voids at the surface would hinder the flow of electron through the sample for both measurement methods.

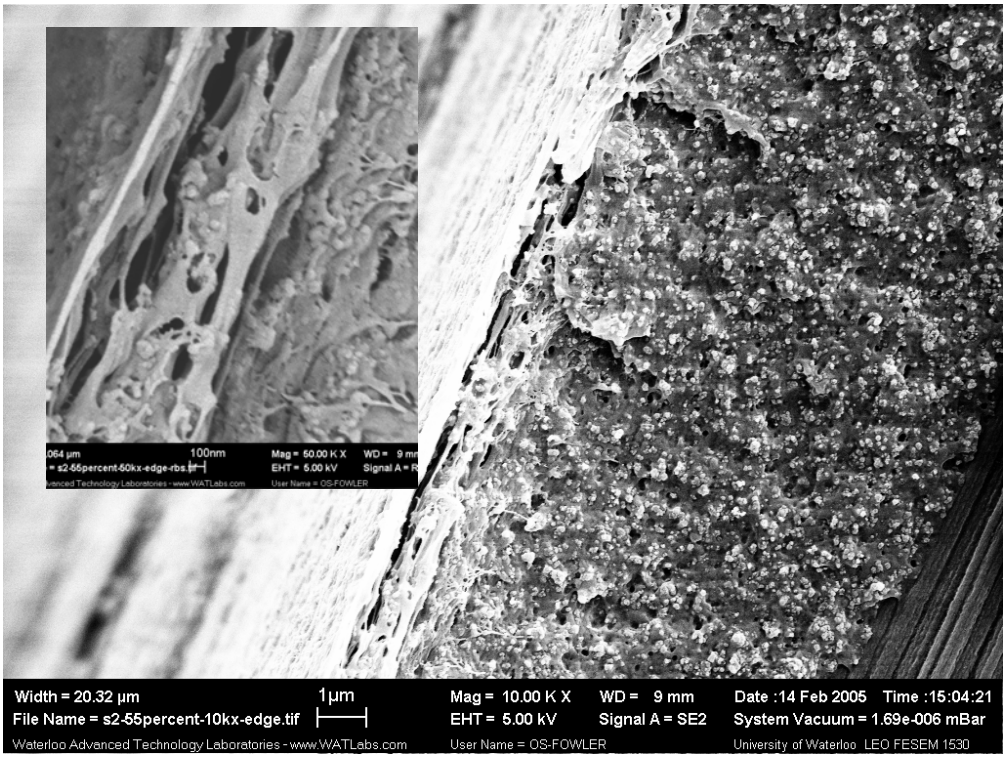

Figure 4-32 – SEM Micrograph of the Edge Composition of a 54 wt% Composite (10k X mag.)

4.2.8 In-situ Fuel Cell Testing of the Plates

The best conductivity results have been achieved with 54 wt% filler loading and a filler ratio of 1:1:1. The potential application of the developed material was best verified by exposure to

the intended application. In this case the application is a PEM fuel cell. The test apparatus and environmental conditions have been described previously in Chapter 3 and the 16 cm^2 single cell fuel cell assembly is shown in Figure 4-33. The results are presented in Figure 4-34 for both graphite (traditionally used material) and the composite material developed within this work. It should be noted that the composite plates were slightly sanded on both faces to ensure flatness for sealing.

Figure 4-33 – Fuel Cell Hardware and Composite Bipolar Plates

From Figure 4-34 the polarization curves both slope from the left to the right with the composite voltage decreasing significantly faster than the traditional graphite flow plate, as expected with lower conductivity plates. The composite material obtained a maximum current density of 0.251 A/cm^2, where as the graphite material obtained a maximum current density of 0.358 A/cm^2. These values correlated to a power output of 1.53 W and 0.78 W for the graphite and composite plates, respectively. The new developed material represented 51% performance as compared to the accepted baseline standard (graphite). This result is promising for future opportunities with composite materials within PEMFCs even though the developed material is currently inferior to the performance of graphite.

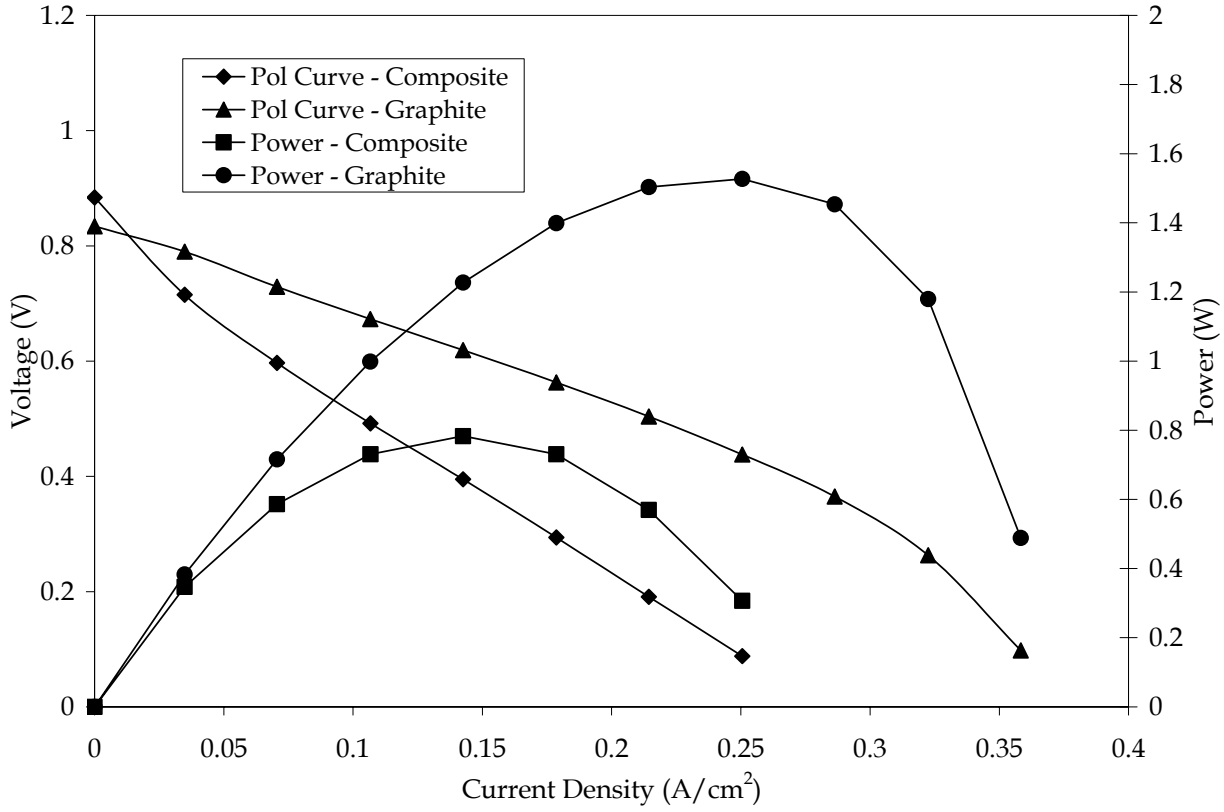

Figure 4-34 – Polarization and Power Curve Results for Composite and Graphite Bipolar Plates

The bipolar plate conductivities for both graphite and composite plates that were used in the in-situ test were also measured using both methods in order to compare conductivity measurement to fuel cell performance. Table 4-24 summarizes the results.

Table 4-24 – Conductivity of Graphite and Composite Bipolar Plates

Test Method	Conductivity (S/m)			
	Composite 1	Composite 2	Graphite 1	Graphite 2
Method 1	2617	2683	87506	88723
Method 2	199	211	2031	2191

Method 2 was the most relevant technique to compare the electrical effectiveness in the direction of interest, but did not give a value which corresponds well to Method 1 for either flow plate material. Poco reports a conductivity of 68000 S/cm (0.00147 ohm-cm) [59] for graphite plates which is reasonably close to the value obtained from the Method 1 results. The Method 2 results give values that are dramatically lower.

These results bring up two important points with respect to accepted conductivity measurement techniques. First the measurement method used must be carefully understood when comparing results and secondly the relative conductivity values do not necessarily correlate to the same ratio in fuel cell performance. Many factors influence the power output in addition to conductivity such as plate thickness, material preparation and contact resistance.

4.2.9 Literature Comparison

Comparing the results of Trial 2 to the literature targets reveals some interesting findings. In Table 4-25 the results indicate, prior to in-situ testing, a conductivity of 12.0% and 2.7% of the target for Method 1 and Method 2, respectively. These results followed from the Trial 1 results that had conductivities representing 2.0% and 0.5% of the literature target.

The molded flow plates for in-situ testing increased the achieved fraction of the conductivity target in the case of Method 1 to 26.5%, but reduced the fraction down to 2.1% for Method 2. The fact that the plates were slightly sanded for sealing has more than doubled the in-plane conductivity and has decreased (or unchanged) the conductivity in the through-plane direction. The graphite bipolar plates exhibited expected results using Method 1; however, using Method 2 the conductivity was significantly less.

Although the Method 2 measurement technique was the most relevant approach with respect to the direction of electron flow, the proposed target seemed to be more tailored to the Method 1 technique. This discrepancy is one of the many issues that are faced in fuel cell research when comparing literature results. The most interesting result, however, was the

polarization curve attained by the 54 wt% bipolar plate material. The overall goal was of course a high efficiency and power output.

Table 4-25 – Comparison of Literature Targets to Trial 2 Results [13]

	Literature Target	Trial 2 Results	Fraction of Target
Conductivity (S/cm)	>100	METHOD 1	
		12.0 (No flow path)	12.0%
		26.5 (Flow path/sanded)	26.5%
		881 (Graphite flow path)	881%
		METHOD 2	
		2.7 (No flow path)	2.7%
		2.1 (Flow path/sanded)	2.1%
		21.1 (Graphite flow path)	21.1%
Tensile Strength (MPa)	41	27.7	68%
Flexural Strength (MPa)	49 – 59	82.8	100%

4.3 Cost Analysis

Assessing the cost of producing bipolar plates based on the materials used in this project and the manufacturing technique of extrusion followed by injection molding was important for comparison, but difficult to predict accurately. Based on the cost models presented in the literature review the materials represented 45% to 70% of the overall fuel cell cost of production for mid to high production levels. This was the basis of this estimation.

Table 4-26 – Assumptions for Cost Estimations [6,33,45]

Annual part production	Material Scrap Efficiency	Material Cost as a percentage of total cost	Material Cost Reduction due to volume
100 (Low)	80%	20%	0%
10000 (Mid)	80%	45%	10%
1000000 (High)	80%	60%	20%

Other assumptions included a plate thickness of 3mm or 0.3 cm. The 1:1:1 54 wt% composite was used for calculations, which had a density of 1.2 g/cm$^{3.}$

Table 4-27 – Material Cost in US Dollars for Increasing Volumes of Production [60,61]

Annual part production	Material Cost USD/lb				Total Plate Cost USD	
	PP	ACB	VCB	CF	Small Applications 200 cm^2 / 0.20 lbs	Large Applications 800 cm^2 / 0.79 lbs
100 (Low)	1.50	2.00	1.75	11.00	$3.35/plate	$13.23/plate
10000 (Mid)	1.25	1.80	1.58	9.90	$1.31/plate	$5.22/plate
1000000 (High)	1.00	1.60	1.40	8.80	$0.86/plate	$3.40/plate

For each level of production the cost based on the cross-sectional area of the plate was $0.0168/cm^2, $0.0066/cm^2, $0.0043/cm^2, for low, mid and high production volumes, respectively. Comparing these values to the targets previously presented of $0.0045/cm^2 (USD 2003) the low production level is not competitive; mid level production does not meet the target but is still reasonably competitive. High production output meets the suggested targets. Therefore at high production levels the developed materials meet the suggested bipolar plate cost which would make fuel cell a competitive technology.

5 Conclusions

During this work two series of experimental runs were conducted in order to develop new material for polymer electrolyte membrane fuel cell (PEMFC) bipolar plates using composite blends of polypropylene, carbon blacks, and carbon fiber.

The first series of experiments used a designed experiment to establish a relationship between the four components, which covered a design space of 35 wt% of each filler and varying filler ratios. The second series focused on a 1:1:1 filler ratio and extended the filler loading up to 60 wt% in order to produce a conductivity percolation relationship.

The density associated with these materials ranged from 0.9 g/cm^3 to 1.2 g/cm^3 and combined with the ability to produce relatively thin plates (as compared to graphite) represents a power density that is very appealing to the transportation industry where both weight and volume are at a premium.

The best result was obtained in Trial 2 with a 54 wt% filler loading and a 1:1:1 filler blend. The conductivity achieved varied with the two methods of measurement used, specifically 2.2 S/cm with a fuel cell industry procedure, and 12.0 S/cm with a 4 point ASTM method. These values represent 3% to 12% of the industry target. The mechanical strength reached 27.7 MPa and 82.8 MPa for tensile and flexural strength, respectively. This represented 68% and 100% of the industry targets. Actual 16 cm^2 fuel cell plates were produced, fuel cells constructed, and the power output was found to be 51% relative to graphite plates.

The rheology results showed the consistency factor increasing linearly at filler loadings less than 40 wt%, and increased dramatically faster at greater than 40 wt% loading, suggesting processing challenges at the higher range. This was also observed in sample fabrication.

Microstructure of the samples exhibited varying degrees of particle and fiber distribution. The limiting factors that contributed to the performance of the material (specifically conductivity) were the edge effects of the composite and the synergy of the fillers. The fibers

and particles had some difficulty penetrating the most outside layers of the polymer skin within the sample creating a small insulating layer which would obstruct electron flow. The interaction between the carbon fibers and the carbon particles played an important role in the effectiveness of the fibers on conductivity. When the particles were not present the carbon fiber was very ineffective in facilitating electron flow due to inter-facial voids between the polymer and the fibers and the large distances between adjacent fibers within the polymer matrix. When particles were present to bridge the distance between the carbon fibers, their contribution to conductivity was much higher.

Fuel cell testing compared the produced material to graphite bipolar plates in a 16 cm^2 single cell fuel cell, tested on the University of Waterloo fuel cell test station. The results showed the composite material performing at 51% of the power output using the same hardware and operating conditions. This result indicated the importance of all the associated factors, not just the conductivity which was only a small fraction of that seen for graphite plates and the literature targets.

Based on the cost analysis the use of this type of composite material would meet suggested financial requirement if produced at high volumes. Low volumes showed exceedingly high costs associated with production.

The research conducted in this project has shown the potential of using composite material as bipolar plates in a PEMFC. The performance is currently below that of the industry targets but with further development could achieve acceptable performance at a significantly reduced power density and cost. These improvements once achieved will facilitate the commercial deployment of PEMFCs and the continued growth of the Hydrogen Economy.

5.1 Recommendations for Further Study

Recommendations for further study include:

- Investigation of alternative polymer resins for the composite matrix. The melt flow index as well as wetting characteristics between the polymer and the fillers is both important for the processability and property characteristics within the composite. Alternative polymers could help to improve these properties.
- The use of additional types of fillers may add an additional synergetic interaction with the composite. Specifically synthetic graphite should be investigated to determine the advantage of combining different filler types.
- The method of processing can impact the resulting material properties, injection molding of the flow path into the plates is necessary to determine if the fillers adequately reach the lands of the flow design and do not create any physical tolerances. Other types of processing including compression molding should also be considered and compared.
- The concept of over molding metal inserts into the composite may be another area of development, combing composites which are appealing in a fuel cell environment with metal which would improve conductivity could prove to be very advantageous.
- In depth mathematical model development regarding the percolation and synergy effects of each filler – polymer system would enable a better comparison of different systems and the ability to predict properties.
- Further economic analysis is key to enabling industry acceptance into the development of new technology, more robust models are necessary for the facilitation of this transition.

References

1. Schultz, M.G.., Diehl, T., Brasseur, G..P., Zittel, W., “Air Pollution and Climate-Forcing Impacts of a Global Hydrogen Economy”, Science, **302 (**2003) 624-628

2. Veziroglu, T.N., “Hydrogen Action and the Next Action: Fossil Fuels Industry and Sustainability Economics”, International Journal for Hydrogen Energy, **22(6)** (1996) 551-556

3. EG&G Services Parsons, Inc., “Fuel Cell Handbook (5^{th} ed.)”, U.S. Department of Energy Office of Fossil Energy, Morgantown, West Virginia (2000)

4. Fowler, M., Stevens, M., “MMO Interact Proposal”, University of Waterloo, September, 2003

5. LaConti, A.B., Hamdan, M., and McDonald, R.C., “Handbook of Fuel Cells”, John Wiley and Sons Ltd, Chichester, England, **3** (2003) 647

6. Bar-On, I., Kirchain, R., Roth, R., “Technical cost analysis for PEM fuel cells”, Journal of Power Sources, **109** (2002) 71-75

7. Li, X., Sabir, I., “Review of bipolar plates in PEM fuel cells: Flow-field designs”, International Journal of Hydrogen Energy, **30** (2005) 359-371

8. Heiser, J.A., “Conductive, shielding, tensile, and impact properties of carbon-filled nylon 6,6 based resins”, Michigan Technological University, Houghton, Michigan (2002)

9. Stauffer, D., “Introduction to Percolation Theory”, Taylor & Francis Ltd., Philadelphia, Pennsylvania (1985)1-11, 87-98

10. Clingerman, M.L., “Development and Modelling of Electrically Conductive Composite Materials”, Michigan Technological University, Houghton, Michigan (2001)

11. Cooper, J.S., “Design analysis of PEMFC bipolar plates considering stack manufacturing and environment impact”, Journal of Power Sources, **129** (2004) 152-169

12. Cho, E.A., Jeon, U.S., Ha, H.Y., Hong, S.A., Oh, I.H., “Characteristics of composite bipolar plates for polymer electrolyte membrane fuel cells”, Journal of Power Sources, **125** (2004) 178-182

13. Huang, J., Baird, D.G.., McGrath, J.E., “Development of fuel cell bipolar plates from graphite filled wet-lay thermoplastic composite materials”, Journal of Power Sources, **150** (2005) 110-119

14. Besmann, T.M., Klett, J.W., Henry, J.J., Lara-Curzio, E., “Carbon/Carbon Composite Bipolar Plate for Proton Exchange Membrane Fuel Cells”, Journal of the Electrochemical Society, **147(11)** (2000) 4083-4086

15. Mehta, V., Cooper, J.S., “Review and analysis of PEM fuel cell design and manufacturing”, Journal of Power Sources, **114** (2002) 32-53

16. Hentall, P.L., Lakeman, B.L., Mepsted, G.O., Adcock, P.L., Moore, J.M., “New materials for polymer electrolyte membrane fuel cell current collectors”, Journal of Power Sources, **80** (1999) 235-241

17. Hornung, R., Kappelt, G., “Bipolar plate materials development using Fe-based alloys for solid polymer fuel cells”, Journal of Power Sources, **72** (1998) 20-21

18. Ma, L., Warthesen, S., Shores, D.A., “Evaluation of materials for bipolar plates in PEMFCs”, Journal of New Materials for Electrochemical Systems, **3** (2000) 221-228

19. Hodgson, D.R., May, B., Adcock, P.L., Davies, D.P., “New lightweight bipolar plate system for polymer electrolyte membrane fuel cells”, Journal of Power Sources, **96** (2001) 233-235

20. Lee, S.J., Huang, C.H., Chen, Y.P., “Investigation of PVD coating on corrosion resistance of metallic bipolar plates in PEM fuel cells”, Journal of Materials Processing Technology, **140** (2003) 688-693

21. Kumar, A., Reddy, R.G., “Materials and design development for bipolar/end plates in fuel cells”, Journal of Power Sources, **129** (2004) 62-67

22. Wind, J., Spah, R., Kaiser, W., Bohm, G., “Metallic bipolar plates for PEM fuel cells”, Journal of Power Sources, **105** (2002) 256-260

23. Davies, D.P., Adcock, P.L., Turpin, M., Rowen, S.J., “Stainless steel as a bipolar plate material for solid polymer fuel cells”, Journal of Power Sources, **86** 2000 237-242

24. Josepha, S., McClurea, J.C., Chianellia, R., Picha, P., Sebastian, P.J., “Conducting polymer-coated stainless steel bipolar plates for proton exchange membrane fuel cells (PEMFC)”, International Journal of Hydrogen Energy, **30** (2005) 1339-1344

25. Hung, Y., El-Khatib, K.M., Tawfik, H., “Corrosion-resistant lightweight metallic bipolar plates for PEM fuel cells”, Journal of Applied Electochemistry, **35** (2005) 445-447

26. Del Rio,C., Ojeda, M.C., Acosta, J.L., Escudero, M.J., Hontanon, E., Daza, L., “New Polymer Bipolar Plates for Polymer Electrolyte Membrane Fuel Cells: Synthesis and Characterization”, Journal of Applied Polymer Science, **83** (2002) 2817-2822

27. Ryu, S.K., Hwang, T.S., Lee, S.G., Lee, S.A., Kim, C.S., Jeong, D.H., “Modification of C/C Composite Bipolar Plate by Addition of Electro-Conductive Carbon Black”, Cabon Science, **2(3-4)** (2001) 165-169

28. Acosta, J.L., Gonzalez, L., Del Rio, C., Ojeda, C., Rodriguez, A., “Elastomeric Conducting Systems Based on Ethylene-Propylene-Norbornene Composites”, Journal of Applied Polymer Science, **79** (2001) 2136-2145

29. Arai, T., Tominaga, Y., Asai, S., Sumita, M., “A Study on Correlation Between Physical Properties and Interfacial Characteristics in Highly Loaded Graphite–Polymer Composites”, Journal of Polymer Science: Part B: Polymer Physics, **43** (2005) 2568-2577

30. Wu, M., Shaw, L.L., “A novel concept of carbon-filled polymer blends for applications in PEM fuel cell bipolar plates”, International Journal of Hydrogen Energy, **30** (2005) 373-380

31. Mighri, F., Huneault, M.A., Champagne, M.F., “Electrically Conductive Thermoplastic Blends for Injection and Compression Molding of Bipolar Plates in the Fuel Cell Application”, Polymer Engineering and Science, **44(9)** (2004) 1755-1765

32. Huang, J., Baird, D.G., “Compression Molding of Highly Conductive Fuel Cell Bipolar Plates from a Thermoplastic Composite”, Antec 2003, (2003) 2151-2155

33. Middelman, E., Kout, W., Vogelaar, B., Lenssen, J., de Waal, E., “Bipolar plates for PEM fuel cells”, Journal of Power Sources, **118** (2003) 44-46

34. Blunk, R.H.J., Lisi, D.J., Yoo, Y.E., Tucker, C.L., “Enhanced Conductivity of Fuel Cell Plates through Controlled Fiber Orientation”, AIChE Journal, **49(1)** (2003) 18-29

35. Feller, J.F., Linossier, I., Grohens, Y., “Conductive polymer composites: comparative study of poly(ester)-short carbon fibres and poly(epoxy)-short carbon fibres mechanical and electrical properties”, Materials Letters, **57** (2002) 64-71

36. Zhang, Q.H., Chen, D.J., “Percolation threshold and morphology of composites of conducting carbon black/polypropylene/EVA”, Journal of Materials Science, **39** (2004) 1751-1757

37. Tchmutin, I.A., Ponomarenko, A.T., Krinichnaya, E.P., Kozub, G.I., Efimov, O.N., “Electrical properties of composites based on conjugated polymers and conductive fillers”, Carbon, **41** (2003) 1391-1395

38. Huang, J.C., “Carbon Black Filled Conducting Polymers and Polymer Blends”, Advances in Polymer Technology, **21(4)** (2002) 299-313

39. Narkis, M., Lidor, G., Vaxman, A., Zuri, L., "New injection moldable electrostatic dissipative (ESD) composites based on very low carbon black loadings", Journal of Electrostatics, **47** (1999) 201-214

40. Chodak, I., Omastova, M., Pionteck, J., "Relation Between Electrical and Mechanical Properties of Conducting Polymer Composites**",** Journal of Applied Polymer Science, **82** (2001) 1903-1906

41. Thongruang, W., Spontak, R.J., Balik, C., "Correlated electrical conductivity and mechanical property analysis of high-density polyethylene filled with graphite and carbon fiber", Polymer, **43** (2002) 2279-2286

42. Taipalus, R., Harmia, T., Zhang, M.Q., Friedrich, K., "The electrical conductivity of carbon-fibre-reinforced polypropylene/polyaniline complex-blends: experimental characterization and modelling", Composites Science and Technology, **61** (2001) 801-814

43. Fu, S.Y., Lauke, B., Mader, E., Yue, C.Y., Hu, X., "Tensile properties of short-glass-fiber- and short-carbon-fiber-reinforced polypropylene composites", Composites: Part A, **31** (2000) 1117-1125

44. HyPM Hydrogenics 65 kW Fuel Cell Power Module, http://www.hydrogenics.com/power/pdf/HyPM_HD-XR_Brochure.pdf (Last acquired December 14, 2006)

45. Heinzel, A., Mahlendorf, F., Niemzig, O., Kreuz, C., "Injection moulded low cost bipolar plates for PEM fuel cells", Journal of Power Sources, **131** (2004) 35-40

46. Equistrar, Petrothene Data Sheet, http://www.equistarchem.com/html/polymer/polypropylene/Impact_IM.htm (Last acquired March 30, 2005), in Appendix F

47. Equistar, Petrothene MSDS, http://www.equistarchem.com/html/polymer/polypropylene/Impact_IM.htm (Last acquired March 30, 2005)

48. CPChem, Shawinagan Data Sheet, as provided with material, in Appendix F

49. Youngs, I.J., "A geometric percolation model for non-spherical excluded volumes", Journal of Physics D: Applied Physics, **36** (2003) 738-747

50. Vulcan Data Sheet, as provided with material, in Appendix F

51. Fortafil Data Sheet, as provided with material, in Appendix F

52. Perry, R.H. (ed.), Green, D.W. (ed.), "Perry's Chemical Engineers' Handbook – Seventh Edition", McGraw-Hill, (1999) 91-92

53. American Society for Testing and Materials (ASTM), “Standard Test Method for Rubber Property – Volume Resistivity of Electrically Conductive and Antistatic Products”, **09-01** (2004) 195-199

54. US Fuel Cell Council, “Electrical Conductivity Testing Protocols Task Force Draft Guidelines, Materials & Components Working Group”, (2003)

55. American Society for Testing and Materials (ASTM), “Standard Test Method for Tensile Properties of Polymer Matrix Composite Materials”, **15-03** (2004) 61-73

56. American Society for Testing and Materials (ASTM), “Standard Test Method for Determination of Modulus of Elasticity for Rigid and Semi-Rigid Plastic Specimens by Controlled Rate of Loading Using Three-Point Bending”, **08-01** (2004) 709-712

57. American Society for Testing and Materials (ASTM), “Standard Test Method for Compressive Properties of Polymer Matrix Composite Materials with Unsupported Gage Section by Shear Loading”, **15-03** (2004) 84-99

58. Ng, Z., “Internal course report for Dr. Fowler, ChE 048 course – Chemical Engineering”, University of Waterloo, April, 2005

59. Poco Graphite, Specification Sheet, http://www.poco.com/us/Graphite/axf.asp (Last Acquired December 15, 2006)

60. Estimate from polymer industry expert Chris Bennett, Polymer Technologies Inc., September 21, 2006

61. Carbon filler costs based on low volume orders as quoted from manufacturers to the University of Waterloo, December 2003 to August 2004

Appendix A – Thermal Gravimetric Analysis and Density Measurement Procedures

Thermal Gravimetric Analysis

Using a 'TA SDT 2960 Simultaneous DTA-TGA' the method equilibrated at 75^{o}C and increased at a rate of 20^{o}C/min up to 1000^{o}C. The chamber environment was a 5% O_2 - 95% He mixture. This gas continuously sweeps through the TGA chamber. Data was collected at a rate of 10/s.

The method was first calibrated without a sample to create a baseline that compensated for the induced increase in measured mass do to the thermal expansion of the internal components. The computer software automatically considers this calibration curve prior to data output.

The sequential procedure for each sample run follows.

1. Clean the platinum sample and reference holders using a hot flame to burn off any foreign residue.
2. Place the reference and sample holders inside the TGA chamber, close the chamber and 'tare' the holder weights.
3. Open the chamber and place approximately 10 mg of sample in the sample holder and close the chamber
4. Initiate the testing procedure as specified above and allow test to run.
5. Obtain results from the computer and repeat procedure for sequential samples.

Density Measurement

Density measurements were conducted using an analytical balance – water displacement technique. The sequential procedure for each sample run follows.

1. Using an analytical balance the dry composite sample mass is measured and recorded.
2. A beaker filled with ultra-pure water at a known temperature (approximately room temperature) is measured on an analytical balance with submerged sample clamp and attached guide (nylon string). The clamp and guide are hung from a stationary support from above, independent of the balance. The baseline mass of the test apparatus is recorded.
3. The sample is placed in the clamp and is submerged in the water the new mass (due to the elevated water height) is recorded.
4. Based on the mass of the displaced water, the sample volume is calculated using the water density (displaced water volume and sample volume will be equal).
5. Sample density is the ratio of sample mass (Step 1) over the sample volume (Step 4).
6. Dry equipment and repeat procedure for each sample.

Appendix B - Conductivity Testing Procedures

Plates were tested using an Enlight Corp. Model EN 820212 power source. Voltage and current measurements were performed using a Agilent Model 34401A 6.5 Digit, Dual Input Multimeter. Both methods are arranged to measure voltage and current independently as shown in the figure below. Calculations are presented in section 3.4.3 of the report.

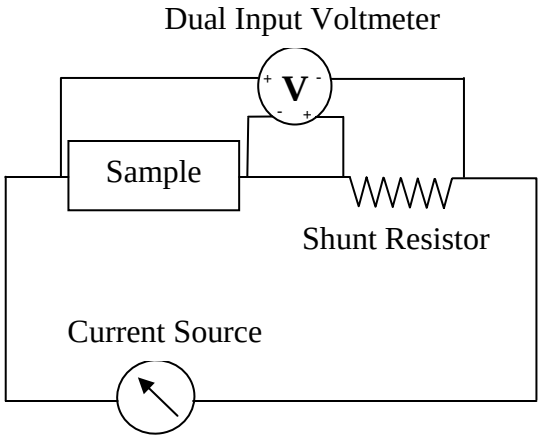

Method 1

The Method 1 measurement technique followed ASTM D-991, the figure below illustrates the specified 4-point probe test apparatus for this method.

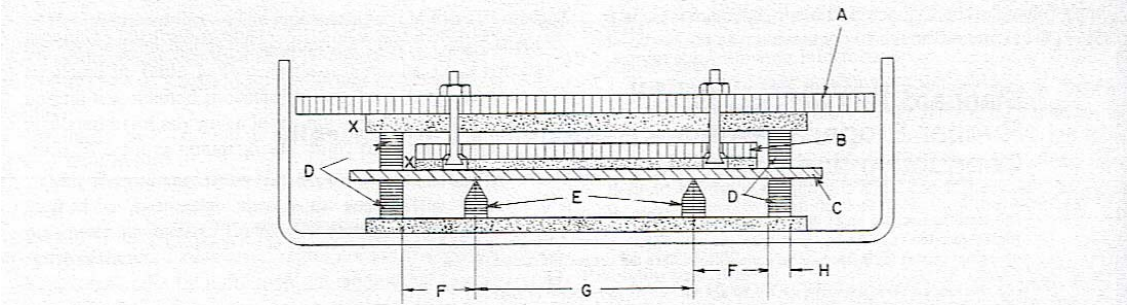

The Method 1 procedure follows.

1. The test apparatus is tightened at each corner by applying an evenly distributed torque of 40 cN-m, which clamped the sample between the current electrodes (‘D’ above).

2. The multimeter outputs are checked ensuring a current and voltage of zero prior to test.
3. The power source is turned on and the current and voltage are recorded at 10 s, 1 min, and 3 min intervals following power source commencement. Calculations are based on the 3 min value.
4. Repeat procedure for each sample.

Method 2

The Method 2 measurement technique followed the recommended US fuel cell council guidelines, the figure below illustrates the specified through-plane test apparatus for this method.

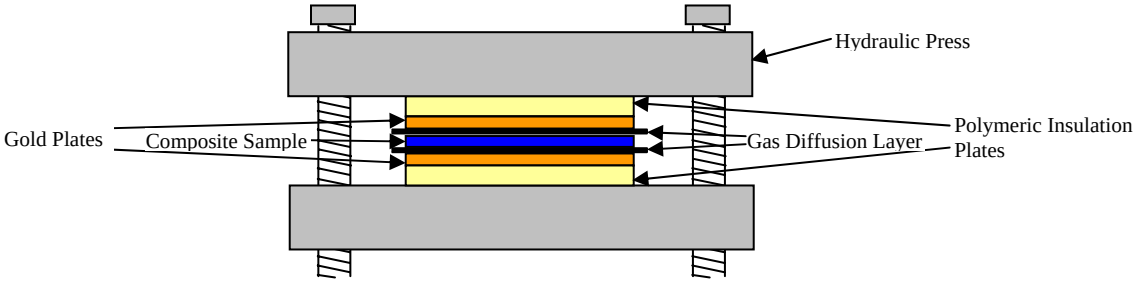

The Method 2 procedure is as follows.

1. Place clean sample between GDL and Gold plates, ensuring a complete contact.
2. Clamp the layered assembly to a pressure of 1000 psig.
3. The multimeter outputs are checked ensuring a current and voltage of zero prior to test.
4. The power source is turned on and the current and voltage are recorded at 10 s, 1 min, and 3 min intervals following power source commencement. Calculations are based on the 3 min value.
5. Repeat procedure for each sample.

Appendix C – Mechanical Property Measurement Procedures

Mechanical modulus and yield strength were determined for tensile, and flexural properties using a Rheometric Scientific Mini-Mat test apparatus. The test procedures that were used for tensile, and flexural analysis in order include: ASTM D-3039/D-3039M-00, and ASTM D-5934.

Deviations:

- Testing speed used was 1 mm per minute.
- Sample size was dictated by the 200 N maximum achievable by the instrument, in some cases the cross-sectional area of the sample was decreased to achieve complete results. In some cases complete results were not practical.

The procedure for mechanical testing follows.

1. Measure and record sample dimensions with digital calipers, repeat 3 times for improved accuracy.
2. Start Mini-mat computer software and select “Tensile” or “Flexural” Testing as appropriate.
3. Input sample parameters, and experiment criteria as shown in the figures that follow.
4. Run the experiment (total duration 90-150 s)
5. Export force versus displacement data and analyze to determine Young’s modulus and the material’s yield strength (0.2% offset used).
6. Repeat steps for each sample, 3-5 samples completed for each experimental run.

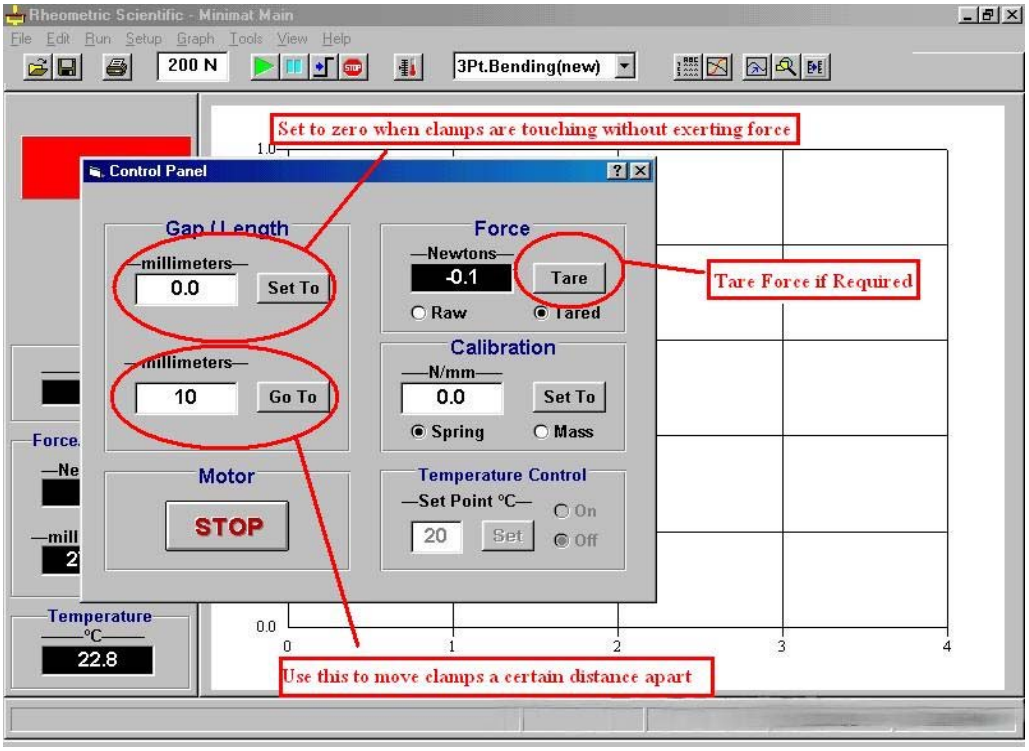
Rheometric Scientific - Minimat Main
File Edit Run Setup Graph Tools View Help
200 N
3Pt.Bending(new)
Set to zero when clamps are touching without exerting force
Control Panel
Gap / Length
millimeters
0.0
Set To
millimeters
10
Go To
Force
Newtons
-0.1
Tare
Raw
Tared
Tare Force if Required
Calibration
N/mm
0.0
Set To
Spring
Mass
Motor
STOP
Temperature Control
Set Point °C
20
Set
On
Off
Force
Temperature
°C
22.8
Use this to move clamps a certain distance apart

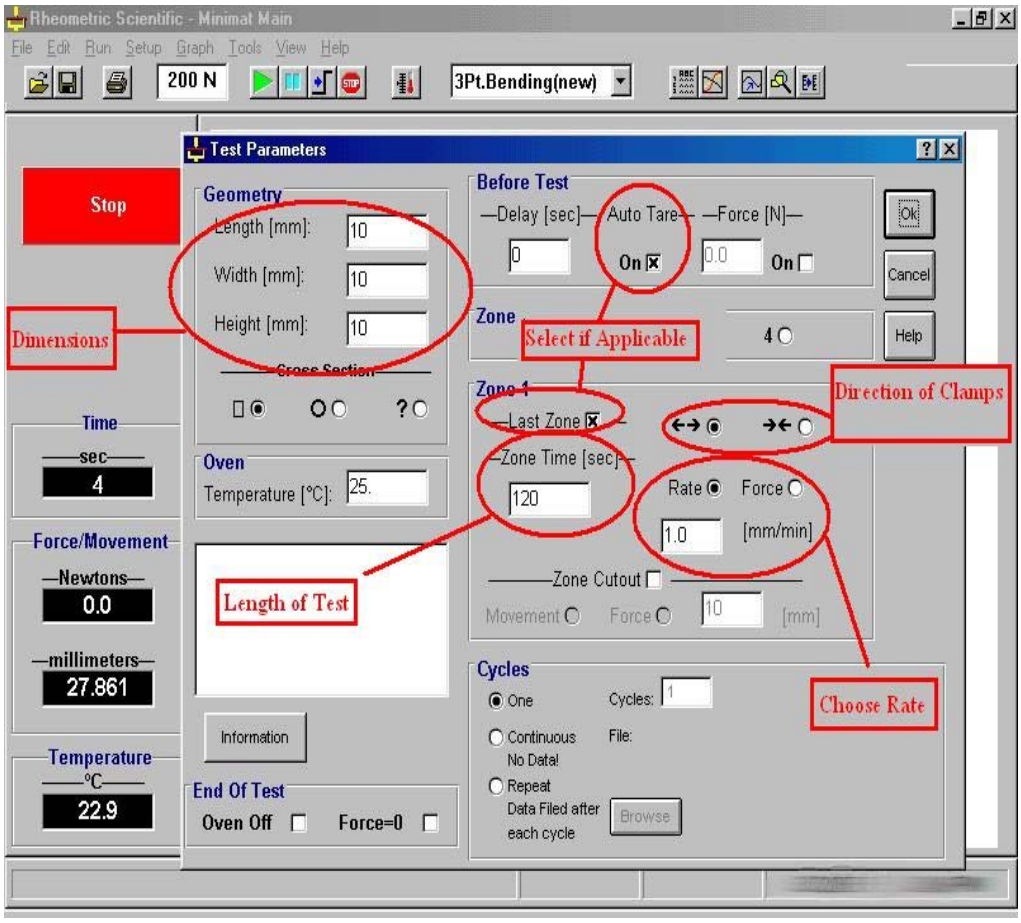
Rheometric Scientific - Minimat Main
File Edit Run Setup Graph Tools View Help
200 N
3Pt.Bending(new)
Test Parameters
Stop
Geometry
Length [mm]: 10
Width [mm]: 10
Height [mm]: 10
Cross Section
Dimensions
Before Test
Delay [sec]
Auto Tare
Force [N]
0
On
0.0
On
Ok
Cancel
Help
Zone
Select if Applicable
4
Zone 1
Last Zone
Direction of Clamps
Zone Time [sec]
120
Rate
Force
1.0
[mm/min]
Zone Cutout
Movement
Force
10
[mm]
Time
sec
4
Oven
Temperature [°C]: 25.
Force/Movement
Newtons
0.0
millimeters
27.861
Length of Test
Information
Cycles
One
Cycles: 1
Continuous
No Data!
File:
Repeat
Data Filed after each cycle
Browse
Choose Rate
Temperature
°C
22.9
End Of Test
Oven Off
Force=0

Appendix D – Rheology Measurement Procedure

The apparatus used for rheological testing was the Dynisco Galaxy V Capillary Rheometer 8052, with a load cell of 2000lb_f maximum capacity. An X5020 die was used (0.05cm diameter, an aspect ratio of 20, and an entrance angle of 120^o). ASTM D3835-02 was followed.

The method developed using the apparatus software for the testing of these materials and characteristics are indicated below.

- Melt Time = 300 s
- TEMP = 220 °C
- Rate # = 4, 2, 1, 0.8, 0.4, 0.2, 0.1, 0.06, 0.03 (cm/min)
- Melt Force = 150 (lb_f)
- Term Force = 1900 (lb_f)
- Start Pos = 3.2 (cm)
- Pos #= 4.46, 6.406, 7.059, 7.792, 8.401, 8.667, 8.784, 8.874, 8.942

1. A sample of approximately 20mL is loaded using the packing plunger in small shots and packed periodically until the entire barrel is filled.
2. Following the melt time the plunger proceeded to move into the chamber.
3. When the force displayed on the screen reached a constant value (+/- 0.05), the END button is pressed to record the value, and allow the load cell speed to proceed to the next shear rate specified.
4. Step 3 continues until all 9 points have been recorded, or until all material has depleted inside the barrel.
5. The plunger returns to the starting position at the end of the run.
6. Repeat the steps for all samples, cleaning the apparatus between runs.

Appendix E –Fuel Cell Test Station Procedure

The fuel cell test station conditions were held constant where possible to ensure easy comparison between runs and different bipolar plates. The parameters that were held constant are given below with their respective values.

- Hydrogen Flow Rate = 0.10 SLPM
- Air Flow Rate = 0.20 SLPM
- Fuel Cell Temperature = 80°C

The procedure that was used follows.

1. Break-in fuel cell for approximately 1 hour by varying the current demand and allow voltage to come to a steady state.
2. Starting at the maximum current demand (determined during the break-in period) allow the fuel cell voltage to stabilize and record.
3. Decrease the voltage by 0.5 Amps
4. Hold the current for 5 minutes and record the corresponding voltage.
5. Repeat steps 3 and 4 until the current reduces to zero (open circuit voltage)
6. The voltage-current or voltage-current density relationship is plotted.

Appendix F – Material Data Sheets

Petrothene®

PP 36KK01

Polypropylene
Injection Molding Grade
Melt Flow Rate 7.0

Applications

PETROTHENE PP 36KK01, formerly known as PP TR311, is a medium impact polypropylene copolymer formulated for injection molding applications requiring a balance of stiffness and cold temperature impact strength. It is heat stabilized for use at elevated temperatures and can be used in FDA food contact applications. Consult with your Equistar sales representative for further details.

Processing Techniques

PP 36KK01 can be processed at normal molding conditions at a melt temperature range of 430°-470°F (221°-243°C). Specific recommendations for conditions under which PP 36KK01 should be processed can be made only when the end use and the type of processing equipment are known. For further suggestions, please contact your Equistar sales representative.

Physical Properties

PP 36KK01 offers the benefits of gas-phase technology along with medium stiffness and high impact strength.

Property	Nominal Value	Units	ASTM Test Method
Melt Flow Rate	7.0	g/10 min	D 1238
Tensile Strength @ Yield	3,200 (22.0)	psi (MPa)	D 638
Elongation @ Yield	6	%	D 638
Flexural Modulus	160,000 (1,100)	psi (MPa)	D 790
Izod Impact, Notched @ 23°C	9.5 (500)	ft-lb/in. (J/m)	D 256
Izod Impact, Notched @ -18°C	1.4 (75)	ft-lb/in. (J/m)	D 256
Unnotched Impact @ -18°C	31 (1,655)	ft-lb/in. (J/m)	D 4812
Gardner Impact @ -18°C	320 (36)	in-lb. (J)	D 5420
Rockwell Hardness	78	R	D 785
Heat Deflection @ 66 psi	73 (163)	°C (°F)	D 648
Heat Deflection @ 264 psi	56 (163)	°C (°F)	D 648

Equistar Chemicals, LP
1221 McKinney, Suite 700
P.O. Box 2583
Houston, Texas 77252-2583
(800) 615-8999
http://www.equistarchem.com

9371/0704

EQUISTAR

Technical Data Sheet

Shawinigan Black®
Acetylene Black

AB100%

SHAWINIGAN BLACK® made from acetylene gas is the purest form of carbon black available. Its unique structural properties offer high liquid absorption, high electrical conductivity, and the ability to impart this conductivity into plastics, rubber, and other materials. This product is available in paper bags, plastic inclusion bags, and bulk bags. For additional information contact the Acetylene Black Business Development Representative at 877-895-4773 or by email at aceblack@cpchem.com.

SPECIFICATIONS	LIMITS	TYPICALS
Moisture, Wt. %	.2 Max.	.05
Ash, Wt. %	.05 Max.	.005
Grit (325 Mesh Sieve), Wt. %	.02 Max.	.006
Absorption Stiffness, ml/5gm	19.0 Min.	19.5
Bulk Density, lbs./ft.^{3}	12.5 – 14.5	12.9
DESCRIPTIVE PROPERTIES	**LIMITS**	**TYPICALS**
Actual Density, gm/cc		1.75
DBPA No., cc/100g		199
Mean Particle Size, nm		42
Surface Area BET Method, m^2/gm Iodine Absorption Number		 75 90
Carbon content, %		>99.9

Chevron Phillips Chemical Company LP
Olefins & Polyolefins Division
10001 Six Pines Drive, The Woodlands, TX 77380
P.O. Box 4910, The Woodlands, TX 77387-4910
Phone (832) 813-4100

Revised 04/01
Replaces 01/01

CABOT
creating what matters

Cabot Corporation
Pampa Plant
3 Miles West Highway
Attn: Mark Lang
1-806-661-3111
Pampa, TX 79065

CARBON BLACK CERTIFICATE OF ANALYSIS

SIS No.	0111017877 9SO / 2		27348
Vehicle No			L V Lomas Limited
Customer Order	V1404604		99 Summerlea Road
Shipping Date	02/20/2004		Brampton ON L6T 4V2
Packing Lot No	254234		Attn : Attn: Brian Fair/Della Shephard
Grade	VULCAN® XC72R		905-458-0462
ASTM Code			
Customer Grade	CABVXC72R		
Quantity	2,250 LB		

Production Date 1/17/2004

Pack Date 2/15/2004

PHYSICAL AND CHEMICAL PROPERTIES

Property Description	Unit	Ref	Specification Min	Individual Values			Specification Max
					Individual		
PH		D-1512	3.5		7.1		9.5
TAP-DENSITY-IMP	lb/cu ft	121	3.00		5.20		9.00
ASH	%	D-1506			0.03		0.20

Property Description	Unit	Ref	Specification Min	Average Values			Specification Max
				Min	Average	Max	
I2NO	g/Kg	D-1510	235.0	255.3	255.7	256.5	271.0
OAN	ml/100g	D-2414	182.0	190.2	190.7	191.4	202.0
MOISTURE	%	D-1509		0.5	0.6	0.7	3.0
TINT	%	D-3265	83.0	84.2	86.6	88.6	91.0
RES-325	ppm	D-1514		1	2	4	10

The data above was obtained from tests on samples taken during the time of production and/or packaging of this product. We do not guarantee the same results will be obtained by others in other laboratories and we disclaim liability resulting from the use of the contents of this report. BLACK PEARLS, ELFTEX, EMPEROR, MOGUL, MONARCH, REGAL, STERLING, VULCAN, CRX, CSX and IRX are registered trademarks for Carbon Blacks produced by Cabot Corporation. Rubber results are reported as difference from IRB7.

Pallet No / Container ID 254234: 30, 40-43, 46

Page 1 of 1

FORTAFIL® FIBERS

CONTINUOUS IN QUALITY. ECONOMICAL BY DESIGN.

Product Literature Sheet

CHOPPED PRODUCTS

Chopped carbon fiber products provide good processability, resin matrix compatibility, and good translation of mechanical and electrical properties. The chopped fibers are easily mixed into a uniform preblend prior to compounding. The chopped products are produced in ⅛" (3 mm) and ¼" (6 mm) lengths and other lengths are available on request. Fiber sizings are available directed toward thermoplastic and thermoset matrices.

Typical Continuous Fiber Properties	English		SI		Metric	
Tensile Strength	>500	ksi	>3,450	MPa	>350	kgf/mm^2
Tensile Modulus	>30.0	Msi	>207	GPa	>21,100	kgf/mm^2
Ultimate Elongation	1.7	%	1.7	%	1.7	%
Density	0.065	lb/in^3	1.8	g/cm^3	1.8	g/cm^3
Cross-Sectional Area/Filament	4.7 or 6.5 x 10^{-8}	in^2	3.3 or 4.2 x 10^{-5}	mm^2	3.3 or 4.2 x 10^{-5}	mm^2
Filament Shape	Round		Round		Round	
Filament Diameter	0.24 or 0.29 x 10^{-3}	in	6 or 7	µm	6 or 7	µm
Electrical Resistivity			1,670	µΩ-cm		
Chopped Products						
Physical Form	Flakes					
Fiber Length	1/8, 1/4	in	3,6	mm	3,6	mm
Bulk Density	Dictated by the fiber length, sizing level, and sizing type					
Moisture Content			<0.3	%		
Sizing Content	Dependent on the fiber length, fiber grade, and end use					
Ferromagnetic Metals Content			None >0.25	mm		
Product Selection						
See the Short Carbon Fiber Selector Chart for specific products						

PLS 004 Rev. D, 05/29/03

Appendix G – Sample of Raw Data (Trial 2 54 wt%)

Thermal Gravimetric Analysis Data

Module TGA-DTA 1500 øC
Sample TJM54MB
Size 22.5075 mg
Method TJM
Operator TJM
Comment 54 MASTER BATCH SAMPLE
Nsig 4
Sig1 Time (min)
Sig2 Temperature (øC)
Sig3 Weight (mg)
Sig4 Temperature Difference (øC)
Kcell 1.0000
Date 4-Feb-05
Time 16:50

Sig1 Time (min)	Sig2 Temperature (øC)	Sig3 Weight (mg)	Sig4 Temperature Difference (øC)	Weight Differential
0	76.0582	22.5232	0.349985	3.141867527
0.166667	76.2886	22.5233	0.33755	3.141881477
0.333333	77.1053	22.5231	0.295365	3.141853578
0.5	78.6713	22.5231	0.226075	3.141853578
0.666667	80.8931	22.5232	0.14158	3.141867527
0.833333	83.6103	22.5232	0.05675	3.141867527
1	86.6951	22.5232	-0.018985	3.141867527
1.16667	89.9973	22.5237	-0.079695	3.141937275
1.33333	93.3654	22.5244	-0.12386	3.142034921
1.5	96.6593	22.5251	-0.153155	3.142132567
1.66667	99.9047	22.5257	-0.17163	3.142216264
1.83333	103.131	22.5263	-0.18472	3.142299961
2	106.331	22.5267	-0.19491	3.142355759
2.16667	109.446	22.5269	-0.203485	3.142383658
2.33333	112.543	22.5274	-0.212455	3.142453405
2.5	115.66	22.528	-0.223235	3.142537102
2.66667	118.808	22.5282	-0.236095	3.142565001
2.83333	121.951	22.5289	-0.250195	3.142662647
3	125.096	22.5293	-0.265275	3.142718445
3.16667	128.281	22.5294	-0.281495	3.142732395
3.33333	131.509	22.5298	-0.299235	3.142788193
3.5	134.718	22.5301	-0.31753	3.142830041
3.66667	137.925	22.5304	-0.33672	3.142871889
3.83333	141.161	22.5305	-0.357795	3.142885839
4	144.417	22.5309	-0.38159	3.142941637
4.16667	147.648	22.5316	-0.40947	3.143039283
4.33333	150.875	22.5319	-0.443595	3.143081132

4.5	154.119	22.5324	-0.485985	3.143150879
4.66667	157.366	22.5331	-0.542135	3.143248525
4.83333	160.56	22.5348	-0.62047	3.143485666
5	163.729	22.5363	-0.73416	3.143694908
5.16667	166.9	22.5373	-0.876585	3.143834403
5.33333	170.275	22.5364	-0.87611	3.143708858
5.5	173.815	22.5353	-0.66505	3.143555414
5.66667	177.291	22.535	-0.52317	3.143513565
5.83333	180.703	22.5346	-0.459045	3.143457767
6	184.047	22.5346	-0.43219	3.143457767
6.16667	187.385	22.5346	-0.422115	3.143457767
6.33333	190.732	22.5342	-0.419975	3.143401969
6.5	194.052	22.5339	-0.42121	3.143360121
6.66667	197.357	22.5337	-0.4239	3.143332222
6.83333	200.689	22.5333	-0.427565	3.143276424
7	204.032	22.5332	-0.431995	3.143262475
7.16667	207.353	22.5328	-0.43614	3.143206677
7.33333	210.689	22.5325	-0.44026	3.143164828
7.5	214.045	22.5325	-0.44452	3.143164828
7.66667	217.38	22.532	-0.448265	3.143095081
7.83333	220.721	22.5318	-0.45183	3.143067182
8	224.076	22.5312	-0.455245	3.142983485
8.16667	227.43	22.5307	-0.45836	3.142913738
8.33333	230.768	22.5301	-0.46119	3.142830041
8.5	234.119	22.5299	-0.463615	3.142802142
8.66667	237.475	22.5294	-0.46608	3.142732395
8.83333	240.81	22.5291	-0.468075	3.142690546
9	244.161	22.5284	-0.470265	3.1425929
9.16667	247.512	22.5278	-0.472105	3.142509203
9.33333	250.857	22.5272	-0.473755	3.142425506
9.5	254.204	22.5266	-0.47464	3.142341809
9.66667	257.562	22.526	-0.47603	3.142258113
9.83333	260.903	22.5253	-0.47671	3.142160466
10	264.245	22.5245	-0.4773	3.142048871
10.1667	267.6	22.5235	-0.47734	3.141909376
10.3333	270.945	22.5227	-0.477205	3.14179778
10.5	274.294	22.5219	-0.475315	3.141686184
10.6667	277.658	22.5211	-0.471035	3.141574589
10.8333	281.02	22.5196	-0.46196	3.141365346
11	284.388	22.5184	-0.446325	3.141197953
11.1667	287.769	22.5173	-0.42655	3.141044509
11.3333	291.137	22.5159	-0.410915	3.140849216
11.5	294.48	22.5138	-0.40527	3.140556277
11.6667	297.828	22.5113	-0.408155	3.14020754
11.8333	301.165	22.5085	-0.414035	3.139816955
12	304.497	22.5052	-0.420565	3.139356622
12.1667	307.841	22.5021	-0.426305	3.138924189
12.3333	311.183	22.4988	-0.430455	3.138463856
12.5	314.523	22.4951	-0.432945	3.137947726

12.6667	317.876	22.4912	-0.4339	3.137403696
12.8333	321.231	22.4869	-0.43349	3.136803869
13	324.575	22.4826	-0.431895	3.136204042
13.1667	327.926	22.4777	-0.429075	3.135520518
13.3333	331.284	22.4723	-0.425435	3.134767246
13.5	334.632	22.4669	-0.42117	3.134013975
13.6667	337.988	22.4607	-0.41635	3.133149107
13.8333	341.346	22.454	-0.41117	3.132214493
14	344.69	22.4468	-0.405645	3.131210131
14.1667	348.041	22.4385	-0.39991	3.130052324
14.3333	351.397	22.4299	-0.39418	3.12885267
14.5	354.744	22.4207	-0.388105	3.127569318
14.6667	358.098	22.4103	-0.38184	3.126118573
14.8333	361.455	22.3985	-0.3743	3.124472536
15	364.805	22.3854	-0.36535	3.122645155
15.1667	368.164	22.3714	-0.355735	3.120692229
15.3333	371.51	22.3557	-0.34565	3.118502161
15.5	374.862	22.3384	-0.335595	3.116088903
15.6667	378.222	22.319	-0.326595	3.113382705
15.8333	381.576	22.2974	-0.316825	3.110369619
16	384.92	22.2731	-0.30676	3.106979897
16.1667	388.278	22.2454	-0.295075	3.103115894
16.3333	391.637	22.214	-0.28196	3.098735759
16.5	394.992	22.1784	-0.267215	3.093769747
16.6667	398.353	22.1378	-0.251495	3.088106261
16.8333	401.708	22.0902	-0.234945	3.081466313
17	405.065	22.0353	-0.217995	3.073808052
17.1667	408.427	21.9723	-0.20194	3.065019885
17.3333	411.783	21.8994	-0.186205	3.05485072
17.5	415.139	21.8151	-0.172135	3.043091315
17.6667	418.499	21.7174	-0.158955	3.02946268
17.8333	421.845	21.6043	-0.14611	3.013685827
18	425.192	21.4735	-0.109225	2.995439918
18.1667	428.542	21.3212	-0.080355	2.974194871
18.3333	431.893	21.1431	-0.06442	2.949350861
18.5	435.248	20.9355	-0.054045	2.920391757
18.6667	438.599	20.692	-0.047925	2.886424792
18.8333	441.948	20.4057	-0.042605	2.846487453
19	445.306	20.0684	-0.028395	2.799435883
19.1667	448.691	19.6661	0.00623	2.743317157
19.3333	452.149	19.1761	0.09757	2.674964743
19.5	455.7	18.5721	0.272865	2.59070993
19.6667	459.274	17.8388	0.483955	2.488418451
19.8333	462.847	16.9752	0.69563	2.367950809
20	466.427	16.0054	0.91246	2.232668827
20.1667	470.03	14.984	1.15852	2.090188918
20.3333	473.72	14.0079	1.4742	1.954028119
20.5	477.542	13.2	1.90938	1.841330333
20.6667	481.441	12.659	2.45024	1.765863689
20.8333	485.551	12.4069	2.80948	1.730697069

21	488.693	12.3381	2.89015	1.721099832
21.1667	490.55	12.3174	2.10049	1.718212291
21.3333	492.976	12.3023	1.46359	1.716105921
21.5	495.828	12.2897	1.11209	1.714348288
21.6667	498.923	12.2782	0.910205	1.712744098
21.8333	502.131	12.2676	0.78911	1.711265454
22	505.387	12.2575	0.716135	1.709856558
22.1667	508.663	12.2475	0.67351	1.70846161
22.3333	511.946	12.2379	0.65073	1.707122461
22.5	515.224	12.228	0.64139	1.705741463
22.6667	518.505	12.218	0.64106	1.704346516
22.8333	521.796	12.2074	0.64749	1.702867872
23	525.087	12.1966	0.659385	1.701361329
23.1667	528.386	12.1856	0.676075	1.699826887
23.3333	531.687	12.1741	0.696945	1.698222698
23.5	534.991	12.1619	0.721525	1.696520862
23.6667	538.302	12.1494	0.749165	1.694777178
23.8333	541.619	12.1362	0.779795	1.692935848
24	544.943	12.1218	0.81323	1.690927124
24.1667	548.274	12.1069	0.849685	1.688848652
24.3333	551.605	12.0916	0.88903	1.686714383
24.5	554.94	12.075	0.931225	1.684398771
24.6667	558.28	12.0576	0.976625	1.681971563
24.8333	561.625	12.0395	1.02494	1.679446708
25	564.987	12.0201	1.07679	1.676740511
25.1667	568.346	11.9997	1.13193	1.673894818
25.3333	571.708	11.9779	1.19084	1.670853833
25.5	575.078	11.9546	1.25328	1.667603606
25.6667	578.447	11.9302	1.32012	1.664199935
25.8333	581.828	11.9042	1.39111	1.660573072
26	585.217	11.8767	1.46665	1.656736967
26.1667	588.615	11.8473	1.54674	1.652635823
26.3333	592.019	11.8162	1.63136	1.648297537
26.5	595.421	11.7833	1.72046	1.64370816
26.6667	598.833	11.748	1.81464	1.638783997
26.8333	602.256	11.7107	1.91458	1.633580843
27	605.688	11.6709	2.01981	1.628028954
27.1667	609.125	11.629	2.13057	1.622184125
27.3333	612.567	11.5845	2.24681	1.61597661
27.5	616.013	11.5368	2.36858	1.609322711
27.6667	619.466	11.4864	2.49527	1.602292177
27.8333	622.923	11.4327	2.62669	1.594801311
28	626.399	11.3759	2.76297	1.58687801
28.1667	629.867	11.3157	2.90358	1.578480428
28.3333	633.338	11.252	3.04819	1.569594614
28.5	636.807	11.1847	3.19592	1.56020662
28.6667	640.286	11.1135	3.34664	1.550274595
28.8333	643.773	11.0386	3.50046	1.539826441
29	647.253	10.9596	3.65615	1.528806358

29.1667	650.732	10.8766	3.81266	1.517228296
29.3333	654.218	10.7893	3.96927	1.505050406
29.5	657.705	10.6976	4.12634	1.49225874
29.6667	661.194	10.6018	4.283	1.478895146
29.8333	664.673	10.5019	4.43825	1.464959623
30	668.15	10.3975	4.59209	1.450396374
30.1667	671.627	10.2884	4.74329	1.4351775
30.3333	675.102	10.1751	4.89171	1.419372748
30.5	678.578	10.0574	5.03812	1.402954219
30.6667	682.042	9.93528	5.18081	1.385919124
30.8333	685.498	9.80878	5.32	1.368273041
31	688.959	9.67781	5.45562	1.350003418
31.1667	692.409	9.54241	5.58652	1.331115832
31.3333	695.859	9.40281	5.7126	1.311642369
31.5	699.298	9.25943	5.83337	1.291641616
31.6667	702.727	9.11224	5.94829	1.271109388
31.8333	706.151	8.96095	6.05617	1.250005231
32	709.566	8.80626	6.15783	1.228426792
32.1667	712.972	8.64837	6.25129	1.206401971
32.3333	716.372	8.48767	6.33708	1.183985169
32.5	719.775	8.32466	6.41928	1.161246134
32.6667	723.165	8.15927	6.49484	1.138175102
32.8333	726.557	7.99164	6.57079	1.114791602
33	729.968	7.82109	6.65454	1.091000777
33.1667	733.375	7.64759	6.74026	1.066798443
33.3333	736.767	7.47243	6.81588	1.042364547
33.5	740.147	7.29705	6.87251	1.017899963
33.6667	743.519	7.12225	6.91853	0.993516285
33.8333	746.88	6.94723	6.95555	0.969101919
34	750.242	6.77229	6.99159	0.944698712
34.1667	753.605	6.59733	7.02825	0.920292716
34.3333	756.969	6.42244	7.064	0.895896484
34.5	760.33	6.24735	7.09558	0.871472353
34.6667	763.69	6.07193	7.11915	0.847002189
34.8333	767.044	5.89632	7.14273	0.822505521
35	770.394	5.72117	7.15801	0.79807302
35.1667	773.727	5.54583	7.16682	0.773614015
35.3333	777.058	5.37057	7.16873	0.74916617
35.5	780.383	5.19569	7.16632	0.724771333
35.6667	783.707	5.02122	7.1584	0.700433689
35.8333	787.03	4.84761	7.14635	0.67621601
36	790.338	4.67509	7.12963	0.652150381
36.1667	793.641	4.50366	7.10847	0.628236801
36.3333	796.937	4.33331	7.07907	0.604473875
36.5	800.23	4.16404	7.04267	0.580861603
36.6667	803.516	3.99608	7.00067	0.55743207
36.8333	806.801	3.82959	6.95601	0.534207593
37	810.089	3.66425	6.91081	0.511143536
37.1667	813.38	3.50078	6.86808	0.488340334
37.3333	816.675	3.33845	6.82775	0.465696155

37.5	819.966	3.17709	6.78827	0.443187287
37.6667	823.261	3.01717	6.75029	0.420879291
37.8333	826.551	2.85874	6.71226	0.398779142
38	829.838	2.70171	6.674	0.376874286
38.1667	833.121	2.54655	6.63399	0.355230285
38.3333	836.408	2.39243	6.59202	0.333731358
38.5	839.692	2.24031	6.54559	0.312511421
38.6667	842.977	2.08956	6.5012	0.291482592
38.8333	846.249	1.94094	6.44779	0.270750886
39	849.519	1.7939	6.39434	0.250239582
39.1667	852.792	1.64884	6.33713	0.230004478
39.3333	856.056	1.50577	6.27378	0.210046968
39.5	859.3	1.36545	6.19592	0.190473068
39.6667	862.552	1.22714	6.11789	0.171179553
39.8333	865.797	1.09127	6.03823	0.152226406
40	869.031	0.958555	5.95124	0.133713363
40.1667	872.247	0.829165	5.85257	0.115664141
40.3333	875.449	0.70371	5.73357	0.098163831
40.5	878.628	0.58254	5.5939	0.081261255
40.6667	881.778	0.466675	5.42554	0.065098699
40.8333	884.874	0.35765	5.21516	0.049890287
41	887.883	0.256625	4.93344	0.035797833
41.1667	890.724	0.16712	4.51516	0.023312358
41.3333	892.773	0.09971	3.50818	0.013909019
41.5	895.017	0.070175	2.29592	0.009789042
41.6667	897.928	0.05575	1.79626	0.007776831
41.8333	901.018	0.04879	1.50423	0.006805947
42	904.252	0.04661	1.34195	0.006501849
42.1667	907.591	0.04612	1.29559	0.006433497
42.3333	910.946	0.045625	1.29173	0.006364447
42.5	914.307	0.04531	1.29692	0.006320506
42.6667	917.663	0.04502	1.30438	0.006280052
42.8333	921.02	0.04478	1.31307	0.006246574
43	924.372	0.044305	1.3226	0.006180314
43.1667	927.716	0.044195	1.33272	0.006164969
43.3333	931.062	0.043915	1.34288	0.006125911
43.5	934.411	0.043605	1.35346	0.006082667
43.6667	937.761	0.04328	1.36416	0.006037332
43.8333	941.102	0.043215	1.37478	0.006028264
44	944.436	0.042615	1.38529	0.005944568
44.1667	947.775	0.042375	1.39578	0.005911089
44.3333	951.114	0.04221	1.40617	0.005888072
44.5	954.461	0.042055	1.41655	0.005866451
44.6667	957.794	0.041945	1.42702	0.005851106
44.8333	961.13	0.041705	1.43756	0.005817627
45	964.471	0.041315	1.4479	0.005763224
45.1667	967.812	0.041145	1.45817	0.00573951
45.3333	971.148	0.04088	1.46836	0.005702544
45.5	974.479	0.0408	1.47819	0.005691385
45.6667	977.814	0.04065	1.48779	0.00567046

Density Data

RUN	SAMPLE	MASS (g)	VOLUME (cm3)	DENSITY (g/cm3)	AVERAGE DENSITY (g/cm3)	ST. DEV.
2	3	0.47857	0.40	1.196425		
	4	0.58176	0.49	1.187265		
54%	5	0.61809	0.52	1.188635		
	6	0.60125	0.50	1.202500		
	7	0.69634	0.56	1.243464	**1.203658**	**0.02309**

Conductivity Data

Run 2, Method 2, Pressure of 1000 psi and 3 min duration used for calculations

RUN	SAMPLE	PRESS. (PSI)	TIME	CURRENT (A)	VOLTAGE (mV)	THICK-NESS (mm)	WIDTH (mm)	AVG. LENGTH (mm)
2	*3*	1000	10 s	0.4880	0.91	2.95	99.51	75.18
			1 min	0.4880	0.89	2.95	99.51	75.18
			3 min	0.4885	0.88	2.95	99.51	75.18
		3000	10 s	0.4885	0.74	2.95	99.51	75.18
			1 min	0.4885	0.73	2.95	99.51	75.18
			3 min	0.4885	0.72	2.95	99.51	75.18
	4	1000	10 s	0.4890	0.96	2.96	99.68	74.88
			1 min	0.4890	0.95	2.96	99.68	74.88
			3 min	0.4890	0.94	2.96	99.68	74.88
		3000	10 s	0.4890	0.77	2.96	99.68	74.88
			1 min	0.4890	0.76	2.96	99.68	74.88
			3 min	0.4890	0.76	2.96	99.68	74.88
	5	1000	10 s	0.4880	0.81	2.96	99.57	75.28
			1 min	0.4885	0.80	2.96	99.57	75.28
			3 min	0.4885	0.79	2.96	99.57	75.28
		3000	10 s	0.4885	0.69	2.96	99.57	75.28
			1 min	0.4885	0.69	2.96	99.57	75.28
			3 min	0.4885	0.68	2.96	99.57	75.28
	6	1000	10 s	0.4880	0.93	2.94	99.44	74.83
			1 min	0.4885	0.91	2.94	99.44	74.83
			3 min	0.4885	0.89	2.94	99.44	74.83
		3000	10 s	0.4885	0.72	2.94	99.44	74.83
			1 min	0.4885	0.71	2.94	99.44	74.83
			3 min	0.4885	0.71	2.94	99.44	74.83
	7	1000	10 s	0.4880	0.90	2.95	99.54	74.92
			1 min	0.4880	0.89	2.95	99.54	74.92
			3 min	0.4885	0.89	2.95	99.54	74.92
		3000	10 s	0.4880	0.73	2.95	99.54	74.92
			1 min	0.4880	0.72	2.95	99.54	74.92
			3 min	0.4885	0.72	2.95	99.54	74.92

Tensile Data

Run 2, Sample 3, Axial Direction

Time sec	Delta_L mm	Force N	Strain %	Stress KPa	LZn_Time sec
0	0	0.27	0.00E+00	5.04E+01	0
0.24	0.004	0.26	1.42E-02	4.80E+01	0.24
0.48	0.008	0.31	2.90E-02	5.76E+01	0.48
0.72	0.012	0.34	4.43E-02	6.24E+01	0.72
0.96	0.016	0.38	5.91E-02	6.90E+01	0.96
1.2	0.02	0.38	7.39E-02	7.05E+01	1.2
1.44	0.024	0.4	8.92E-02	7.26E+01	1.44
1.68	0.028	0.38	1.04E-01	7.06E+01	1.68
1.92	0.032	0.39	1.19E-01	7.16E+01	1.92
2.16	0.036	0.42	1.34E-01	7.74E+01	2.16
2.4	0.04	0.41	1.49E-01	7.60E+01	2.4
2.64	0.044	0.43	1.64E-01	7.97E+01	2.64
2.88	0.048	0.44	1.79E-01	8.04E+01	2.88
3.12	0.052	0.44	1.94E-01	8.06E+01	3.12
3.36	0.056	0.46	2.09E-01	8.46E+01	3.36
3.6	0.06	0.48	2.24E-01	8.79E+01	3.6
3.84	0.064	0.49	2.39E-01	9.06E+01	3.84
4.08	0.068	0.52	2.54E-01	9.63E+01	4.08
4.32	0.072	0.76	2.69E-01	1.40E+02	4.32
4.56	0.076	1.46	2.84E-01	2.68E+02	4.56
4.8	0.08	1.99	2.99E-01	3.65E+02	4.8
5.04	0.084	2.44	3.14E-01	4.48E+02	5.04
5.28	0.088	2.76	3.29E-01	5.07E+02	5.28
5.52	0.092	3.11	3.44E-01	5.72E+02	5.52
5.76	0.096	3.44	3.59E-01	6.32E+02	5.76
6	0.1	3.76	3.74E-01	6.90E+02	6
6.24	0.104	4.11	3.89E-01	7.55E+02	6.24
6.48	0.108	4.46	4.04E-01	8.19E+02	6.48
6.72	0.112	4.77	4.19E-01	8.75E+02	6.72
6.96	0.116	5.11	4.35E-01	9.39E+02	6.96
7.2	0.12	5.45	4.49E-01	1.00E+03	7.2
7.44	0.124	5.8	4.64E-01	1.06E+03	7.44
7.68	0.128	6.13	4.79E-01	1.13E+03	7.68
7.92	0.132	6.49	4.94E-01	1.19E+03	7.92
8.16	0.136	6.81	5.10E-01	1.25E+03	8.16
8.4	0.14	7.15	5.24E-01	1.31E+03	8.4
8.64	0.144	7.5	5.39E-01	1.38E+03	8.64
8.88	0.148	7.92	5.54E-01	1.45E+03	8.88
9.12	0.152	8.31	5.69E-01	1.53E+03	9.12
9.36	0.156	8.71	5.84E-01	1.60E+03	9.36
9.6	0.16	9.12	5.99E-01	1.67E+03	9.6
9.84	0.164	9.56	6.15E-01	1.75E+03	9.84
10.08	0.168	10.01	6.29E-01	1.84E+03	10.08
10.32	0.172	10.41	6.44E-01	1.91E+03	10.32

10.56	0.176	10.93	6.59E-01	2.01E+03	10.56
10.8	0.18	11.67	6.74E-01	2.14E+03	10.8
11.04	0.184	12.46	6.90E-01	2.29E+03	11.04
11.28	0.188	13.1	7.04E-01	2.41E+03	11.28
11.52	0.192	13.58	7.19E-01	2.49E+03	11.52
11.76	0.196	14.07	7.34E-01	2.58E+03	11.76
12	0.2	14.58	7.49E-01	2.68E+03	12
12.24	0.204	15.06	7.65E-01	2.77E+03	12.24
12.48	0.208	15.61	7.79E-01	2.87E+03	12.48
12.72	0.212	16.17	7.95E-01	2.97E+03	12.72
12.96	0.216	16.79	8.09E-01	3.08E+03	12.96
13.2	0.22	17.51	8.24E-01	3.22E+03	13.2
13.44	0.224	18.5	8.39E-01	3.40E+03	13.44
13.68	0.228	19.62	8.54E-01	3.60E+03	13.68
13.92	0.232	20.55	8.70E-01	3.77E+03	13.92
14.16	0.236	21.44	8.84E-01	3.94E+03	14.16
14.4	0.24	22.33	8.99E-01	4.10E+03	14.4
14.64	0.244	23.32	9.14E-01	4.28E+03	14.64
14.88	0.248	24.44	9.29E-01	4.49E+03	14.88
15.12	0.252	25.73	9.45E-01	4.72E+03	15.12
15.36	0.256	27.23	9.59E-01	5.00E+03	15.36
15.6	0.26	28.72	9.75E-01	5.27E+03	15.6
15.84	0.264	30.13	9.89E-01	5.53E+03	15.84
16.08	0.268	31.46	1.00E+00	5.78E+03	16.08
16.32	0.272	32.77	1.02E+00	6.02E+03	16.32
16.56	0.276	33.99	1.03E+00	6.24E+03	16.56
16.8	0.28	35.11	1.05E+00	6.45E+03	16.8
17.04	0.284	36.17	1.06E+00	6.64E+03	17.04
17.28	0.288	37.15	1.08E+00	6.82E+03	17.28
17.52	0.292	38.03	1.09E+00	6.98E+03	17.52
17.76	0.296	38.72	1.11E+00	7.11E+03	17.76
18	0.3	39.28	1.13E+00	7.21E+03	18
18.24	0.304	39.69	1.14E+00	7.29E+03	18.24
18.48	0.308	39.97	1.16E+00	7.34E+03	18.48
18.72	0.312	40.11	1.17E+00	7.36E+03	18.72
18.96	0.316	40.11	1.18E+00	7.36E+03	18.96
19.2	0.32	40.06	1.20E+00	7.36E+03	19.2
19.44	0.324	39.95	1.21E+00	7.33E+03	19.44
19.68	0.328	39.74	1.23E+00	7.30E+03	19.68
19.92	0.332	39.48	1.24E+00	7.25E+03	19.92
20.16	0.336	39.15	1.26E+00	7.19E+03	20.16
20.4	0.34	38.8	1.27E+00	7.12E+03	20.4
20.64	0.344	38.54	1.29E+00	7.08E+03	20.64
20.88	0.348	38.3	1.31E+00	7.03E+03	20.88
21.12	0.352	37.97	1.32E+00	6.97E+03	21.12
21.36	0.356	37.64	1.34E+00	6.91E+03	21.36
21.6	0.36	37.31	1.35E+00	6.85E+03	21.6
21.84	0.364	37.01	1.36E+00	6.79E+03	21.84
22.08	0.368	36.74	1.38E+00	6.75E+03	22.08
22.32	0.372	36.52	1.39E+00	6.71E+03	22.32

22.56	0.376	36.29	1.41E+00	6.66E+03	22.56
22.8	0.38	36.06	1.42E+00	6.62E+03	22.8
23.04	0.384	35.81	1.44E+00	6.58E+03	23.04
23.28	0.388	35.58	1.46E+00	6.53E+03	23.28
23.52	0.392	35.38	1.47E+00	6.50E+03	23.52
23.76	0.396	35.18	1.49E+00	6.46E+03	23.76
24	0.4	34.95	1.50E+00	6.42E+03	24
24.24	0.404	34.71	1.52E+00	6.37E+03	24.24
24.48	0.408	34.43	1.53E+00	6.32E+03	24.48
24.72	0.412	34.17	1.55E+00	6.27E+03	24.72
24.96	0.416	33.94	1.56E+00	6.23E+03	24.96
25.2	0.42	33.68	1.57E+00	6.18E+03	25.2
25.44	0.424	33.46	1.59E+00	6.14E+03	25.44
25.68	0.428	33.24	1.60E+00	6.10E+03	25.68
25.92	0.432	33.03	1.62E+00	6.07E+03	25.92
26.16	0.436	32.82	1.64E+00	6.03E+03	26.16
26.4	0.44	32.59	1.65E+00	5.98E+03	26.4
26.64	0.444	32.29	1.67E+00	5.93E+03	26.64
26.88	0.448	32.04	1.68E+00	5.88E+03	26.88
27.12	0.452	31.79	1.70E+00	5.84E+03	27.12
27.36	0.456	31.53	1.71E+00	5.79E+03	27.36
27.6	0.46	31.24	1.73E+00	5.74E+03	27.6
27.84	0.464	31.02	1.74E+00	5.69E+03	27.84
28.08	0.468	30.81	1.75E+00	5.66E+03	28.08
28.32	0.472	30.57	1.77E+00	5.61E+03	28.32
28.56	0.476	30.36	1.78E+00	5.58E+03	28.56
28.8	0.48	30.12	1.80E+00	5.53E+03	28.8
29.04	0.484	29.83	1.82E+00	5.48E+03	29.04
29.28	0.488	29.59	1.83E+00	5.43E+03	29.28
29.52	0.492	29.39	1.85E+00	5.40E+03	29.52
29.76	0.496	29.15	1.86E+00	5.35E+03	29.76
30	0.5	28.97	1.88E+00	5.32E+03	30
30.24	0.504	28.77	1.89E+00	5.28E+03	30.24
30.48	0.508	28.57	1.91E+00	5.25E+03	30.48
30.72	0.512	28.39	1.92E+00	5.21E+03	30.72
30.96	0.516	28.22	1.93E+00	5.18E+03	30.96
31.2	0.52	28.03	1.95E+00	5.15E+03	31.2
31.44	0.524	27.86	1.97E+00	5.11E+03	31.44
31.68	0.528	27.68	1.98E+00	5.08E+03	31.68
31.92	0.532	27.5	2.00E+00	5.05E+03	31.92
32.16	0.536	27.35	2.01E+00	5.02E+03	32.16
32.4	0.54	27.2	2.03E+00	4.99E+03	32.4
32.64	0.544	27.07	2.04E+00	4.97E+03	32.64
32.88	0.548	26.93	2.06E+00	4.94E+03	32.88
33.12	0.552	26.8	2.07E+00	4.92E+03	33.12
33.36	0.556	26.66	2.09E+00	4.89E+03	33.36
33.6	0.56	26.53	2.10E+00	4.87E+03	33.6
33.84	0.564	26.4	2.11E+00	4.85E+03	33.84
34.08	0.568	26.27	2.13E+00	4.82E+03	34.08

34.32	0.572	26.11	2.15E+00	4.79E+03	34.32
34.56	0.576	25.96	2.16E+00	4.77E+03	34.56
34.8	0.58	25.85	2.18E+00	4.75E+03	34.8
35.04	0.584	25.7	2.19E+00	4.72E+03	35.04
35.28	0.588	25.56	2.21E+00	4.69E+03	35.28
35.52	0.592	25.44	2.22E+00	4.67E+03	35.52
35.76	0.596	25.33	2.24E+00	4.65E+03	35.76
36	0.6	25.18	2.25E+00	4.62E+03	36
36.24	0.604	25.1	2.27E+00	4.61E+03	36.24
36.48	0.608	25	2.28E+00	4.59E+03	36.48
36.72	0.611	24.85	2.29E+00	4.56E+03	36.72
36.96	0.616	24.73	2.31E+00	4.54E+03	36.96
37.2	0.62	24.61	2.33E+00	4.52E+03	37.2
37.44	0.624	24.45	2.34E+00	4.49E+03	37.44
37.68	0.628	24.33	2.36E+00	4.47E+03	37.68
37.92	0.632	24.18	2.37E+00	4.44E+03	37.92
38.16	0.636	24.02	2.39E+00	4.41E+03	38.16
38.4	0.639	23.91	2.40E+00	4.39E+03	38.4
38.64	0.644	23.74	2.42E+00	4.36E+03	38.64
38.88	0.648	23.54	2.43E+00	4.32E+03	38.88
39.12	0.652	23.39	2.45E+00	4.29E+03	39.12
39.36	0.656	23.21	2.46E+00	4.26E+03	39.36
39.6	0.659	23.09	2.48E+00	4.24E+03	39.6
39.84	0.664	22.9	2.49E+00	4.20E+03	39.84
40.08	0.667	22.71	2.51E+00	4.17E+03	40.08
40.32	0.672	22.5	2.52E+00	4.13E+03	40.32
40.56	0.676	22.27	2.54E+00	4.09E+03	40.56
40.8	0.68	22.14	2.55E+00	4.07E+03	40.8
41.04	0.684	21.97	2.57E+00	4.03E+03	41.04
41.28	0.687	21.83	2.58E+00	4.01E+03	41.28
41.52	0.692	21.72	2.60E+00	3.99E+03	41.52
41.76	0.695	21.56	2.61E+00	3.96E+03	41.76
42	0.7	21.44	2.63E+00	3.94E+03	42
42.24	0.704	21.29	2.64E+00	3.91E+03	42.24
42.48	0.708	21.2	2.66E+00	3.89E+03	42.48
42.72	0.712	21.11	2.67E+00	3.88E+03	42.72
42.96	0.715	21.04	2.69E+00	3.86E+03	42.96
43.2	0.72	20.94	2.70E+00	3.85E+03	43.2
43.44	0.723	20.83	2.72E+00	3.83E+03	43.44
43.68	0.728	20.72	2.73E+00	3.80E+03	43.68
43.92	0.732	20.62	2.75E+00	3.79E+03	43.92
44.16	0.735	20.5	2.76E+00	3.76E+03	44.16
44.4	0.74	20.39	2.78E+00	3.74E+03	44.4
44.64	0.743	20.28	2.79E+00	3.72E+03	44.64
44.88	0.748	20.19	2.81E+00	3.71E+03	44.88
45.12	0.751	20.09	2.82E+00	3.69E+03	45.12
45.36	0.756	20	2.84E+00	3.67E+03	45.36
45.6	0.76	19.86	2.85E+00	3.65E+03	45.6
45.84	0.763	19.76	2.87E+00	3.63E+03	45.84
46.08	0.768	19.62	2.88E+00	3.60E+03	46.08

46.32	0.771	19.51	2.90E+00	3.58E+03	46.32
46.56	0.776	19.39	2.91E+00	3.56E+03	46.56
46.8	0.779	19.26	2.93E+00	3.54E+03	46.8
47.04	0.783	19.1	2.94E+00	3.51E+03	47.04
47.28	0.788	18.93	2.96E+00	3.48E+03	47.28
47.52	0.791	18.82	2.97E+00	3.46E+03	47.52
47.76	0.796	18.7	2.99E+00	3.43E+03	47.76
48	0.799	18.58	3.00E+00	3.41E+03	48
48.24	0.804	18.41	3.02E+00	3.38E+03	48.24
48.48	0.807	18.29	3.03E+00	3.36E+03	48.48
48.72	0.811	18.14	3.05E+00	3.33E+03	48.72
48.96	0.816	18.03	3.06E+00	3.31E+03	48.96
49.2	0.819	17.87	3.08E+00	3.28E+03	49.2
49.44	0.824	17.78	3.09E+00	3.26E+03	49.44
49.68	0.827	17.68	3.11E+00	3.25E+03	49.68
49.92	0.831	17.5	3.12E+00	3.21E+03	49.92
50.16	0.835	17.36	3.14E+00	3.19E+03	50.16
50.4	0.839	17.21	3.15E+00	3.16E+03	50.4
50.64	0.844	17.06	3.17E+00	3.13E+03	50.64
50.88	0.847	16.91	3.18E+00	3.11E+03	50.88
51.12	0.852	16.84	3.20E+00	3.09E+03	51.12
51.36	0.855	16.73	3.21E+00	3.07E+03	51.36
51.6	0.859	16.64	3.23E+00	3.05E+03	51.6
51.84	0.863	16.56	3.24E+00	3.04E+03	51.84
52.08	0.867	16.46	3.26E+00	3.02E+03	52.08
52.32	0.872	16.35	3.27E+00	3.00E+03	52.32
52.56	0.875	16.26	3.29E+00	2.98E+03	52.56
52.8	0.88	16.18	3.30E+00	2.97E+03	52.8
53.04	0.883	16.07	3.32E+00	2.95E+03	53.04
53.28	0.887	15.98	3.33E+00	2.93E+03	53.28
53.52	0.891	15.94	3.35E+00	2.93E+03	53.52
53.76	0.895	15.91	3.36E+00	2.92E+03	53.76
54	0.899	15.85	3.38E+00	2.91E+03	54
54.24	0.903	15.86	3.39E+00	2.91E+03	54.24
54.48	0.907	15.82	3.41E+00	2.91E+03	54.48
54.72	0.911	15.74	3.42E+00	2.89E+03	54.72
54.96	0.915	15.67	3.44E+00	2.88E+03	54.96
55.2	0.919	15.57	3.45E+00	2.86E+03	55.2
55.44	0.923	15.51	3.47E+00	2.85E+03	55.44
55.68	0.928	15.45	3.48E+00	2.84E+03	55.68
55.92	0.931	15.36	3.50E+00	2.82E+03	55.92
56.16	0.935	15.23	3.51E+00	2.80E+03	56.16
56.4	0.939	15.09	3.53E+00	2.77E+03	56.4
56.64	0.943	14.95	3.54E+00	2.75E+03	56.64
56.88	0.947	14.85	3.56E+00	2.73E+03	56.88
57.12	0.951	14.7	3.57E+00	2.70E+03	57.12
57.36	0.955	14.57	3.59E+00	2.68E+03	57.36
57.6	0.959	14.42	3.60E+00	2.65E+03	57.6
57.84	0.963	14.24	3.62E+00	2.62E+03	57.84
58.08	0.967	14.06	3.63E+00	2.58E+03	58.08

58.32	0.971	13.91	3.65E+00	2.55E+03	58.32
58.56	0.975	13.76	3.66E+00	2.53E+03	58.56
58.8	0.979	13.59	3.68E+00	2.50E+03	58.8
59.04	0.983	13.47	3.69E+00	2.47E+03	59.04
59.28	0.987	13.31	3.71E+00	2.44E+03	59.28
59.52	0.991	13.14	3.72E+00	2.41E+03	59.52
59.76	0.995	12.97	3.74E+00	2.38E+03	59.76
60	0.999	12.79	3.75E+00	2.35E+03	60
60.24	1.003	12.6	3.77E+00	2.31E+03	60.24
60.48	1.007	12.41	3.78E+00	2.28E+03	60.48
60.72	1.011	12.21	3.80E+00	2.24E+03	60.72
60.96	1.015	11.99	3.81E+00	2.20E+03	60.96
61.2	1.019	11.78	3.83E+00	2.16E+03	61.2
61.44	1.023	11.56	3.84E+00	2.12E+03	61.44
61.68	1.027	11.33	3.86E+00	2.08E+03	61.68
61.92	1.031	11.11	3.87E+00	2.04E+03	61.92
62.16	1.035	10.91	3.89E+00	2.00E+03	62.16
62.4	1.039	10.7	3.90E+00	1.97E+03	62.4
62.64	1.043	10.51	3.92E+00	1.93E+03	62.64
62.88	1.047	10.34	3.93E+00	1.90E+03	62.88
63.12	1.051	10.13	3.95E+00	1.86E+03	63.12
63.36	1.055	9.92	3.96E+00	1.82E+03	63.36
63.6	1.059	9.65	3.98E+00	1.77E+03	63.6
63.84	1.063	8.97	3.99E+00	1.65E+03	63.84
64.08	1.067	8.99	4.01E+00	1.65E+03	64.08
64.32	1.071	8.94	4.02E+00	1.64E+03	64.32
64.56	1.075	8.89	4.04E+00	1.63E+03	64.56
64.8	1.079	8.78	4.05E+00	1.61E+03	64.8
65.04	1.083	8.67	4.07E+00	1.59E+03	65.04
65.28	1.087	8.55	4.08E+00	1.57E+03	65.28
65.52	1.091	8.46	4.10E+00	1.55E+03	65.52
65.76	1.095	8.39	4.11E+00	1.54E+03	65.76
66	1.099	8.31	4.13E+00	1.53E+03	66
66.24	1.103	8.23	4.14E+00	1.51E+03	66.24
66.48	1.107	8.13	4.16E+00	1.49E+03	66.48
66.72	1.111	8.03	4.17E+00	1.48E+03	66.72
66.96	1.115	7.92	4.19E+00	1.45E+03	66.96
67.2	1.119	7.84	4.20E+00	1.44E+03	67.2
67.44	1.123	7.73	4.22E+00	1.42E+03	67.44
67.68	1.127	7.66	4.23E+00	1.41E+03	67.68
67.92	1.131	7.59	4.25E+00	1.39E+03	67.92
68.16	1.135	7.48	4.26E+00	1.37E+03	68.16
68.4	1.139	7.44	4.28E+00	1.37E+03	68.4
68.64	1.143	7.33	4.29E+00	1.35E+03	68.64
68.88	1.147	7.21	4.31E+00	1.32E+03	68.88
69.12	1.151	7.11	4.32E+00	1.31E+03	69.12
69.36	1.155	6.99	4.34E+00	1.28E+03	69.36
69.6	1.159	6.84	4.35E+00	1.26E+03	69.6
69.84	1.163	6.7	4.37E+00	1.23E+03	69.84

70.08	1.167	6.6	4.38E+00	1.21E+03	70.08
70.32	1.171	6.49	4.40E+00	1.19E+03	70.32
70.56	1.175	6.42	4.41E+00	1.18E+03	70.56
70.8	1.179	6.32	4.43E+00	1.16E+03	70.8
71.04	1.183	6.27	4.44E+00	1.15E+03	71.04
71.28	1.187	6.18	4.46E+00	1.14E+03	71.28
71.52	1.191	6.14	4.47E+00	1.13E+03	71.52
71.76	1.195	6.08	4.49E+00	1.12E+03	71.76
72	1.199	6.08	4.50E+00	1.12E+03	72
72.24	1.203	6.03	4.52E+00	1.11E+03	72.24
72.48	1.207	6.04	4.53E+00	1.11E+03	72.48
72.72	1.211	6.09	4.55E+00	1.12E+03	72.72
72.96	1.215	6.08	4.56E+00	1.12E+03	72.96
73.2	1.219	6.08	4.58E+00	1.12E+03	73.2
73.44	1.223	6.08	4.59E+00	1.12E+03	73.44
73.68	1.227	6.06	4.61E+00	1.11E+03	73.68
73.92	1.231	6.05	4.62E+00	1.11E+03	73.92
74.16	1.235	6.06	4.64E+00	1.11E+03	74.16
74.4	1.239	6.04	4.65E+00	1.11E+03	74.4
74.64	1.243	6.04	4.67E+00	1.11E+03	74.64
74.88	1.247	6.02	4.68E+00	1.10E+03	74.88
75.12	1.251	5.97	4.70E+00	1.10E+03	75.12
75.36	1.255	5.94	4.71E+00	1.09E+03	75.36
75.6	1.259	5.92	4.73E+00	1.09E+03	75.6
75.84	1.263	5.87	4.74E+00	1.08E+03	75.84
76.08	1.267	5.9	4.76E+00	1.08E+03	76.08
76.32	1.271	5.87	4.77E+00	1.08E+03	76.32
76.56	1.275	5.9	4.79E+00	1.08E+03	76.56
76.8	1.279	5.88	4.80E+00	1.08E+03	76.8
77.04	1.283	5.86	4.82E+00	1.08E+03	77.04
77.28	1.287	5.88	4.83E+00	1.08E+03	77.28
77.52	1.291	5.89	4.85E+00	1.08E+03	77.52
77.76	1.295	5.9	4.86E+00	1.08E+03	77.76
78	1.299	5.94	4.88E+00	1.09E+03	78
78.24	1.303	6.01	4.89E+00	1.10E+03	78.24
78.48	1.307	6.03	4.91E+00	1.11E+03	78.48
78.72	1.311	6.04	4.92E+00	1.11E+03	78.72
78.96	1.315	6.04	4.94E+00	1.11E+03	78.96
79.2	1.319	6.07	4.95E+00	1.11E+03	79.2
79.44	1.323	6.13	4.97E+00	1.13E+03	79.44
79.68	1.327	6.18	4.98E+00	1.13E+03	79.68
79.92	1.331	6.21	5.00E+00	1.14E+03	79.92
80.16	1.335	6.24	5.01E+00	1.15E+03	80.16
80.4	1.339	6.26	5.03E+00	1.15E+03	80.4
80.64	1.343	6.23	5.04E+00	1.14E+03	80.64
80.88	1.347	6.27	5.06E+00	1.15E+03	80.88
81.12	1.351	6.32	5.07E+00	1.16E+03	81.12
81.36	1.355	6.33	5.09E+00	1.16E+03	81.36
81.6	1.359	6.37	5.10E+00	1.17E+03	81.6
81.84	1.363	6.39	5.12E+00	1.17E+03	81.84

82.08	1.367	6.43	5.13E+00	1.18E+03	82.08
82.32	1.371	6.48	5.15E+00	1.19E+03	82.32
82.56	1.375	6.57	5.16E+00	1.21E+03	82.56
82.8	1.379	6.61	5.18E+00	1.21E+03	82.8
83.04	1.383	6.65	5.19E+00	1.22E+03	83.04
83.28	1.387	6.68	5.21E+00	1.23E+03	83.28
83.52	1.391	6.66	5.22E+00	1.22E+03	83.52
83.76	1.395	6.72	5.24E+00	1.23E+03	83.76
84	1.399	6.71	5.25E+00	1.23E+03	84
84.24	1.403	6.73	5.27E+00	1.24E+03	84.24
84.48	1.407	6.71	5.28E+00	1.23E+03	84.48
84.72	1.411	6.72	5.30E+00	1.23E+03	84.72
84.96	1.415	6.71	5.31E+00	1.23E+03	84.96
85.2	1.419	6.69	5.33E+00	1.23E+03	85.2
85.44	1.423	6.66	5.34E+00	1.22E+03	85.44
85.68	1.427	6.64	5.36E+00	1.22E+03	85.68
85.92	1.431	6.63	5.37E+00	1.22E+03	85.92
86.16	1.435	6.64	5.39E+00	1.22E+03	86.16
86.4	1.439	6.62	5.40E+00	1.22E+03	86.4
86.64	1.443	6.61	5.42E+00	1.21E+03	86.64
86.88	1.447	6.59	5.43E+00	1.21E+03	86.88
87.12	1.451	6.58	5.45E+00	1.21E+03	87.12
87.36	1.455	6.53	5.46E+00	1.20E+03	87.36
87.6	1.459	6.53	5.48E+00	1.20E+03	87.6
87.84	1.463	6.51	5.49E+00	1.20E+03	87.84
88.08	1.467	6.45	5.51E+00	1.19E+03	88.08
88.32	1.471	6.46	5.52E+00	1.19E+03	88.32
88.56	1.475	6.44	5.54E+00	1.18E+03	88.56
88.8	1.479	6.39	5.55E+00	1.17E+03	88.8
89.04	1.483	6.37	5.57E+00	1.17E+03	89.04
89.28	1.487	6.37	5.58E+00	1.17E+03	89.28
89.52	1.491	6.34	5.60E+00	1.16E+03	89.52
89.76	1.495	6.31	5.61E+00	1.16E+03	89.76
90	1.499	6.3	5.63E+00	1.16E+03	90
90.24	1.503	6.3	5.64E+00	1.16E+03	90.24
90.48	1.507	6.31	5.66E+00	1.16E+03	90.48
90.72	1.511	6.31	5.67E+00	1.16E+03	90.72
90.96	1.515	6.33	5.69E+00	1.16E+03	90.96
91.2	1.519	6.32	5.70E+00	1.16E+03	91.2
91.44	1.523	6.34	5.72E+00	1.17E+03	91.44
91.68	1.527	6.33	5.73E+00	1.16E+03	91.68
91.92	1.531	6.33	5.75E+00	1.16E+03	91.92
92.16	1.535	6.33	5.76E+00	1.16E+03	92.16
92.4	1.539	6.4	5.78E+00	1.18E+03	92.4
92.64	1.543	6.43	5.79E+00	1.18E+03	92.64
92.88	1.547	6.41	5.81E+00	1.18E+03	92.88
93.12	1.551	6.48	5.82E+00	1.19E+03	93.12
93.36	1.555	6.57	5.84E+00	1.21E+03	93.36
93.6	1.559	6.65	5.85E+00	1.22E+03	93.6
93.84	1.563	6.74	5.87E+00	1.24E+03	93.84

94.08	1.567	6.86	5.88E+00	1.26E+03	94.08
94.32	1.571	7.04	5.90E+00	1.29E+03	94.32
94.56	1.575	7.18	5.91E+00	1.32E+03	94.56
94.8	1.579	7.35	5.93E+00	1.35E+03	94.8
95.04	1.583	7.45	5.94E+00	1.37E+03	95.04
95.28	1.587	7.64	5.96E+00	1.40E+03	95.28
95.52	1.591	7.77	5.97E+00	1.43E+03	95.52
95.76	1.595	7.95	5.99E+00	1.46E+03	95.76
96	1.599	8.1	6.00E+00	1.49E+03	96
96.24	1.603	8.27	6.02E+00	1.52E+03	96.24
96.48	1.607	8.44	6.03E+00	1.55E+03	96.48
96.72	1.611	8.6	6.05E+00	1.58E+03	96.72
96.96	1.615	8.79	6.06E+00	1.61E+03	96.96
97.2	1.619	8.96	6.08E+00	1.65E+03	97.2
97.44	1.623	9.14	6.09E+00	1.68E+03	97.44
97.68	1.627	9.31	6.11E+00	1.71E+03	97.68
97.92	1.631	9.45	6.12E+00	1.74E+03	97.92
98.16	1.635	9.57	6.14E+00	1.76E+03	98.16
98.4	1.639	9.67	6.15E+00	1.78E+03	98.4
98.64	1.643	9.73	6.17E+00	1.79E+03	98.64
98.88	1.647	9.77	6.18E+00	1.79E+03	98.88
99.12	1.651	9.84	6.20E+00	1.81E+03	99.12
99.36	1.655	9.89	6.21E+00	1.82E+03	99.36
99.6	1.659	9.98	6.23E+00	1.83E+03	99.6
99.84	1.663	10.01	6.24E+00	1.84E+03	99.84
100.08	1.667	9.99	6.26E+00	1.83E+03	100.08
100.32	1.671	9.93	6.27E+00	1.82E+03	100.32
100.56	1.675	9.9	6.29E+00	1.82E+03	100.56
100.8	1.679	9.87	6.30E+00	1.81E+03	100.8
101.04	1.683	9.8	6.32E+00	1.80E+03	101.04
101.28	1.687	9.75	6.33E+00	1.79E+03	101.28
101.52	1.691	9.68	6.35E+00	1.78E+03	101.52
101.76	1.695	9.59	6.36E+00	1.76E+03	101.76
102	1.699	9.49	6.38E+00	1.74E+03	102
102.24	1.703	9.35	6.39E+00	1.72E+03	102.24
102.48	1.707	9.16	6.41E+00	1.68E+03	102.48
102.72	1.711	9.01	6.42E+00	1.65E+03	102.72
102.96	1.715	8.87	6.44E+00	1.63E+03	102.96
103.2	1.719	8.77	6.45E+00	1.61E+03	103.2
103.44	1.723	8.66	6.47E+00	1.59E+03	103.44
103.68	1.727	8.57	6.48E+00	1.57E+03	103.68
103.92	1.731	8.53	6.50E+00	1.57E+03	103.92
104.16	1.735	8.41	6.51E+00	1.54E+03	104.16
104.4	1.739	8.35	6.53E+00	1.53E+03	104.4
104.64	1.743	8.26	6.54E+00	1.52E+03	104.64
104.88	1.747	8.19	6.56E+00	1.50E+03	104.88
105.12	1.751	8.18	6.57E+00	1.50E+03	105.12
105.36	1.755	8.16	6.59E+00	1.50E+03	105.36
105.6	1.759	8.17	6.60E+00	1.50E+03	105.6

105.84	1.763	8.15	6.62E+00	1.50E+03	105.84
106.08	1.767	8.13	6.63E+00	1.49E+03	106.08
106.32	1.771	8.18	6.65E+00	1.50E+03	106.32
106.56	1.775	8.22	6.66E+00	1.51E+03	106.56
106.8	1.779	8.28	6.68E+00	1.52E+03	106.8
107.04	1.783	8.36	6.69E+00	1.54E+03	107.04
107.28	1.787	8.44	6.71E+00	1.55E+03	107.28
107.52	1.791	8.48	6.72E+00	1.56E+03	107.52
107.76	1.795	8.57	6.74E+00	1.57E+03	107.76
108	1.799	8.67	6.75E+00	1.59E+03	108
108.24	1.803	8.78	6.77E+00	1.61E+03	108.24
108.48	1.807	8.93	6.78E+00	1.64E+03	108.48
108.72	1.811	9.1	6.80E+00	1.67E+03	108.72
108.96	1.815	9.24	6.81E+00	1.70E+03	108.96
109.2	1.819	9.4	6.83E+00	1.73E+03	109.2
109.44	1.823	9.55	6.84E+00	1.75E+03	109.44
109.68	1.827	9.71	6.86E+00	1.78E+03	109.68
109.92	1.831	9.87	6.87E+00	1.81E+03	109.92
110.16	1.835	10.02	6.89E+00	1.84E+03	110.16
110.4	1.839	10.2	6.90E+00	1.87E+03	110.4
110.64	1.843	10.4	6.92E+00	1.91E+03	110.64
110.88	1.847	10.54	6.93E+00	1.93E+03	110.88
111.12	1.851	10.7	6.95E+00	1.96E+03	111.12
111.36	1.855	10.87	6.96E+00	2.00E+03	111.36
111.6	1.859	11.01	6.98E+00	2.02E+03	111.6
111.84	1.863	11.16	6.99E+00	2.05E+03	111.84
112.08	1.867	11.26	7.01E+00	2.07E+03	112.08
112.32	1.871	11.38	7.02E+00	2.09E+03	112.32
112.56	1.875	11.52	7.04E+00	2.12E+03	112.56
112.8	1.879	11.66	7.05E+00	2.14E+03	112.8
113.04	1.883	11.85	7.07E+00	2.18E+03	113.04
113.28	1.887	11.98	7.08E+00	2.20E+03	113.28
113.52	1.891	12.09	7.10E+00	2.22E+03	113.52
113.76	1.895	12.19	7.11E+00	2.24E+03	113.76
114	1.899	12.3	7.13E+00	2.26E+03	114
114.24	1.903	12.41	7.14E+00	2.28E+03	114.24
114.48	1.907	12.45	7.16E+00	2.29E+03	114.48
114.72	1.911	12.56	7.17E+00	2.31E+03	114.72
114.96	1.915	12.67	7.19E+00	2.33E+03	114.96
115.2	1.919	12.82	7.20E+00	2.35E+03	115.2
115.44	1.923	12.88	7.22E+00	2.37E+03	115.44
115.68	1.927	12.94	7.23E+00	2.38E+03	115.68
115.92	1.931	12.99	7.25E+00	2.39E+03	115.92
116.16	1.935	13.06	7.26E+00	2.40E+03	116.16
116.4	1.939	13.12	7.28E+00	2.41E+03	116.4
116.64	1.943	13.22	7.29E+00	2.43E+03	116.64
116.88	1.947	13.31	7.31E+00	2.44E+03	116.88
117.12	1.951	13.43	7.32E+00	2.47E+03	117.12
117.36	1.955	13.46	7.34E+00	2.47E+03	117.36
117.6	1.959	13.48	7.35E+00	2.48E+03	117.6

117.84	1.963	13.53	7.37E+00	2.49E+03	117.84
118.08	1.967	13.64	7.38E+00	2.51E+03	118.08
118.32	1.971	13.7	7.40E+00	2.52E+03	118.32
118.56	1.975	13.79	7.41E+00	2.53E+03	118.56
118.8	1.979	13.88	7.43E+00	2.55E+03	118.8
119.04	1.983	13.93	7.44E+00	2.56E+03	119.04
119.28	1.987	13.97	7.46E+00	2.57E+03	119.28
119.52	1.991	14.03	7.47E+00	2.58E+03	119.52
119.76	1.995	14.06	7.49E+00	2.58E+03	119.76

Summary of Run 2 for All Sample in both Directions

RUN	SAMPLE	TYPE	Length (mm)	Width (mm)	Height (mm)	MODULUS (MPa)	Yield (kPa)	Stress at Yield Strength (%)	Ultimate Yield (kPa)
2	3	AT2	23.37	2.92	0.89	1483.0	12910	1.967	15340
		TT2	24.28	2.89	2.16	1017.0	5405	1.625	5425
	4	AT2	23.94	2.90	1.19	2507.0	23310	2.317	23840
		TT2	26.24	2.97	1.28	2742.0	10460	1.017	10470
	5	AT3	29.31	2.97	0.79	3227.0	34230	1.759	34770
		TT2	21.06	2.94	1.06	1898.0	16740	2.050	17060
	6	AT2	29.98	2.86	1.71	2514.0	20470	1.490	20630
		TT3	26.75	2.95	1.23	2233.0	16090	1.733	16230
	7	AT2	25.99	2.89	1.00	4691.0	32930	1.372	33070
		TT3	30.85	2.92	1.37	2601.0	18120	1.779	18120

Flexural Data

Run 2, Sample 6, Transverse Direction

Time sec	Delta_L mm	Force N	Strain %	Stress KPa	LZn_Time sec
0	0	0.02	0.00E+00	1.42E+01	0
0.18	0.002	0.14	6.02E-03	1.15E+02	0.18
0.36	0.004	0.1	1.25E-02	8.38E+01	0.36
0.54	0.007	0.14	1.93E-02	1.11E+02	0.54
0.72	0.009	0.13	2.58E-02	1.04E+02	0.72
0.9	0.011	0.16	3.27E-02	1.30E+02	0.9
1.08	0.013	0.16	3.91E-02	1.30E+02	1.08
1.26	0.016	0.11	4.60E-02	9.06E+01	1.26
1.44	0.018	0.19	5.24E-02	1.49E+02	1.44
1.62	0.02	0.24	5.89E-02	1.95E+02	1.62
1.8	0.022	0.18	6.57E-02	1.48E+02	1.8
1.98	0.025	0.2	7.22E-02	1.62E+02	1.98
2.16	0.027	0.28	7.91E-02	2.23E+02	2.16
2.34	0.029	0.31	8.55E-02	2.52E+02	2.34
2.52	0.031	0.41	9.24E-02	3.32E+02	2.52
2.7	0.034	0.39	9.88E-02	3.17E+02	2.7
2.88	0.036	0.46	1.05E-01	3.73E+02	2.88
3.06	0.038	0.43	1.12E-01	3.44E+02	3.06
3.24	0.04	0.54	1.19E-01	4.32E+02	3.24
3.42	0.043	0.67	1.26E-01	5.35E+02	3.42
3.6	0.045	0.7	1.32E-01	5.61E+02	3.6
3.78	0.047	0.8	1.39E-01	6.42E+02	3.78
3.96	0.049	0.9	1.45E-01	7.22E+02	3.96
4.14	0.051	1.01	1.52E-01	8.12E+02	4.14
4.32	0.054	1.1	1.59E-01	8.79E+02	4.32
4.5	0.056	1.21	1.65E-01	9.73E+02	4.5
4.68	0.058	1.4	1.72E-01	1.12E+03	4.68
4.86	0.061	1.52	1.78E-01	1.22E+03	4.86
5.04	0.063	1.67	1.85E-01	1.34E+03	5.04
5.22	0.065	1.8	1.92E-01	1.44E+03	5.22
5.4	0.067	1.93	1.98E-01	1.55E+03	5.4
5.58	0.07	2.02	2.05E-01	1.62E+03	5.58
5.76	0.072	2.12	2.11E-01	1.71E+03	5.76
5.94	0.074	2.3	2.18E-01	1.84E+03	5.94
6.12	0.076	2.41	2.25E-01	1.94E+03	6.12
6.3	0.078	2.58	2.31E-01	2.07E+03	6.3
6.48	0.081	2.72	2.38E-01	2.18E+03	6.48
6.66	0.083	2.79	2.45E-01	2.24E+03	6.66
6.84	0.085	2.89	2.51E-01	2.32E+03	6.84
7.02	0.088	2.96	2.58E-01	2.38E+03	7.02
7.2	0.09	3.12	2.65E-01	2.50E+03	7.2
7.38	0.092	3.23	2.71E-01	2.59E+03	7.38
7.56	0.094	3.32	2.78E-01	2.67E+03	7.56
7.74	0.097	3.43	2.84E-01	2.75E+03	7.74

7.92	0.099	3.5	2.91E-01	2.81E+03	7.92
8.1	0.101	3.67	2.98E-01	2.95E+03	8.1
8.28	0.103	3.75	3.04E-01	3.01E+03	8.28
8.46	0.106	3.8	3.11E-01	3.05E+03	8.46
8.64	0.108	3.91	3.18E-01	3.14E+03	8.64
8.82	0.11	4.03	3.24E-01	3.23E+03	8.82
9	0.112	4.11	3.31E-01	3.29E+03	9
9.18	0.114	4.11	3.37E-01	3.29E+03	9.18
9.36	0.117	4.14	3.44E-01	3.32E+03	9.36
9.54	0.119	4.09	3.51E-01	3.28E+03	9.54
9.72	0.121	4.12	3.57E-01	3.30E+03	9.72
9.9	0.124	4.15	3.64E-01	3.33E+03	9.9
10.08	0.126	4.12	3.70E-01	3.31E+03	10.08
10.26	0.128	4.13	3.77E-01	3.32E+03	10.26
10.44	0.13	4.2	3.84E-01	3.37E+03	10.44
10.62	0.133	4.24	3.91E-01	3.40E+03	10.62
10.8	0.135	4.25	3.97E-01	3.41E+03	10.8
10.98	0.137	4.36	4.03E-01	3.50E+03	10.98
11.16	0.139	4.4	4.10E-01	3.53E+03	11.16
11.34	0.141	4.42	4.17E-01	3.55E+03	11.34
11.52	0.144	4.55	4.24E-01	3.65E+03	11.52
11.7	0.146	4.54	4.30E-01	3.64E+03	11.7
11.88	0.148	4.65	4.37E-01	3.73E+03	11.88
12.06	0.151	4.7	4.43E-01	3.77E+03	12.06
12.24	0.153	4.79	4.50E-01	3.84E+03	12.24
12.42	0.155	4.84	4.57E-01	3.89E+03	12.42
12.6	0.157	5.04	4.63E-01	4.04E+03	12.6
12.78	0.16	5.05	4.70E-01	4.05E+03	12.78
12.96	0.162	5.2	4.77E-01	4.17E+03	12.96
13.14	0.164	5.3	4.83E-01	4.25E+03	13.14
13.32	0.166	5.37	4.90E-01	4.31E+03	13.32
13.5	0.168	5.48	4.96E-01	4.40E+03	13.5
13.68	0.171	5.63	5.03E-01	4.51E+03	13.68
13.86	0.173	5.82	5.10E-01	4.67E+03	13.86
14.04	0.175	5.93	5.16E-01	4.75E+03	14.04
14.22	0.177	6.06	5.23E-01	4.86E+03	14.22
14.4	0.18	6.05	5.30E-01	4.85E+03	14.4
14.58	0.182	6.17	5.36E-01	4.95E+03	14.58
14.76	0.184	6.35	5.43E-01	5.10E+03	14.76
14.94	0.187	6.38	5.50E-01	5.12E+03	14.94
15.12	0.189	6.47	5.56E-01	5.19E+03	15.12
15.3	0.191	6.54	5.63E-01	5.25E+03	15.3
15.48	0.193	6.58	5.69E-01	5.28E+03	15.48
15.66	0.195	6.73	5.76E-01	5.40E+03	15.66
15.84	0.198	6.76	5.83E-01	5.42E+03	15.84
16.02	0.2	6.78	5.89E-01	5.44E+03	16.02
16.2	0.202	6.91	5.96E-01	5.54E+03	16.2
16.38	0.204	6.95	6.02E-01	5.58E+03	16.38
16.56	0.207	7.02	6.09E-01	5.63E+03	16.56
16.74	0.209	6.97	6.16E-01	5.59E+03	16.74
16.92	0.211	6.95	6.22E-01	5.57E+03	16.92
17.1	0.214	6.98	6.29E-01	5.60E+03	17.1

17.28	0.216	6.98	6.35E-01	5.60E+03	17.28
17.46	0.218	6.97	6.42E-01	5.59E+03	17.46
17.64	0.22	7.01	6.49E-01	5.63E+03	17.64
17.82	0.223	7.04	6.56E-01	5.64E+03	17.82
18	0.225	7.03	6.62E-01	5.64E+03	18
18.18	0.227	7.11	6.69E-01	5.70E+03	18.18
18.36	0.229	7.18	6.75E-01	5.76E+03	18.36
18.54	0.231	7.22	6.82E-01	5.79E+03	18.54
18.72	0.234	7.26	6.89E-01	5.82E+03	18.72
18.9	0.236	7.28	6.95E-01	5.84E+03	18.9
19.08	0.238	7.31	7.02E-01	5.87E+03	19.08
19.26	0.24	7.3	7.09E-01	5.86E+03	19.26
19.44	0.243	7.35	7.15E-01	5.89E+03	19.44
19.62	0.245	7.37	7.22E-01	5.91E+03	19.62
19.8	0.247	7.31	7.28E-01	5.86E+03	19.8
19.98	0.25	7.36	7.35E-01	5.91E+03	19.98
20.16	0.252	7.37	7.42E-01	5.92E+03	20.16
20.34	0.254	7.36	7.48E-01	5.90E+03	20.34
20.52	0.256	7.37	7.55E-01	5.91E+03	20.52
20.7	0.258	7.37	7.61E-01	5.91E+03	20.7
20.88	0.261	7.33	7.68E-01	5.88E+03	20.88
21.06	0.263	7.4	7.75E-01	5.94E+03	21.06
21.24	0.265	7.35	7.82E-01	5.89E+03	21.24
21.42	0.267	7.4	7.88E-01	5.93E+03	21.42
21.6	0.27	7.39	7.94E-01	5.93E+03	21.6
21.78	0.272	7.37	8.01E-01	5.91E+03	21.78
21.96	0.274	7.41	8.08E-01	5.95E+03	21.96
22.14	0.277	7.52	8.15E-01	6.03E+03	22.14
22.32	0.279	7.43	8.21E-01	5.96E+03	22.32
22.5	0.281	7.49	8.28E-01	6.01E+03	22.5
22.68	0.283	7.51	8.34E-01	6.03E+03	22.68
22.86	0.285	7.53	8.41E-01	6.04E+03	22.86
23.04	0.288	7.49	8.48E-01	6.01E+03	23.04
23.22	0.29	7.5	8.54E-01	6.02E+03	23.22
23.4	0.292	7.52	8.61E-01	6.03E+03	23.4
23.58	0.294	7.55	8.68E-01	6.06E+03	23.58
23.76	0.297	7.57	8.74E-01	6.07E+03	23.76
23.94	0.299	7.55	8.81E-01	6.06E+03	23.94
24.12	0.301	7.58	8.87E-01	6.08E+03	24.12
24.3	0.303	7.56	8.94E-01	6.07E+03	24.3
24.48	0.306	7.61	9.01E-01	6.11E+03	24.48
24.66	0.308	7.6	9.07E-01	6.10E+03	24.66
24.84	0.31	7.61	9.14E-01	6.11E+03	24.84
25.02	0.312	7.61	9.20E-01	6.11E+03	25.02
25.2	0.315	7.62	9.27E-01	6.11E+03	25.2
25.38	0.317	7.63	9.34E-01	6.12E+03	25.38
25.56	0.319	7.62	9.41E-01	6.12E+03	25.56
25.74	0.321	7.65	9.47E-01	6.13E+03	25.74
25.92	0.324	7.65	9.54E-01	6.14E+03	25.92
26.1	0.326	7.65	9.60E-01	6.14E+03	26.1
26.28	0.328	7.7	9.67E-01	6.18E+03	26.28
26.46	0.33	7.72	9.74E-01	6.19E+03	26.46

26.64	0.333	7.79	9.80E-01	6.25E+03	26.64
26.82	0.335	7.81	9.87E-01	6.26E+03	26.82
27	0.337	7.81	9.93E-01	6.26E+03	27
27.18	0.34	7.91	1.00E+00	6.35E+03	27.18
27.36	0.342	8	1.01E+00	6.42E+03	27.36
27.54	0.344	8.11	1.01E+00	6.50E+03	27.54
27.72	0.346	8.18	1.02E+00	6.56E+03	27.72
27.9	0.348	8.31	1.03E+00	6.67E+03	27.9
28.08	0.351	8.39	1.03E+00	6.73E+03	28.08
28.26	0.353	8.48	1.04E+00	6.80E+03	28.26
28.44	0.355	8.54	1.05E+00	6.85E+03	28.44
28.62	0.357	8.68	1.05E+00	6.96E+03	28.62
28.8	0.36	8.73	1.06E+00	7.00E+03	28.8
28.98	0.362	8.86	1.07E+00	7.11E+03	28.98
29.16	0.364	8.94	1.07E+00	7.17E+03	29.16
29.34	0.366	9.07	1.08E+00	7.27E+03	29.34
29.52	0.369	9.15	1.09E+00	7.34E+03	29.52
29.7	0.371	9.24	1.09E+00	7.41E+03	29.7
29.88	0.373	9.32	1.10E+00	7.48E+03	29.88
30.06	0.375	9.45	1.11E+00	7.58E+03	30.06
30.24	0.378	9.58	1.11E+00	7.68E+03	30.24
30.42	0.38	9.67	1.12E+00	7.76E+03	30.42
30.6	0.382	9.73	1.13E+00	7.81E+03	30.6
30.78	0.384	9.86	1.13E+00	7.91E+03	30.78
30.96	0.387	10.03	1.14E+00	8.04E+03	30.96
31.14	0.389	10.1	1.15E+00	8.10E+03	31.14
31.32	0.391	10.17	1.15E+00	8.16E+03	31.32
31.5	0.393	10.28	1.16E+00	8.25E+03	31.5
31.68	0.396	10.35	1.17E+00	8.30E+03	31.68
31.86	0.398	10.51	1.17E+00	8.43E+03	31.86
32.04	0.4	10.62	1.18E+00	8.52E+03	32.04
32.22	0.402	10.81	1.19E+00	8.67E+03	32.22
32.4	0.405	10.96	1.19E+00	8.80E+03	32.4
32.58	0.407	11.18	1.20E+00	8.97E+03	32.58
32.76	0.409	11.33	1.21E+00	9.09E+03	32.76
32.94	0.411	11.52	1.21E+00	9.24E+03	32.94
33.12	0.414	11.68	1.22E+00	9.37E+03	33.12
33.3	0.416	11.86	1.23E+00	9.52E+03	33.3
33.48	0.418	12.06	1.23E+00	9.68E+03	33.48
33.66	0.42	12.25	1.24E+00	9.82E+03	33.66
33.84	0.423	12.43	1.25E+00	9.97E+03	33.84
34.02	0.425	12.62	1.25E+00	1.01E+04	34.02
34.2	0.427	12.84	1.26E+00	1.03E+04	34.2
34.38	0.429	13.07	1.27E+00	1.05E+04	34.38
34.56	0.432	13.36	1.27E+00	1.07E+04	34.56
34.74	0.434	13.66	1.28E+00	1.10E+04	34.74
34.92	0.436	13.88	1.29E+00	1.11E+04	34.92
35.1	0.438	14.17	1.29E+00	1.14E+04	35.1
35.28	0.441	14.43	1.30E+00	1.16E+04	35.28
35.46	0.443	14.75	1.31E+00	1.18E+04	35.46
35.64	0.445	15.06	1.31E+00	1.21E+04	35.64

35.82	0.447	15.3	1.32E+00	1.23E+04	35.82
36	0.45	15.65	1.33E+00	1.26E+04	36
36.18	0.452	15.94	1.33E+00	1.28E+04	36.18
36.36	0.454	16.27	1.34E+00	1.31E+04	36.36
36.54	0.456	16.54	1.35E+00	1.33E+04	36.54
36.72	0.459	16.89	1.35E+00	1.36E+04	36.72
36.9	0.461	17.18	1.36E+00	1.38E+04	36.9
37.08	0.463	17.48	1.37E+00	1.40E+04	37.08
37.26	0.465	17.75	1.37E+00	1.42E+04	37.26
37.44	0.468	18.06	1.38E+00	1.45E+04	37.44
37.62	0.47	18.37	1.38E+00	1.47E+04	37.62
37.8	0.472	18.66	1.39E+00	1.50E+04	37.8
37.98	0.474	18.93	1.40E+00	1.52E+04	37.98
38.16	0.477	19.24	1.40E+00	1.54E+04	38.16
38.34	0.479	19.49	1.41E+00	1.56E+04	38.34
38.52	0.481	19.78	1.42E+00	1.59E+04	38.52
38.7	0.483	20.07	1.42E+00	1.61E+04	38.7
38.88	0.486	20.39	1.43E+00	1.64E+04	38.88
39.06	0.488	20.68	1.44E+00	1.66E+04	39.06
39.24	0.49	20.99	1.44E+00	1.68E+04	39.24
39.42	0.492	21.25	1.45E+00	1.71E+04	39.42
39.6	0.495	21.61	1.46E+00	1.73E+04	39.6
39.78	0.497	21.92	1.46E+00	1.76E+04	39.78
39.96	0.499	22.23	1.47E+00	1.78E+04	39.96
40.14	0.501	22.53	1.48E+00	1.81E+04	40.14
40.32	0.504	22.8	1.48E+00	1.83E+04	40.32
40.5	0.506	23.12	1.49E+00	1.86E+04	40.5
40.68	0.508	23.43	1.50E+00	1.88E+04	40.68
40.86	0.51	23.73	1.50E+00	1.90E+04	40.86
41.04	0.513	24.02	1.51E+00	1.93E+04	41.04
41.22	0.515	24.27	1.52E+00	1.95E+04	41.22
41.4	0.517	24.61	1.52E+00	1.97E+04	41.4
41.58	0.519	24.9	1.53E+00	2.00E+04	41.58
41.76	0.522	25.21	1.54E+00	2.02E+04	41.76
41.94	0.524	25.5	1.54E+00	2.05E+04	41.94
42.12	0.526	25.82	1.55E+00	2.07E+04	42.12
42.3	0.528	26.12	1.56E+00	2.10E+04	42.3
42.48	0.531	26.42	1.56E+00	2.12E+04	42.48
42.66	0.533	26.69	1.57E+00	2.14E+04	42.66
42.84	0.535	27.02	1.58E+00	2.17E+04	42.84
43.02	0.537	27.32	1.58E+00	2.19E+04	43.02
43.2	0.54	27.59	1.59E+00	2.21E+04	43.2
43.38	0.542	27.92	1.60E+00	2.24E+04	43.38
43.56	0.544	28.21	1.60E+00	2.26E+04	43.56
43.74	0.546	28.55	1.61E+00	2.29E+04	43.74
43.92	0.549	28.81	1.62E+00	2.31E+04	43.92
44.1	0.551	29.12	1.62E+00	2.34E+04	44.1
44.28	0.553	29.44	1.63E+00	2.36E+04	44.28
44.46	0.555	29.76	1.64E+00	2.39E+04	44.46
44.64	0.558	30.09	1.64E+00	2.41E+04	44.64
44.82	0.56	30.44	1.65E+00	2.44E+04	44.82
45	0.562	30.78	1.66E+00	2.47E+04	45

45.18	0.564	31.15	1.66E+00	2.50E+04	45.18
45.36	0.567	31.5	1.67E+00	2.53E+04	45.36
45.54	0.569	31.91	1.68E+00	2.56E+04	45.54
45.72	0.571	32.31	1.68E+00	2.59E+04	45.72
45.9	0.573	32.71	1.69E+00	2.62E+04	45.9
46.08	0.576	33.13	1.70E+00	2.66E+04	46.08
46.26	0.578	33.5	1.70E+00	2.69E+04	46.26
46.44	0.58	33.91	1.71E+00	2.72E+04	46.44
46.62	0.582	34.3	1.72E+00	2.75E+04	46.62
46.8	0.585	34.76	1.72E+00	2.79E+04	46.8
46.98	0.587	35.1	1.73E+00	2.82E+04	46.98
47.16	0.589	35.52	1.74E+00	2.85E+04	47.16
47.34	0.591	35.89	1.74E+00	2.88E+04	47.34
47.52	0.594	36.24	1.75E+00	2.91E+04	47.52
47.7	0.596	36.67	1.76E+00	2.94E+04	47.7
47.88	0.598	37.06	1.76E+00	2.97E+04	47.88
48.06	0.6	37.44	1.77E+00	3.00E+04	48.06
48.24	0.603	37.84	1.78E+00	3.04E+04	48.24
48.42	0.605	38.2	1.78E+00	3.07E+04	48.42
48.6	0.607	38.61	1.79E+00	3.10E+04	48.6
48.78	0.609	38.99	1.80E+00	3.13E+04	48.78
48.96	0.612	39.36	1.80E+00	3.16E+04	48.96
49.14	0.614	39.73	1.81E+00	3.19E+04	49.14
49.32	0.616	40.09	1.82E+00	3.22E+04	49.32
49.5	0.618	40.46	1.82E+00	3.25E+04	49.5
49.68	0.621	40.81	1.83E+00	3.27E+04	49.68
49.86	0.623	41.21	1.84E+00	3.31E+04	49.86
50.04	0.625	41.56	1.84E+00	3.33E+04	50.04
50.22	0.627	41.93	1.85E+00	3.36E+04	50.22
50.4	0.63	42.33	1.86E+00	3.40E+04	50.4
50.58	0.632	42.66	1.86E+00	3.42E+04	50.58
50.76	0.634	43.03	1.87E+00	3.45E+04	50.76
50.94	0.636	43.36	1.88E+00	3.48E+04	50.94
51.12	0.639	43.68	1.88E+00	3.50E+04	51.12
51.3	0.641	44.08	1.89E+00	3.54E+04	51.3
51.48	0.643	44.4	1.90E+00	3.56E+04	51.48
51.66	0.645	44.78	1.90E+00	3.59E+04	51.66
51.84	0.648	45.13	1.91E+00	3.62E+04	51.84
52.02	0.65	45.47	1.91E+00	3.65E+04	52.02
52.2	0.652	45.82	1.92E+00	3.68E+04	52.2
52.38	0.654	46.15	1.93E+00	3.70E+04	52.38
52.56	0.657	46.48	1.93E+00	3.73E+04	52.56
52.74	0.659	46.83	1.94E+00	3.76E+04	52.74
52.92	0.661	47.14	1.95E+00	3.78E+04	52.92
53.1	0.663	47.45	1.95E+00	3.81E+04	53.1
53.28	0.666	47.77	1.96E+00	3.83E+04	53.28
53.46	0.668	48.12	1.97E+00	3.86E+04	53.46
53.64	0.67	48.44	1.97E+00	3.89E+04	53.64
53.82	0.672	48.72	1.98E+00	3.91E+04	53.82
54	0.675	49.01	1.99E+00	3.93E+04	54
54.18	0.677	49.36	1.99E+00	3.96E+04	54.18
54.36	0.679	49.63	2.00E+00	3.98E+04	54.36

54.54	0.681	49.95	2.01E+00	4.01E+04	54.54
54.72	0.684	50.22	2.01E+00	4.03E+04	54.72
54.9	0.686	50.53	2.02E+00	4.05E+04	54.9
55.08	0.688	50.81	2.03E+00	4.08E+04	55.08
55.26	0.69	51.08	2.03E+00	4.10E+04	55.26
55.44	0.693	51.34	2.04E+00	4.12E+04	55.44
55.62	0.695	51.59	2.05E+00	4.14E+04	55.62
55.8	0.697	51.86	2.05E+00	4.16E+04	55.8
55.98	0.699	52.11	2.06E+00	4.18E+04	55.98
56.16	0.702	52.38	2.07E+00	4.20E+04	56.16
56.34	0.704	52.64	2.07E+00	4.22E+04	56.34
56.52	0.706	52.91	2.08E+00	4.24E+04	56.52
56.7	0.708	53.12	2.09E+00	4.26E+04	56.7
56.88	0.711	53.39	2.09E+00	4.28E+04	56.88
57.06	0.713	53.64	2.10E+00	4.30E+04	57.06
57.24	0.715	53.86	2.11E+00	4.32E+04	57.24
57.42	0.717	54.09	2.11E+00	4.34E+04	57.42
57.6	0.72	54.33	2.12E+00	4.36E+04	57.6
57.78	0.722	54.56	2.13E+00	4.38E+04	57.78
57.96	0.724	54.78	2.13E+00	4.39E+04	57.96
58.14	0.726	54.94	2.14E+00	4.41E+04	58.14
58.32	0.729	55.16	2.15E+00	4.43E+04	58.32
58.5	0.731	55.38	2.15E+00	4.44E+04	58.5
58.68	0.733	55.6	2.16E+00	4.46E+04	58.68
58.86	0.735	55.74	2.17E+00	4.47E+04	58.86
59.04	0.737	55.95	2.17E+00	4.49E+04	59.04
59.22	0.74	56.14	2.18E+00	4.50E+04	59.22
59.4	0.742	56.31	2.19E+00	4.52E+04	59.4
59.58	0.744	56.49	2.19E+00	4.53E+04	59.58
59.76	0.747	56.67	2.20E+00	4.55E+04	59.76
59.94	0.749	56.86	2.21E+00	4.56E+04	59.94
60.12	0.751	56.98	2.21E+00	4.57E+04	60.12
60.3	0.753	57.1	2.22E+00	4.58E+04	60.3
60.48	0.756	57.3	2.23E+00	4.60E+04	60.48
60.66	0.758	57.45	2.23E+00	4.61E+04	60.66
60.84	0.76	57.59	2.24E+00	4.62E+04	60.84
61.02	0.762	57.76	2.25E+00	4.63E+04	61.02
61.2	0.765	57.9	2.25E+00	4.64E+04	61.2
61.38	0.767	58.07	2.26E+00	4.66E+04	61.38
61.56	0.769	58.18	2.27E+00	4.67E+04	61.56
61.74	0.771	58.32	2.27E+00	4.68E+04	61.74
61.92	0.774	58.46	2.28E+00	4.69E+04	61.92
62.1	0.776	58.61	2.29E+00	4.70E+04	62.1
62.28	0.778	58.74	2.29E+00	4.71E+04	62.28
62.46	0.78	58.85	2.30E+00	4.72E+04	62.46
62.64	0.783	58.98	2.31E+00	4.73E+04	62.64
62.82	0.785	59.08	2.31E+00	4.74E+04	62.82
63	0.787	59.15	2.32E+00	4.75E+04	63
63.18	0.789	59.27	2.33E+00	4.76E+04	63.18
63.36	0.792	59.33	2.33E+00	4.76E+04	63.36
63.54	0.794	59.41	2.34E+00	4.77E+04	63.54

63.72	0.796	59.45	2.35E+00	4.77E+04	63.72
63.9	0.798	59.47	2.35E+00	4.77E+04	63.9
64.08	0.8	59.5	2.36E+00	4.77E+04	64.08
64.26	0.803	59.48	2.37E+00	4.77E+04	64.26
64.44	0.805	59.4	2.37E+00	4.77E+04	64.44
64.62	0.807	59.25	2.38E+00	4.75E+04	64.62
64.8	0.81	59.02	2.39E+00	4.74E+04	64.8
64.98	0.812	58.65	2.39E+00	4.71E+04	64.98
65.16	0.814	58.1	2.40E+00	4.66E+04	65.16
65.34	0.816	57.43	2.41E+00	4.61E+04	65.34
65.52	0.819	56.73	2.41E+00	4.55E+04	65.52
65.7	0.821	55.94	2.42E+00	4.49E+04	65.7
65.88	0.823	55.17	2.43E+00	4.43E+04	65.88
66.06	0.825	54.37	2.43E+00	4.36E+04	66.06
66.24	0.827	53.58	2.44E+00	4.30E+04	66.24
66.42	0.83	52.8	2.45E+00	4.24E+04	66.42
66.6	0.832	51.98	2.45E+00	4.17E+04	66.6
66.78	0.834	51.13	2.46E+00	4.10E+04	66.78
66.96	0.837	50.24	2.46E+00	4.03E+04	66.96
67.14	0.839	49.32	2.47E+00	3.96E+04	67.14
67.32	0.841	48.36	2.48E+00	3.88E+04	67.32
67.5	0.843	47.39	2.48E+00	3.80E+04	67.5
67.68	0.846	46.41	2.49E+00	3.72E+04	67.68
67.86	0.848	45.42	2.50E+00	3.64E+04	67.86
68.04	0.85	44.39	2.50E+00	3.56E+04	68.04
68.22	0.852	43.4	2.51E+00	3.48E+04	68.22
68.4	0.855	42.41	2.52E+00	3.40E+04	68.4
68.58	0.857	41.43	2.52E+00	3.32E+04	68.58
68.76	0.859	40.54	2.53E+00	3.25E+04	68.76
68.94	0.861	39.62	2.54E+00	3.18E+04	68.94
69.12	0.863	38.76	2.54E+00	3.11E+04	69.12
69.3	0.866	37.83	2.55E+00	3.04E+04	69.3
69.48	0.868	36.84	2.56E+00	2.96E+04	69.48
69.66	0.87	35.7	2.56E+00	2.86E+04	69.66
69.84	0.873	34.51	2.57E+00	2.77E+04	69.84
70.02	0.875	33.3	2.58E+00	2.67E+04	70.02
70.2	0.877	32.07	2.58E+00	2.57E+04	70.2
70.38	0.879	30.85	2.59E+00	2.48E+04	70.38
70.56	0.882	29.66	2.60E+00	2.38E+04	70.56
70.74	0.884	28.5	2.60E+00	2.29E+04	70.74
70.92	0.886	27.41	2.61E+00	2.20E+04	70.92
71.1	0.888	26.36	2.62E+00	2.12E+04	71.1
71.28	0.89	25.39	2.62E+00	2.04E+04	71.28
71.46	0.893	24.49	2.63E+00	1.96E+04	71.46
71.64	0.895	23.62	2.64E+00	1.89E+04	71.64
71.82	0.897	22.73	2.64E+00	1.82E+04	71.82
72	0.9	21.95	2.65E+00	1.76E+04	72
72.18	0.902	21.14	2.66E+00	1.70E+04	72.18
72.36	0.904	20.38	2.66E+00	1.63E+04	72.36
72.54	0.906	19.71	2.67E+00	1.58E+04	72.54
72.72	0.909	19.02	2.68E+00	1.53E+04	72.72
72.9	0.911	18.43	2.68E+00	1.48E+04	72.9

73.08	0.913	17.87	2.69E+00	1.43E+04	73.08
73.26	0.915	17.36	2.70E+00	1.39E+04	73.26
73.44	0.917	16.9	2.70E+00	1.36E+04	73.44
73.62	0.92	16.45	2.71E+00	1.32E+04	73.62
73.8	0.922	16.02	2.72E+00	1.29E+04	73.8
73.98	0.924	15.63	2.72E+00	1.25E+04	73.98
74.16	0.926	15.28	2.73E+00	1.23E+04	74.16
74.34	0.929	14.93	2.74E+00	1.20E+04	74.34
74.52	0.931	14.63	2.74E+00	1.17E+04	74.52
74.7	0.933	14.31	2.75E+00	1.15E+04	74.7
74.88	0.936	13.99	2.76E+00	1.12E+04	74.88
75.06	0.938	13.71	2.76E+00	1.10E+04	75.06
75.24	0.94	13.39	2.77E+00	1.07E+04	75.24
75.42	0.942	13.12	2.78E+00	1.05E+04	75.42
75.6	0.944	12.81	2.78E+00	1.03E+04	75.6
75.78	0.947	12.55	2.79E+00	1.01E+04	75.78
75.96	0.949	12.31	2.80E+00	9.88E+03	75.96
76.14	0.951	12.05	2.80E+00	9.67E+03	76.14
76.32	0.953	11.77	2.81E+00	9.45E+03	76.32
76.5	0.956	11.52	2.82E+00	9.24E+03	76.5
76.68	0.958	11.22	2.82E+00	9.00E+03	76.68
76.86	0.96	10.96	2.83E+00	8.79E+03	76.86
77.04	0.963	10.66	2.84E+00	8.55E+03	77.04
77.22	0.965	10.34	2.84E+00	8.30E+03	77.22
77.4	0.967	10.07	2.85E+00	8.08E+03	77.4
77.58	0.969	9.77	2.86E+00	7.84E+03	77.58
77.76	0.972	9.49	2.86E+00	7.62E+03	77.76
77.94	0.974	9.2	2.87E+00	7.38E+03	77.94
78.12	0.976	8.9	2.88E+00	7.14E+03	78.12
78.3	0.978	8.54	2.88E+00	6.85E+03	78.3
78.48	0.98	8.17	2.89E+00	6.56E+03	78.48
78.66	0.983	7.8	2.90E+00	6.26E+03	78.66
78.84	0.985	4.37	2.90E+00	3.50E+03	78.84
79.02	0.987	3.41	2.91E+00	2.73E+03	79.02
79.2	0.989	3.24	2.92E+00	2.60E+03	79.2
79.38	0.992	3.12	2.92E+00	2.51E+03	79.38
79.56	0.994	3.06	2.93E+00	2.46E+03	79.56
79.74	0.996	3.01	2.94E+00	2.42E+03	79.74
79.92	0.999	3	2.94E+00	2.40E+03	79.92
80.1	1.001	2.96	2.95E+00	2.37E+03	80.1
80.28	1.003	2.94	2.96E+00	2.36E+03	80.28
80.46	1.005	2.89	2.96E+00	2.32E+03	80.46
80.64	1.007	2.9	2.97E+00	2.33E+03	80.64
80.82	1.01	2.86	2.98E+00	2.29E+03	80.82
81	1.012	2.84	2.98E+00	2.28E+03	81
81.18	1.014	2.8	2.99E+00	2.25E+03	81.18
81.36	1.016	2.83	3.00E+00	2.27E+03	81.36
81.54	1.019	2.78	3.00E+00	2.23E+03	81.54
81.72	1.021	2.79	3.01E+00	2.24E+03	81.72
81.9	1.023	2.78	3.01E+00	2.23E+03	81.9
82.08	1.026	2.71	3.02E+00	2.18E+03	82.08
82.26	1.028	2.76	3.03E+00	2.21E+03	82.26

82.44	1.03	2.74	3.04E+00	2.20E+03	82.44
82.62	1.032	2.73	3.04E+00	2.19E+03	82.62
82.8	1.034	2.72	3.05E+00	2.18E+03	82.8
82.98	1.037	2.7	3.05E+00	2.17E+03	82.98
83.16	1.039	2.66	3.06E+00	2.13E+03	83.16
83.34	1.041	2.66	3.07E+00	2.13E+03	83.34
83.52	1.043	2.66	3.07E+00	2.14E+03	83.52
83.7	1.046	2.65	3.08E+00	2.12E+03	83.7
83.88	1.048	2.62	3.09E+00	2.10E+03	83.88
84.06	1.05	2.59	3.09E+00	2.08E+03	84.06
84.24	1.052	2.61	3.10E+00	2.09E+03	84.24
84.42	1.055	2.57	3.11E+00	2.06E+03	84.42
84.6	1.057	2.54	3.11E+00	2.04E+03	84.6
84.78	1.059	2.55	3.12E+00	2.05E+03	84.78
84.96	1.061	2.53	3.13E+00	2.03E+03	84.96
85.14	1.064	2.51	3.13E+00	2.01E+03	85.14
85.32	1.066	2.48	3.14E+00	1.99E+03	85.32
85.5	1.068	2.49	3.15E+00	2.00E+03	85.5
85.68	1.07	2.47	3.15E+00	1.98E+03	85.68
85.86	1.073	2.46	3.16E+00	1.97E+03	85.86
86.04	1.075	2.45	3.17E+00	1.96E+03	86.04
86.22	1.077	2.44	3.17E+00	1.96E+03	86.22
86.4	1.079	2.43	3.18E+00	1.95E+03	86.4
86.58	1.082	2.4	3.19E+00	1.93E+03	86.58
86.76	1.084	2.38	3.19E+00	1.91E+03	86.76
86.94	1.086	2.37	3.20E+00	1.90E+03	86.94
87.12	1.089	2.36	3.21E+00	1.89E+03	87.12
87.3	1.091	2.33	3.21E+00	1.87E+03	87.3
87.48	1.093	2.36	3.22E+00	1.89E+03	87.48
87.66	1.095	2.32	3.23E+00	1.86E+03	87.66
87.84	1.097	2.31	3.23E+00	1.86E+03	87.84
88.02	1.1	2.28	3.24E+00	1.83E+03	88.02
88.2	1.102	2.26	3.25E+00	1.81E+03	88.2
88.38	1.104	2.27	3.25E+00	1.82E+03	88.38
88.56	1.106	2.24	3.26E+00	1.80E+03	88.56
88.74	1.109	2.22	3.27E+00	1.78E+03	88.74
88.92	1.111	2.19	3.27E+00	1.76E+03	88.92
89.1	1.113	2.21	3.28E+00	1.77E+03	89.1
89.28	1.115	2.18	3.29E+00	1.75E+03	89.28
89.46	1.118	2.15	3.29E+00	1.73E+03	89.46
89.64	1.12	2.12	3.30E+00	1.70E+03	89.64
89.82	1.122	2.12	3.31E+00	1.70E+03	89.82

Summary of Run 2 for All Sample in both Directions

Run	Sample	Type	Length (mm)	Width (mm)	Height (mm)	Modulus (MPa)	Yield (kPa)	Stress at Yield Strength (%)	Ultimate Yield (kPa)
2	3	AF2	29.86	2.86	6.20	5066	62900	1.884	65260
		TF2	27.33	2.86	6.37	1865	27500	2.072	30540
	4	AF2	23.39	2.87	4.41	4362	44860	2.416	48060
		TF2	26.11	2.90	4.06	2596	37060	3.263	39430
	5	AF2	30.49	2.84	4.51	9102	93400	2.712	94760
		TF2	31.69	2.87	3.91	7809	60820	2.038	61780
	6	AF2	30.30	2.85	3.88	15980	1E+05	1.755	110000
		TF2	30.09	2.85	4.45	4749	47690	2.345	47730
	7	AF2	31.51	2.82	4.67	10860	91960	2.066	92980
		TF2	27.00	2.85	4.24	4445	45530	2.613	47920

Rheology Data

Date Run #	2	Shear Rate 1/s	Viscosity Pa*s	Temperature C	L/D	Time min
ACB		4.52	50252.39	220	20	12.13
VCB		9.05	27056.34	220	20	11.21
CF		15.08	18272.04	220	20	10.41
MB	54%	30.16	9848.89	220	20	8.84
		60.32	5970.58	220	20	8.02
		120.64	3467.83	220	20	7.38
		150.8	2871.54	220	20	6.91
		301.6	1705.99	220	20	6.25
		603.2	1045.75	220	20	5.71